

See discussions, stats, and author profiles for this publication at: <https://www.researchgate.net/publication/376799918>

What are the mechanical factors altering the sprinting performance in the curve?

Thesis · December 2023

DOI: 10.13140/RG.2.2.27197.44002

CITATION

1

READS

56

1 author:



[Benjamin Millot](#)

French Athletics Federation

11 PUBLICATIONS 30 CITATIONS

SEE PROFILE

Université Paris Cité

Ecole doctorale 566 : Sciences du sport, de la motricité et du mouvement humain

Laboratoire Sport, Expertise et Performance

What are the mechanical factors altering the sprinting performance in the curve?

Quels sont les facteurs mécaniques explicatifs de la diminution de la performance lors de la course de sprint en virage ?

Par Benjamin MILLOT

Thèse de doctorat en Sciences du Mouvement Humain

Dirigée par Jean SLAWINSKI

Présentée et soutenue publiquement le 7 décembre 2023

Devant un jury composé de :

- Rapporteur.e.s :** **Emilie SIMONEAU**, Professeure des Universités, HDR, Université Polytechnique des Hauts de France, Valenciennes, France
Sylvain DOREL, Professeur des Universités, HDR, Université de Nantes, Nantes, France
- Examineur.e.s :** **Elena BERGAMINI**, Associate Professor, Università degli Studi "Foro Italico," Rome, Italy
Neil BEZODIS, Professor, Swansea University, Swansea, United Kingdom of Great Britain and Northern Island
- Directeur de thèse** **Jean SLAWINSKI**, PhD, HDR, Institut National du Sport, de l'Expertise et de la Performance, Paris, France
- Co-encadrant** **Daniel DINU**, PhD, Institut National du Sport, de l'Expertise et de la Performance, Paris, France

ACKNOWLEDGMENTS

Tout d'abord, je souhaiterais remercier Prof. **Emilie Simoneau** et Prof. **Sylvain Dorel** d'avoir accepté d'être les rapporteurs de mon manuscrit de thèse. Je me sens très privilégié de bénéficier de votre expertise. J'attends avec impatience vos retours qui seront, j'en suis certain, d'une grande richesse.

I would also like to warmly thank Prof. **Elena Bergamini** and Prof. **Neil Bezodis** for accepting of being part of my jury. I feel very honoured and grateful to benefit from your expertise and I am looking forward to discussing through this work together.

Je souhaite également remercier **Hélène**, quelques années après les TD de L2, je souhaite de nouveau te remercier d'avoir fait partie de mon comité de suivi individuel. Merci également pour les conseils précieux dès que j'en avais besoin.

%%%

```
clear all, close all, clc;
```

```
Load(« merci_Tonton_Matlab.mat »)
```

```
[vent_de_face,ça_monte_a_Saint_Cloud] =  
btkGetAnalog(h,'Didier_j''ai_une_heure_de_velo_pour_venir')
```

```
If vent_de_face == 1
```

```
Disp('Ouais désolé Didier je dois être à l'INSEP aujourd'hui, j''ai une réunion super importante')
```

```
else
```

```
Disp('J'arrive à 9h30 Didier')
```

```
End
```

%%%

Didier, merci également d'avoir fait partie de mon CSI et d'avoir apporté ton expérience, ton expertise et ta franchise. Outre cela, je me rappelle ces jours de janvier 2022 où j'ai commencé mes périples en direction de Garches. Mille mercis à toi pour les innombrables heures passées ensemble devant l'écran avec Matlab ouvert, où je te voyais comme le Messi qui a réponse à tout. Jamais je n'aurais pu en arriver là sans toi et je t'en serai éternellement reconnaissant. Merci tonton Matlab !!

Je souhaite également remercier mon co-encadrant et mon directeur de thèse qui m'accompagnent depuis mon stage de master 2. Quelle aventure ! Je commence avec toi, **Daniel**. Je me souviens encore de notre première rencontre ! J'avais toqué à ton bureau et tu m'avais accueilli avec le grincement de ta chaise. Une poignée de main ferme plus tard, tu m'as déroulé tout ton savoir-faire et les missions d'ASP avec les différentes fédé. Et même si je n'avais pas pu en placer une, l'aventure était commencée. Merci à toi pour tout et je te serai toujours reconnaissant de m'avoir « mis le pied à l'étrier » comme tu aimes si bien le dire.

Et enfin, **Jean-senseï**. Je t'avais découvert à l'escrime en novembre 2018 en début d'après-midi, avec ton sandwich. Tu m'as tout de suite fait confiance. J'ai énormément appris à tes côtés, tu m'as toujours mis en confiance, bref, je pense tout ce qu'on peut rêver d'un directeur de thèse, ou d'un senseï. Tes commentaires dans la relecture du manuscrit m'ont beaucoup fait rire, parfois fait grincer des dents, mais je pense que je ne peux être qu'éternellement

reconnaissant pour tout ce que tu m'as apporté. Je ne vais pas faire trop long (c'est trop tard...), j'en garde pour le saké post-soutenance et comme tu dirais : Marseille !!!

This is it! Après 3 ans à travailler sur le virage, me voilà au bout de cette dernière (longue) ligne droite... Zabardast ! Comme disaient Thomas Delphino et son équipe en apercevant la Biacherahi Tower au fin fond du Karakoram au Pakistan. Mais plus que ces trois années, je retiendrai tout le chemin qui m'a mené jusque-là (oui, parce que : « It's not the destination, it's the journey »). Et ça a commencé lors de mon entrée en Master à Valenciennes.

Jenn, comment te remercier... C'est toi qui m'as donné envie de prendre cette voie-là lors de mon année à « VA », puis à UVIC. Merci également pour les innombrables heures passées ensemble dans les différents stades du Nord. Merci également à tous les amis de l'US Valenciennes Athlétisme. Un merci particulier à **Julie** (et Boulette...) pour les moments passés ensembles, ton écoute sans faille, tes conseils de haut-rang et ton soutien inconditionnel à travers ces trois années. **Romain**, merci pour tous les fous rires ensemble, je t'attends à Paris pour un volley loute ! Merci également à **Tristan, Mouad, Ilona, Carole, David**, et tous les autres qui m'ont rendu mon année dans votre Ch'nord si agréable et épanouissante.

Merci également à **Julien** pour m'avoir fait confiance pour ce stage extrêmement enrichissant. Merci également à toute l'équipe du **Décathlon Sports Lab** pour votre accueil et en particulier **Cédric** pour nos échanges intéressants en congrès depuis.

Then I moved to west coast of Canada, in Victoria, BC for a full year and I would like to thank all my friends back in "Vic". A special thanks to **Claire & Shayla**, what a pleasure I had to meet you and discover your island alongside you! **Leah, Kim** and **Matthew**, many thanks for having me over when I arrived. I really enjoyed my stay at your lovely place. **Meg, Allison, Ben, Max**, you took care of your "Second Ben" as a family would do! Thank you to the UVIC friends and professors as well (a special thanks for **Drew!**), thank you so much. Merci également à **Geoff** avec qui je me suis jeté à l'eau pour traverser l'Atlantique et vivre cette aventure incroyable.

Je souhaite également remercier mes amis qui m'ont donné beaucoup de force sur ces trois dernières années. Un merci particulier à **Loulou, Anton, Yougz, Polo, Marwinch, Anne, Laurette, Daphny, Jojo, Juju**. Ces petits week-ends sur cette dernière année m'ont permis de bien m'aérer et j'en avais fort besoin ! **Coco, Gato**, merci pour les relais appuyés et les fringales cet été, maintenant place au jus ! Un merci très particulier à mon **KAL** pour toutes ces années de baroude. Plein d'autres sont à venir maintenant que je vais avoir du temps ! Merci également à **Pierrick, Marie, Hugo, Lili, Arnaud, Cass, Marie, Flo, Yankou, Manon, Adrien, Eva, Val, Antho, Flo, Théo** pour votre soutien et votre force tout au long de ces trois années ! Merci également à mon club d'athlétisme de l'UAI Nogent-sur-Marne et en particulier à **Olivier** pour ton engagement quotidien pour nous tous. Merci à tous les collègues de souffrance et notamment **Samir, Victor, Alexis, Thomas, Laurent** et tous les autres pour ces belles sessions d'entraînement ensemble.

Depuis maintenant 5 ans je prends la direction de l'INSEP. Merci, donc, à l'**INSEP** dans son ensemble et plus particulièrement aux équipes de **Frédéric Chasles**, au **pôle Hospitalité**, **Isabelle Amaudry** ou encore à l'**IRMES**. Merci également à **Mohammed** qui s'occupe du ménage au RDJ du bâtiment C.

J'adresse également un immense merci au laboratoire Sport, Expertise et Performance pour son accueil sur ces cinq années. Merci à tous les membres du labo et notamment à **Alexis, Claire** et **Bruno** pour votre soutien. **Charly**, merci d'avoir systématiquement répondu à mes « dis-moi, j'ai une question ». Merci à **Antoine** pour ton aide avec Origin, j'ai pu faire des belles figures de daltonien ! Merci également à **Caro** pour les échanges toujours très riches et tout soutien systématique. Merci à **Franck** pour les conseils toujours avisés, notamment la fameuse

théorie des 120 h lors de la dernière semaine avant le rendu du manuscrit. Merci **Janne** pour tes encouragements quasi-quotidiens depuis plusieurs mois maintenant. A huge thanks to **Andras** for your extensive help with the sEMG stuff! Merci également à **Adrien** et **Jean-François** pour tout. Nous ne pourrions rien faire sans les assistantes administratives alors merci **Isa** ! Enfin, merci à **Sinéad** pour le grain de folie que tu apportes au labo et en dehors ainsi que ta spontanéité.

Le RDJ !! Merci à vous, à tous les doctorants que j'ai pu croiser depuis 2018 et mon stage de M2. Merci à **Joffrey** pour toutes nos pauses café où nous refaisons le monde. Merci à **Mathilde P.** qui représente le X-bar et pour tous tes conseils à travers ces années. Merci également à **Valentine** pour avoir tant de fois répondu à mes questions avec un calme exemplaire. Merci à **Mildred** qui m'a permis de me remplir la panse (chose très importante pour moi) pendant la période transitoire fin de stage/début de thèse qui est toujours délicate à gérer. Enfin, merci à **Chloé, Jérôme, Allison, Enzo, Antoine, Anis**, bref, tous les « anciens », dont j'ai pu bénéficier de l'expérience, des compétences et des conseils avisés.

Merci à mes camarades « djeuns » du RDJ, les nouveaux arrivants : **Quentin, Max, Raph, Simon, Pauline**. Ça a été un plaisir de fermer la boutique à vos côtés tous les soirs. Vous verrez, c'est une belle aventure la dernière ligne droite... Faites mieux. **Mathilde D.** courage à toi pour cette dernière ligne droite, tu touches le bout !

Une mention très spéciale pour **Vincent**. Merci pour ton expertise, ta passion, ton sérieux, ton aide. Je repense à toutes nos heures passées ensemble à discuter de tout, de rien, à échanger sur des graphs, des pensées, des idées. Merci également de m'avoir sorti du bureau pour aller tourner les guiboles à Pershing ou dans le bois dans cette dernière ligne droite, ça m'a bien aidé à turbocharger. Enfin, souviens-toi... Généralement, quand c'est flou...

Je remercie également à mes amis Québécois **Paul-Eric & Jérémie** qui étaient là lors de mon arrivée à l'INSEP en M2 et qui m'ont poussé à me lancer dans le code.

Gaël, je voulais t'adresser un grand merci pour ta confiance accordée, mais également pour tous les échanges, pro ou perso, que nous avons pu avoir ces dernières années. J'ai beaucoup apprécié représenter les doctorants au sein du labo cette année, ça a été extrêmement enrichissant.

Et enfin **Adèle**, ostie ! Le *little-shit* a bien évolué depuis ton départ et je suis le point de rejoindre ton rang ! Merci de m'avoir supporté moi et mon bazar pendant ces 3 ans. Tu as été un exemple de sérieux depuis l'Open Space en 2018 jusqu'à notre somptueux loft, porte fenêtre aménagée, avec vue sur cour CRJ16. Enfin, merci pour tous tes conseils si précieux dans cette dernière ligne droite qui m'ont beaucoup rassuré.

Paul, tu as été omniprésent lors des pré-manips, manips, post-manips, post-post-manips, etc... Pour préparer, installer et ranger les bandes, monter sur les appareils de muscu, car « faut pas qu'ça bouuge !! ». Tu as été une pièce maîtresse de ce travail de thèse, alors merci infiniment ! Merci également à **Axelle** pour toute ton aide apportée sur ces manips, ton sérieux et ton savoir-faire. Je tiens également à remercier **Jean-Pierre** et la société **Sartorius** pour m'avoir fourni le gabarit ainsi qu'à **Margaux** et **DimaSport** pour vos belles bandes blanches qui ont permis de reproduire à la perfection ce couloir 5.

どうもありがとう **Daichi-sensei, Laura-sama, Arata-sama, Hana-sama, Itsuko-sama, Takeshi-sama, Hirotaaka-sama, Katsuyoshi-sama** and all the other wonderful persons I had the privilege to meet at the Japan Institute of Sport Sciences. This experience was the cherry on top of this PhD thesis and I am very grateful that you gave me this opportunity.

Je tiens également à remercier la **Fédération Française d'Athlétisme** dans son ensemble pour l'accueil depuis 3 ans. Cette thèse CIFRE a été une expérience extrêmement enrichissante

personnellement et professionnellement. Je souhaite remercier en particulier l'équipe du pôle orga' pour votre travail et votre sérieux dans leur globalité qui m'ont permis d'évoluer dans des conditions idéales lors des compétitions. Merci tout particulièrement à **Eric, Mike, Margot, Charles, Ingrid, Joseph, Pauline, Thomas, Sylvaine, Geoff**. Merci également à tous les autres collègues de la fédé, parmi lesquels **Julien, Joost, Alberto, Arnaud, Jean-Seb, Sabrina, Margaux, Constance, Laurie, Clément, Patricia, Emilie, Souad** et **tous les autres**. J'adresse également un merci tout particulier à **Catherine, Pierre-Yves, Adrien, Geoff** et enfin **Louise**, membres du CSE, qui font un travail extraordinaire. Une mention très spéciale pour **Louise** qui se plie en quatre au quotidien pour nous proposer le meilleur et qui m'a toujours aidé quand j'avais « une p'tite question », merci ! Merci également à **Claudine**, notre représentante du personnel.

Merci également à **Philippe** pour toutes les discussions extrêmement enrichissantes, en particulier à l'INSEP cet été. Merci également à **Pierre-Jean** pour tes connaissances sans limites de notre sport. C'est toujours un immense plaisir d'échanger et d'apprendre avec toi.

Je souhaite également remercier tous les entraîneurs pour leur confiance accordée depuis 3 ans. Je remercie en particulier **Guy & Bruno** avec qui j'ai eu la chance d'évoluer dès le début. Merci également à tout le groupe des combinards et notamment **Gaëtan** pour ta confiance depuis 2020. Merci également à **Manu** pour tous nos échanges ainsi qu'à **Sullivan, Ketty** et **tous les autres** pour votre confiance et votre bienveillance. Du côté des athlètes, j'adresse un merci particulier à **Jules, Amandine, Kevin, Mak, Mélina, Alexandra, David, Téo** et d'une manière générale tous les combinard(e)s, les sprinters(euses) et les lanceurs(euses) avec qui j'ai eu la chance de travailler pendant 3 ans.

Ce travail sur le terrain n'était pas individuel et puisqu'on est plus fort à plusieurs, j'adresse un immense merci à **Arnaud** et **Dorian** pour toute l'aide apportée lors des compétitions. **Dorian**, des beaux souvenirs sur ce week-end de folie entre Clermont et Lyon ! **Arnaud**, des beaux moments également à Albi cet été à griller au soleil ! Merci également à **Yanis**, Monsieur le Président, toujours prêt à m'apporter de l'aide.

Guillaume, merci à toi pour tous ces échanges et tout ce que tu m'as appris ces dernières années. **Giuseppe**, merci infiniment pour toute ton aide extrêmement précieuse lors du traitement de données et sur toutes les réflexions très riches que nous avons eu ensemble. J'arrive au bout de mon 400, je te passe désormais le témoin, qui sera, j'en suis certain, entre de bonnes mains pour le prochain tour de piste (ou d'aire de lancer). **Canelle**, merci pour toute l'aide que tu m'as apportée sur mes différentes questions stats ainsi que pour les conseils en cette fin de thèse. Merci également à m'sieur **Chiron** pour ton soutien systématique et nos fameuses lunes de miel à Munich & Budapest. Courage pour ta dernière ligne droite !! Merci également à **Simon & Jerem**, les deux derniers membres de notre petite équipe initiale. Enfin, merci à **Christine**, notre maman à tous qui chapotait tout cela d'une main de maître. Tu as été tout simplement parfaite à tous égards avec moi : perso, pro, toujours le conseil qui faut, toujours à me mettre en confiance et à valoriser mon travail... Merci pour ton humanité, merci pour ta bienveillance, merci pour tout.

Hugo, merci pour ton aide dans cette dernière ligne droite avec cette relecture express qui m'a beaucoup apporté. Merci également pour ta confiance, ton soutien et tes conseils depuis ton arrivée à la FFA !

Bertrand, nous nous sommes rencontrés un midi de décembre 2020 à la cafet' de l'hôtel à la Réunion. Tu m'as tout de suite pris sous ton aile et accordé une confiance sans failles depuis, merci ! Merci également pour notre étroite collaboration sur les cursives de Liévin cet hiver, les mains tremblantes !

Papi, que dire, tu m'as mis les pieds dans le sport quand j'étais encore petit et je ne l'ai jamais quitté depuis. Merci pour tout ce que tu m'as apporté depuis que je suis petit et ça dépasse largement le cadre du sport. Tu es une source d'inspiration pour moi au quotidien et ce que tu as montré cette dernière année le prouve encore plus.

Cathy, Fred, on s'est malheureusement peu vu ces trois dernières années, mais les quelques barbecues chez vous dans cette dernière ligne droite m'ont fait un bien fou ! « On est là... On est lààà ». **Jenna**, merci également pour ton soutien à chaque fois qu'on s'est vu.

Antoine, mon reuf, j'ai suivi le chemin que tu avais tracé et 3 ans plus tard, j'y suis enfin ! 2 docteurs dans la mif ! Les parents vont être fiers de nous ! Merci d'avoir toujours été là pour moi. Je vais enfin avoir du temps pour venir voir l'épicerie fine Délicatessen.

Sarah, comment te remercier... Ton soutien dans cette dernière ligne droite est tellement précieux. Merci dans l'ensemble pour tout ce que tu m'apportes au quotidien depuis plus de 19 mois maintenant. Merci également pour ton temps passé dans cette dernière ligne droite à corriger mes fautes en anglais. Merci de m'avoir fait remonter du creux de la vague tant de fois ces derniers mois. Merci pour tout, merci pour toi dans l'ensemble et ces quelques phrases ne suffisent pas pour exprimer toute la gratitude que j'éprouve à ton égard.

Maman, Papa, un merci infini à vous deux, pour tout. Merci d'avoir toujours cru en moi, de m'avoir toujours fait confiance et de vous être pliés en quatre pour que je puisse m'épanouir au quotidien. Merci pour votre soutien inconditionnel, depuis toujours, et en particulier sur ces 3 dernières années. Si j'en suis là aujourd'hui, c'est en très grande partie grâce à vous. Je ne pourrai pas résumer en quelques lignes l'ampleur de ma reconnaissance à votre égard, alors je conclurai en disant tout simplement, merci.

"Let's change the way we eat, let's change the way we live and let's change the way we treat each other." (Tupac Amaru Shakur, 1992)

PUBLICATIONS AND CONFERENCE PRESENTATIONS

Published peer-reviewed articles related to the thesis

Millot, B., Blache, P., Dinu, D., Arnould, A., Jusseaume, J., Hanon, C. & Slawinski, J. (2022). Centre of mass velocity comparison using a whole body magnetic inertial measurement unit system and force platforms in well trained sprinters in straight-line and curve sprinting. *Gait Posture*. <https://doi.org/10.1016/j.gaitpost.2022.11.002>

Conference communications related to the thesis

Millot, B., Blache, P., Dinu, D., Arnould, A., Jusseaume, J., Hanon, C. & Slawinski, J. (2021). Kinetic analysis of curve sprinting in male and female track athletes. 19ème congrès de l'Association des Chercheurs en Activités Physiques et Sportives, Montpellier, France.

Millot, B., Blache, P., Dinu, D., Arnould, A., Jusseaume, J., Hanon, C. & Slawinski, J. (2022). Centre of mass velocity comparison using a whole body magnetic inertial measurement unit system and force platforms in well trained sprinters in straight-line and curve sprinting. 27th European College of Sport Science, Sevilla, Spain.

Millot, B., Pradon, D., Blache, P., Dinu, D., Cecchelli, G., Arnould, A., Hegyi, A. & Slawinski, J. (2023). Muscle activity timings in the early acceleration phase of straight-line and curve sprinting. 28th European College of Sport Science, Paris, France.

Published peer-reviewed article outside of the scope of the thesis

Fornasier-Santos, C., Arnould, A., Jusseaume, J., **Millot, B.**, Guilhem, G., Couturier, A., Samozino, P., Slawinski, J. & Morin, J. B. (2022). Sprint Acceleration Mechanical Outputs Derived from Position- or Velocity-Time Data: A Multi-System Comparison Study. *Sensors* 22, 8610. <https://doi.org/10.3390/s22228610>

Dinu, D., Delaveau, G., Blache, P., Slawinski, J. & **Millot, B.** (2023). Etude des contraintes biomécaniques exercées sur les articulations de l'épaule et de la hanche chez le pongiste de haut niveau. *Journal de Traumatologie du Sport* 40(3) : 184-191. <http://dx.doi.org/10.1016/j.jts.2023.06.008>

Published article outside of the scope of the thesis

Slawinski, J., Chiron, F., **Millot, B.**, Taouji, A. & Brocherie, F. (2019). Effect of a 16-Day Altitude Training Camp on 3,000-m Steeplechase Running Energetics and Biomechanics: A Case Study. *Frontiers in Sports and Active Living*, 1. <https://www.frontiersin.org/articles/10.3389/fspor.2019.00063>

Millot, B. (2020). Les déterminants mécaniques de la course de sprint en virage. *La Revue de l'Association des Entraîneurs Français d'Athlétisme*. <https://www.aefathle.org/produit/n238/>

Simon, M., Jusseaume, J., Chiron, F., Guyot, V., **Millot, B.** & Hanon, C. (2021). Quand la science s'invite sur les pistes d'athlétisme. *La Revue de l'Association des Entraîneurs Français d'Athlétisme*. <https://www.aefathle.org/produit/n243/>

Conference communication outside of the scope of the thesis

Millot, B. (2020). Les contraintes mécaniques de la course de sprint en virage : début d'une thèse CIFRE au sein de la FFA. Assises du sprint de la Fédération Française d'Athlétisme, Boulouris, France.

Millot, B. (2022). L'Accompagnement Scientifique à la Performance au sein de la Fédération Française d'Athlétisme au cours de la saison 2021-2022. Assises du sprint de la Fédération Française d'Athlétisme, Lyon, France.

Slawinski, J., Houel, N., **Millot, B.**, Mahlig, A. & Dinu, D. (2022). Kinetic energy of the trunk, a key parameter to explain performance in sprint running acceleration? 27th European College of Sport Science, Sevilla, Spain.

Millot, B. (2023). Analyse cinématique et musculaire lors de la phase de transition en ligne droite et en virage. Colloque medical de la Fédération Française d'Athlétisme, Paris, France.

Millot, B. (2023). Analyse cinématique lors de la phase de transition en ligne droite et en virage. Coaching Summit Series by European Athletics. Liévin, France.

LIST OF ABBREVIATIONS

ANOVA	Analysis of variance	F_V	Vertical component of the ground reaction force
AGLR	Approximated Generalized Likelihood Ratio	g	Gravitational acceleration
ADD	<i>Adductor</i>	GCS	Global coordinate system
A_{A-P}	Antero-posterior acceleration	GM	<i>Gastrocnemius Medialis</i>
$A_{A-P MAX}$	Maximum antero-posterior acceleration	GMax	<i>Gluteus Maximus</i>
BLL	<i>Body lateral lean</i>	GPS	Global positioning system
BF_{lh}	<i>Biceps Femoris long head</i>	GRF	Ground reaction forces
BW	Body weight	IMP_{A-P}	Antero-posterior component of the impulse
CM	Centre of mass	IMP_{A-P-}	Braking antero-posterior impulse
DLT	Direct Linear Transformation	IMP_{A-P+}	Propulsive antero-posterior impulse
F_C	Norm of the centripetal force	IMP_{M-L}	Medial-lateral component of the impulse
F_{A-P}	Norm of the antero-posterior component of the ground reaction force	IMP_{TOT}	Resultant impulse
F_{A-P-}	Norm of the antero-posterior braking force	IMP_V	Vertical component of the impulse
F_{A-P+}	Norm of the antero-posterior propulsive force	ISB	International Society of Biomechanics
F_{M-L}	Norm of the medial-lateral component of the ground reaction force	LCS	<i>Local coordinate system</i>
FP	Force platforms	MIMU	Magneto inertial measurement unit
F-v	Force-velocity	MTP	<i>Metatarsophalangeal</i>

F_{TOT}	Norm of the resultant ground reaction force	MTU	Muscle-tendon unit
MVIC	Maximal Voluntary Isometric Contraction	V_{CM}	Centre of mass velocity
OS	Optoelectronic system	V_{A-P}	Antero-posterior velocity
PB	Personnal best	$V_{A-P CM}$	Centre of mass antero-posterior velocity
RF	<i>Rectus Femoris</i>	$V_{A-P CM MAX}$	Centre of mass maximal antero-posterior velocity
sEMG	Surface electromyography	$V_{A-P CM MEAN}$	Centre of mass mean antero-posterior velocity
SD	Standard deviation	$V_{A-P MAX}$	Maximal antero-posterior velocity
SF	<i>Step frequency</i>	$V_{A-P MEAN}$	Mean antero-posterior velocity
SL	<i>Step length</i>	VL	<i>Vastus Lateralis</i>
SOL	<i>Soleus</i>	3D	Three-dimensional
TKEO	Teager-Kaiser Energy Operator	VM	<i>Vastus Medialis</i>

TABLE OF CONTENT

GENERAL INTRODUCTION.....	14
LITERATURE REVIEW.....	18
Part I – The sprinting velocity determines the performance	18
The sources of the human movement	18
1. The sprinting velocity from the starting blocks to the maximal antero-posterior power (from ~0 m to ~4 m).....	24
2. The sprinting velocity from the maximal antero-posterior power to the maximal antero-posterior velocity (from ~4 m to ~40 m)	28
3. The sprinting velocity at the maximal antero-posterior velocity (from ~40 m to ~70 m)	29
Part II – Ground Reaction Forces and impulse	34
1. The ground reaction forces and impulses from the starting blocks to the maximal antero-posterior power (from ~0 m to ~4 m)	36
2. The ground reaction forces from the maximal antero-posterior power to the maximal antero-posterior velocity (from ~4 m to ~40 m)	41
3. The ground reaction forces and impulses at the maximal antero-posterior velocity (from ~40 m to ~70 m).....	48
Part III – Sprinting kinematics	53
1. The sprinting kinematics from the starting blocks to the maximal antero-posterior power (from ~0 m to ~4 m)	53
2. The sprinting kinematics from the maximal antero-posterior power to the maximal antero-posterior velocity (from ~4 m to ~40 m)	59
3. The sprinting kinematics during the maximal antero-posterior velocity (from ~40 m to ~70 m).....	63
Part IV – The use of surface electromyography to understand the sprinting technique	67
1. The muscle activity from the starting blocks to the maximal antero-posterior power (from ~0 m to ~4 m).....	67
2. The muscle activity from the maximal antero-posterior power to the maximal antero-posterior velocity (from ~4 m to ~40 m)	70
3. The muscle activity at the maximal antero-posterior velocity (from ~40 m to ~70 m)	72
RESEARCH QUESTIONS AND AIMS OF THE THESIS.....	76
GENERAL METHODOLOGY	79
1. Participants.....	79
2. Protocol	79
3. Materials	89
4. Synchronization	90
5. Data processing	92
6. Study 1: Comparison of the centre of mass velocity between a reference system and a MIMU-based system	97

7. Study 2: Are the ground reaction forces altered by the curve and with the increasing sprinting velocity through the transition phase?	99
8. Study 3: Are the lower limb joint kinematics altered by the curve and with the increasing sprinting velocity through the transition phase?	104
9. Study 4: Are the muscular activities altered by the curve and with the increasing sprinting velocity through the transition phase?	106
10. Statistical analyses	110
STUDY 1	115
1. Results	116
2. Discussion	119
3. Limitations	123
4. Conclusion	124
STUDY 2	126
1. Results	127
2. Discussion	136
3. Limitations	140
4. Conclusion	140
STUDY 3	142
1. Results	143
2. Discussion	151
3. Limitations	159
4. Conclusion	159
STUDY 4	161
1. Results	162
2. Discussion	167
3. Limitations	172
4. Conclusion	173
GENERAL DISCUSSION	175
1. A pioneer exploration in the curve from the starting blocks on to the maximal antero-posterior velocity	176
2. An explanatory factor for the hamstrings' injury during the late swing phase?	182
GENERAL CONCLUSION	189
1. Research perspectives	189
REFERENCES	192

GENERAL INTRODUCTION

In the 100-m dash, after the gun goes off, the female and the male who cross the finish line in the shortest elapsed time will be crowned. As the mean antero-posterior velocity ($V_{A-P\ MEAN}$) reached during the 100-m dash is defined by the elapsed time over this distance, it is pretty straightforward to assume that the $V_{A-P\ MEAN}$ is eventually the most important parameter that must be enhanced.

Decades of research have now addressed quite thoroughly the different parameters that can influence the $V_{A-P\ MEAN}$ and the performance over a 100-m dash. By using data from lasers, radars and video cameras, Slawinski et al. (2017) showed that the maximal antero-posterior velocity ($V_{A-P\ MAX}$) strongly predicted the 100-m dash performance among World-Class sprinters (correlation coefficient (r) of -0.90). During his 9.59 World Record, Usain Bolt reached the astonishing $V_{A-P\ MAX}$ of $12.34\ \text{m} \cdot \text{s}^{-1}$ (Graubner & Nixdorf, 2009). Consequently, anyone who is willing to beat Bolt's World Record would likely have to reach a greater $V_{A-P\ MAX}$. Likewise, we can quite confidently predict the next female and male Olympic Champion in August 2024 based on the $V_{A-P\ MAX}$ that the athletes will reach during the race. The centre of mass (CM) antero-posterior velocity ($V_{A-P\ CM}$) although more challenging to capture than the $V_{A-P\ MEAN}$ or the $V_{A-P\ MAX}$ was also related to the sprinting expertise (Slawinski, Bonnefoy Mazure, Levêque, et al., 2010). Consequently, the greater the $V_{A-P\ CM}$, the better the sprinter (Slawinski, Bonnefoy Mazure, Levêque, et al., 2010).

Based on Newton's Second Law the CM velocity (V_{CM}) can be described from the ground reaction forces (GRF) (Kawamori et al., 2013). In the straight, it has been shown that applying a greater magnitude of antero-posterior force (F_{A-P}) is key to a better sprinting performance (Hunter et al., 2005; Kawamori et al., 2013; Morin et al., 2012; Rabita et al., 2015). Indeed, within a group of sprinters, those with the better performances were able to produce more F_{A-P} than their less experienced counterparts (Rabita et al., 2015). Nevertheless, as sprinting is not an unloaded activity, sprinters cannot only apply F_{A-P} . In fact, a vertical force (F_V) must be applied as well in order to overcome the gravitational acceleration (g) and not fall (Morin et al., 2011). Similarly, as a 100-m dash is assumed to be performed strictly in the straight, the medial-lateral force (F_{M-L}) is usually neglected or is not reported, although its magnitude can reach up to 1/3rd of the body weight (BW) during the initial stances (Nagahara et al., 2017).

In contrast, in the curve, the F_{M-L} becomes central as the sprinter has to adopt a curvilinear motion (Chang & Kram, 2007). On top of that, this curvilinear motion is fundamental in athletics as the 100-m dash remains the only event (with the 100-m and the 110-m hurdles) to be performed strictly in the straight. Indeed, for all the track events starting from the 200 m onwards, 57.84% of the total distance is run in the curve which is equal to 115.68 m for a 200 m. For a 400 m, this distance is doubled and the athletes must cover 231.36 m in the curve. At the Olympics, 10 sprint events are run in the curve and can be considered as “curve sprinting events”: the 4*100, the 200 m, the 400 m, the 400-m hurdles, and the 4*400 m. Plus, in 2019, an additional Olympic discipline, the 4*400-m mixed relay, has appeared. Thus, considering the number of curve sprinting events in track and field, it is quite paradoxical that most of the research that has been conducted until now has mostly focused on the straight.

Consequently, the French Athletics Federation, via its coaches, has positioned itself to initiate a PhD thesis aiming to address and understand the challenges when sprinting in the curve. Indeed, it is well accepted that in this sprinting condition, the performance is reduced in comparison to the straight, likely due to the apparition of the centripetal force (Greene, 1985; Jain, 1980). For example, during a 200-m race, the performance would be ~0.4 second (s) better if the same distance was to be run in the straight instead of in the curve (Jain, 1980). Therefore, it appears mandatory to study the underlying reasons explaining this reduced performance.

In sprinting, several mechanical parameters directly account for the performance and can be investigated to compare both sprinting conditions to address a better understanding of the different factors altering the sprinting performance in the curve. Among these parameters, the V_{CM} provide a global approach of the sprinting performance. As the V_{CM} is directly impacted by the GRF and as the GRF has been described as key parameters in the sprinting performance, they should be studied concomitantly. Furthermore, a sprinter's capacity to optimally produce the GRF depends on the sprinting technique which is itself impacted by the muscle activity of the muscles surrounding the joints. Consequently, straight-line and curve sprinting can be compared using a multi-dimensional experimental approach to address some mechanical factors that reduce the sprinting performance in the curve.

Thus far, a few experimental studies have been conducted to understand the reasons that account for the poorer sprinting performance in the curve. However, some of these studies were conducted at radii not typical of track events (Chang & Kram, 2007; Filter et al., 2020), or with athletes sprinting at sub-maximal velocities (Alt et al., 2015). Overall, only a few studies have investigated the GRF (Churchill et al., 2016; Judson et al., 2019) and the kinematics (Churchill et al., 2015; Judson, Churchill, Barnes, Stone,

Brookes, et al., 2020; Judson, Churchill, Barnes, Stone, & Wheat, 2020) in the curve, at radii typical of track events and with athletes sprinting with maximal efforts. Nevertheless, these experimentations investigated 2 specific instants of the sprint: at 13 m (Judson, Churchill, Barnes, Stone, Brookes, et al., 2020; Judson, Churchill, Barnes, Stone, & Wheat, 2020; Judson et al., 2019) and 40 m (Churchill et al., 2015, 2016). Yet, in the curve, the centripetal force applied to the CM is strongly influenced by the antero-posterior V_{CM} ($V_{A-P CM}$) (Greene, 1985). Consequently, it is mandatory to compare the curve to the straight not at an isolated moment of the curve, but rather, throughout the transition phase.

Thus, the present PhD thesis aimed to compare the GRF, the joints' kinematics and the sEMG activity between the curve and the straight from the starting block on to the $V_{A-P MAX}$.

Over the past decade, technological improvements have permitted to conduct *in-field* analyses to explore the sprinting kinematics (Blair et al., 2018; Nijmeijer et al., 2023) and the surface electromyographic (sEMG) activity with wireless devices benefiting from an adequate range. These devices together with innovating protocols (Cavagna et al., 1971; Rabita et al., 2015) now permit to investigate the GRF, the kinematics and the sEMG activity throughout an entire sprint within *in-field* conditions in order to strengthen the study's ecological validity. In the present PhD thesis, the experimentations conducted were tailored into four separate studies.

At first, we have tried to determine whether the V_{CM} computed with a commercially available Magneto-Inertial Measurement Unit (MIMU)-based system matched the V_{CM} computed with a reference system (*i.e.*, force platforms (FP)). **In a secondary study**, we have compared the GRF and the impulses in the straight and in the curve to better appreciate how the human body adopts the curvilinear trajectory. **Thirdly**, the lower-limb joint kinematics were explored to comprehend how the human body adapts to make the CM turn while leaning inwards. **Finally**, as the sprinting technique itself relies on the sEMG activity of the different muscles surrounding the joints, we have investigated the sEMG activity of four muscles that have a meaningful impact in the straight-line sprinting performance in a fourth study.

This manuscript is composed out of four main chapters. The **first chapter** is a literature review detailing the current knowledge regarding the V_{CM} , the GRF, the kinematics and the sEMG activity from the starting blocks on to $V_{A-P MAX}$ in the straight and in the curve. The **second chapter** presents the general methodology employed to carry out the different experimentations conducted during this PhD thesis. The **third chapter** details the experimental contributions of the present thesis within four successive

studies. Finally, the **fourth chapter** discusses the overall contribution of this PhD thesis and address a general picture of the characteristics of curve sprinting. Practical recommendations emerging from this PhD thesis are also made, together with research perspectives that emerge from the present work.

LITERATURE REVIEW

Part I – The sprinting velocity determines the performance

The sources of the human movement

Walking and running

Humans are capable of locomotion over a wide range of velocities. Progressing from one to the subsequent velocity requires mechanical adaptations. Three main means of displacements are common: walking, running and sprinting. At the lowest velocities, walking is characterized by a double support (*i.e.*, both limbs are in contact with the ground) (Nilsson et al., 1985; Novacheck, 1998; Segers et al., 2006). With a velocity approaching and eventually exceeding $\sim 2 \text{ m} \cdot \text{s}^{-1}$, humans transition towards running (Segers et al., 2007; Thorstensson & Roberthson, 1987). In running, double support phases disappear and successive stance and swing phases appear (see figure 1) (Segers et al., 2007). With the increasing running velocity, the touchdown contact eventually shifts from rearfoot to forefoot and can characterize the change between running to sprinting (Novacheck, 1998). Regardless of the velocity, sprinting also consists of a maximal effort aiming to cover a given (generally short) distance, in the shortest time.

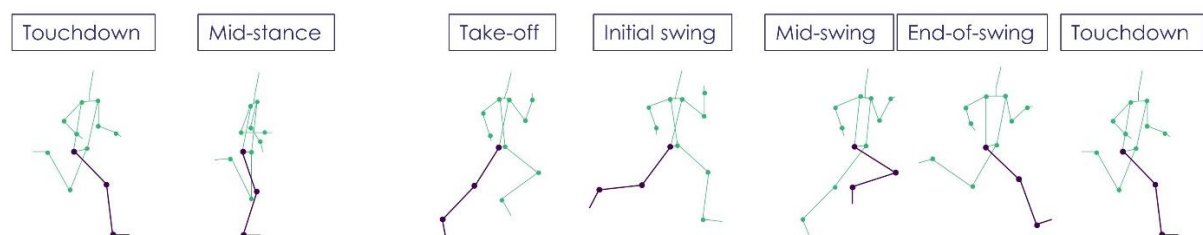


Figure 1. Representation of the right leg from entire running gait cycle (from one touchdown to the following touchdown).

Sprinting

Depending on the sport, the sprinting demand and the characteristics associated with it can vary. In track and field sprint events, the 100-m dash is considered to be the showpiece event and eventually honors the fastest female and male in the world. This event is also unique in itself as it is the only outdoor track event to be run strictly in the straight. In all other track events (200 m and above), the curve represents ~58% of the total distance, which means that sprinting efficiently in the curve is key for these events. For the 200 m, the distance to cover in the curve is 115.60 m for all the lanes. For the 400 m, the distance to cover in the curve is doubled and equals to 231.20 m for all lanes.

Sprinting in the curve

It is a common statement among coaches and athletes to assume that the curve portion of the race results in a decreased sprinting performance in comparison to the straight. In addition to that, within the curve, further discrepancies result from the lane allocated to the athlete. The inner lanes yield greater disadvantages in comparison to the outer ones due to the smaller radii of curvature. Following the World Athletics Track and Field Facilities Manual, international events can be held on lanes 1 to 9. Their radius of curvature typically ranges from 36.50 m (lane 1) to 46.26 m (lane 9) with 1.22-m wide lanes. Likely aware of the disparities between lanes, World Athletics have recently built new rules regarding the lane allocation for the 200 and 400 m that will be applied starting from the 2023 World Championships onwards. For the first round, the lane allocation in track competitions “shall be drawn by lot”. For the subsequent rounds, three draws for lanes will be made. For the 200 m, the following rules will apply:

1. “The 3 top ranked athletes to determine placings in lanes 5, 6 and 7;
2. Another for the three following athletes to determine placings in lane 3, 4 & 8;
3. A third draw for the two last ranked athletes or teams to determine placings in lanes 1 and 2.”

For the 400 m on the other hand, the following drawing will apply:

1. “The 4 top ranked athletes to determine placings in lanes 4, 5, 6 and 7;
2. Another for the two following athletes to determine placings in lane 3 & 8;
3. A third draw for the two last ranked athletes or teams to determine placings in lanes 1 and 2.”

Thus, this regulation somehow confirms the empirical statement postulating that inner lanes yield greater disadvantages than the outer lanes.

A couple of mathematical models confirmed this empirical evidence. For example, Jain (1980) estimated that in average, the advantage of the outer lane between two adjacent lanes would be approximately 0.012 s. Therefore, in their example of a seven lanes track, differences between the innermost and the outermost lanes would be 0.069 s for a 200 m (Jain, 1980). Using a diverging mathematical model, Greene (1985) suggested that the differences between lane 1 and lane 7 would be 0.123 s for a 200-m race, which is almost the double of Jain's (1980) estimations. Overall, although these mathematical models do not fully agree regarding the magnitude of the difference between each lane in the curve, they are in line with the empirical statements stipulating that 1) the curve results in a decrease in performance in comparison to the straight; and 2) the innermost lanes place the athletes at a greater disadvantage in comparison to the outermost lanes.

The 2017 200-m World Championships men's final provides an illustration of the uneven nature of the curve in track and field events. Ramil Guliyev won the gold medal by 0.02 s over Wayde Van Niekerk: respectively 20.09 and 20.11 s. Guliyev ran on lane 5 while the lane 3 was attributed to Van Niekerk. It is interesting to note that the final time difference between both sprinters resulted in the differences that arose from the first 100 m of this race (10.13 vs 10.15 s respectively), strictly ran on the curve portion of the track. Following Jain's (1980) estimations, this two-lane staggered position would yield a 0.023 s difference, making Wayde Van Niekerk win the gold medal if this assumption was found to be correct and if the athletes were to run on the same lane (although this is very unlikely to happen). Many similar examples can be found in the track and field 200- and 400-m history, confirming the uneven nature of the curve and strongly encourage to understand the underpinning reasons.

From basic physics, a body moving in a circular motion requires a centripetal force to be applied to that body. The norm of the centripetal force (F_C) is defined by:

$$F_C = m * \left(\frac{V_T^2}{r} \right) \quad (1)$$

where, m is the subject's mass, V_T his tangential linear velocity and r the radius of curvature. Since this F_C is proportional to the V_T squared, thus, the magnitude of F_C strongly depends on the runner's $V_{A-P_{CM}}$. Therefore, at a given radius of curvature, close to the runner's $V_{A-P_{CM_{MAX}}}$, F_C is maximal. Given that the F_C is inversely proportional to the radius of curvature, and following Jain's (1980) and Greene's (1985) models, one would state that the most outer lane would yield the least reduction in performance in comparison to the straight. Yet, it is a common statement

among track and field coaches and athletes to postulate that sprinting “blind” without seeing another athlete in front is detrimental. Thus, the middle lanes are commonly considered as being the most advantageous in the curve as they represent a trade-off between radius of curvature and having opponents in front (World Athletics does not allocate the lane 8 to the best seeded athlete).

The different phases of a sprint

Track and field coaches agree with researchers and describe sprinting as a multi-phase event. From a practical point of view and although the phases' names and its number diverge among authors a 100-m dash can be divided within three main phases. Volkov & Lapin (1979) divided the sprint within 1. Acceleration, 2. $V_{A-P MAX}$ and 3. Deceleration phases. On the other hand, Moravec et al. (1988) divided the 100-m dash within 1. Acceleration, 2. $V_{A-P MAX}$ and 3. Velocity endurance, based on their work during the 100-m dash 1987 World Championships. Finally, Mero et al. (1992) separated the acceleration phase within two sub-phases which breaks down the 100-m dash within 4 separate parts: starting blocks, acceleration, constant velocity and deceleration phases (Mero et al., 1992).

Recently, simple methods were developed to compute the Force-Velocity (F-v) relationship of a 40-m sprint in overground sprinting (Morin et al., 2019; Samozino et al., 2016). Computing the F-v relationship helps to individualize the training programs (Morin & Samozino, 2016) and has become of greater interest in coaching over the past decade. Thus, for the present manuscript, we thought it would be of interest to suggest a new break-down of the 100-m dash into different sprinting phases that ultimately correspond to distinct training zones. This layout would eventually draw an interesting overview of the main characteristics of each phase associated with each specific strength and conditioning training zones.

Consequently, in the present manuscript, we have decided to divide a 100-m dash within four different phases based on Volkov & Lapin's (1979) sprinting definition (figure 2):

- **Phase 1:** From the starting blocks push-off – (maximal F_{A-P}) to the maximal antero-posterior power ($P_{A-P MAX}$);
- **Phase 2:** From the $P_{A-P MAX}$ to the $V_{A-P MAX}$ (the transition phase);
- **Phase 3:** The $V_{A-P MAX}$;
- **Phase 4:** The deceleration.

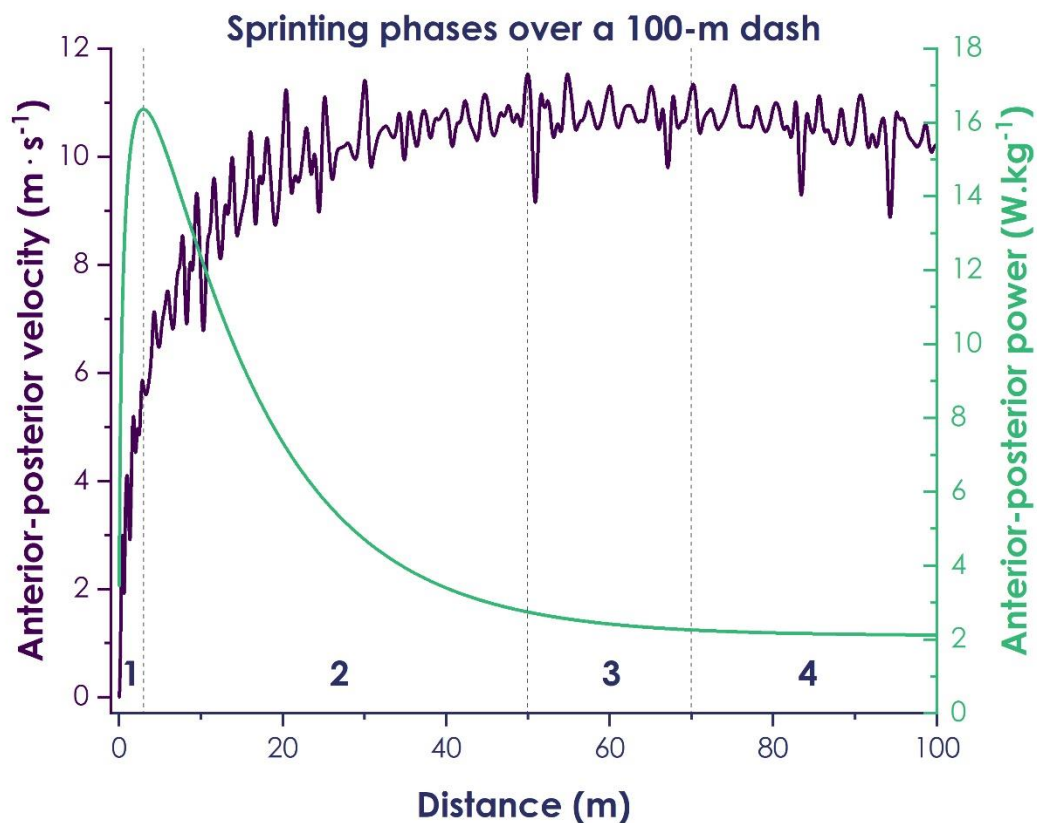


Figure 2. An example of a raw 100-m dash antero-posterior velocity (in purple) and the antero-posterior power (in green, computed using Samozino et al.'s (2016) method) with respect to the distance (expressed in m) recorded with a laser device. The dashed vertical lines represent each sprinting phase. The phase 1 includes the starting blocks pushing phase and lasts until the maximal antero-posterior power ($P_{A-P MAX}$). The phase 2 spans from the $P_{A-P MAX}$ to the maximal antero-posterior velocity ($V_{A-P MAX}$). The phase 3 corresponds to the $V_{A-P MAX}$ phase. Finally, the phase 4 corresponds to the deceleration phase.

Based on personal unpublished data using wearable global positioning systems (GPS), we found that the same 4 phases can be found during 200- and 400-m sprints (see figure 3).

Within the present manuscript, we have decided to focus our analysis over the first three phases of the sprint. Thus, in the following literature review, the experimentations discussing the V_{A-P} , the GRF, the joints' kinematics as well as the muscular activity within these first three phases of a 100-m dash in the straight and in the curve will be discussed. For clarity's sake, when experimentations refer to multiple instants of the sprint that include the phases 1 and 2, we will refer to the "transition phase".

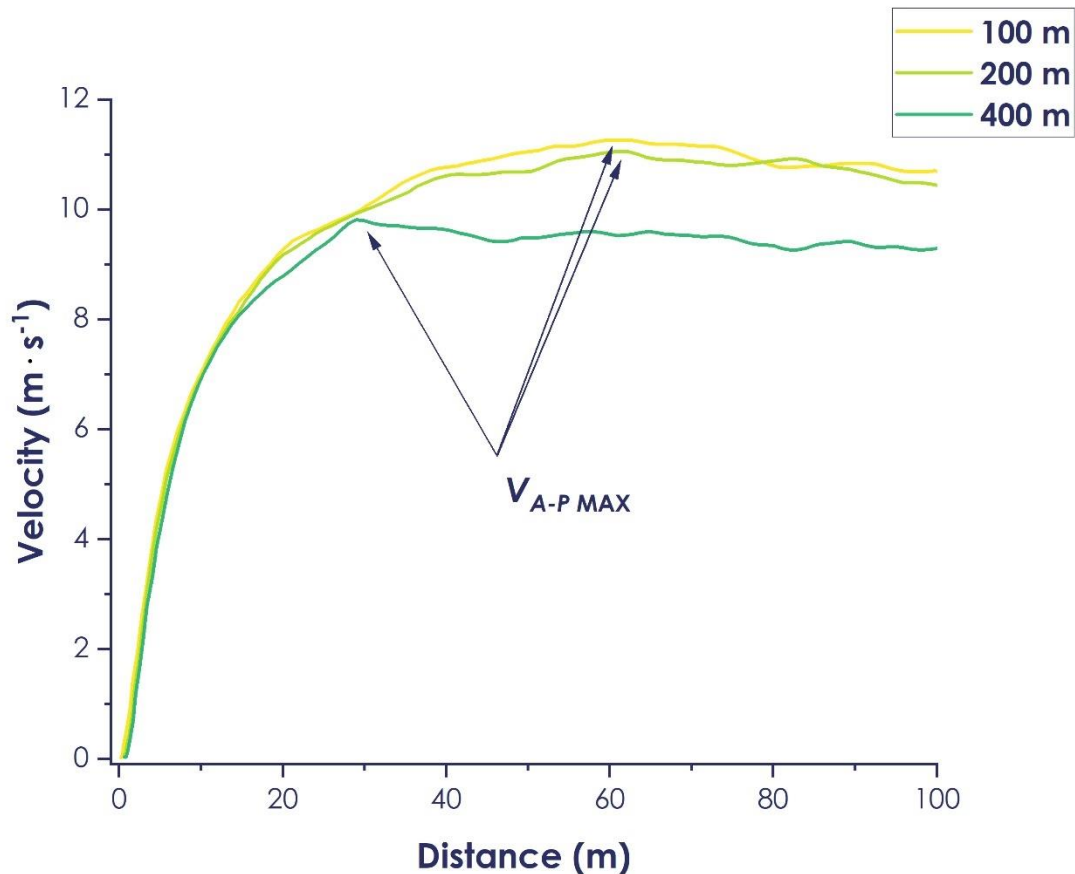


Figure 3. Sprinting velocity measured with a Global Positioning System device during a 100-, 200- and 400-m sprints by the same athlete. The arrows point the instant where the maximal antero-posterior velocity ($V_{A-P MAX}$) is reached. Although the $V_{A-P MAX}$ changes between each sprinting distance, the same four phases are recognizable.

Velocity as a pledge of performance

Strictly speaking, the V_{A-P} is defined as the time taken to cover a given antero-posterior distance. Thus, the main aim of a 100-m race consists of covering the given distance over the shortest time. It is pretty straight-forward to acknowledge that the sprinter's $V_{A-P MEAN}$ over the distance is ultimately the most important parameter for straight-line sprinting performance. Thereafter, through the three different phases, we will present the sprinter's V_{A-P} -time curve reported in the literature.

1. The sprinting velocity from the starting blocks to the maximal antero-posterior power (from ~0 m to ~4 m)

1. The starting blocks pushing phase

i. Straight

In track and field, all sprint events (*i.e.*, 60, 100, 200 and 400 m) are initiated with a starting blocks phase. This phase spans from the “On your marks” on to the front block exit (Bezodis et al., 2019). Before entering into the starting blocks, the sprinter must setup the plates antero-posterior position and inclination as these eventually influence the starting blocks pushing phase performance.

According to Slawinski et al. (2012), the best trade-off between the starting block V_{A-P} exit and the pushing time on the blocks corresponds to a “medium start” (inter-blocks spacing of 36.8 ± 3.5 cm). In addition to that, the blocks inclination is also a key feature in the sprint start. Guissard et al. (1992) reported a greater V_{A-P} at starting blocks exit with a front block angle of 30° in comparison to 70° (respectively 2.94 ± 0.20 m · s⁻¹ and 2.37 ± 0.31 m · s⁻¹), without any increase in the starting blocks pushing phase duration.

As we will develop in the present manuscript, the V_{A-P} is a central metric in sprinting. Therefore, different experimentations evaluated this parameter. The figure 4 presents the $V_{A-P\ CM}$ (computed from FP), optoelectronic systems (OS) or manual digitation from video footage) or V_{A-P} (radar, laser) at the starting blocks exit as reported in the literature when 100-m dash personal bests (PBs) were also reported. Overall, we can observe a trend suggesting that the $V_{A-P\ CM}$ or V_{A-P} at the starting blocks exit increases together with the sprinting expertise.

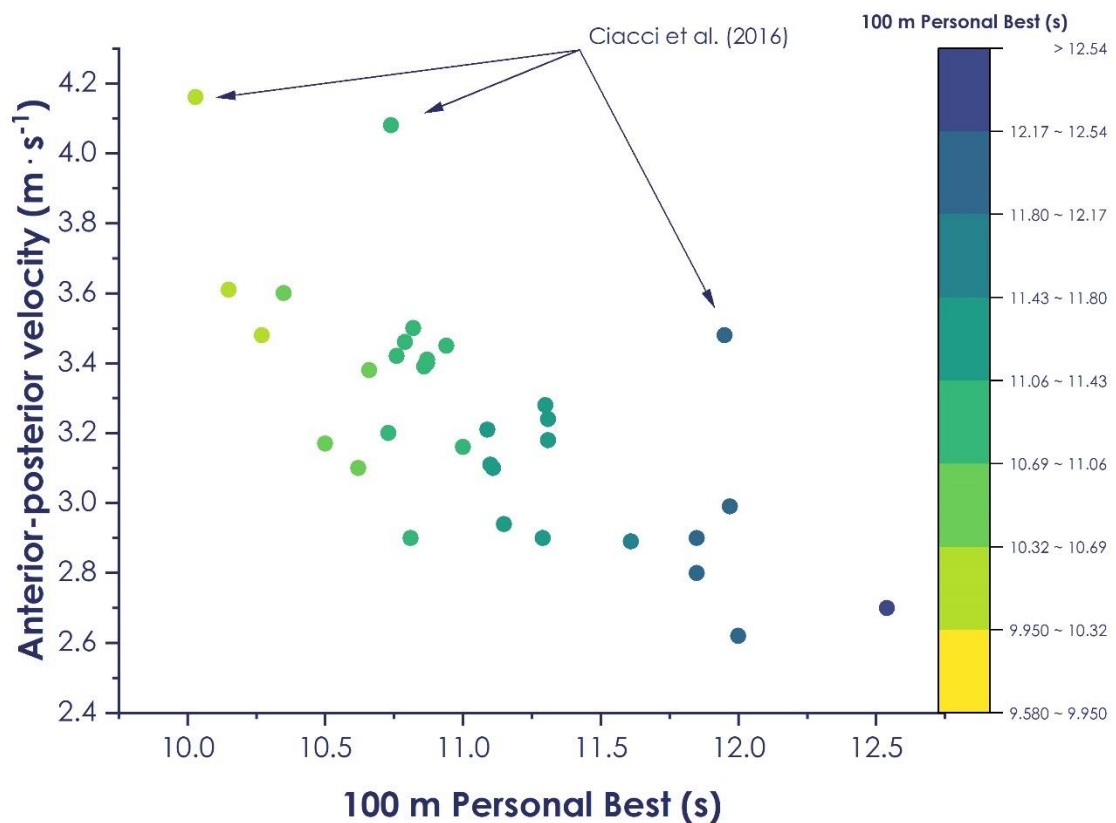


Figure 4. Centre of mass' or sprinter's antero-posterior velocity (expressed in $\text{m} \cdot \text{s}^{-1}$) at the starting blocks exit with respect to the 100 m personal best (PB; expressed in s) retrieved from the available literature. The color map corresponds to the 100 m PB.

Slawinski et al. (2010) used an OS and 63 retro-reflective markers positioned on anatomical landmarks in order to compute the CM V_{A-P} ($V_{A-P CM}$) over the starting blocks pushing phase. From the reconstructed spatial trajectories of the markers, the segments' mass and the CM position ($V_{A-P CM}$ was computed using the time differentiation of the CM position) were estimated with scaling equations (Dumas et al., 2007). The authors reported a greater $V_{A-P CM}$ at the front block exit between elite (100-m PBs of 10.27 ± 0.14 s) and experienced (100-m PBs of 11.31 ± 0.28 s) sprinters (respectively 3.48 ± 0.05 vs 3.24 ± 0.18 $\text{m} \cdot \text{s}^{-1}$) (Slawinski, Bonnefoy Mazure, Levêque, et al., 2010).

Ciacci et al. (2016) compared the $V_{A-P CM}$ of "world-class" (derived from Diamond League track meets) and "elite" (derived from the Italian junior athletics championships) sprinters using 3 video cameras. From the video footage, the authors computed the partial and global $V_{A-P CM}$ through manual digitation of 21 anatomical landmarks on the three videos and Direct Linear Transformation (DLT) (Abdel-Aziz & Karara, 1971) was used in order to perform a three-dimensional (3D) calibration and

segmental data (de Leva, 1996). In their experimentation, world-class male sprinters (100-m PBs of 10.03 ± 0.14 s) reached greater $V_{A-P_{CM}}$ than their elite (100-m PBs of 10.74 ± 0.21 s) counterparts (4.16 ± 0.39 vs 4.08 ± 0.08 $\text{m} \cdot \text{s}^{-1}$, respectively) and represent the highest values available in the literature (Ciacci et al., 2016) (see the two highest points in figure 4).

However, the utilization of an OS or cameras has been criticized as this “inverse dynamics” methods relies on assumptions regarding the anthropometry and the body segments' rigidity (Pavei et al., 2017). In addition, markers movement on the skin as well as operator errors originating from manual digitation during video footage clicking on the anatomical landmarks constitute other limitations of this method. In order to overcome those limitations, other authors have used FP to compute the $V_{H_{CM}}$ using a “forward dynamics” approach as none of the above-mentioned assumptions are needed (Pavei et al., 2017).

Using FP, Rabita et al. (2015) compared the $V_{A-P_{CM}}$ at the front starting blocks exit between elite (100-m PBs ranging from 9.95 to 10.29 s) and sub-elite (100-m PBs ranging from 10.40 to 10.60 s) sprinters. In their experimentation, the elite athletes reached a $V_{A-P_{CM}}$ of 3.61 ± 0.08 $\text{m} \cdot \text{s}^{-1}$ which corresponds to a 12.1% higher $V_{A-P_{CM}}$ than their less experienced counterparts (3.17 ± 0.19 $\text{m} \cdot \text{s}^{-1}$) (Rabita et al., 2015). Those findings corroborate with those of Slawinski et al. (2010) postulating that the starting blocks exit $V_{A-P_{CM}}$ is positively associated with the sprinting expertise.

Ciacci et al.'s (2016) values are ~15% greater than those reported by Rabita et al. (2015) despite that the participants in both studies were at a quasi similar sprinting expertise. The large discrepancies between the two experimentations could be twofold. First, the conditions under which the measurements were made differed. In Ciacci et al.'s (2016) experimentation, the data were retrieved from international track meets, with opponents next to the athletes. In contrasts, in Rabita et al.'s (2015) experimentation, those measurements were made during a training session. Thus, the engagement might have been maximal during the track meet and could explain the ~15% greater values than the findings of Rabita et al. (2015). In addition to that, the $V_{A-P_{CM}}$ processing varied between both studies. While Rabita et al. (2015) used FP, Ciacci et al. (2016) used video cameras and manual digitation of anatomical landmarks to reconstruct the body CM after applying segmental parameters.

Two experimentations reported the $V_{A-P_{CM}}$ at the starting blocks exit and at $V_{A-P_{MAX}}$. Rabita et al.'s (2015) showed that elite and sub-elite sprinters are able to reach ~35% of their maximal $V_{A-P_{CM}}$ ($V_{A-P_{CM_{MAX}}}$) at the starting blocks exit. On the other hand, Debaere et al. (2013) found that national level female and male athletes reached a

$V_{A-P CM}$ at the starting blocks exit which correspond to ~31% of their $V_{A-P CM MAX}$. In their study, the female sprinters had a $V_{A-P CM}$ of $2.76 \pm 0.40 \text{ m} \cdot \text{s}^{-1}$ at the starting blocks exit and $8.88 \pm 0.11 \text{ m} \cdot \text{s}^{-1}$ at $V_{A-P CM MAX}$. The male sprinters, on the other hand, had a $V_{A-P CM}$ of $3.14 \pm 0.18 \text{ m} \cdot \text{s}^{-1}$ at the front block exit and $10.01 \pm 0.16 \text{ m} \cdot \text{s}^{-1}$ at $V_{A-P CM MAX}$ (Debaere, Jonkers, et al., 2013).

Overall, these two experimentations show that the starting blocks pushing-phase leads the sprinters to reach ~1/3rd of their $V_{A-P CM MAX}$ over a short time (~0.35 s (Slawinski, Bonnefoy Mazure, Levêque, et al., 2010)) and emphasize the major role of this phase.

ii. Curve

To the author's knowledge, no experimentation investigated the $V_{A-P CM}$ during the starting blocks pushing phase in the curve. In the 200- and 400-m sprint starts, athletes are usually advised to position their starting blocks on the outside of their lane, pointing towards the inside of the lane, a few meters ahead, in order to sprint in a straight-line during the first steps. Thus, based on the coaches' empirical evidence, it is likely that small differences if any will be found between the two sprinting conditions during the starting blocks pushing-phase.

2. The sprinting velocity from the starting blocks exit on to the maximal antero-posterior power (from ~0 m to ~4 m)

i. Straight

After the starting blocks phase, a sprinter still undergoes a large increase in his V_{A-P} while in an uprising position (Nagahara et al., 2014). With the increasing V_{A-P} , the sprinter's ability to generate F_{A-P} onto the ground decreases. The antero-posterior power (P_{A-P}) can be defined as the product of the V_{A-P} and the F_{A-P} . Thus, the maximal P_{A-P} ($P_{A-P MAX}$) corresponds to the apex of the antero-posterior power-velocity relationship and is reached at 50% of V_{A-P0} (Samozino et al., 2016).

In treadmill sprinting, the $P_{A-P MAX}$ was typically reached after ~2 s (Morin et al., 2010) for physically active students, ~2.5 s (Jaskólski et al., 1996) for healthy-male students and at sprinting V_{A-P} comprised between ~4.5 and ~6.5 $\text{m} \cdot \text{s}^{-1}$ with a mixed population of physically active students and track sprinters (Morin et al., 2012).

In overground sprinting on the other hand, the $P_{A-P MAX}$ was reached at ~5.5 $\text{m} \cdot \text{s}^{-1}$ and ~6 $\text{m} \cdot \text{s}^{-1}$ (~3-3.3 m) by female and male world-class athletes and at ~6.5 $\text{m} \cdot \text{s}^{-1}$ for Usain Bolt during his 9.59 s World Record in 2009 which corresponded to ~50% of their $V_{A-P MAX}$

(Slawinski et al., 2017). Thus, overall, from the starting blocks exit on to the $P_{A-P MAX}$, the sprinter's V_{A-P} increases from ~30% to ~50% of the sprinter's $V_{A-P MAX}$ within 2-to-3 steps.

ii. Curve

To the author's knowledge, no experimentation investigated the $V_{A-P CM}$ between the starting blocks exit and the $P_{A-P MAX}$ in the curve. As the initial steps are expected to be mostly in the straight, little (if any) changes are expected for the $V_{A-P CM}$ between the straight and the curve.

2. The sprinting velocity from the maximal antero-posterior power to the maximal antero-posterior velocity (from ~4 m to ~40 m)

1. Straight

After the $P_{A-P MAX}$ is reached, the so-called "transition phase" spans on to the instant of $V_{A-P CM MAX}$ or $V_{A-P MAX}$ from ~4 m to ~40 m. This phase's duration varies with the athlete's expertise (Slawinski et al., 2017; Volkov & Lapin, 1979). Throughout this phase, the sprinter's $V_{A-P CM}$ increases to a lesser extent than during the first phase of the race.

Usain Bolt's V_{A-P} -distance curve from his 9.59 s World Record in 2009 illustrates this (see Graubner & Nixdorf's (2009) figure A page 27 in their study). Bolt reached a $V_{A-P MEAN}$ of $9.99 \text{ m} \cdot \text{s}^{-1}$ during the 10-20 m interval which corresponds to ~81% of his $V_{A-P MAX}$. Over the 20-30 m interval, his $V_{A-P MEAN}$ increased to $11.11 \text{ m} \cdot \text{s}^{-1}$, corresponding to ~90% of his $V_{A-P MAX}$. In the 30-40 m interval, his $V_{A-P MEAN}$ further increased to $11.63 \text{ m} \cdot \text{s}^{-1}$, which corresponds to ~94% of his $V_{A-P MAX}$. Overall, Usain Bolt reached ~50% of his $V_{A-P MAX}$ with the starting blocks push-off and the initial 3 steps. From ~50% to ~90% of his $V_{A-P MAX}$, Bolt needed 16 more steps. Thus, it is clear that once the $P_{A-P MAX}$ has been reached, the increase in V_{A-P} is slower.

Aerenthouts et al. (2012) evaluated the V_{A-P} of female and male junior and senior Finish sprinters using a laser during the transition phase. These authors found that, regardless of the gender, the sprinters with the best sprinting expertise were at a significantly greater (all $p < 0.05$) V_{A-P} at 5, 10, 15 and 20 m than their less experienced counterparts (Aerenthouts et al., 2012). Those findings suggest that in addition to the starting blocks exit and the $P_{A-P MAX}$ phases, the sprinters with a greater expertise are also able to reach higher V_{A-P} than their less skilled counterparts throughout the transition phase.

2. Curve

Judson et al. (2020) used an OS and applied segment inertial parameters (de Leva, 1996) to compute the $V_{A-P CM}$ from maximal effort sprints, both in the straight and in the curve and at 13 m on a reconstructed lane 1 ($r = 36.50$ m). These authors reported similar $V_{A-P CM}$ in the curve in comparison to the straight (both $p > 0.05$). Those findings mean that the $V_{A-P CM}$ is not affected by the curve at 13 m on lane 1. However, due to the restricted calibrated volume, these authors focussed their analysis on two steps at a specific instant of the transition phase which limits the global understanding of how the curve alters the $V_{A-P CM}$ during this phase.

3. The sprinting velocity at the maximal antero-posterior velocity (from ~40 m to ~70 m)

1. Straight

At the end of the transition phase, a sprinter reaches $V_{A-P MAX}$ after ~22 steps in overground sprinting (Nagahara et al., 2020). Using a linear encoder that measures the rate at which a 200-m long wire is unrolled, Volkov & Lapin (1979) were the first to compare the $V_{A-P MAX}$ between two groups with a different sprinting expertise. These authors found that sprinters with 100-m PBs of 11.17 ± 0.33 s reached greater $V_{A-P MAX}$ than non sprinters (9.01 ± 0.22 vs 7.59 ± 0.57 $m \cdot s^{-1}$ respectively) (Volkov & Lapin, 1979). In their study, Rabita et al. (2015) found a significantly greater $V_{A-P MAX}$ for the elite group in comparison to their sub-elite counterparts (respectively 10.24 ± 0.19 vs 9.33 ± 0.31 $m \cdot s^{-1}$); thus, confirming the previous findings that sprinters with a greater expertise are able to reach higher $V_{A-P MAX}$ than their least experienced counterparts.

More recently, Slawinski et al. (2017) congregated instantaneous V_{A-P} from laser and $V_{A-P MEAN}$ over 10-m interval retrieved from female and male video footage during 100-m dash at the World Championships and the Olympic Games finals between 1987 and 2012. Fifty-one races were compiled for the female sprinters and fifty for the male athletes with mean performances of 10.85 ± 0.15 s and 9.82 ± 0.15 s respectively in the 100-m dash. Thus, it is clear that this study gathered world class performances for both female and male sprinters. Slawinski et al. (2017) reported that male sprinters reached a significantly greater $V_{A-P MAX}$ than the females (11.53 ± 0.23 $m \cdot s^{-1}$ vs 10.39 ± 0.17 $m \cdot s^{-1}$ respectively) (Slawinski et al., 2017). In addition to that, the $V_{A-P MAX}$ reached during the race was strongly correlated with the 100-m performance of the female and male sprinters ($r = -0.74$ and -0.90 ; $p < 0.001$, respectively) (Slawinski et al., 2017).

The figure 5 gathers the $V_{A-P MAX}$ reported through the literature as a function of the 100-m PB. From the figure 5, it is also interesting to note that with a 100-m PB of ~ 11.00 s or better, the increase in the 100-m dash performance and the $V_{A-P MAX}$ are almost linear.

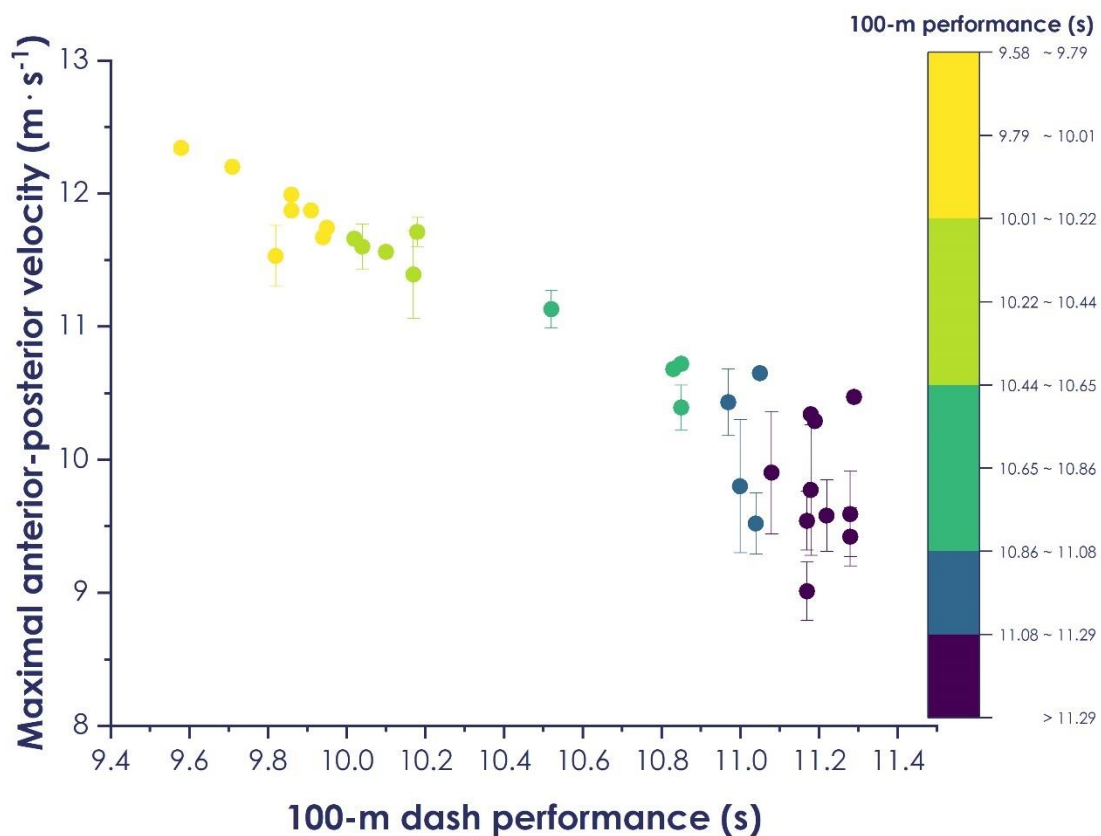


Figure 5. Centre of mass' and sprinter's antero-posterior velocity (in $m \cdot s^{-1}$) expressed as a function of the sprinters' 100 m personal best (in s) among male and female sprinters. Data retrieved from the available literature.

The three greatest $V_{A-P MAX}$ recorded were reached during the 2009 World Championships male 100-m final. During this race, Usain Bolt beat his own 100-m World Record with a time of 9.58 s while Tyson Gay (silver medalist) and Asafa Powell (bronze medalist) set a time of respectively 9.71 s and 9.84 s. Using lasers positioned behind the three medalists, Graubner & Nixdorf (2009) assessed the instantaneous V_{A-P} -distance curve of these three outstanding sprinters. Usain Bolt reached a $V_{A-P MAX}$ of $12.34 m \cdot s^{-1}$ while the other two medalists reached a $V_{A-P MAX}$ of $12.20 m \cdot s^{-1}$ and $11.90 m \cdot s^{-1}$ (Graubner & Nixdorf, 2009). As the greatest $V_{A-P MAX}$ for male was recorded during the male World Record, any sprinter attempting to beat Bolt's performance would likely have to reach $V_{A-P MAX}$ greater than $12.34 m \cdot s^{-1}$.

In addition to the $V_{A-P MAX}$, the time or the distance taken to reach this $V_{A-P MAX}$ are also key parameters in straight-line sprinting that are well associated with the sprinting expertise. Volkov & Lapin (1979) showed that the sprinters reach their $V_{A-P MAX}$ later than the non-sprinters (after 4.66 ± 0.36 s vs 4.22 ± 0.21 s for the sprinters and the non-sprinters, respectively; $p < 0.001$), meaning that the sprinters are able to accelerate over a longer duration. More than 30 years later, Debaere et al. (2013), using a laser, investigated the V_{A-P} of the 20 best performing female and male Flanders sprinters of the 100-m sprint rankings in 2009. These authors showed that male with better 100-m PBs reached their $V_{A-P MAX}$ at 50.75 ± 5.35 m which was $\sim 20\%$ later than their female counterparts, who reached their $V_{A-P MAX}$ at 42.26 ± 5.42 m (Debaere, Jonkers, et al., 2013). Slawinski et al. (2017) later confirmed Debaere et al.'s (2013) findings with world-class male sprinters reaching their $V_{A-P MAX}$ significantly later than their female counterparts (after 6.44 ± 0.86 s and 5.70 ± 0.69 s, respectively; $p < 0.001$) (Slawinski et al., 2017). Finally, in the 2009 World Championships final, Usain Bolt reached his $V_{A-P MAX}$ at 67.90 m while the other two medalists reached their $V_{A-P MAX}$ at 55.23 and 53.75 m (Graubner & Nixdorf, 2009), meaning that all three athletes were able to accelerate over a large portion of the 100-m dash which can testify their sprinting expertise.

Overall, these experimentations suggest that a) greater $V_{A-P MAX}$ are reached by sprinters with greater expertise; and b) sprinters with better 100-m expertise reach their $V_{A-P MAX}$ later than their least experienced counterparts.

2. Curve

Hanon & Gajer (2009) computed the sprinting $V_{A-P MEAN}$ over 50-m segments of regional-to-international level female and male 400-m races. These authors showed that regardless the expertise or the gender, the athletes' greatest $V_{A-P MEAN}$ over 50-m segments were reached within the 50-100 m segment (Hanon & Gajer, 2009). Although providing preliminary insights, Hanon & Gajer's (2009) study presents limitations as the V_{A-P} was averaged over 50-m intervals and sprinting with maximal effort is characterized by step-by-step changes. As the 0-50 m interval encompasses the early transition phase and the very low V_{A-P} associated with it, the $V_{A-P MEAN}$ is underestimated during the 0-50 m interval. Thus, it is possible that the $V_{A-P MAX}$ was reached before the 50-m mark, as it could be the case in the straight. For that sake, it would be of great interest to seek for the $V_{A-P MEAN}$ over smaller intervals (*i.e.*, 10 m) or directly for the instantaneous V_{A-P} . This would in turn provide unique information regarding the instant at which the $V_{A-P MAX}$ is reached during 200- and 400-m races.

Churchill et al. (2015) were the first authors who investigated the $V_{H CM}$ at a distance that could correspond to $V_{A-P CM MAX}$ in the curve (*i.e.*, 40 m). The authors used two

cameras, manual digitation and the DLT (Abdel-Aziz & Karara, 1971) in order to create a 16-segment kinematic model, to combine body segment inertia (de Leva, 1996) and to determine the CM using the segmental approach (Eng & Winter, 1993).

Thereafter, the authors compared the $V_{A-P CM MAX}$ between straight-line and curve sprinting at 40 m on lane 2 ($r = 37.72$ m) averaged during both left and right steps. Churchill et al. (2015) reported a significant $\sim 4.7\%$ decrease of the $V_{A-P CM MAX}$ during both left and right steps in the curve in comparison to the straight (from ~ 9.83 m \cdot s $^{-1}$ in the straight to ~ 9.37 m \cdot s $^{-1}$ in the curve). However, these authors only investigated the $V_{A-P CM}$ averaged over one single step on each limb. In addition to that, the 3-D kinematic analysis was realized using video cameras and manual digitation and this methodology can yield several errors as previously discussed (section 1.1.i.). Thus, the understanding of how the curve affects the V_{A-P} or $V_{A-P CM}$ remains limited and further experimentations should be led.

Part I - Summary

- ✎ The V_{A-P} over the different sprinting phases strongly predicts the sprinting performance during a 100-m dash. In addition, sprinters with a greater expertise reach their $V_{A-P MAX}$ later on during a 100 m making the deceleration phase shorter.
- ✎ Thus far, only a few experimentations investigated the V_{A-P} in the curve. These studies either averaged the V_{A-P} over large intervals which makes almost impossible any attempt in comparing both sprinting conditions, or analyzed the $V_{A-P CM}$ at 13 and 40 m into the curve, making the understanding of V_{A-P} in the curve rather limited and challenge anyone attempting to draw conclusions.
- ✎ Recently, technologies more broadly used (MIMU-based system, GPS) could help to investigate the V_{A-P} throughout the curve. Therefore, investigating the V_{A-P} from the starting blocks pushing phase onwards during maximal effort sprinting in the curve is required to better understand the V_{A-P} -time kinetics in the curve.

Based on Newton's Second Law of Motion, the change in the V_{A-P} results from the magnitude and the direction of the GRF vector during the stance phase. Thus, investigating the GRF in the curve would provide a deeper understanding of the V_{A-P} -time kinetics.

Part II – Ground Reaction Forces and impulse

The $V_{A-P\ CM}$ -time kinetics -hence, performance- can be examined through Newton's second law of motion:

$$\vec{F} = m \cdot \vec{a} \quad (2)$$

Where \vec{F} corresponds to the net forces acting on the body, m to the body mass and \vec{a} to the body acceleration. The ability to reach higher $V_{A-P\ MAX}$ later during a 100-m dash corresponds to one's aptitude to keep accelerating despite the increasing V_{A-P} and eventually reflects the ability to keep producing F_{A-P} at very high V_{A-P} (Morin et al., 2011). Thus, investigating the GRF in sprint running is mandatory to understand how the change in V_{A-P} occur at the CM.

The CM motion of someone sprinting is determined by three external forces:

- The GRF;
- The BW;
- Air resistance;

A representation of the GRF (F_{TOT} , F_V , F_{A-P} and F_{M-L}) and the acceleration due to gravity (g) (dark blue arrow pointing downwards) are represented in figure 6. Although not represented in this figure 6, the air resistance acts backward.

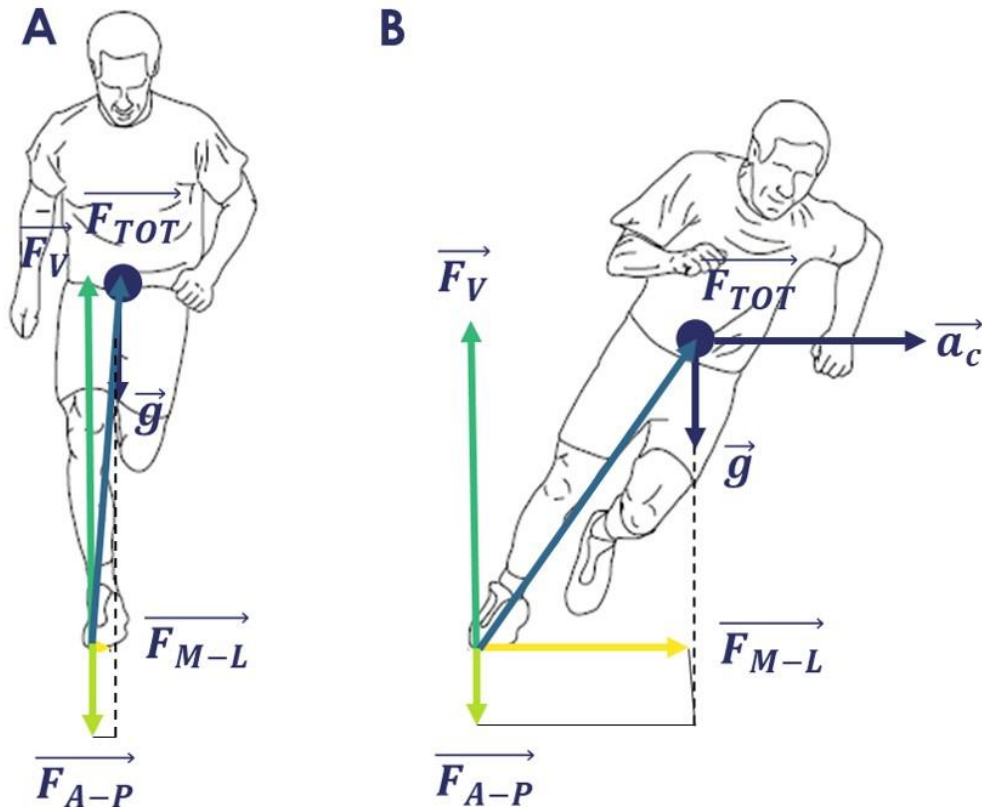


Figure 6. Graphical representation of the ground reaction forces (GRF) a) in the straight and b) in the curve. On each panel the gravitational acceleration (g) is in dark blue and is directed at the centre of mass (dark blue circle), downwards. The GRF components are represented as follow: in blue, the resultant force (F_{TOT}); in green, the vertical component (F_V); in light green, the antero-posterior component (F_{A-P}) and in yellow, the medial-lateral component (F_{M-L}). In the panel B, the centripetal acceleration (a_c) is directed towards the centre of the radius. Finally, the air resistance is not represented but acts backwards. The figure was reproduced from Chang & Kram (2007).

Considering their role for understanding the CM motion, researchers are often seeking to investigate the GRF. Historically, the GRF in running and sprinting were studied within a laboratory using instrumented treadmills (Morin et al., 2010, 2011, 2012; Weyand et al., 2000, 2010) or FP (Fenn, 1930; Kawamori et al., 2013); or directly within *in-field* environment using FP embedded underneath the track surface (Cavagna et al., 1971; Hunter et al., 2005; Morin, Slawinski, et al., 2015; Nagahara et al., 2018b, 2020; Rabita et al., 2015; Samozino et al., 2016).

The norm of the resultant GRF (F_{TOT}) applied to the body at the centre of pressure can be broken down within three orthogonal components and corresponds to the sum of each of the three orthogonal components (see figure 6):

$$F_{TOT} = \sqrt{F_V^2 + F_{A-P}^2 + F_{M-L}^2} \quad (3)$$

Where F_V , F_{A-P} and F_{M-L} correspond to the vertical, the antero-posterior and the medial-lateral components of the F_{TOT} , respectively (see figure 6).

Someone sprinting forward (either in the straight or in the curve) must generate F_V in order to counteract the g directed to his CM. In addition to that, in straight-line sprinting a sprinter must translate his body from the starting blocks to the finish line in the antero-posterior direction, making F_{A-P} a mandatory feature. Thus, F_V and F_{A-P} are the two greatest GRF components of the F_{TOT} in the straight. Additionally, most of the experimentations that investigated the GRF in the straight focussed their analysis on F_V and F_{A-P} . In contrast, in the curve, a sprinter must adopt a curvilinear motion, meaning that F_{M-L} cannot be ignored anymore and must be analyzed. Thus, this sprinting condition diverges from the straight and this **part II** will discuss, to a certain extent how the straight and the curve diverge from a GRF aspect.

1. The ground reaction forces and impulses from the starting blocks to the maximal antero-posterior power (from ~0 m to ~4 m)

1. The ground reaction forces and impulses during the starting blocks pushing phase

i. The resultant force & impulse in the straight

During the starting blocks phase, in the “set” position, the sprinter has to maintain an unstable position. For that sake, the sprinter exerts force onto the ground through the hands and the feet. The two starting blocks plates are usually positioned such that the “preferred” leg is on the front block. An example of the GRF during the starting blocks pushing phase is presented in the figure 7. The first peak on the F_{TOT} , the F_V the and F_{A-P} is produced mainly by the rear leg while the second peak corresponds to the front leg's push-off which approximately lasts twice longer (Otsuka et al., 2014; Slawinski, Bonnefoy Mazure, Levêque, et al., 2010).

Otsuka et al. (2014) compared the 3D GRF of the rear and the front legs during the starting blocks pushing phase between well-trained (100-m PBs of 10.87 ± 0.41 s), trained (100-m PBs of 11.31 ± 0.42 s) and non-trained (no 100-m PBs history) athletes. These authors found that the well-trained athletes produced respectively ~17% and ~11% greater mean F_{TOT} on the rear and the front legs in comparison to the non-trained athletes.

A few years later, Bezodis et al. (2019) found that the ability to produce a large F_{TOT} on the rear block was the best performance predictor during the starting blocks pushing-phase, followed by the ability to produce a large F_{TOT} on the front block. Consequently, overall, the ability to produce larger F_{TOT} on the blocks appears of great importance in order to improve the starting blocks performance.

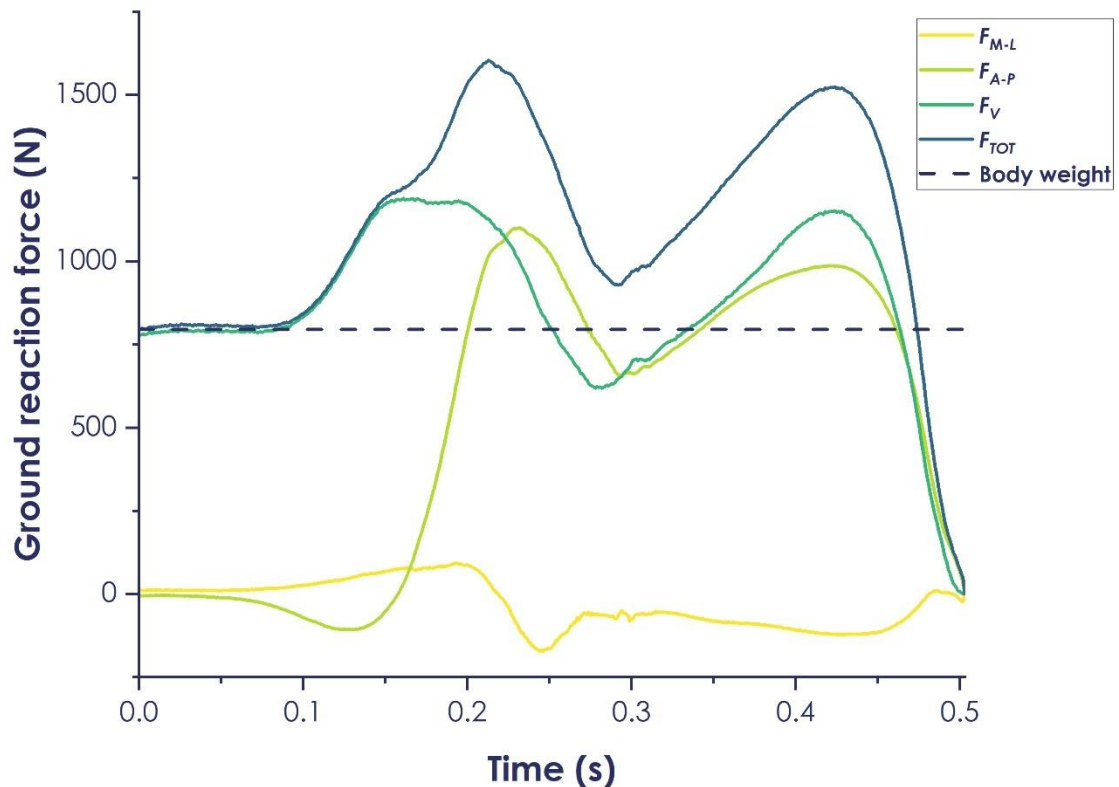


Figure 7. Example of the resultant force (F_{TOT}) and its 3 orthogonal components during the starting blocks pushing phase. F_{M-L} : medial-lateral force; F_{A-P} : antero-posterior force and F_V : vertical force.

ii. The resultant force & impulse in the curve

In the curve, no experimentation investigated the GRF over the starting blocks pushing phase. The 200- and 400-m races differ from the 60- and 100-m dash as the starting blocks are positioned in the curve. However, among coaches and sprinters, it is well admitted that athletes should position their starting blocks on the outer part of their respective lane. In addition to that, the starting blocks should be pointing out towards a point, tangent to the inner part of their lane, so the starting blocks push-off phase and the initial steps that follow are roughly in straight-line.

This was visually confirmed with qualitative video analysis by Judson et al. (2020). However, these authors questioned this strategy and stated that “sprinting with the aim of maintaining a straight path during the transition phase may not be an effective strategy” (Judson, Churchill, Barnes, Stone, Brookes, et al., 2020). Yet, this assumption remains to be investigated as it goes against the common statement and strategies adopted during 200 and 400 m races. Overall, in the curve, as the sprinter is expected to sprint in a linear fashion for the first steps, we hypothesize the mean F_{M-L} to be low, yet, this remains to be evaluated.

iii. The vertical force & impulse in the straight

Regarding the F_V , well-trained and trained sprinters produced a similar mean F_V over the starting blocks pushing phase (Otsuka et al., 2014). In addition to that, no differences were reported at the front and rear legs' level between groups. On the other hand, the front leg produced a mean F_V ~33% greater than the rear leg (Otsuka et al., 2014), meaning that a greater CM rising in the vertical direction is explained by the front leg in comparison to the rear leg. As the front leg pushing-time duration was ~2 times longer than that of the rear leg, the front leg vertical impulse (IMP_V) was ~3 times greater than that of the rear leg. Finally, despite a significantly longer pushing-time for the trained participants and a similar mean F_V , no differences were found for the IMP_V between the well-trained and trained groups (Otsuka et al., 2014).

iv. The antero-posterior force & impulse in the straight

Rabita et al. (2015) showed that the F_{A-P} is at its maximum (Otsuka et al., 2014; Rabita et al., 2015) in this phase of the sprint. Additionally, the elite sprinters (100-m PBs ranging between 9.95 and 10.29 s) produced a greater mean F_{A-P} when the F_{A-P} was averaged over the starting blocks pushing phase than their sub-elite (100-m PBs ranging between 10.40 and 10.60 s) counterparts (Rabita et al., 2015). These authors also reported that producing a large magnitude of mean F_{A-P} over the starting blocks strongly predicted the starting blocks clearing V_{A-P} ($r = 0.873$), the measured 40-m $V_{A-P MAX}$ ($r = 0.836$) and the 40-m performance ($r = 0.850$) among elite and sub-elite sprinters (Rabita et al., 2015). Thus, those findings attest the necessity to produce a large mean F_{A-P} over the starting blocks pushing phase.

Rabita et al.'s (2015) findings are in line with those of Otsuka et al.'s (2014) as the well-trained sprinters produced a greater mean F_{A-P} during the starting blocks than the trained group (9.72 ± 0.36 vs 8.41 ± 0.49 N · kg⁻¹, respectively). On the other hand, the trained group had longer pushing time (which is detrimental for performance),

meaning that the mean antero-posterior impulse (IMP_{A-P}) did not differ between the well-trained and the trained groups (Otsuka et al., 2014).

v. The medial-lateral force & impulse in the straight

Only one experimentation reported the F_{M-L} during the starting blocks pushing phase (Otsuka et al., 2014). These authors showed that the mean F_{M-L} in this phase of the sprint could be neglected and that no differences were reported between well-trained and trained groups of sprinters (-0.27 ± 0.49 vs -0.36 ± 0.20 N · kg⁻¹, respectively) which might explain why most studies did not report the mean F_{M-L} .

2. The ground reaction forces from the starting blocks exit on to the maximal antero-posterior power

i. The resultant force & impulse in the straight

In the literature, many studies investigated the GRF from the first stance after the starting blocks exit on to the $P_{A-P MAX}$. During this phase, the mean F_{TOT} increases in a linear fashion with the V_{A-P} (Rabita et al., 2015). This was mainly associated with an increase in the mean F_V and despite a linear concomitant decrease in the mean F_{A-P} (Nagahara et al., 2020; Rabita et al., 2015).

ii. The resultant force & impulse in the curve

Thus far, no experimentation investigated the GRF in the curve from the starting blocks exit on to $P_{A-P MAX}$. However, as the initial steps that follow the starting blocks exit are expected to be run in the straight, it is likely that the no differences in the mean F_{TOT} , F_V , F_{A-P} and F_{M-L} between the straight and the curve would be observed.

iii. The vertical force & impulse in the straight

Among the three orthogonal F_{TOT} components, the F_V is the greatest in magnitude during both treadmill (Morin et al., 2011) and overground (Nagahara et al., 2020; Rabita et al., 2015) sprinting since the CM undergoes the g in the vertical direction. Thus, the F_V contains the BW and must be subtracted to the F_V to have the "effective F_V and IMP_V " (see the **general methodology** for more details). In order to make the sprinting motion possible and raise the CM, a sprinter must generate a F_V magnitude larger than the BW. In sprinting, a typical stance starts with a downward displacement of the CM (F_V lower than BW), followed by an upward displacement of the CM (F_V greater than BW). If the averaged F_V over a stance exceeds BW, this will result in an elevation of the CM during the stance, if not, the CM will lower.

During the $P_{A-P\ MAX}$ phase, the mean F_V over a stance increases linearly from $\sim 10\ \text{N} \cdot \text{kg}^{-1}$ at the first stance to $\sim 15\ \text{N} \cdot \text{kg}^{-1}$ at $P_{A-P\ MAX}$ (Nagahara et al., 2018b). Otsuka et al. (2014) reported significant differences between the non-trained and the trained groups in the mean F_V applied at the first stance (13.59 ± 0.82 vs $12.23 \pm 1.03\ \text{N} \cdot \text{kg}^{-1}$, respectively; $p < 0.05$). However, these differences between both groups disappeared at the second stance (13.22 ± 1.15 vs $12.94 \pm 0.79\ \text{N} \cdot \text{kg}^{-1}$, respectively; $p > 0.05$). Thus, it is not clear whether applying greater mean F_V over a stance from the starting blocks exit on to $P_{A-P\ MAX}$ necessarily demonstrates better sprinting abilities during this phase.

iv. The antero-posterior force & impulse in the straight

The F_{A-P} determines the CM motion in the antero-posterior direction. In sprinting, after the starting blocks exit, a stance is composed of a braking phase (F_{A-P-} i.e., backward orientation of the F_{A-P} vector) at the beginning of the stance, followed by a propulsive phase (F_{A-P+} i.e., forward orientation of the F_{A-P} vector). Averaged over the stance, the mean F_{A-P} corresponds to the sum of the F_{A-P-} and the F_{A-P+} . Overall, when the air resistance is retrieved, if the mean F_{A-P} over a stance is positive, the sprinter is accelerating, otherwise, the sprinter decelerates. From the starting blocks exit on to the $P_{A-P\ MAX}$, the mean F_{A-P} decreases due to a concomitant decrease in F_{A-P+} and an increase in F_{A-P-} (Nagahara et al., 2018b).

In addition to that, the braking phase duration increases while the propulsive phase duration decreases (Nagahara et al., 2020). This eventually results in a decreased IMP_{A-P} due to an increase in the IMP_{A-P-} concomitantly with a decrease in IMP_{A-P+} (Nagahara et al., 2018b).

v. The medial-lateral force & impulse in the straight

The magnitude of the F_{M-L} applied onto the ground determines how the CM will move medially or laterally. Usually, during the left and right stances, the F_{M-L} are opposite in direction and have approximately the same magnitude so that they cancel up and the athlete can sprint in a more or less linear fashion (Nagahara et al., 2017). Nonetheless, the F_{M-L} are usually neglected or not investigated at all in straight-line walking (Cavagna et al., 1963), running (Cavanagh & Lafortune, 1980; Kyröläinen et al., 1999) or sprinting (Cavagna, 1975; Matsuo et al., 2019; Rabita et al., 2015). Nagahara et al. (2017) were amongst the rare studies that investigated the medial-lateral impulses (IMP_{M-L}) from the first stance on to the $P_{A-P\ MAX}$. These authors showed that the IMP_{M-L} were limited during this phase ($0.29 \pm 0.11\ \text{m} \cdot \text{s}^{-1}$), meaning that the sprinters leave the ground at take-off (TO) with a slight IMP_{M-L} and sprint in a more or less linear fashion.

2. The ground reaction forces from the maximal antero-posterior power to the maximal antero-posterior velocity (from ~4 m to ~40 m)

1. The resultant force & impulse in the straight

In overground sprinting, Rabita et al. (2015) reported a linear increase in the mean F_{TOT} throughout the transition phase among both elite and sub-elite sprinters. However, the mean F_{TOT} over a stance expressed relative to body mass was not correlated neither with the sprinting expertise nor the sprinting performance (Rabita et al., 2015). Therefore, the best sprinters were actually not the one who were able to produce the largest mean F_{TOT} during the entire transition phase.

2. The resultant force & impulse in the curve

No experimentation investigated the mean F_{TOT} in the curve during the transition phase.

3. The vertical force & impulse in the straight

In treadmill sprinting, when the V_{A-P} increases between different steady-states V_{A-P} , the mean F_V increases concomitantly in a linear way (Weyand et al., 2000, 2010). Similar findings were reported in overground sprinting whereby the mean F_V increased from $P_{A-P MAX}$ and until $V_{A-P MAX}$ in the straight (Nagahara et al., 2018b, 2019).

The figure 8 presents the F_V -time curve of the 8th, 12th, 16th and 20th stances. In this example, we can visually see that the peak F_V increases through this phase, which is in line with Nagahara et al.'s (2018) findings, yet this peak F_V is reached approximately at the same time through the transition phase. On the other hand, despite the decreasing stance time after the $P_{A-P MAX}$, the effective mean IMP_V keeps increasing until $V_{A-P MAX}$.

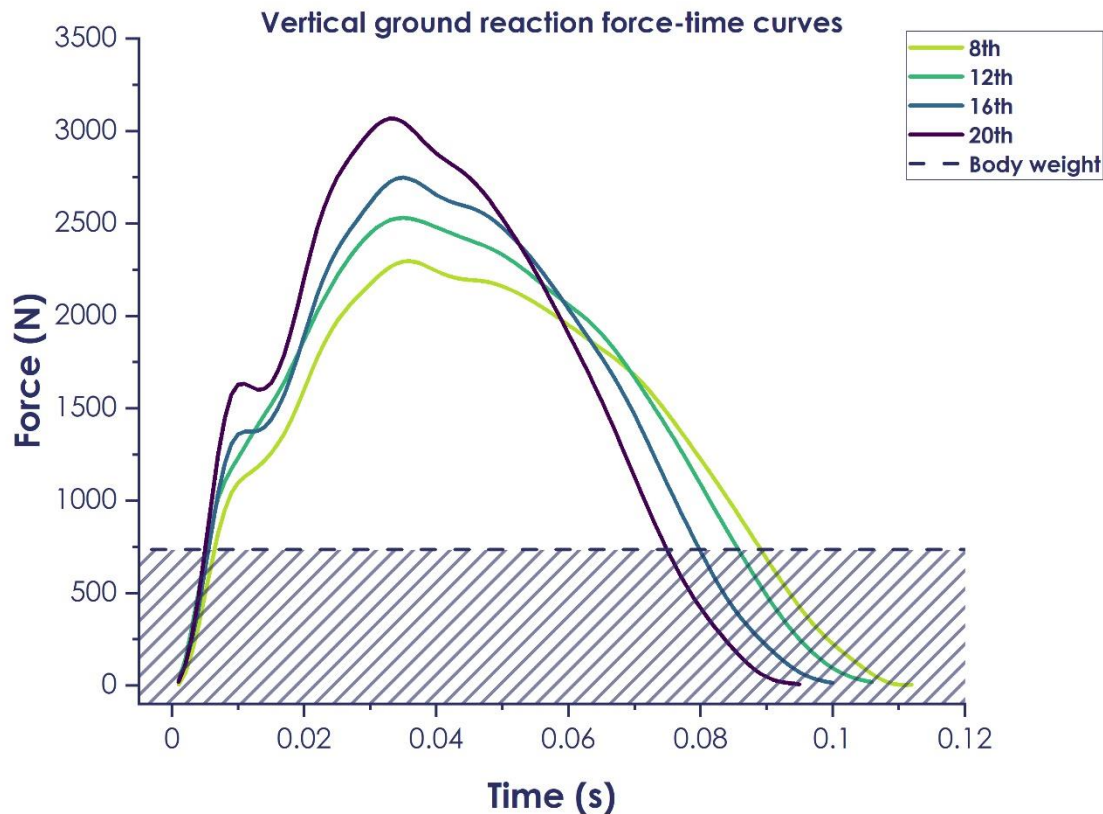


Figure 8. Graphical representation of a participant's vertical force-time curves over different stances (8th, 12th, 16th and 20th stances after the starting blocks exit) during the transition phase of a sprint with maximal effort. The horizontal dashed line corresponds to the participant's body weight. The effective vertical impulse corresponds to the area under the curve above this horizontal dashed line.

During the transition phase of overground sprinting, no evidence regarding the association of F_V and performance were found (Rabita et al., 2015). Therefore, it seems that although mandatory for the sprinting motion in order to overcome the negative vertical acceleration due to the g , the sprinting performance over the transition phase does not rely on the sprinter's ability to produce large magnitude of F_V and this parameter is not itself a performance determinant in this phase of the sprint.

4. The vertical force & impulse in the curve

No experimentation investigated the F_V in the curve from the $P_{A-P MAX}$ on to $V_{A-P MAX}$, phase. However, Greene (1985) followed by Usherwood and Wilson (2006) postulated that F_V would be altered in the curve. According to the authors' hypotheses, the peak F_{TOT} in the curve would remain similar to that of the straight. However, due to the additional requirement to produce F_{M-L} in the curve in order to maintain a curvilinear motion, the F_V would inevitably decrease (Greene, 1985; Usherwood & Wilson, 2006).

5. The antero-posterior force & impulse in the straight

In maximal effort sprinting, we saw that the mean F_{A-P} is maximum during the starting blocks pushing phase and started to decrease from the first stance on to the $P_{A-P MAX}$ (Otsuka et al., 2014; Rabita et al., 2015). For the rest of the transition phase, the F_{A-P} keeps decreasing linearly with the increasing V_{A-P} and eventually corresponds to the F-v relationship that was described in many multi-joints activities (Giroux et al., 2014; Rahmani et al., 2001; Samozino et al., 2016; Vandewalle et al., 1987). Thus, at the end of the transition phase, (*i.e.*, when the athlete's antero-posterior acceleration is almost null) the mean F_{A-P} is almost null.

When the V_{A-P} increased successively between different steady-states V_{A-P} , the mean F_{A-P} increased concomitantly (Hamner & Delp, 2013; Nilsson & Thorstensson, 1989), thus strengthening the assumption that the sprinting demand should not be investigated with successively increased steady-states V_{A-P} but rather with maximal effort accelerated sprinting.

In overground sprinting, after the $P_{A-P MAX}$ has been reached, the decrease in this mean F_{A-P} results from an increase in the mean F_{A-P-} , from $\sim -3 \text{ N} \cdot \text{kg}^{-1}$ to $\sim -4 \text{ N} \cdot \text{kg}^{-1}$ while the F_{A-P+} plateaus concomitantly (see figure 9 and Nagahara et al., 2018), meaning that more braking occurs at greater V_{A-P} (Morin, Slawinski, et al., 2015). Interestingly, the time at which the peak F_{A-P-} occurs does not vary (see figure 9).

Similar to what was observed between the starting blocks exit on to the $P_{A-P MAX}$ (Nagahara et al., 2020), we can see on the figure 9 that the braking phase duration increases while the propulsive phase duration decreases. This eventually results in a decreased IMP_{A-P} due to an increase in the IMP_{A-P-} concomitantly with a decrease in IMP_{A-P+} (Morin et al., 2015; Nagahara et al., 2018; see figure 10). The IMP_{A-P-} undergoes a threefold increase (from $-0.06 \pm 0.02 \text{ m} \cdot \text{s}^{-1}$ to $-0.18 \pm 0.03 \text{ m} \cdot \text{s}^{-1}$) that results from both the increase in the mean F_{A-P-} and in the braking time (Nagahara et al., 2017 and see figure 10). In contrast the twofold decrease of the IMP_{A-P+} from $0.49 \pm$

$0.03 \text{ m} \cdot \text{s}^{-1}$ to $0.26 \pm 0.04 \text{ m} \cdot \text{s}^{-1}$ results from a decrease in the propulsion time as the mean F_{A-P+} plateaus at $P_{A-P \text{ MAX}}$ (Nagahara et al., 2020).

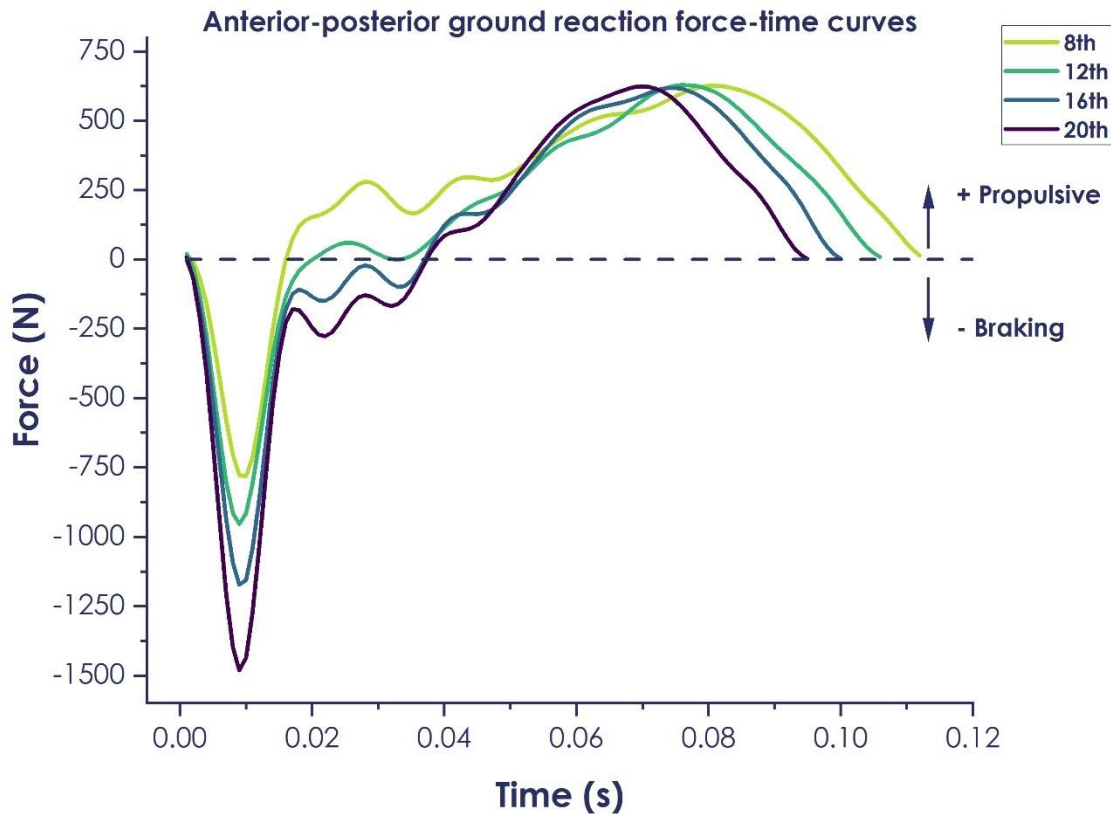


Figure 9. Graphical representation of a participant's antero-posterior force (F_{A-P})-time curves over different stances (8th, 12th, 16th and 20th stances after the starting blocks exit) during the transition phase of a sprint with maximal effort. The data below the horizontal dashed line correspond to negative values of the F_{A-P} (i.e., the braking phase). On the other hand, the data above the dashed line correspond to positive values of the F_{A-P} (i.e., the propulsive phase).

During the past decade, several experimentations reported the major role of the mean F_{A-P} generated over a stance in maximal effort sprinting either in treadmill (Morin et al., 2010; Morin & Sève, 2011) and overground (Mero, 1988; Morin et al., 2011, 2012; Rabita et al., 2015) straight-line sprinting.

In overground sprinting, elite sprinters produced greater mean F_{A-P} than the sub-elites when mean F_{A-P} was averaged over the transition phase (Rabita et al., 2015). In addition to that, the authors found that a sprinter's ability to produce large magnitude of mean F_{A-P} over 40 m was strongly associated with the 40-m performance ($r = 0.816$) and 40-m $V_{A-P \text{ MAX}}$ ($r = 0.904$) (Rabita et al., 2015).

Similarly, both the IMP_{A-P} and the IMP_{A-P+} were significantly correlated with sprinting performance at 8 m (Kawamori et al., 2013), 16 m (Hunter et al., 2005), when averaged over the 0-20 m distance (Morin et al., 2015) or over 40 m (Morin et al., 2015). As these experimentations gathered heterogeneous populations with both sprinters and non-sprinters and as the IMP_{A-P} were computed at different instants of the transition phase, these studies confirm the high relevance of producing the largest IMP_{A-P} and IMP_{A-P+} from the $P_{A-P MAX}$ on to $V_{A-P MAX}$. Since increased stance times would in turn result in decreased SF, it is likely that the greater IMP_{A-P} and IMP_{A-P+} with better sprinting expertise would result from increased F_{A-P} applied over the corresponding time-period rather than the same F_{A-P} production applied over a longer time.

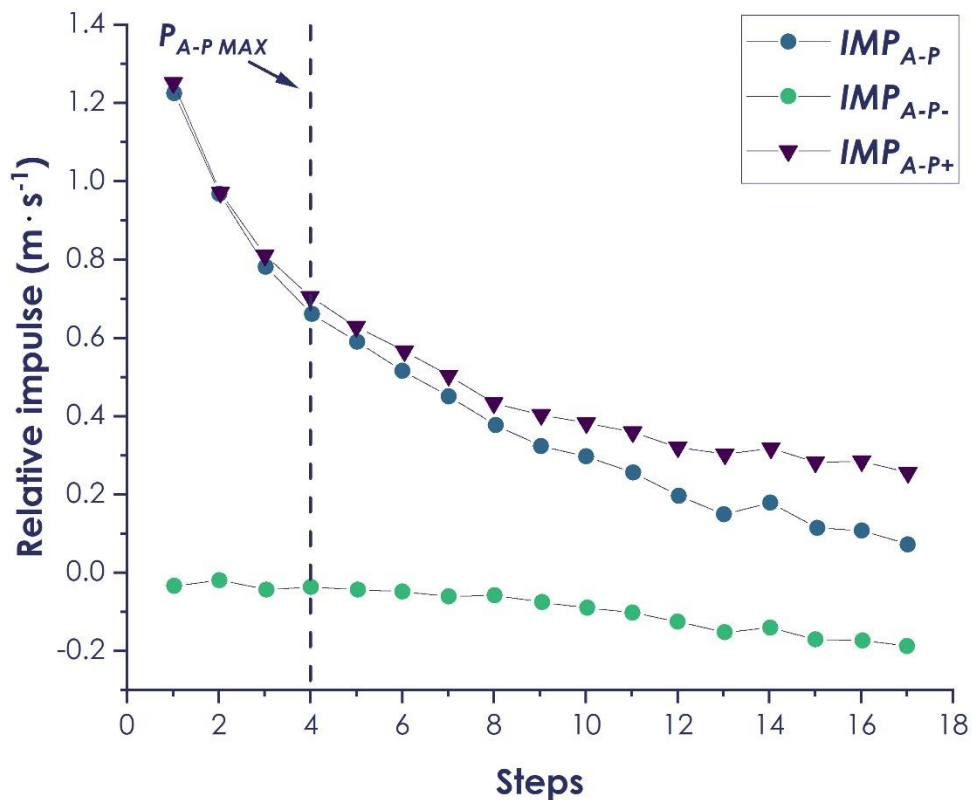


Figure 10. Net (filled circles), propulsive (triangles) and braking (empty circles) relative antero-posterior impulses for the 17 stances analyzed over the 40-m sprints. Starting blocks push-off data are not presented. Figure reproduced from Morin et al. (2015).

6. The antero-posterior force & impulse in the curve

The understanding of whether the curve impacts the F_{A-P} is limited as a single experimentation compared the F_{A-P} between the straight and the curve during the transition phase of the sprint at 13 m on a reconstructed lane 1 (Judson et al., 2019).

However, rather than investigating the mean F_{A-P} or IMP_{A-P} over a stance, the authors performed Statistical Parametrical Mapping (SPM) in order to compare the point-by-point “force production across the entire stance phase between conditions” (Judson et al., 2019). Using this statistical approach, the authors reported a main effect for condition between 37 and 44% of the stance duration, with the F_{A-P} being lower in the curve than in the straight ($p < 0.001$). However, not only the authors investigated a single stance during the transition phase which limits the understanding of the whole phase, but also the statistical approach utilized cannot be used to compare the mean F_{A-P} between both sprinting conditions. Thus, overall, this study lacks details and further experimentations should be led in order to better understand whether the mean F_{A-P} is modified in the curve; and whether both the left and right limbs are impacted in the curve.

7. The medial-lateral force & impulse in the straight

After the $P_{A-P MAX}$, Nagahara et al. (2017) reported a decrease in the net IMP_{M-L} that resulted from both an increase in the medial-lateral IMP_{M-L} (IMP_{M-L-}) and a decrease in the medial IMP_{M-L} (IMP_{M-L+}) (see figure 11). The net IMP_{M-L} progressed from $0.17 \pm 0.10 \text{ m} \cdot \text{s}^{-1}$ when averaged over the 5th to 8th stance, to $0.00 \pm 0.08 \text{ m} \cdot \text{s}^{-1}$ when averaged over the 21st and 22nd stances (Nagahara et al., 2017). Thus, at the end of the transition phase in the straight, while in an upright posture, sprinters have a null change in the V_{M-L} through the stance. This means that the medial-lateral motion decreases through the transition phase.

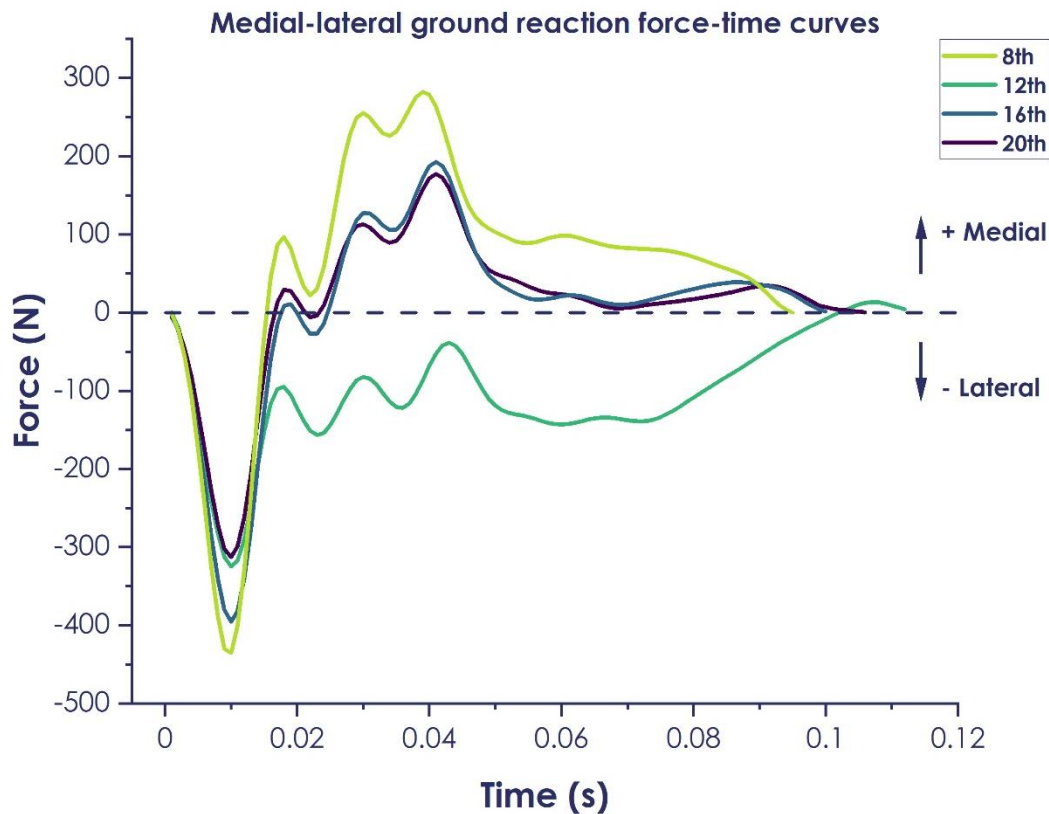


Figure 11. Graphical representation of the medial-lateral force curves during different stances (2nd, 8th, 12th, 16th and 20th stances after the starting blocks exit) of a 40-m sprint with maximal effort.

8. The medial-lateral force & impulse in the curve

In their experimentation, Judson et al. (2019) reported a significant main effect for condition between 3 to 96% of the stance duration, whereby the F_{M-L} was greater in the curve than in the straight in the mean period (Judson et al., 2019). Thus, although it is unclear whether the trajectory is linear over the initial stances, Judson et al. (2019) showed that their participants were following a curvilinear motion at 13 m after the starting blocks.

Unfortunately, these authors did not provide the magnitude of the F_{M-L} neither in the straight nor in the curve. In addition to that, a single stance was analyzed at 13 m after the starting blocks. In the straight we saw that IMP_{M-L} decreases after the $P_{A-P MAX}$. In the curve, it might be opposite, whereby the IMP_{M-L} increases with the increasing V_{A-P} in order to cope for the additional F_C requirement. However, further experimentations should be conducted to confirm this hypothesis.

3. The ground reaction forces and impulses at the maximal antero-posterior velocity (from ~40 m to ~70 m)

1. The resultant force & impulse in the straight

Mero & Komi (1986) compared the mean F_{TOT} during the braking and propulsive phases of the stance in overground sprinting at $V_{A-P MAX}$ between two groups of male sprinters with different expertise. The male sprinters with the greatest sprinting expertise were able to produce a significantly greater mean F_{TOT} during both the braking and propulsive phases of the stance than their less experienced counterparts.

In addition to that, the authors reported significant correlations between the $V_{A-P MAX}$ and the mean F_{TOT} during the braking ($r = 0.65$, $p < 0.01$) and propulsive phases ($r = 0.84$, $p < 0.001$). Thus, these authors assumed that the sprinters able to produce the largest F_{TOT} during both the braking and the propulsive phases would, to some extent, reach higher $V_{A-P MAX}$.

2. The resultant force & impulse in the curve

Chang & Kram (2007) compared the GRF of five recreational men obtained in the straight at $V_{A-P MAX}$ to the GRF at radii of 1, 2, 3, 4 and 6 m. At these extremely tight radii, the authors did not report any significant difference in the right leg's peak F_{TOT} between the straight and the curve. On the other hand, the left leg peak F_{TOT} was reduced in the curve (Chang & Kram, 2007) which refutes the "constant limb force" stipulating that the peak F_{TOT} in the curve would remain similar to the straight (Usherwood & Wilson, 2006). However, Chang & Kram's (2007) study was conducted at radii of curvature far from representing the track sprinting conditions. In addition to that, the statistical power was small and this could have hidden some statistical differences between the two sprinting conditions.

A decade later, Churchill et al. (2016) confirmed Chang & Kram's (2007) findings on a reconstructed lane 2 ($r = 37.72$ m) using two FP positioned 40 m after the starting blocks. The seven male experienced sprinters involved in this experimentation performed two 60-m sprints in the straight and in the curve. Churchill et al. (2016) did not report modifications on the right limb peak or the mean F_{TOT} , which confirms Chang & Kram's (2007) findings. For the left limb, on the other hand, the peak F_{TOT} decreased by ~6% in the curve in comparison to the straight which rejects the "constant limb hypothesis" for the left limb in the curve. However, the mean F_{TOT} remained similar to the straight; consequently, due to the additional requirement to

generate the F_C , alterations would likely be observed on either or both the mean F_V and the mean F_{A-P} .

3. The vertical force & impulse in the straight

In overground sprinting, at $V_{A-P MAX}$, the mean F_V over a stance reaches its greatest magnitude (Nagahara et al., 2018a; Nagahara & Girard, 2021). On a treadmill, the IMP_V decreases at $V_{A-P MAX}$ due to a larger decrease in stance times in comparison to the concomitant increase in F_V applied onto the ground (Weyand et al., 2000). In overground sprinting, on the other hand, the IMP_V keeps increasing at $V_{A-P MAX}$ (Nagahara et al., 2018b, 2020), further indicating that sprinting analyses should not be conducted on a treadmill as the sprinting demands vary with overground sprinting.

4. The vertical force & impulse in the curve

On lane 2 in the curve, Churchill et al. (2016) reported a ~5% decrease on the left leg mean F_V . As the mean F_{TOT} did not change concomitantly, this reduction in the mean F_V likely results from the necessity to apply the F_C in the curve. In contrast, no modifications were found for the right limb's F_V between the two sprinting conditions. Thus, overall, only the left limb mean F_V was affected at $V_{A-P MAX}$ in the curve at typical radii of track events (Churchill et al., 2016).

Since the GRF were collected at $V_{A-P MAX}$ in this experimentation, it is expected that sprinting performance would be related -to some extent-, to the sprinter's ability to exert large mean F_V onto the ground (Nagahara et al., 2018a; Weyand et al., 2000). Considering that the mean F_V was reduced on the left leg in the curve, this further raises the question of whether the mean F_V remains related to the performance at $V_{A-P MAX}$ in the curve. If so, this suggests that the 2.5% reduction in the left leg's sprinting V_{A-P} (Churchill et al., 2016) could be -at least partially- related to the reduced mean F_V .

5. The antero-posterior force & impulse in the straight

The distance at which a sprinter reaches his $V_{A-P MAX}$ partially depends on his expertise as discussed in **part I** and his ability to produce F_{A-P} despite the increase in V_{A-P} . At $V_{A-P MAX}$, the mean F_{A-P} and the IMP_{A-P} become almost null, just slightly positive to overcome air resistance (Nagahara & Girard, 2021) and the athlete is not accelerating in the antero-posterior direction anymore.

As these metrics are close to zero during the $V_{A-P MAX}$ phase, the mean F_{A-P} and the IMP_{A-P} have not been thoroughly examined in the literature. For instance, Weyand et

al. (2000) postulated that the F_{A-P} produced at $V_{A-P MAX}$ could not explain the differences in the $V_{A-P MAX}$ reached and in turn “were not included in the analysis”. Indeed, it is likely that the authors postulated that other parameters would be of greater importance during this phase.

6. The antero-posterior force & impulse in the curve

As Churchill et al.'s (2016) study was conducted at $V_{A-P MAX}$, the mean F_{A-P} was also expected to be close to zero. Unfortunately, the authors did not report the mean F_{A-P} . Yet, it is likely that, as the mean F_{TOT} was unchanged on the left limb and due to the additional requirement of F_{M-L} in order to maintain a curvilinear motion, the mean F_{A-P} would be reduced in the curve, similarly to the mean F_V .

7. The medial-lateral force & impulse in the straight

Similar to the transition phase, the F_{M-L} at $V_{A-P MAX}$ has not received a major attention in straight-line sprinting in the existing literature. The work of Nagahara et al. (2017) suggests that the F_{M-L} is rather small during this phase.

8. The medial-lateral force & impulse in the curve

At radii of 1, 2, 3, 4 and 6 m, both the peak and mean F_{M-L} were systematically greater in the curve than those obtained in the straight (Chang & Kram, 2007). On the other hand, the authors did not report any radius effect on the peak F_{M-L} suggesting that at extremely tight radii, the F_{M-L} magnitude is not impacted by the radius of curvature. As the stance duration was longer in the curve, the IMP_{M-L} was also greater in the curve in comparison to the straight.

At 40 m on lane 2, at the sprinter's $V_{A-P MAX}$ and with a F_C expected to be large, Churchill et al. (2016) showed that the peak F_{M-L} increased by ~161% on the left limb and ~110% on the right limb. Those findings contrast with those previously reported by Chang & Kram (2007) at radii <6 m stipulating that the right leg's peak F_{M-L} exceeded the left peak F_{M-L} .

In addition to that, Churchill et al. (2016) reported an elevenfold increase on the left leg IMP_{M-L} while the right IMP_{M-L} underwent a fourfold increase in comparison to the straight (Churchill et al., 2016). These extremely large increases in the left and right IMP_{M-L} were mainly explained by a large increase in the mean F_{M-L} (even though this parameter was not reported). Indeed, the left leg's ST only underwent a significant ~9% increase while the right leg's ST did not change. Thus, in the curve, both the mean

F_{M-L} and IMP_{M-L} over a stance largely increase and likely explain the unchanged F_{TOT} despite the decreased F_V .

In addition to that, the left leg's F_{M-L} and IMP_{M-L} were ~60% greater than the right F_{M-L} and IMP_{M-L} . Consequently, the sprinters' CM turned 1.6% more during the left stance than during the right stance (Churchill et al., 2015, 2016).

Part II - Summary

- In the straight, the GRF were mainly approached throughout the F_V and the F_{A-P} components and both limbs are assumed to perform symmetrically. The available literature well emphasized the importance to produce large F_{A-P} from the starting blocks pushing phase on to the end of the transition phase to improve the sprinting performance in the straight.
- In the curve, the peak F_{M-L} and the IMP_{M-L} largely increase in comparison to the straight. In turn, the mean F_V and so does the mean F_{TOT} in the curve. However, to date, no experimentation clearly investigated the mean F_{A-P} in the curve and whether this metric changes in comparison to the straight remains to be studied.
- Furthermore, the only analysis that investigated these metrics focussed on two steps at $V_{A-P MAX}$. Since the F_C increases with the increasing V_{A-P} , it is likely that the sprinting V_{A-P} directly affects the GRF in the curve. Thus, it seems mandatory to carry out a comprehensive analysis of the GRF in the curve, from the starting blocks on to the $V_{A-P MAX}$, at the same radius of curvature in order to better understand how the curve alters the GRF in comparison to the straight and how the increase in V_{A-P} within the curve modifies the GRF.

With the increasing V_{A-P} , the GRF change. These modifications in the sprinting GRF are eventually the consequences of modifications in the sprinting technique from the starting blocks on to the $V_{A-P MAX}$ with the sprinter being progressively in a more upright posture. The sprinting technique can be described with a kinematic analysis of the sprinter. In the curve, the mean F_{M-L} largely increases together with a decrease in the mean F_V to maintain a curvilinear motion. Changes in the sprinting technique are likely to be observed such as the athlete lean into the curve. Thus, it is of interest to investigate which modifications in the sprinting technique lead to these changes in the GRF.

Part III – Sprinting kinematics

1. The sprinting kinematics from the starting blocks to the maximal antero-posterior power (from ~0 m to ~4 m)

1. The sprinting kinematics during the starting blocks pushing phase

i. The spatiotemporal parameters & joint kinematics in the straight

In the starting blocks, the spatiotemporal analysis can be considered as the pushing phase duration and was discussed in **part I**. The starting blocks pushing phase is a key phase of the sprint which requires specific technical abilities of the whole body. As previously discussed, the starting blocks setup (*i.e.*, the antero-posterior distance between the front and rear blocks and the plates inclination) strongly influences the starting blocks V_H exit, but also the joints' kinematics and thus the position in which the sprinter produces force.

In the “set” position, the sprinters raised their CM and adopted an unstable position that has to be maintained. Slawinski et al. (2010) showed that the elite sprinters were able to sustain a more unstable position than their less experienced counterparts by increasing their rear knee angle, positioning their CM closer to the starting-line in the antero-posterior direction and with the shoulders above the hips (see figure 12).

The figure 12 presents examples of the lower limb joint kinematics in the “set” position retrieved from the literature. In the “set” position, both the rear and front ankles have a similar dorsiflexion angle (Debaere, Delecluse, et al., 2013; Mero & Komi, 1990). However, the other lower limb joint show more discrepancies between the rear and front limbs. As such, both the front knee and hip are more flexed than the respective rear joints (see figure 12).

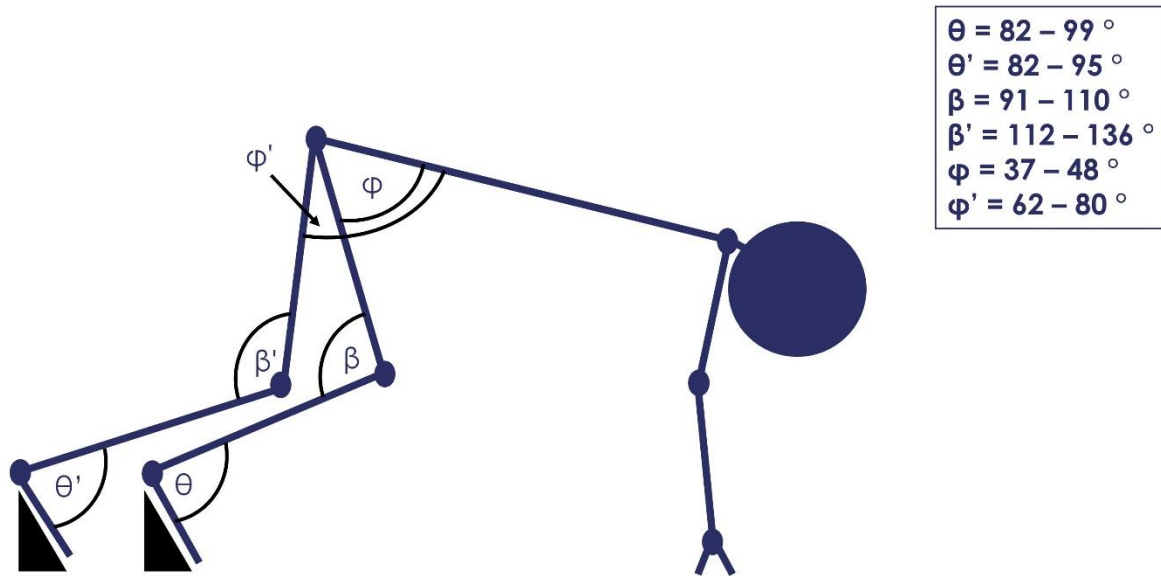


Figure 12. Body schematic denoting joint and segment angles measured in the set position retrieved from the literature (N. E. Bezodis et al., 2015; Ciacci et al., 2016; Debaere, Delecluse, et al., 2013; Mero & Komi, 1990; Slawinski, Bonnefoy Mazure, Levêque, et al., 2010).

After the starting-gun fires, the hips and knees start to extend and greater extension velocities are observed at the front joints in comparison to the rear joints (see table 1). The rear hip reaches its peak extension velocity ($\sim 200 \text{ }^\circ \cdot \text{s}^{-1}$) around the middle of the rear block push-off, approximately when the hands leave the ground (2010). Afterwards, the rear hip extension velocity decreases and the rear hip starts to flex slightly before rear block exit. In contrast, the front hip reaches its peak extension velocity at around 80% of the starting blocks pushing phase ($\sim 400 \text{ }^\circ \cdot \text{s}^{-1}$) and is extending through the entire pushing-phase (Slawinski, Bonnefoy Mazure, Ontanon, et al., 2010).

Table 1. Peak hip and knee extension and ankle plantarflexion velocities (expressed in $^\circ \cdot \text{s}^{-1}$) reported from the first to the fourth stance. Data retrieved from Bezodis et al. (2010); Brazil et al. (2016); Charalambous et al. (2012).

	Bezodis et al. 2014	Brazil et al. 2016	Charalambous et al. 2012
Hip ($^\circ \cdot \text{s}^{-1}$)	~ 200	~ 150	~ 200
Knee ($^\circ \cdot \text{s}^{-1}$)	~ 200	~ 150	~ 150
Ankle ($^\circ \cdot \text{s}^{-1}$)	~ 400	~ 300	~ 300

The rear knee reaches its peak extension velocity at $\sim 35\%$ of the rear block pushing phase ($\sim 100 \text{ }^\circ \cdot \text{s}^{-1}$) and keeps extending afterwards until $\sim 60\text{-}70\%$ of the rear block pushing phase then flexes until the rear block exit. In contrast, the front knee is

exclusively extending and reaches its peak extension velocity at approximately 80-90% of the front leg push-off ($\sim 700 \text{ }^\circ \cdot \text{s}^{-1}$).

At the ankle joint, a brief dorsiflexion at both ankles is observed at the beginning of the starting blocks pushing phase, directly followed by a plantarflexion, showing a stretch-shortening cycle (Brazil et al., 2016; Debaere, Delecluse, et al., 2013; Slawinski, Bonnefoy Mazure, Ontanon, et al., 2010). The rear ankle reaches its peak plantarflexion velocity $\sim 2/3^{\text{rd}}$ into the rear block pushing phase ($\sim 100 \text{ }^\circ \cdot \text{s}^{-1}$). The front ankle on the other hand reaches its peak plantarflexion velocity at $\sim 90\%$ of the starting blocks pushing phase ($\sim 700 \text{ }^\circ \cdot \text{s}^{-1}$).

ii. The spatiotemporal parameters & joint kinematics in the curve

In the curve, no experimentation investigated the starting blocks kinematics. However, we assume that little difference would be observed in comparison to the straight as the starting blocks pushing phase in the curve is assumed to be performed in an almost linear fashion as discussed at different occasions in this manuscript.

2. The sprinting kinematics from the starting blocks exit to the maximal antero-posterior power

i. The spatiotemporal parameters & joint kinematics in the straight

In sprinting, the V_{A-P} can be expressed as the product of the step frequency (SF) and the step length (SL) (which are also further determined by subsequent parameters) (Hunter et al., 2004). Hence, increased V_{A-P} can result from endless combinations of increase in either one (as long as the other parameter does not undergo a concomitant similar or larger decrease), or both parameters. In maximal effort accelerated overground sprinting, the SL increased from ~ 0.9 m at the first step after the starting blocks exit to ~ 1.4 m at the 3rd step (Debaere, Jonkers, et al., 2013; Rabita et al., 2015).

Regarding the SF, on the other hand, ~ 80 and $\sim 90\%$ of the maximum SF were reached at the 1st and 2nd steps after the starting blocks exit, respectively (~ 4.0 Hz) and then plateaus around $P_{A-P MAX}$, at the 3rd step ($\sim 4.3-4.5$ Hz) (Debaere, Delecluse, et al., 2013; Nagahara et al., 2014; Rabita et al., 2015). Thus, in maximal effort overground sprinting, the increase in V_{A-P} from the front block exit and until the $P_{A-P MAX}$ almost exclusively relies on the sprinter's ability to increase his SL.

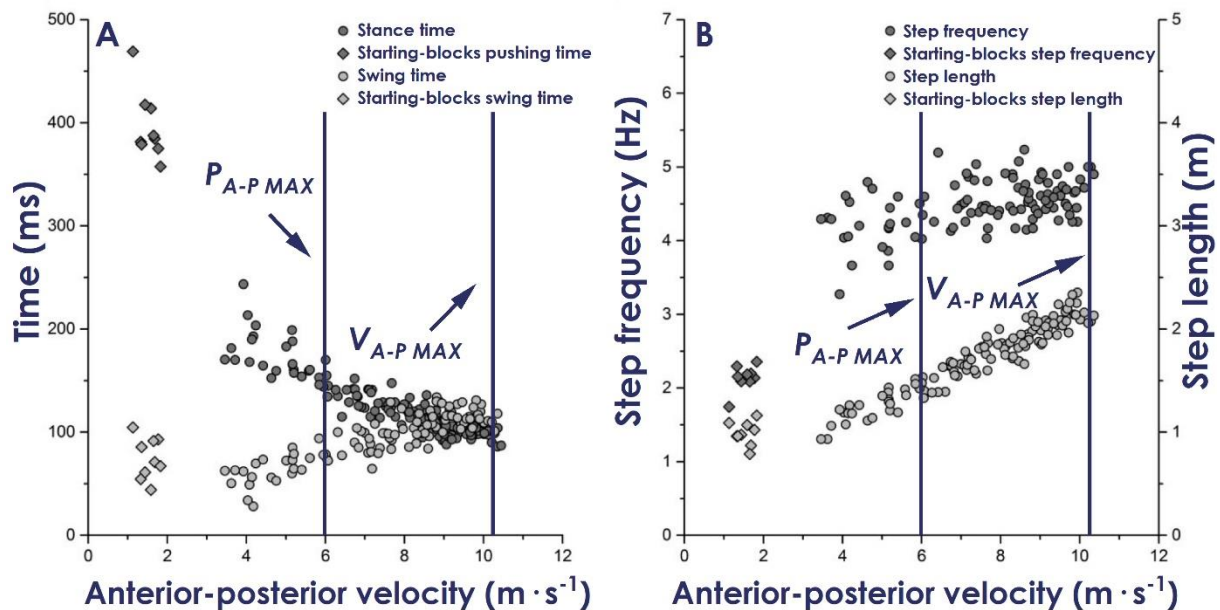


Figure 13. Spatiotemporal characteristics of a) the stance and the swing times in the starting blocks (diamonds) and after the starting blocks (circles); and b) the step frequency and the step length in the starting blocks (diamonds) and after the starting blocks (circles). Figure reproduced from Rabita et al. (2015).

Rather than performing a 3D analysis, the available literature focussed on the lower limb flexion-extension angles and flexion-extension velocities which are deemed to contribute the most to the forward displacement. Some experimentations investigated the hip, knee and ankle angles and angular velocities at the first (N. E. Bezodis et al., 2014; Brazil et al., 2016; Charalambous et al., 2012; Debaere, Delecluse, et al., 2013) and second (Debaere, Delecluse, et al., 2013; Jacobs & van Ingen Schenau, 1992) stances after the starting blocks exit, while King et al. (2023) averaged the angular velocities over the first four stances.

Overall, these experimentations mostly agreed regarding the pattern of the lower limb joint angles and angular velocities and the peak extension and plantarflexion velocities reported (see table 1). For the first two stances, the hip and knee were extending through the majority of the stance duration (N. E. Bezodis et al., 2014; Brazil et al., 2016; Charalambous et al., 2012). The ankle on the other hand was dorsiflexing for the first 40-50% of the stance and then plantarflexing through the end of the stance. The peak extension and plantarflexion velocities were reached in average at ~ 80 , ~ 80 and $\sim 90\%$ of the stance duration respectively for the hip, knee and ankle.

Steady-state velocities vs maximal effort sprinting

When running at a steady-state V_{A-P} below $7 \text{ m} \cdot \text{s}^{-1}$, several studies reported that an increase in V_{A-P} between two steady-states results from an increase in both the SF and the SL (Dorn et al., 2012; Mero & Komi, 1986; Schache et al., 2014). In contrast, above $7 \text{ m} \cdot \text{s}^{-1}$, an increase in V_{A-P} between two steady-state V_{A-P} only results in a SF increase in both overground (Dorn et al., 2012; Mero & Komi, 1986; Schache et al., 2014) and treadmill (Weyand et al., 2000) sprinting. Thus, the increase in V_{A-P} is not explained by the same parameters whether the V_{A-P} increases from one steady-state V_{A-P} to the following one or whether it is maximal effort sprinting. Therefore, attention should be paid to the protocol used when investigating the spatiotemporal parameters responsible for the increase in V_{A-P} .

To summarize, kinematic analyses aiming to investigate the spatiotemporal parameters associated with the increase in V_{A-P} should be analyzed in overground sprinting, with maximal effort sprints.

At the fourth stance, King et al. (2023) reported a clear change in comparison to the first three stances whereby the knee flexes until $\sim 50\%$ of the stance duration. These findings coincide with those previously reported by Nagahara et al.'s (2014) regarding the so-called "first transition". Indeed, these authors found that the change in the average CM height during the stance (see the white dots in figure 14) increased differently from the starting blocks on to $V_{A-P \text{ MAX}}$, with two transitions (see the vertical lines in figure 14). According to the authors, the "first transition" occurred at the $\sim 4^{\text{th}}$ step which could correspond to the $P_{A-P \text{ MAX}}$. Indeed, from the starting blocks exit to the "first transition", these authors reported a rapid rise up of the CM in the vertical direction with a knee strictly extending through the stance. After the "first transition", "the CM rises up more gradually" and "the knee flexes during the early stance phase" before extending (Nagahara et al., 2014). Therefore, it seems that from the starting blocks exit on to the $P_{A-P \text{ MAX}}$, the knees only extend through the stance, causing the CM to rise up rapidly. Afterwards, the CM rises up more gradually as the knee flexes in the early-stance phase.

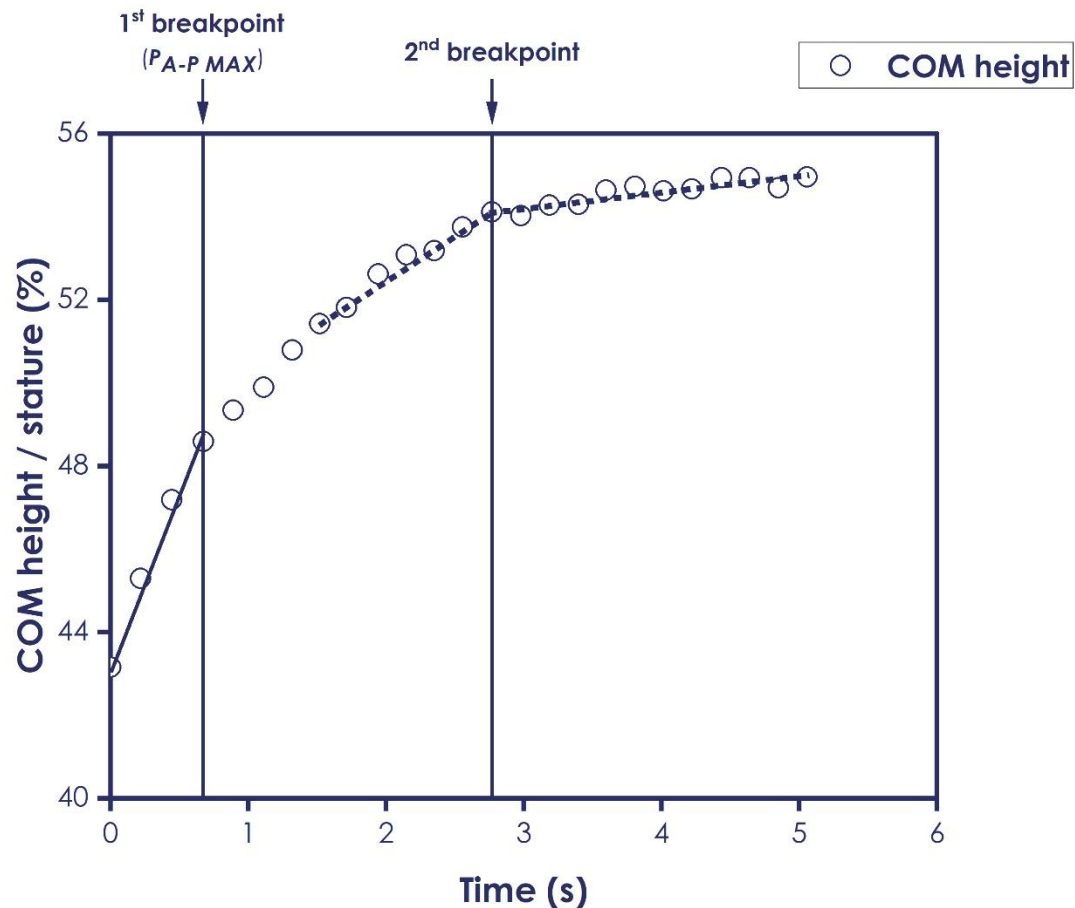


Figure 14. Change in the centre of mass height and indication of the first breakpoint at the fourth step. The figure was reproduced from Nagahara et al. (2014).

ii. The spatiotemporal parameters & joint kinematics in the curve

In the curve, no experimentation investigated the spatiotemporal parameters in this phase of the sprint despite being easily accessible with a camera sampling at 120 Hz during competitions. However, based on the assumption that a sprinter adopts a linear path for the initial steps, we would assume that these metrics in the curve would be similar to the straight.

In addition to that, no experimentation investigated the lower limb joint kinematics from the starting blocks exit on to the $P_{A-P MAX}$ at radii typical of track events. Based on the assumption postulating that a sprinter would adopt a linear path during the initial steps in the curve, we can assume that the lower limb joint kinematics in the curve would be similar to that of the straight. The first modifications between both sprinting conditions would likely occur when the sprinter begins to adopt a curvilinear motion and to lean inward.

2. The sprinting kinematics from the maximal antero-posterior power to the maximal antero-posterior velocity (from ~4 m to ~40 m)

1. The spatiotemporal parameters & joint kinematics in the straight

After the $P_{A-P MAX}$ (i.e., first breakpoint in figure 14), the CM rises up in the vertical direction more gradually until the second breakpoint (Nagahara et al., 2014) (see figure 14) suggesting that changes in the body kinematics are more trivial. This second breakpoint corresponds to the $14^{th} \pm 2$ step, where the sprinter has reached an upright posture (Nagahara et al., 2014). Through the transition phase of overground sprinting, the stance times slightly decrease from ~130 ms to ~100 ms concomitantly with a similar increase in the swing times from ~10 ms to ~130 ms (Debaere, Jonkers, et al., 2013; Rabita et al., 2015). Thus, the SF plateaus at $P_{H MAX}$ and does not meaningfully change during the transition phase, meaning that the increase in the V_{A-P} through this phase exclusively depends on the sprinter's ability to increase his SL (Debaere, Jonkers, et al., 2013; Rabita et al., 2015).

In the transition phase, only a single experimentation described the lower limb joint sagittal plane kinematics (Johnson & Buckley, 2001). The authors investigated the hips, knees and ankles angular velocities at 14 m after the starting blocks during the stance and swing phases. However, this analysis was conducted with manual digitation from video footage at 50 Hz, which is a low sampling rate for rapid movements such as sprinting.

During the transition phase, the authors showed that the hip is extending through the stance which is similar to what is seen during the $P_{A-P MAX}$ phase. The knee, on the other hand, slightly flexes during the early stance phase and then extends through the stance. Finally, the ankle is dorsiflexing through the entire braking phase and the beginning of the propulsive phase (~50% of the stance duration) and plantar-flexes afterwards. The peak extension and plantarflexion velocities in this transition phase are displayed in table 2 and are reached respectively at ~65%, ~75% and ~90% of the stance duration for the hip, knee and ankle.

Table 2. Peak hip and knee extension and ankle plantarflexion velocities (expressed in $^{\circ} \cdot s^{-1}$) during the stance and swing phases at 14 m by Johnson & Buckley (2001).

	Peak extension velocity
Stance hip ($^{\circ} \cdot s^{-1}$)	~750
Stance knee ($^{\circ} \cdot s^{-1}$)	~450
Stance ankle ($^{\circ} \cdot s^{-1}$)	~1150
Swing hip ($^{\circ} \cdot s^{-1}$)	~600
Swing knee ($^{\circ} \cdot s^{-1}$)	~900
Swing ankle ($^{\circ} \cdot s^{-1}$)	~900

2. The spatiotemporal parameters & joint kinematics in the curve

In the curve, the only experimentation that investigated the spatiotemporal alterations in comparison to the straight during the transition phase focussed on a specific instant of this phase (*i.e.*, at 13 m). In contrast to the straight, where a certain symmetry is thought between both limbs, the left and right limbs behave differently in the curve as we will discuss in the rest of this manuscript. Although they should rather be referred as “inside” and “outside” limbs, we will keep the “left” and “right” designation in the rest of this manuscript for clarity sake.

In their study, Judson et al. (2020) analyzed two steps at 13 m and found a significant reduction on the left leg SF, caused by an increased left leg stance time, while the right leg SF did not change in comparison to the straight (Judson, Churchill, Barnes, Stone, Brookes, et al., 2020). On the other hand, no differences were observed for the SL between the straight and the curve (Judson, Churchill, Barnes, Stone, Brookes, et al., 2020).

Thus, the curve results in asymmetrical alterations in the spatiotemporal parameters during the transition phase in comparison to the straight. Overall, the left leg seems more altered by the curve than the right one. However, Judson et al.'s (2020) experimentation only provides a partial understanding of the spatiotemporal alterations in the curve at a very specific instant. In the curve, whether the SF plateaus after $P_{A-P MAX}$ as it is the case in the straight and whether both limbs' SF follow the same trend within the curve remain to be investigated.

In the curve, a major kinematic modification in comparison to the straight occur and can be experienced by anyone attempting to sprint in the curve: the body lateral lean (BLL) (see figure 15) into the curve. Judson et al. (2020) reported a significant increase

in the BLL at touchdown in the curve, in comparison to the straight, during both left and right stances 13 m after the starting blocks exit. This BLL facilitates the F_{M-L} as previously discussed and induces in-series modifications in the sprinting kinematics that are worth mentioning.

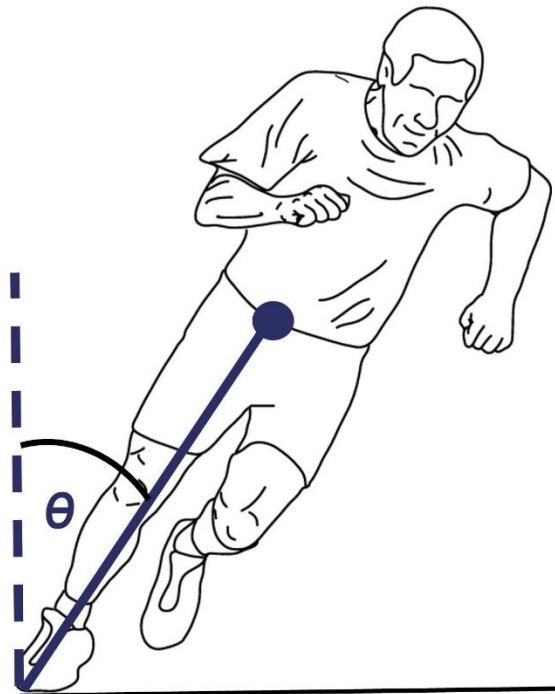


Figure 15. Graphical representation of the body lateral lean (θ) in the curve. The figure was reproduced from Chang & Kram (2007).

Among those modifications, the left foot touchdown kinematics is directly affected by the BLL. At the *Metatarsophalangeal* (MTP) joint, two axes exist about which the foot can push off: the transverse (solid black line on figure 16) and the oblique (dashed black line on figure 16) axes. The transverse axis runs through the heads of the first and second metatarsals whereas the oblique axis runs through the second to fifth metatarsal heads (see figure 16). In the straight, the transverse axis was found to be more effective for the propulsion in comparison to the oblique axis (Bojsen-Møller, 1978). In the curve, the transverse axis was used for the right foot push-off axis (*i.e.*,

transverse) whereas the oblique axis was used for the left foot push-off axis (Judson et al., 2019), suggesting that the propulsion is less effective on the left foot in the curve.

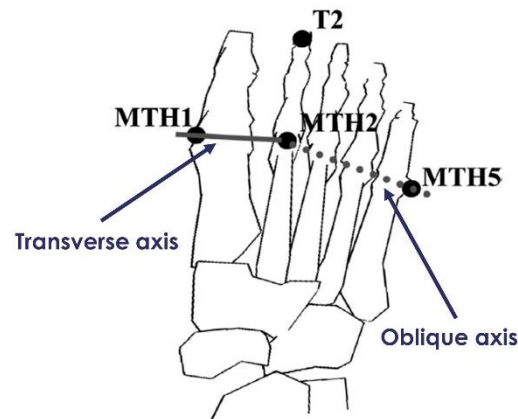


Figure 16. Right foot graphical representation of the transverse (solid) and oblique (dashed) push-off axes of the foot. The T2 marker represents a marker at the second toe. The MTH1, MTH2 and MTH5 markers represent a marker at the first, second and fifth metatarsal heads, respectively. The figure was reproduced from Judson et al. (2019).

Those modifications at the left foot push-off axis resulted in increased touchdown distance (Judson, Churchill, Barnes, Stone, Brookes, et al., 2020) that can result from a restricted “pawing” action before the touchdown. A reduction in the left hip extension velocities just before touchdown could be caused by the BLL into the curve and the inability to produce rapid hip extensions before touchdown while in this position. Unfortunately, Judson et al. (2020) did not report the sagittal plane kinematics and the hip extension velocities during the late swing phase.

Thus, overall, the curve mainly has an impact on the left leg spatiotemporal parameters and kinematics, likely resulting from the sprinter leaning into the curve. However, to date a single experimentation investigated a few kinematic features specifically at 13 m after the starting blocks exit. In addition to that, the authors did not report any findings regarding the sagittal plane kinematics. Despite the changes in the CM posture evolve in a slower fashion during the transition phase until the “second breakpoint (Nagahara et al., 2014), the joints’ kinematics should be investigated

through the whole transition phase in the curve, in order to better understand which metrics are the most affected when sprinting in the curve and with the increasing V_{A-P} .

3. The sprinting kinematics during the maximal antero-posterior velocity (from ~40 m to ~70 m)

1. The spatiotemporal parameters & joint kinematics in the straight

When sprinting at $V_{A-P MAX}$, the stance times are minimum: ~100 ms (see figure 13) (Rabita et al., 2015) and become slightly inferior to the swing times. Yet, the stance times hardly become inferior than 100 ms since one must produce the necessary IMP_{A-P} and IMP_V over a stance to maintain an adequate sprinting motion. At $V_{A-P MAX}$, male national level sprinters have a SF of 4.43 ± 0.18 Hz while their female counterparts have a SF of 4.28 ± 0.17 Hz ($p > 0.05$) (Debaere, Jonkers, et al., 2013). As no statistical differences were found in the SF between genders, the male reached greater $V_{A-P MAX}$ thanks to SL ~11% greater (Debaere, Jonkers, et al., 2013).

During the female and male 100-m dash finals at the 2017 World Championships, a kinematic analysis studied the spatiotemporal parameters over the 47.0-55.5-m section of the race (which approximately corresponds to the $V_{A-P MAX}$ phase). Both genders had a similar SF (~4.80 Hz), however, the 8 male finalists had a ~11% greater SL than their female counterparts.

Thus, between genders with a similar expertise (World Championship finalists), higher $V_{A-P MAX}$ are reached by the male sprinters with longer SL only as the SF were similar between groups. On the other hand, within a gender, a better sprinter reaches higher $V_{A-P MAX}$ by having both higher SF and SL.

At $V_{A-P MAX}$ in overground sprinting, Bezodis et al. (2008) described the hip, knee and ankle joint kinematics during the stance phase with four well-trained sprinters. The authors showed that at $V_{A-P MAX}$, the ankle dorsiflexed and the knee flexed through the entire braking phase and the beginning of the propulsive phase (~60% of the stance duration). Afterwards, the ankle plantarflexed and the knee extended through the end of the stance phase. On the other hand, the hip extended through the stance. The peak extension velocities retrieved from the literature in this $V_{A-P MAX}$ phase are displayed in table 3 and were reached at ~80%, ~90% and ~95% of the stance duration for the hip, knee and ankle respectively (Belli et al., 2002; I. N. Bezodis et al., 2008).

Belli et al. (2002) also investigated the lower limb joint angular velocities at $V_{A-P MAX}$. Although the pattern of the joints angular velocities through the stance were similar to

those reported by Bezodis et al. (2008), Belli et al. (2002) found lower peak extension velocities than the other group (see table 3). The differences between the two experimentations' findings likely originate from the different $V_{A-P MAX}$ reached in the two experimentations. Nine middle-distance runners participated to Belli et al.'s (2002) study while four sprinters were recruited in Bezodis et al.'s (2008) experimentation. In Bezodis et al.'s (2008) study, the four male sprinters reached a $V_{A-P MAX}$ comprised between 9.06 and 10.37 $\text{m} \cdot \text{s}^{-1}$, while the nine middle-distance runners from Belli et al.'s (2002) study reached a $V_{A-P MAX}$ of $8.86 \pm 0.56 \text{ m} \cdot \text{s}^{-1}$. Therefore, those findings further suggest that the greater the $V_{A-P MAX}$, the greater the peak extension velocities at the lower limb joint in overground sprinting.

Table 3. Peak hip, knee and ankle extension velocities (expressed in $^{\circ} \cdot \text{s}^{-1}$) reached during the stance phase at $V_{A-P MAX}$. The data were retried from two experimentations (Belli et al., 2002; I. N. Bezodis et al., 2008).

	Bezodis et al. 2008	Belli et al. 2002
Rear hip ($^{\circ} \cdot \text{s}^{-1}$)	~850	~550
Rear knee ($^{\circ} \cdot \text{s}^{-1}$)	~550	~450
Rear ankle ($^{\circ} \cdot \text{s}^{-1}$)	~1450	~950

2. The spatiotemporal parameters & joint kinematics in the curve

At $V_{A-P MAX}$, in the curve, the left and right legs' spatiotemporal parameters are asymmetrically altered as it is the case during the transition phase. At this point of the curve, the left leg SF is 2.5% lower than in the straight, due to an increased stance time and unchanged swing time (Churchill et al., 2015).

In contrast, the right limb SF was unchanged at $V_{A-P MAX}$ despite this limb had to travel a greater distance during the swing phase in the curve. However, the right limb SL decreased by 4.5% and this confirms the asymmetrical impact of the curve on the spatiotemporal parameters. Eventually, the decreased left leg SF and right leg SL conducted to a significant 4.5% decrease of the $V_{A-P MAX}$ in the curve in comparison to the straight (Churchill et al., 2015).

In the curve, the BLL at touchdown during the $V_{A-P MAX}$ phase was greater in comparison to the straight (Churchill et al., 2015). Additionally, as the values reported at $V_{A-P MAX}$ by Churchill et al. (2015) are greater than those reported by Judson et al. (2020) at 13 m, we can assume that this metric increases in the curve with the increasing V_{A-P} . Since the BLL facilitates the F_{M-L} , the increase in BLL with the increasing V_{A-P} could result from the requirement to apply greater F_C magnitude with the

increasing V_{A-p} . Eventually, the increased BLL also likely induces more alteration in sagittal plane kinematic metrics.

During the late stance phase, the left hip peak extension velocity was reduced by ~11% in the curve in comparison to the straight (Churchill et al., 2015). Those findings suggest that during the left stance in the curve, the hip extensors function could be altered. This alteration could potentially result from the greater BLL and the restricted ability to quickly extend the hip while in this position.

In contrast, the right hip extension velocity was unchanged during the stance phase in the curve. However, the timing of the right hip peak extension was delayed from $50.7 \pm 3.1\%$ of the step duration in the straight to $55.0 \pm 1.9\%$ in the curve. Similarly, the right hip peak flexion was delayed from $45.2 \pm 6.5\%$ of the step cycle in the straight to $50.9 \pm 5.2\%$ in the curve (Churchill et al., 2015). A delayed right hip peak extension and hip flexion could result from delayed onset of muscle activation of respectively the right hip extensors and right hip flexors in the curve in comparison to the straight.

Part III - Summary

- ✎ In overground sprinting in the straight, after the starting blocks exit, the SF reaches its maximum, around the 3rd step (i.e., around $P_{A-P MAX}$). Thereafter, the increase in V_{A-P} almost exclusively results from an increase in the SL.
- ✎ In the curve, the existing literature reported asymmetrical alterations of the spatiotemporal parameters: the left leg's SF and the right leg's SL being reduced in the curve in comparison to the straight. In addition to that, whether the SF plateaus after $P_{A-P MAX}$ in the curve as it is the case in the straight and whether the SL in the curve keeps increasing from the starting blocks onwards remain unknown and should be investigated to better comprehend how the V_{A-P} increases in the curve.
- ✎ In the straight, the sagittal plane hip, knee and ankle angles and angular velocities during the stance and swing phases are well-known. In the curve, as the BLL affects the sagittal plane kinematic, it seems mandatory to investigate the hip, knee and ankle angles and angular velocities during the stance and swing phases through the transition phase in the curve as this has not been realized yet.

Any potential kinematic modifications in the curve would have a muscular origin. According to Kyröläinen et al. (1999): *"The movements of the body segments determine GRF and their directions. Therefore, the roles of muscle actions are important determinants of running mechanics"* (Kyröläinen et al., 1999). Thus, investigating the muscular activity in sprint running is a mandatory requirement for a comprehensive analysis of the motion and its underlying factors. In the curve, little - if any - is known regarding the muscular activity of the lower limbs' muscles. Therefore, conducting a muscular analysis in the curve would likely help better understand the factors affecting the kinematic modifications in this sprinting condition.

Part IV – The use of surface electromyography to understand the sprinting technique

1. The muscle activity from the starting blocks to the maximal antero-posterior power (from ~0 m to ~4 m)

1. The muscle activity during the starting blocks pushing phase

i. The muscle activity in the straight

Otsuka et al.'s (2014) showed that the rear leg starts to produce GRF shortly before the front one. Therefore, it is expected that the rear leg muscles become active first. Mero & Komi (1990) were the first to describe the sEMG activity of the rear and the front *Gastrocnemius Lateralis* (GL), *Vastus Lateralis* (VL), *Biceps Femoris long head* (BF_{lh}), *Rectus Femoris* (RF) and *Gluteus Maximus* (GMax) during the starting blocks pushing phase with 8 experienced male athletes. Contrary to what was expected, Mero & Komi (1990) found that the front leg GL was the first muscle active, followed shortly after by the rear leg GMax. In addition to that, it is interesting to note that none of these muscles were active while in the set position, meaning that other muscles should be active to maintain the set position.

Guissard et al. (1992) studied how different front blocks angles would impact the *Soleus* (SOL), the *Gastrocnemius Medialis* (GM) and the *Vastus Medialis* (VM) sEMG activity of both the rear and the front legs during the starting blocks pushing phase. With a front block angle of 30°, the starting blocks exit V_H was increased (see **part 1 section 1.1.i.**) and this was likely related to a significantly earlier onset and a greater sEMG activity of the front GM in comparison to a front block angle of 70°.

ii. The muscle activity in the curve

In the curve, no experimentation investigated the sEMG activity during the starting blocks phase. However, as already highlighted in the previous sections of this manuscript, the sEMG activity of the hip and the knee extensors, the ankle dorsiflexors and plantar flexors during the starting blocks pushing phase are expected to be close to the sEMG in the straight as the CM trajectory is expected to be linear.

2. The muscle activity from the starting blocks exit to the maximal antero-posterior power

i. The muscle activity in the straight

Mero & Komi (1990) also showed that after the starting blocks exit, the front leg RF was the only muscle active to reposition the front thigh forward during the swing phase (see figure 17). In contrast, the other muscles investigated by the authors (*GMax*, *VL*, *BFlh* and *GM*) were inactive in the corresponding period and started to become active at the end of the swing phase (see figure 17) (Mero & Komi, 1990).

During the first stance phase, the *GMax*, the *VL*, the *RF* and the *GM* showed a peak sEMG activity during the braking phase (Mero & Komi, 1990). Afterwards their sEMG activity decreased until the take-off. In contrast, the *BFlh* sEMG activity remained high through the stance and peaked by the end of the propulsion phase (Mero & Komi, 1990). Based on the sEMG activity timings of the *GMax* and the *BFlh*, it can be hypothesized that the *GMax* is the main (among the muscles investigated) hip extensor during the early stance phase, with a lower hip angle, while the *BFlh* is the main hip extensor during the late stance phase, with a greater hip angle (*i.e.*, with a hip being more extended).

However, Mero & Komi (1990) did not report the sEMG activity timings and the amplitude was not normalized to a reference value. Unfortunately, this annihilates any attempt to compare the sEMG activity found across studies. Indeed, in order to enable between muscle, between study and between subject comparisons, and to provide “a basis of comparison among the differing force capabilities of the subjects’ muscles” (De Luca, 1997), sEMG signals are often expressed as a normalized value which necessitates a rescaling to a percentage of a reference value (Ball & Scurr, 2013). In the literature, several normalization methods exist and have been discussed at different occasions (Albertus-Kajee et al., 2011; Ball & Scurr, 2013; Burden, 2010; Burden & Bartlett, 1999; Halaki & Gi, 2012). Overall, it seems that normalizing to a Maximal Voluntary Isometric Contraction (MVIC) would be more accurate for low-velocity movements (Ball & Scurr, 2013; Burden, 2010) while high-velocity movements should be normalized to the task under investigation (Ball & Scurr, 2013).

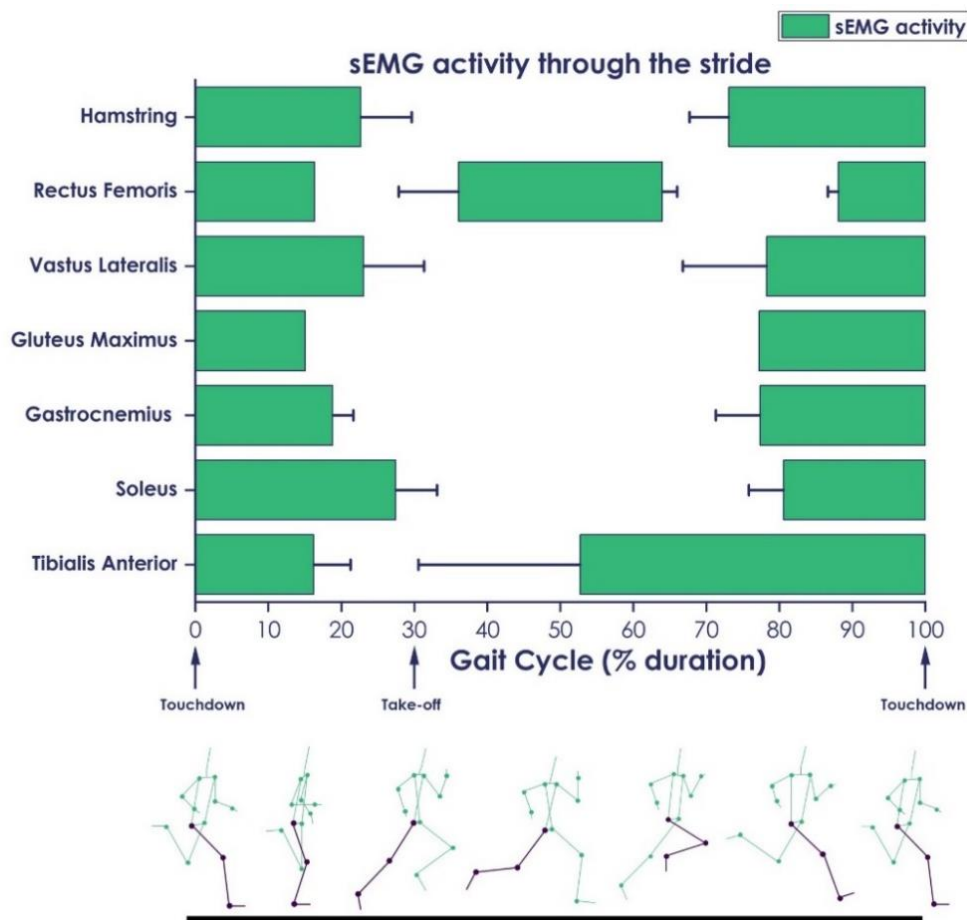


Figure 17. The muscle activation timings of the lower limbs during sprinting across the gait cycle as a percentage of time. Timings gathered from Chumanov et al. (2007); Higashihara et al. (2010); Kuitinen et al. (2002); Kyröläinen et al. (2005); Mero & Komi (1987); Novachek (1998); Pinniger et al. (2000); Thelen et al. (2005); and Yu et al. (2008). The green areas represent the mean (\pm SD) periods where the muscles are active. The figure was reproduced from Howard et al. (2018).

After normalizing their sEMG signal to a reference value, Jacobs & van Ingen Schenau (1992) demonstrated a proximal-to-distal sequencing onset of sEMG activity of the lower limb muscles investigated at the second stance. A hip extensor (GMax) became active first during the stance, following by two knee extensors (VL and VM) and two plantar flexors (GM and SOL) (Jacobs & van Ingen Schenau, 1992). Those findings seem consistent with the kinematic analyses reported by Brazil et al. (2016) and King et al. (2023), stipulating that the peak extension velocities at the lower limb joints were reached in a similar order: the hip first, followed by the knee and finally the ankle.

ii. The muscle activity in the curve

No experimentation investigated the sEMG activity in the curve from the starting blocks exit to $P_{A-P\ MAX}$. As the sprinting motion for the first steps is expected to be linear,

no modifications are expected in the sEMG activity amplitude and timings of hip and knee flexors/extensors and ankle dorsiflexors/plantar flexors.

2. The muscle activity from the maximal antero-posterior power to the maximal antero-posterior velocity (from ~4 m to ~40 m)

1. The muscle activity in the straight

As the hamstrings are the most frequently injured muscle group in sprinting (Askling et al., 2007; Koulouris & Connell, 2003), they have been studied at two occasions during the transition phase of maximal effort sprinting (Higashihara et al., 2018; Yu et al., 2008). Yu et al. (2008) investigated the *BFlh* and the *Semimembranosus* sEMG activities 10 m after the start with 20 male runners (sprinters or middle-distance runners), lacrosse or soccer players. In this study, the participants reached a V_{A-P} of $7.77 \pm 0.11 \text{ m} \cdot \text{s}^{-1}$. On the other hand, Higashihara et al. (2018) investigated the *BFlh* and *Semitendinosus* sEMG activity 15 m after the start with 13 college male sprinters sprinting at a V_H of $8.52 \pm 0.20 \text{ m} \cdot \text{s}^{-1}$.

Both studies showed that the hamstrings were active during the stance phase (see figure 17). In addition to that, their sEMG activity peaked during the early stance phase and decreased afterwards (Higashihara et al., 2018; Yu et al., 2008). Those findings contrast with those previously reported by Mero & Komi (1990) during the first stance phase as these authors reported a *BFlh* peak sEMG activity at the end of the stance phase (Mero & Komi, 1990). The differences between those experimentations can be explained by the different sprinting postures between the first stance and the early transition phase (Nagahara et al., 2014). In the transition phase, with the sprinter being in a more upright posture, the hamstrings are strong hip extensor muscles starting from the touchdown. This could be related to the hip angle at the touchdown. Indeed, from Mero & Komi's (1990) study, we can hypothesize that the *BFlh* becomes a strong hip extensor at a greater hip angle. Through the transition phase, as the sprinter straightens up, it is likely that the hip angle at touchdown increases which in turn conducts the hamstrings to actively extend the hip earlier in the stance.

During the early swing phase, the hip is flexed to reposition the thigh forward and the knee flexes concomitantly, conducting to a shortening of the hamstrings' muscle-tendon unit (MTU) length (Nagano et al., 2014). In this phase, both the *BFlh*, the *Semitendinosus* and the *Semimembranosus* have a low activity (Higashihara et al., 2018; Yu et al., 2008). Starting from the mid-swing phase onwards, their activity began to increase (see figure 17), with the hamstrings' MTU being lengthened as the hip

flexed and the knee extended (Nagano et al., 2014). The hamstrings' sEMG activity peaks by the late swing phase, just before the following touchdown (Yu et al., 2008). It is also interesting to note that the hamstrings' activity during this late swing phase exceed that of the stance (Higashihara et al., 2018; Yu et al., 2008). This could result from the greater hamstrings' MTU lengthening velocity during the swing phase in comparison to that of the stance (Yu et al., 2008). Overall, the greater *BFIh* sEMG activity together with the greater *BFIh* MTU lengthening velocity could partially explain the underlying reasons for the greater hamstring risks of injuries in this phase of the sprint (Chumanov et al., 2012). Therefore, these studies provide knowledge regarding the hamstrings' sEMG activity during the transition phase. Unfortunately, to date, no experimentation investigated the sEMG activity of other lower limb muscles in overground sprinting with maximal effort during the transition phase.

The sEMG activity should be analyzed with maximal effort sprints

Several experimentations investigated how the increase in V_{A-P} would affect the sEMG activity either during treadmill (Cappellini et al., 2006; Chumanov et al., 2007, 2011; Hegyi et al., 2019; Nilsson et al., 1985) or overground (Mero & Komi, 1986, 1987; Schache et al., 2013) sprinting. However, the protocol of these studies was designed such as the participants were running at successively increased steady-states V_{A-P} either on a treadmill (Hegyi et al., 2019) or in overground sprinting (Kuitunen et al., 2002; Kyröläinen et al., 1999, 2001, 2005; Mero & Komi, 1987). For this reason, we decided not to discuss the findings of these studies in the theoretical claim of this manuscript.

Indeed, as previously discussed in the earlier sections of this manuscript (see page 57), sprinting with maximal effort is an un-steady activity by nature whereby characterized by step-by-step V_{A-P} , GRF and kinematics changes (Nagahara et al., 2014). Therefore, the sEMG activity demand would likely differ whether the sprinting V_{A-P} increases between different steady-states or whether this increase in V_{A-P} follows a maximal effort and overall the sEMG analysis in sprinting should be done by investigating maximal effort sprinting.

To date, only a few experimentations reported the muscle activity in overground sprinting with maximal effort at 10 (Yu et al., 2008), 15 (Higashihara et al., 2018) and 40 m (Higashihara et al., 2018; Pinniger et al., 2000; Simonsen et al., 1985). Thus, further studies should be conducted in order to better comprehend how the increase in V_{A-P} within a maximal effort sprint affects the sEMG activity.

2. The muscle activity in the curve

In the curve, no experimentation examined the sEMG activity at radii typical of track events during the transition phase. On a soccer pitch, Filter et al. (2020) positioned sEMG electrodes on the left and right *GMed*, *Semitendinosus*, *BFIh* and *Adductors (ADD)* of nine semi-professional soccer players that sprinted in the straight and in the

curve around the penalty arc of an official soccer field ($r = 9.15 \text{ m}$) (Filter et al., 2020). The authors reported a significantly greater sEMG activity of the right leg's *GMed* and *BFlh* in comparison to the left leg in the curve. According to the authors, this increased sEMG activity was found “to counter the applied valgus and hip internal rotation moments” (Filter et al., 2020). On the other hand, the left *Semitendinosus* and *ADD* had a greater sEMG activity in comparison to the right leg in the curve “to counter the applied varus and hip external rotation moments at the knee” (Filter et al., 2020), confirming the asymmetrical impact of the curve on the left and right limbs, this time with sEMG activity. Despite this study sheds light regarding how the muscles behave in the curve, this experimentation was conducted at a radius far from representative of track events, with non-sprinters and on an artificial grass. Thus, additional studies investigating the sEMG activity on a track, at radii typical of track events and with sprinters would improve the underlying reasons of the asymmetrical nature of the curve.

3. The muscle activity at the maximal antero-posterior velocity (from ~40 m to ~70 m)

1. The muscle activity in the straight

In the late 80's, Mero & Komi (1986) investigated the sEMG activity of the right leg's *VL* and *Gastrocnemius* (the authors did not mention whether it was the *GL* or *GM*) at $V_{A-P \text{ MAX}}$, after a 35-m flying start. These authors reported a greater *VL* and *Gastrocnemius* sEMG activity during the braking phase in comparison to the propulsive phase of the stance, which is similar to what the same authors reported at the first stance after the starting blocks exit (Mero & Komi, 1990). Thus, both at the first stance and at $V_{A-P \text{ MAX}}$, the sEMG activity of a knee extensor and an ankle plantar flexors decrease during the late stance phase despite the knee keeps extending and the ankle keeps plantarflexing during this phase of the stance (Belli et al., 2002; I. N. Bezodis et al., 2008).

Kakehata et al. (2021) investigated the *RF* and *BFlh* sEMG activity timings (i.e., when the muscle switches from inactive to active and from active to inactive) at $V_{A-P \text{ MAX}}$ during the swing phase. All the 18 well-trained sprinters enrolled in this study showed a clear switching between the *BFlh* activity in the late stance and the *RF* sEMG activity at the beginning of the swing. Afterwards, in the mid/late swing phase, 10 out of the 18 participants showed a clear switching between the *RF* and the *BFlh* sEMG activities, meaning that the *RF* activity ceased before its antagonist's activity begun (Kakehata

et al., 2021). However, the authors reported co-contractions for the remaining 8 sprinters. For these sprinters, the *BFlh* became active in the late swing phase while the RF was still active as well. In other words, a hip extensor became active while its antagonist (*i.e.*, a hip flexor) was still active and these co-contractions were found to be deleterious at $V_{A-P MAX}$ whereby a clear switching between the RF offset and the *BFlh* onset in the mid/late swing phase seems more appropriate in order to reach higher SF in this phase (Takehata et al., 2021).

To the author's knowledge, only Higashihara et al. (2018) compared the *BFlh* and *Semitendinosus* sEMG activity between the transition phase (*i.e.*, at 15 m) and at $V_{A-P MAX}$ following two maximal effort sprints. These authors did not report any increase in the sEMG activity, despite a significantly increased V_{A-P} between the two phases. As the hamstring injury risks apparently increase with the increasing V_{A-P} , it is likely metrics other than the sEMG can be responsible for these increased injury risks. Nonetheless, Higashihara et al. (2018) studied two muscles from the hamstring muscle group. Thus, further studies investigating additional muscles should be conducted in overground sprinting with maximal effort in order to better comprehend whether the increased V_{A-P} affects the sEMG activity.

2. The muscle activity in the curve

In the curve Pietraszewski et al. (2021) evaluated the peak sEMG activity of the GM, *BFlh*, GMax, TA and VL during 200-m sprints at the inner and outer lanes of an indoor banked track (*i.e.*, smaller radii than outdoor tracks). The authors compared the sEMG peak activity reached between the straight and the curve portions of the two 200-m. The authors eventually reported a greater peak sEMG activity of the right GM and left and right VL in the curve in comparison to the straight.

However, the confusing data processing description in both experimentations challenges to understand how the curve impacts these muscles sEMG activity. Indeed, the authors reported the peak sEMG amplitude over 50-m sections which, in indoor track venues includes both curve and straight sections. In addition to that, these 50-m sections also gather successive phases of the sprint which we attempted to dissociate in the present manuscript (see **Part 1**) and this means that the sEMG activity was not specifically investigated at $V_{A-P MAX}$. Overall, the multiple limitations highlighted above indicate that the sEMG activity in the curve at radii typical of track events is rather unknown.

Thus, overall, no experimentation with a sufficiently robust experimental design investigated the sEMG activity of lower limb muscles in the curve. We have previously

seen in the **Part 3** of the manuscript that the left hip peak extension velocity during the stance was reduced in the curve in comparison to the straight (Churchill et al., 2015). This could in turn result from alterations of hip extensors muscle activity during the stance phase and hip extensors sEMG activity should be investigated in the curve.

Finally, as we have previously discussed in the **Part 3**, the left leg's SF is reduced in the curve in comparison to the straight during the transition phase (Judson, Churchill, Barnes, Stone, Brookes, et al., 2020) and at $V_{A-P MAX}$ (Churchill et al., 2015). As we have discussed, co-contractions between *BFlh* and *RF* in the late swing phase in turn reduce the SF (Kakehata et al., 2021). In the curve, the left leg SF is reduced due to an increased left stance time as developed in the **Part 3**. Therefore, investigating the sEMG activity timings and amplitude of these muscles in the curve could help understand the underlying reasons of the increased stance times. For instance, hip or knee extensors or ankle plantar flexors might show a lower sEMG activity or these muscles could be active for a longer duration, which could in turn induce lower hip or knee extension or ankle plantarflexion velocities and consequently longer stance times.

Part IV – Summary

- 👉 Only a few experimentations investigated the sEMG activity in overground sprinting with maximal effort. As the sprinter straightens up during the transition phase, it seems that the hip extensors' sEMG activity changes as well. However, to date neither study investigated the change in the sEMG activity with the sprinting kinematics.
- 👉 In addition to that, these studies focussed their analysis on specific timestamps of the sprint. Therefore, an analysis from the starting blocks exit onward would help better understand how the muscle activity impacts the sprinting technique.
- 👉 To date, a single experimentation compared the sEMG activity of the *BFlh* and *Semitendinosus* at 15 m and at $V_{A-P MAX}$. These authors did not report any increase in the sEMG activity with the increasing V_{A-P} , suggesting that it is not the sEMG activity that is responsible for the greater risks of injuries as the V_{A-P} increases.
- 👉 In the curve, to date, two studies explored the sEMG activity and compared it to the sEMG activity obtained in the straight. However, one showed large methodological limitations while the other was realized on a soccer pitch with soccer players, meaning that the sEMG activity in the curve at radii typical of track events remains rather limited. Thus, a clear investigation of the sEMG activity timings and amplitude at radii typical of track events with sprinters is still lacking.

RESEARCH QUESTIONS AND AIMS OF THE THESIS

From a biomechanical aspect, the sprinting performance can be thoroughly characterized through the $V_{A-P\ CM}$, the GRF, the kinematics and the sEMG features. These parameters have been well detailed in the straight in the existing literature. However, the straight only represents a minor portion of the performance in curve sprinting events (200, 400, 400-m hurdles, 4*100, 4*400, 4*400 mixed relay) and a clear gap remains in the literature regarding the $V_{A-P\ CM}$, the GRF, the kinematics and the sEMG in the curve. Consequently, the sprinting performance in the curve is not well understood hitherto.

- **Thus, the first main aim of the present thesis was to compare the sprinting activity between the straight and the curve using the different metrics that we mentioned.**

In addition, we have seen in the **literature review** that overground straight-line sprinting with maximal effort is an un-steady activity by nature. With the increasing $V_{A-P\ CM}$, several mechanical and kinematic changes are observed as a sprinter progresses into the sprint and straightens up. In the curve, neither experimentation reported whether the mechanical and the kinematic parameters undergo similar changes throughout the transition phase. Furthermore, as the F_C magnitude is strongly influenced by the sprinting V_{A-P} , additional changes between the curve and the straight could result from the increasing F_C .

- **Therefore, the secondary main aim of the present thesis was to investigate whether the CM, the GRF, the kinematics and the sEMG activities modifications in the curve change with the increasing V_{A-P} through the transition phase.**

As this PhD thesis was conducted at the French Institute of Sport and with the French Athletics Federation, in a context of sport performance, we paid special attention to the parameters that could eventually a) alter the sprinting performance and b) increase the injury risks in the curve in comparison to the straight.

In addition, the sprinting activity must be studied in overground sprinting with maximal effort with *in-field* experimentations. In addition to that, as the curve requires specific technical abilities in itself, we wanted to investigate those parameters among experienced curve sprinters.

In the **literature review**, we saw that the $V_{A-P\ CM}$ was a key feature of the sprinting performance in the straight and directly provides information regarding the sprinting

expertise. In the curve, only a few studies investigated the $V_{A-P\ CM}$. Moreover, these studies were limited to a specific portion of the curve due to technological limits which attests the challenge to assess the $V_{A-P\ CM}$ in the curve, especially within *in-field* conditions. Nevertheless, investigating the $V_{A-P\ CM}$ in the curve throughout the transition phase seems of great importance. Considering their portability, their convenience and their range, full-body MIMU-based systems have become popular over the past decade. Yet, to our knowledge, no study compared the stance-averaged V_{CM} computed from a MIMU-based system to a reference system.

Thus, the aim of the study #1 was to compare the stance-averaged V_{CM} computed from a MIMU-based system to the V_{CM} measured with a reference system (i.e., FP) over the starting blocks pushing phase and the initial 1-to-4 stances both in the straight and in the curve.

It was hypothesized that this MIMU-based system would provide comparable data for the V_{CM} in comparison to the PF. If this system is found to be suitable for *in-field* computation of the V_{CM} , this would provide the unique opportunity to easily and rapidly access the V_{CM} in the curve over the entire transition phase.

Based on Newton Second Law of Motion the V_{CM} can be described using the GRF and several experimentations have used the GRF approach in the straight. Numerous studies showed that the mean F_{A-P} over a stance was a key feature in straight-line sprinting performance. In the curve, the additional requirement of the F_{M-L} in order to maintain a curvilinear motion likely affects the F_{A-P} which would in turn alter the sprinting performance. In addition, mathematical models hypothesized that the F_V would be altered as well. Overall despite the ability to produce a similar F_{TOT} in the curve would not be affected, the sprinter would need to increase the stance times in order to produce an IMP_V similar to the straight.

Thus, the main aim of the study #2 was to compare the GRF from the starting blocks pushing phase to the $V_{A-P\ MAX}$ between the straight and the curve. A secondary aim was to investigate how the GRF evolve in the curve with the increasing V_{A-P} .

It was hypothesized that the mean F_{TOT} would remain similar to the straight. Concomitantly, we would observe a substantially increase in the mean F_{M-L} , meaning that the mean F_V and F_{A-P} would decrease in comparison to the straight. A second hypothesis of the present study was that the mean F_{M-L} over the first stances in the curve would be similar to the straight as the first steps are thought to be performed in the straight.

Anyone sprinting in the curve will automatically lean in order to exert the F_{M-L} . As it has been previously suggested, those changes in the frontal plane likely yield changes in the sagittal plane kinematics as well and these changes in the sagittal plane must be investigated. Additionally, the reduced F_{A-P} in the curve likely results from alterations in the hip, knee and ankle extension/plantarflexion during the stance phase. Furthermore, we saw that the BLL increased with the increasing V_{A-P} , meaning that the sagittal plane kinematic modifications in the curve in comparison to the straight could potentially increase with the increasing V_{A-P} .

Thus, the main aim of this study #3 was to compare the peak hip, knee and ankle extension and plantarflexion angles and angular velocities during the stance and the swing phases through the transition phase. During the swing phase, as the hip and knee flexions are meaningful in terms of performance, they will also be investigated.

Based on the previous literature and due to the BLL, it was hypothesized that the left limb sagittal plane kinematics would be the most affected by the curve. Specifically, we are expecting a lower left hip extension velocity during the stance phase.

The modifications in the sagittal plane kinematics are eventually originating from changes in the sEMG activity of the muscles surrounding the joints. For instance, a lower left hip extension velocity can result from a lower sEMG activity of a hip extensor (*i.e.*, the *BFlh*), or this muscle being active over a shorter period in comparison to the straight. Consequently, investigating the sEMG activity of muscles directly involved in sagittal plane movements would likely provide meaningful knowledge regarding the changes in the sagittal plane kinematics.

Thus, the main aim of this study #4 was to compare the sEMG activity of hip flexors and extensors, knee flexors and extensors and ankle plantar flexors during both the stance and the swing phases. A secondary aim was to investigate whether the sEMG activity of these muscles change with the increasing V_{A-P} .

Based on the GRF changes and the kinematics modifications expected in the curve, it was hypothesized that the sEMG activity of a left hip extensor would be decreased in the curve. Moreover, based on the BLL, we expect the left limb muscles to undergo the greatest changes.

GENERAL METHODOLOGY

This chapter outlines the general methodology for the experimentations conducted within the Halle Maigrot of the French Institute of Sport (INSEP, Paris, France). These experimentations were in accordance with the Declaration of Helsinki and have been approved by the Ethical Committee for Research in Sport Sciences (n° **IRB00012476-2021-29-04-107**). The four studies that will be detailed thereafter all emerge from the same experimentations.

1. Participants

The participants' characteristics are presented in table 4. Four female and fifteen male sprinters, experienced-to-elite 200- and 400-m specialists were enrolled in these experimentations. Four of them recently participated to international competitions (2016 Olympic Games, 2021 Paralympic Games as a guide, 2021 under 20 European and World Championships).

Table 4. Mean \pm SD characteristics of the participants recruited for the four experimentations.

	Age (years)	Height (cm)	Body mass (kg)	Personal best 200 m (s)	Personal best 400 m (s)
Female	23.75 \pm 2.9	170.25 \pm 4.2	65.87 \pm 4.03	26.30 (range 24.85 – 27.75)	57.67 (range 57.40 – 57.93)
Male	23.93 \pm 3.9	178.80 \pm 5.7	76.10 \pm 6.78	22.89 (range 20.45 – 23.83)	49.56 (range 47.60 – 53.31)

2. Protocol

1. Participants' arrival and informed consent

The recordings took place on an indoor track facility between June and July 2021, which corresponded to the track competition period. Upon the participants' arrival, they were informed of the aims, risks and benefits of the experimentation and signed the informed consent (see figure 18, panel A).

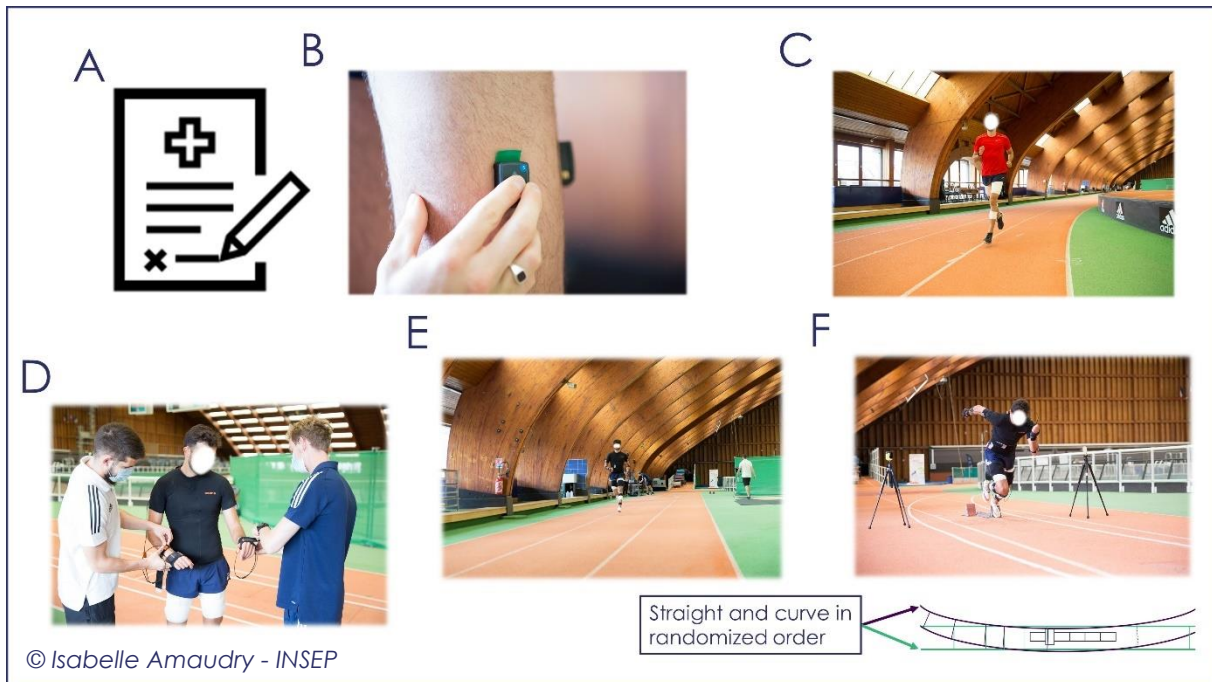


Figure 18. Graphical representation of the experimental protocol. A. the participant is signing the informed consent; B. the surface electromyography electrodes are positioned on the middle of each muscle's belly following the SENIAM recommendations; C. the participant warms-up for at least 45 minutes; D. the Magneto-Inertial Measurement Unit (MIMU)-based system is positioned on the participants; E. with the MIMUs and the straps on, the participant familiarize for an additional 10-to-15 minutes; and F. the data collection begins with 10-, 15-, 20-, 30- and 40-m sprints in the straight and in the curve with the sprinting condition (straight or curve) order being randomized.

2. Material detecting and recording the muscles' surface electromyography

In order to compare the sEMG activity of four muscles in the curve, to that of the straight, we positioned 8 single sEMG electrodes (Trigno, Delsys INC. Boston, USA, see figure 19) sampling at 2148 Hz on the muscle belly of 4 muscles on each leg (see figure 18 panel B) following the SENIAM recommendations (Hermens et al., 2000). Considering the previous kinematics and sEMG activity literature that analyzed the sprint, we have chosen to collect the sEMG activities of the following four muscles: the *BFlh*, the *RF*, the *VL* and the *GM*. Once accurate positioning of the muscles was identified, a black pencil was used to mark its location. Thereafter, the participants were asked to gently isometrically contract the different muscles to ensure correct electrode positioning. Afterwards, the surface was shaved and abraded (Merletti et al., 2001). Finally, the sEMG electrodes were positioned longitudinally to the muscle fiber in order to guarantee the detection of the maximum muscle activity amplitude (Merletti et al., 2001); and firmly attached to the skin using straps (see figure 18, panel C).

In sprinting, the four muscles analyzed have the following anatomical characteristics and functions:

- The *BFlh* is a bi-articular muscle and is the longest portion of the *Biceps Femoris*. The *BFlh* has a conjoined tendon proximally with the *Semitendinosus* on the ischial tuberosity (Stępień et al., 2019). The distal tendon is common with the *Semimembranosus* on the styloid process of the fibula (Terry & LaPrade, 1996). This muscle works as a knee flexor before the touchdown (eccentric contraction during the late swing phase) and a hip extensor through the stance (concentric contraction).
- The *RF* is bi-articular and is located in the anterior part of the thigh. Proximally, its tendon origin is on the anterior inferior iliac spine. Distally, the *RF* tendon terminates on the patella with the quadriceps tendon. During the stance phase, the *RF* has “an important role in tolerating impact loads in running” (Nummela et al., 1994). In the swing phase, this muscle works as a hip flexor to reposition the thigh ahead of the trunk (Takehata et al., 2021, 2022; Mero & Komi, 1987).
- The *VL* is mono-articular. Its proximal tendon origin is on the lateral lip of the linea aspera and the distal tendon terminates on the *Patella* with the quadriceps tendon. In sprinting, this muscle contracts concentrically to extend the knee before the touchdown and controls the knee flexion while eccentrically contracted during the stance.
- Finally, the *GM* is the medial head of the bi-articular *Gastrocnemius* muscle. Its origin is above the medial femoral condyle and terminates on the calcaneal tuberosity on the *Calcaneum* through the Achilles tendon. This muscle works mainly as an ankle plantar flexor in sprinting and has a minor role of knee flexor.

Overall, these muscles have major roles in sprinting and were found to be solicited in running and sprinting (Hanon et al., 2005; Higashihara et al., 2010, 2018; Howard et al., 2018; Takehata et al., 2021, 2022; Pinniger et al., 2000; Slawinski et al., 2008; Yu et al., 2008). Due to the asymmetrical nature of curve sprinting between the left and right legs as presented in the **literature review**, we analyzed both the left and right leg's muscles in either sprinting condition. In addition to that, as we wanted to specifically investigate how these muscles mainly involved in sagittal plane movements would perform in the curve in comparison to the straight, we considered the straight as the “reference condition”.

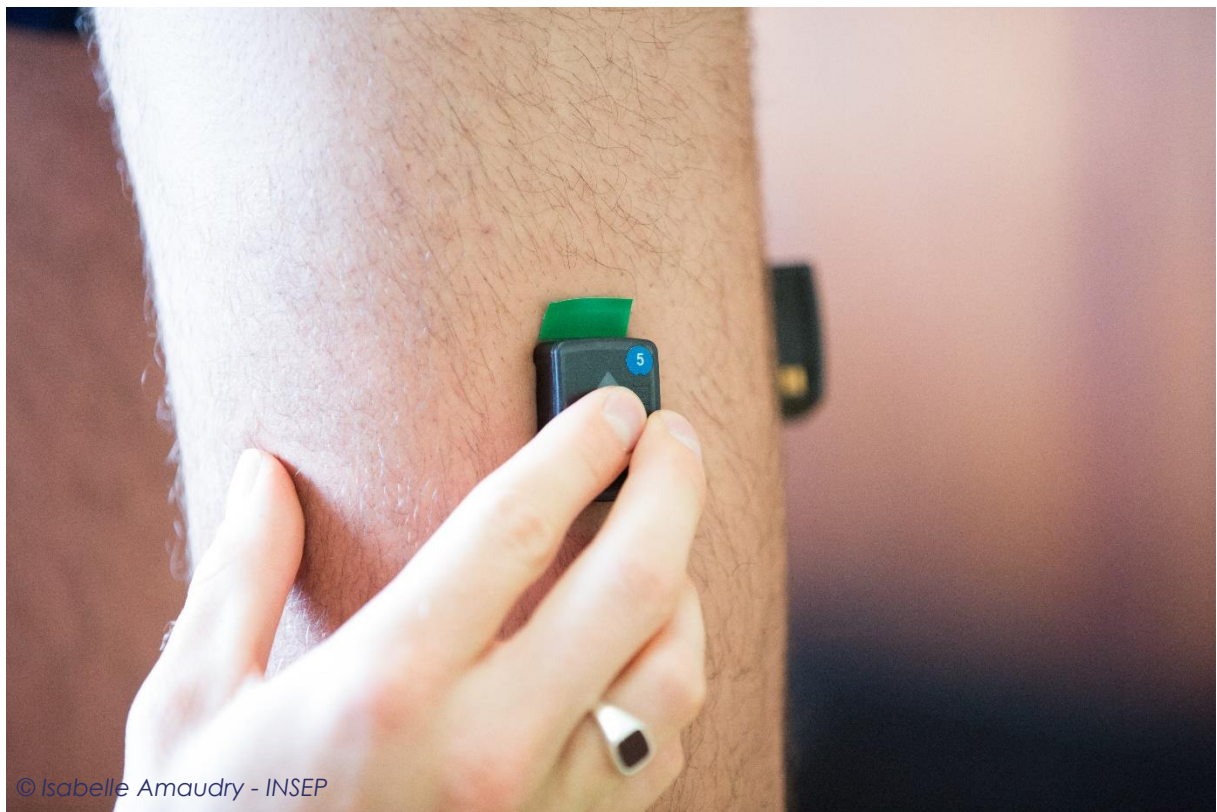


Figure 19. Representation of the surface electromyographic electrodes positioned on a participant.

3. Self-managed warm-up

After the electrodes were positioned, the participants began with a self-managed warm-up (≥ 45 min) that comprised jogging, drills and accelerated sprints with increasing intensity (see figure 18, panel C).

4. Material detecting and recording the joints' kinematic

The sprinting kinematic was computed using a MIMU-based system (MVN Link Xsens Technologies, Enschede, Netherlands, 240 Hz). This MIMU-based system is composed out of 17 individual MIMUs (36 x 24.5 x 10 mm: 10 g) connected through wires. Each MIMU contains a 3D gyroscope (± 2000 °·s⁻¹), a 3D accelerometer (scale: ± 160 m·s⁻²) and a 3D magnetometer (± 1.9 Gauss). The MIMUs were fixed to the participants' segments with straps (see figure 18, panel D) following the manufacturer recommendations (see figure 20 for a representation of the MIMUs' location) after the warm-up.

Afterwards, in order to “estimate the dimensions/proportions of the person being tracked, as well as the orientation of the sensors with respect to the corresponding

segments" (Schepers et al., 2018), a calibration procedure must be done. This calibration starts with the computation of the anthropometrical model.

i. The anthropometrical model

For that sake, the participants' height and foot length were measured and input into the MIMU-based system software which estimates segments' lengths with regression equation (Drillis et al., 1966; Roetenberg et al., 2013; Yeadon & Morlock, 1989) in order to define the MIMU-based anthropometrical model. The MIMU-based system anthropometrical model is defined by 23 segments: pelvis, L5, L3, T12, T8, neck, head, left and right shoulders, upper arms, fore arms, upper legs, lower legs, feet and toes and is based on the International Society of Biomechanics (ISB) biomechanical model (Roetenberg et al., 2013). These 23 segments are linked through 22 joints and the Euler representation of those joints follows the ZXY Euler sequence. In addition to that, the segments' movements that do not have sensors attached on are "estimated by combining the information of connected segments and the anthropometrical model" (Roetenberg et al., 2013; Schepers et al., 2018). Unfortunately, the whole computation is based on the manufacturer's proprietary sensor fusion algorithm and scaling model; and thorough information regarding its processing cannot be accessed.

Robert-Lachaine et al. (2017) have estimated the differences attributed to the MIMU-based system anthropometrical model in comparison to the ISB anthropometrical model. The authors showed that, depending on the joint, small-to-large differences due to the biomechanical model used can be observed for the joint angles. The most affected joints were the shoulder and the elbow (root mean square errors up to 41.3°) (Robert-Lachaine et al., 2017). In contrasts, the hip, knee and ankle joints "were the least affected by the model component" (Robert-Lachaine et al., 2017). As the errors due to the technology were rather small, the anthropometrical model represents the main limitation of this system.

Although the errors associated with the technology were rather small (Robert-Lachaine et al., 2017) an accurate recording using this technology is strongly influenced by the sensors positioning on the segments and the calibration procedure that follow. Consequently, in the present study, the calibration procedure was performed according to the manufacturer instructions (Schepers et al., 2018) and to general guidelines (Camomilla et al., 2015, 2018; Hughes et al., 2021) to generate sensor-to-segment alignment (Roetenberg et al., 2013).

ii. The calibration steps

- **Sensor-to-segment calibration:** This step consists on an estimation of the segments' kinematics based on the sensors' orientation on the body segments. For that sake, the participants were asked to stand in a reference, known position (N-pose, see figure 20), in which the segments' orientation is assumed to be known. Then, the participants were asked to walk back and forth for ~5 m. Thus, a high-quality calibration procedure also strongly relies on the quality of the N-pose adopted by the participant.

In the N-pose, the participant's body is assumed to be a rigid body and the homogeneous matrices between the segments and the MIMU-based system Global Coordinate System (GCS) are computed. From that point on, we can follow the segments' motion based on the MIMU's GCS motion (Roetenberg et al., 2013; Schepers et al., 2018).

- **Axes definition:** Finally, the calibration was applied with the participant standing in the N-pose and facing the direction of the measurement environment. The forward axis, as well as the local coordinate system's (LCS) origin (corresponding to the right heel position) were in turn defined. In our experimentations, the participants positioned their right heel at the origin of the FP GCS (see figure 30, bottom left corner, position (0,0,0)) in order to align the FP and the MIMU-based systems' GCS. Unfortunately, due to sensors drift, the MIMU-based system LCS is unlikely to be perfectly aligned with the FP GCS (see section 6.2. of the **general methodology**).

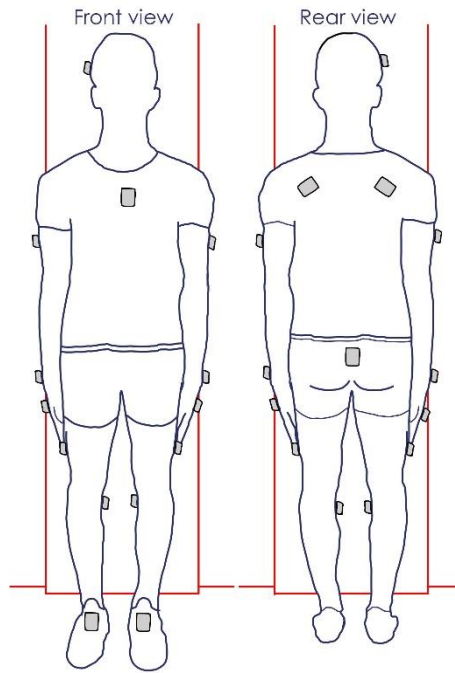


Figure 20. Position of the magneto-inertial measurement units (in gray) with a participant standing in the N-pose.

iii. Familiarization with the electrodes and the sensors on

After the participants were fully equipped with the MIMU-based sensors, they were given an additional 10 minutes to familiarize with the sensors on (see figure, 18 panel E).

5. How to investigate the ground reaction forces in the curve?

Following the familiarization period, the participants performed 10-, 15-, 20-, 30- and 40-m sprints (see figure 18, panel F). The 5 sprints were performed with maximal effort, in the straight and in the curve with a randomized sprinting condition (straight & curve) order. The participants were given 3, 4, 5, 6 and 8 min of rest after the 10-, 15-, 20-, 30- and 40-m sprints, respectively, in order to avoid the onset of fatigue. The participants followed the “on your marks”, “set” and “go” instructions using starting blocks and were wearing their own spikes.

For this experimentation we had access to an indoor track facility (the Halle Maigrot of the French Institute of Sport, Paris, France) where 6 FP are connected in-series and embedded within the track (see figure 21, the FP apparatus will be detailed in the **general methodology** section 3.3.). In order to compute the GRF over multiple stances in both the straight and in the curve, we adapted a protocol based on the original work of Cavagna et al. (1971) and later replicated by Rabita et al. (2015) (see figure 21 for a graphical representation of this protocol). For the 10-m sprints in either the

straight or the curve, the starting blocks were positioned on the first FP (see figure 21). For the subsequent sprints, the starting blocks were progressively positioned further away from the FP so that the GRF of consecutive stances could be computed (see the moving positions of the starting-lines in comparison to the FP). This methodology permitted to collect the GRF of ~17 stances in average in the straight and ~15 stances in average in the curve.

The GRF obtained during the 10-, 15-, 20-, 30- and 40-m sprints correspond to the GRF at the following distances for each sprint. For the 10-m sprints, the GRF were collected at 0-6 m. For the 15-m sprints, the GRF were collected at 8-14 m. For the 20-m sprints, the GRF were collected at 14-19 m. For the 30-m sprints, the GRF were collected at 24-29 m. Finally, for the 40-m sprints, the GRF were collected at 34-39 m (see figures 21 & 22 for graphical representations).

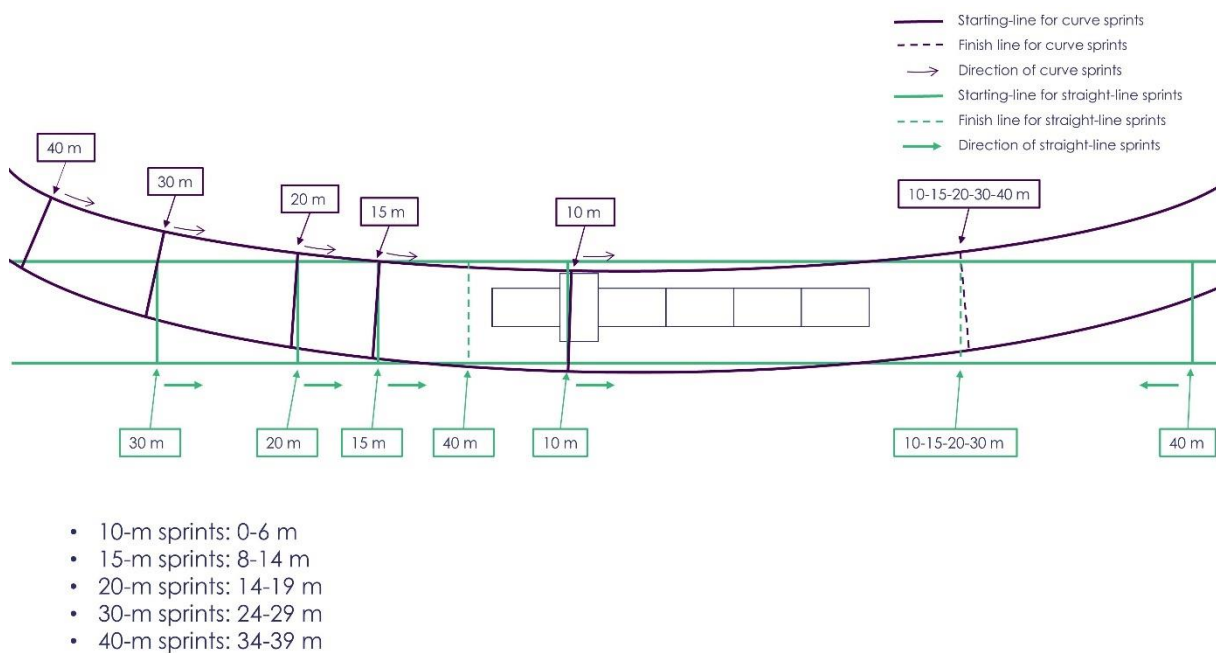


Figure 21. Graphical representation of the protocol used to collect the ground reaction forces (GRF) at different instants of the race. Overall, with the increasing distance, the starting blocks position was positioned further away from the force platforms in order to collect the GRF of the subsequent stances. Note that for the 40-m sprints, the starting blocks were positioned on the other side and the participants were sprinting on the opposite way due to the indoor facility organization. The dimensions are not at a correct scale.

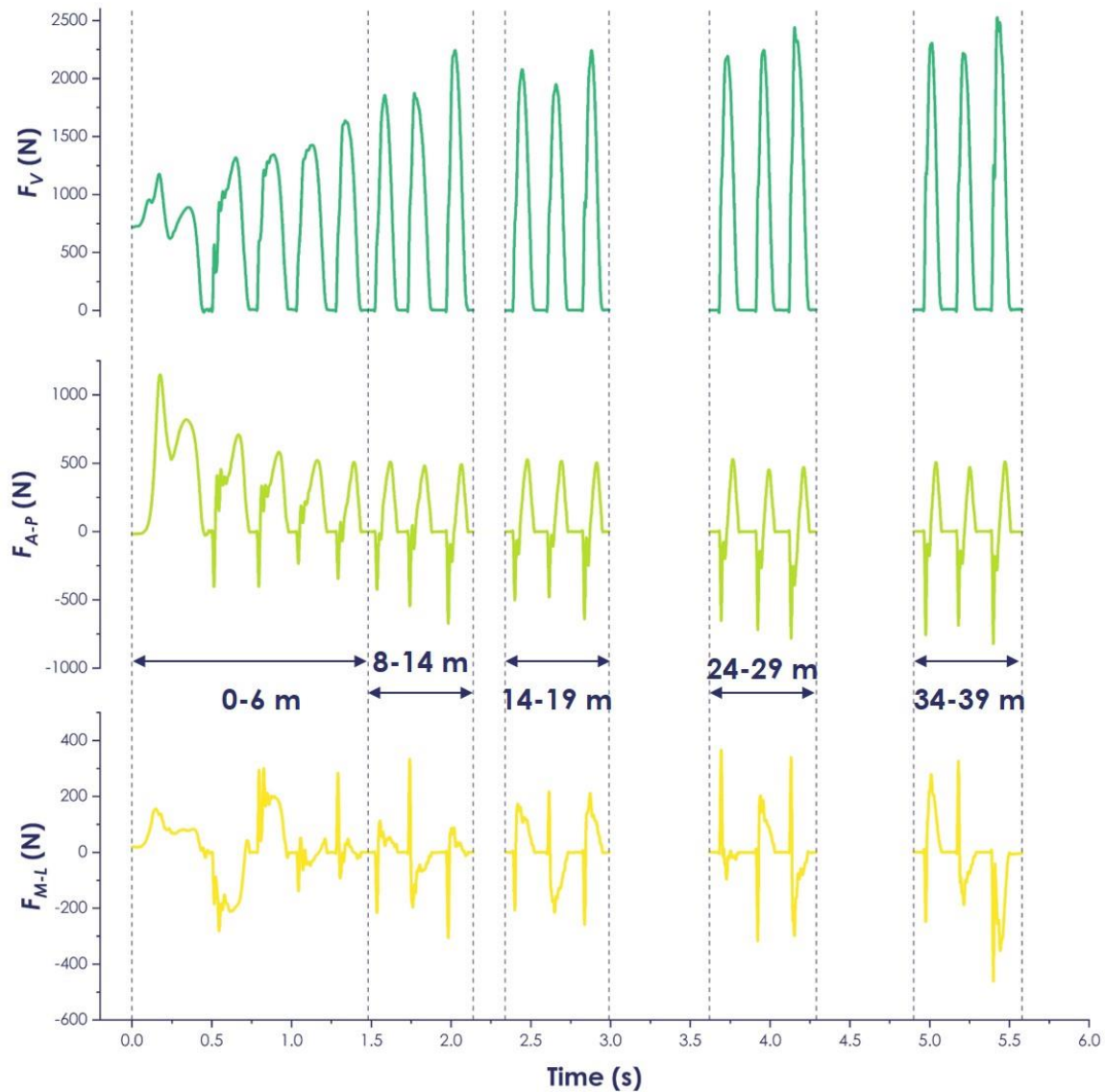


Figure 22. Typical signals of instantaneous vertical (F_V), antero-posterior (F_{A-P}) and medial-lateral (F_{M-L}) components of the ground reaction force obtained during the 10-, 15-, 20-, 30- and 40-m sprints in the straight, and that correspond to the following location of the force platforms area: a) 10-m sprints: Zone 1 (0 to 6 m; 0 corresponding to the starting line); b) 15-m sprints: Zone 2 (8 to 14 m); c) 20-m sprints: Zone 3 (14 to 19 m); d) 30-m sprints: Zone 4 (24 to 29 m) and 40-m sprints: Zone 5 (34 to 39 m).

6. How to reconstruct a curve on a straight-line of an indoor track facility?

In order to investigate the GRF within the curve, we had to reconstruct a curve on the straight-line of the indoor track facility, where the 6 FP are embedded within the track (see figure 23).

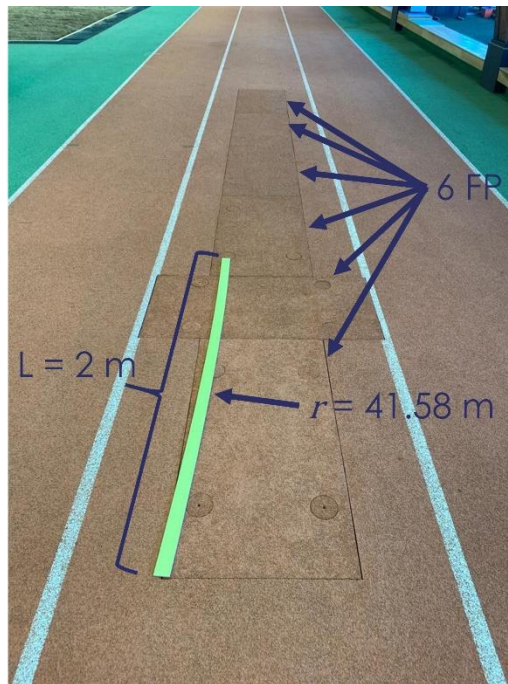


Figure 23. Location of the 6 force platforms (FP) in the straight-line of an indoor track facility. In yellow is the 2-m long template corresponding to the lane 5 of a standard athletics track (radius (r) = 41.58 m) was positioned on the FP in order to reconstruct a curve overlapping the 6 FP.

For the reconstruction of the curve, we used a 2-m long template with a radius of curvature of 41.58 m (Sartorius, la Ferté-sous-Jouarre, France, see figure 23), corresponding to the lane 5 of a standard athletic track. This template was positioned on the inner edge of the FP (see figure 23), in order to reconstruct a curve overlapping the FP area such that the participants were the most likely to hit the FP while sprinting. With this template, we drew the curve onto the track using chalk (see figure 24) and moved the template successively along the track in order to reconstruct a 40-m long lane in the curve (see figure 24). For each experimentation, we positioned two white bands (DimaSport, Ozoir-la-Ferrière, France; see figure 24) on the track to replicate the inner and the outer lanes of a 1.22-m wide lane 5.

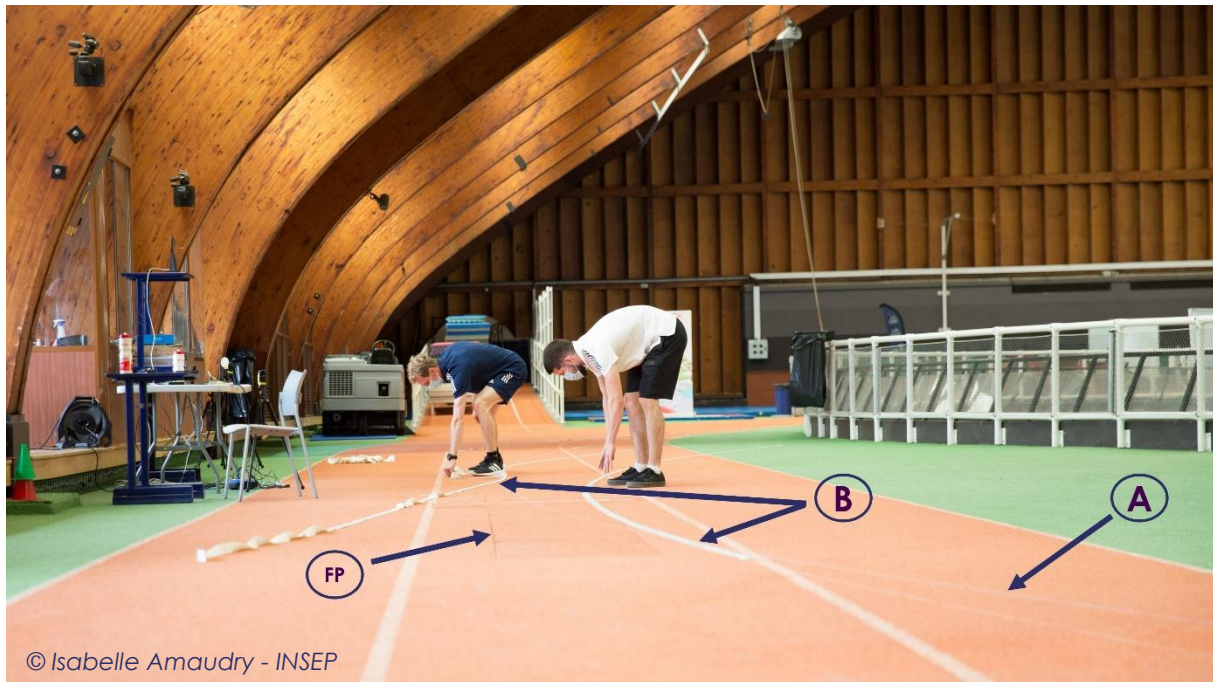


Figure 24. The two experimenters installing the two white bands (B arrows) on top of the chalk line (A arrow) in order to replicate a lane 5 (radius = 41.58 m) of a standard athletic track over the force platforms (FP) area. The reproduced lane was 1.22 m wide.

3. Materials

1. Video cameras

One of the main concerns with the FP data is to make sure the participants' feet made contact strictly within the FP. For that sake, each sprint was filmed using two video cameras (120 Hz, iPhone 11, Apple, California, USA) positioned on either side of the FP (represented in grey and mounted on tripods in the figure 25) in order to make sure each foot was fully within the FP. A stance was considered “valid” when the foot fully landed within the FP.

2. Timing gates

Two pairs of timing gates (Witty, Microgate, Bolzano, Italy) were positioned at the beginning and at the end of each sprinting distance (represented in dark grey in figure 25) to compute the elapsed time between the starting and the finish lines over each sprint. The first pair of timing gates was placed ~10 cm ahead of the starting-line such that the participants were not obstructing the beam while on the starting blocks (see figure 25).

3. Material detecting and recording the ground reaction forces

In the present experimentation, the instantaneous F_V , F_{A-P} and F_{M-L} were measured by a 6.60-m long FP (see figures 21, 22 & 23), composed out of six individual FP (5 length-wise and 1 sideways; 1.2×0.6 m each sampling at 1000 Hz; KI 9067; Kistler, Winterthur, Switzerland) connected in-series and embedded within the track surface. The second FP was oriented perpendicularly so that the participants' hands were positioned on the FP during the starting blocks phase (see figures 21, 23 & 25).

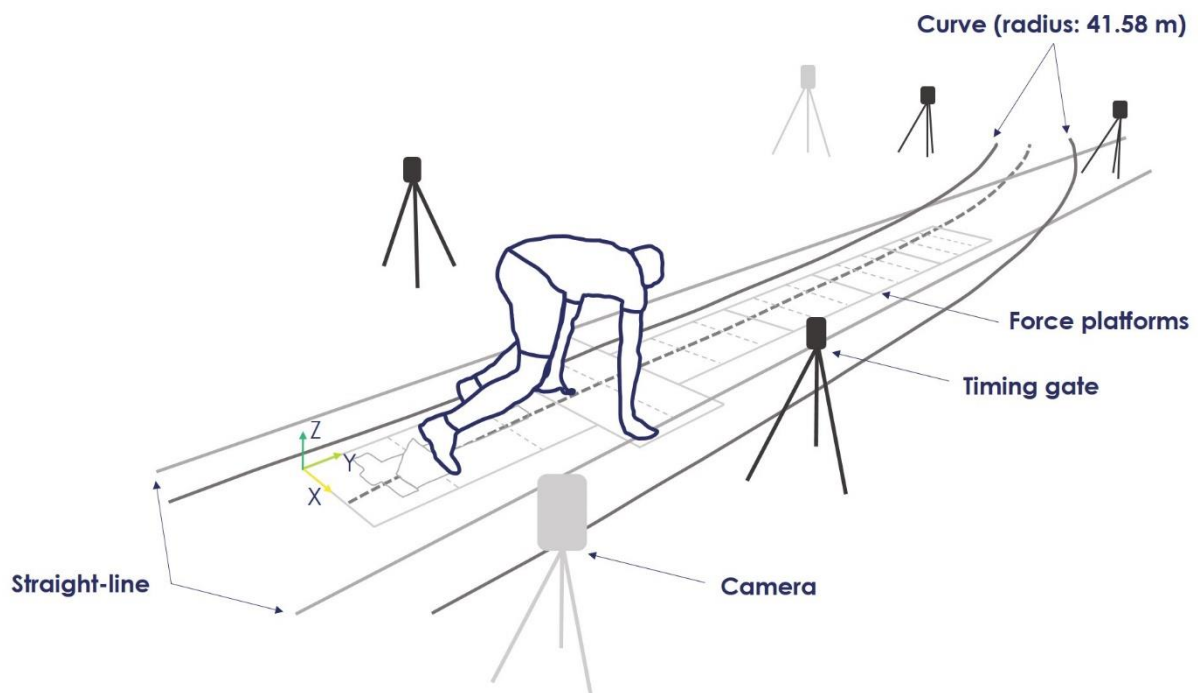


Figure 25. Graphical representation of the experimental set-up for the curve sprinting condition showing the force platforms, the straight-line and the curve lanes, two video cameras (light grey on the tripods) and the timing gates (dark grey on the tripods). For the straight-line condition, the top right corner timing gate was moved outside of the straight-line lane and placed such at 10 m from the starting timing gates.

4. Synchronization

The data originating from the FP, the sEMG and the MIMU-based systems were all time-synchronized to the nearest MIMU-based system frame (thus $\pm 1/240$ s) using a customized cable. With this setup, the FP were the masters while the MIMU-based and the sEMG systems were the slaves. Using this methodology, 2 new channels were added to the FP in complement to the 6 already existing on the 6 FP. The FP recordings began first, with the MIMU-based system and sEMG softwares following (see figure 26; steps 1, 2, 3 & 4).

1. Synchronization between kinematics and kinetics

In order to synchronize the FP and the MIMU-based systems, we connected a BNC cable to the Awinda, sync station (Xsens Technologies, Enschede, Netherlands) on one hand and to the 7th FP channel on the other hand. The beginning and the end of the MIMU-based system recordings both emitted a falling edge to the Kistler software, temporally indicating when the MIMU-based system was initiated (see figure 26, steps 2 & 4).

2. Synchronization between electromyography and kinetics

In order to synchronize the FP and the sEMG systems, we connected a second BNC cable to the Delsys Trigno Module (Delsys INC. Boston, USA) on one hand and to the 8th FP channel on the other hand. The beginning of the sEMG system recordings emitted a falling edge, temporally indicating when the sEMG system was initiated (see figure 26 steps 3 & 5).

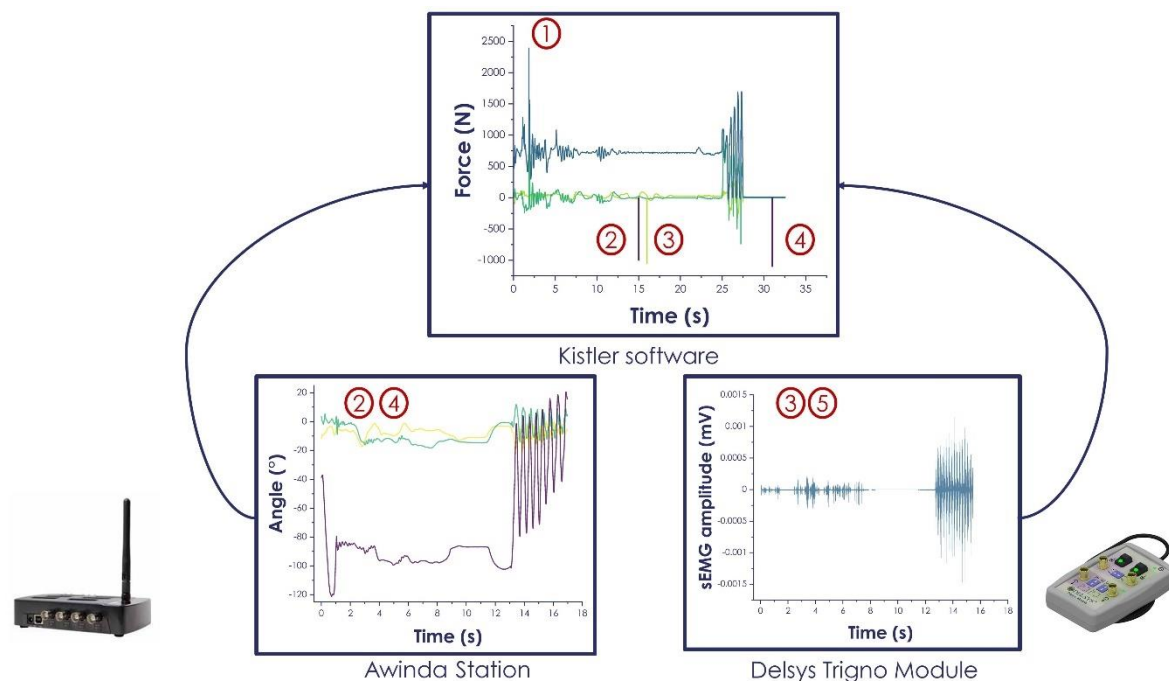


Figure 26. Illustration of the synchronization setup used in the present study. 1. The force platforms' recording is initiated; 2. The magneto-inertial measurement units'(MIMU)-based system recording is initiated. On the top figure, we can see the dark purple falling edge of the synchronization pulse originating from the MIMU-based system; 3. The surface electromyography (sEMG) system recording is initiated. On the top figure, we can see the light green falling edge of the synchronization pulse originating from the sEMG system; 4. At the end of the sprint, the MIMU-based system recording is terminated. On the top figure, we can see the second dark purple falling edge of the synchronization pulse. 5. The sEMG recording is terminated, yet, this does not send any falling edge to the Kistler software.

Synchronization between devices was confirmed during pilot testing by gently pressing on one MIMU positioned over the FP and by checking the temporal events of the F_V and the vertical MIMU acceleration.

5. Data processing

The entire data processing described in the following paragraphs was realized using a customized Matlab (R2017b MathWorks Inc. Natick, MA, USA) script.

1. Timing gates

Sprinting performance (expressed in s) over the different sprints corresponded to the elapsed time over each distance measured with the two pairs of timing gates.

2. Conversion to .c3d file

With the time-synchronization between each system, we created .c3d files that gathered the GRF, the kinematics and the sEMG raw signals using the Biomechanical toolkit github (0.3.0). After the 3 systems were time-synchronized, we analyzed each system's data from each sprint that correspond to the stances that were on the FP. For example, according to the figure 26, the GRF were recorded for the starting blocks pushing phase and until the 4th stance. Thus, for this sprint, we analyzed the GRF, the kinematics and the sEMG from the starting blocks pushing phase and until the 4th stance.

3. How to choose the filtering cut-off frequency: an example with the ground reaction forces

Usually, when a raw data is recorded, it necessitates appropriate filtering in order to remove the signal noise (see figure 27). The cut-off frequency chosen for the filter can strongly influence the signal and the processing that follows (see figure 27). Thus, it is of great importance to appropriately decide which cut-off frequency to choose.

In order to illustrate the impact of the cut-off frequency chosen, we provide an example detailing the different steps to choose the cut-off frequency using the GRF data collected in the present experimentation (see the figures 27 and 28). We can see on the figure 27 that the filtered signals strongly differ depending on the cut-off frequency used for the filter applied to the raw signal. With a 10-Hz cut-off frequency, the signal is completely changed and looks like a sine wave (see the yellow curve on the figure 27). On the other hand, with a cut-off frequency of 200 Hz (the dark blue

curve on the figure 27), the signal nature of the raw data is unchanged, yet the signal noise is smoothed (see figure 27, panel B).

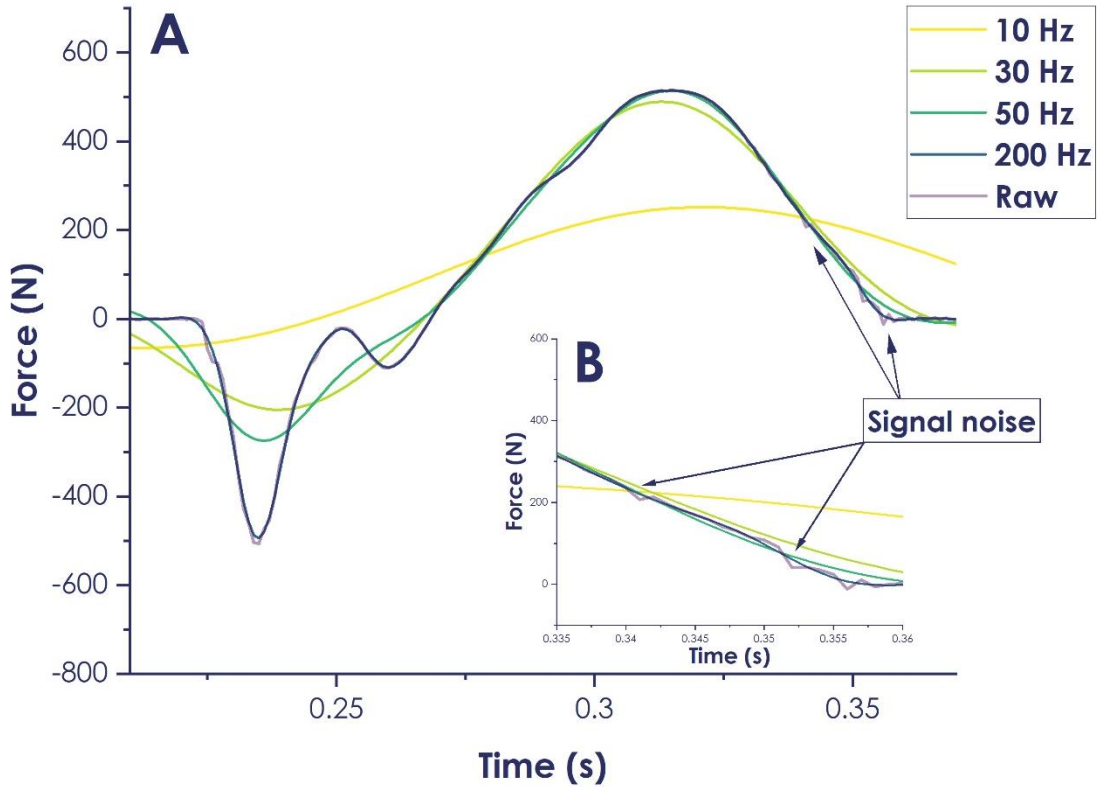


Figure 27. The panel A shows an example of the raw antero-posterior signal and the filtered antero-posterior signals with cut-off frequencies of 10, 30, 50 & 200 Hz with a third-order Butterworth filter. The arrows point out the signal noise on the raw data. The panel B zooms in around the signal noise area.

Nonetheless, the signal shape is not the only indicator to follow for an appropriate cut-off frequency choice. According to Winter (2009), one of the most common method requires a “residual analysis of the difference between the filtered and the unfiltered signals over a wide range of cut-off frequencies”. This method was used for the choice of the cut-off frequencies that were applied to the raw data retrieved from the MIMU-based system, the FP and the sEMG. With this method, the residuals were calculated for a signal of N sample points in time at each cut-off frequency, as follows:

$$R(f_c) = \sqrt{\frac{1}{N} \sum_{i=1}^N (X_i - \hat{X}_i)^2} \quad (4)$$

Where f_c is the cut-off frequency of the 3rd order dual-pass filter, X_i is the raw data at the i th sample and \hat{X}_i corresponds to the filtered data at the i th sample using a 3rd order zero-lag filter.

The left panels of the figure 28 show the residuals (in N) of a participant's F_V , F_{A-P} and F_{M-L} (averaged over 3 successive stances) depending on the cut-off frequency chosen with a 10-Hz step. From those charts, we can visually see that the change in the residuals from one cut-off frequency to the following one (with a 10-Hz step) becomes trivial after respectively ~ 120 Hz, ~ 150 Hz and ~ 200 Hz for the F_V , F_{A-P} and F_{M-L} .

The right panels of the figure 28 on the other hand display the comparison of the mean F_V , F_{A-P} and F_{M-L} over the same 3 stances depending on the cut-off frequency chosen with a 10-Hz step. The mean raw F_V was 830.12 N. On the other hand, the mean F_V with cut-off frequencies of respectively 50, 100 and 200 Hz were 829.58, 830.14 and 830.10 N, respectively. This means that, the differences in the mean F_V between the raw data and each of the cut-off frequency became trivial starting from ~ 50 Hz. Consequently, starting from ~ 50 Hz, an increase in the cut-off frequency will result in trivial changes in the mean F_V . For the F_{A-P} , the differences between the raw and the filtered signals became $<0.50\%$ after a cut-off frequency of ~ 100 Hz. Finally, for the F_{M-L} , the differences between the raw and the filtered data dropped below $<0.50\%$ at a cut-off frequency of ~ 200 Hz.

Overall, both the residuals and the mean F_V , F_{A-P} and F_{M-L} differences became trivial between one cut-off frequency and the subsequent one starting from ~ 200 Hz. Those findings mean that, a cut-off frequency of 200 Hz or higher will not affect neither the residuals nor the mean GRF. Consequently, either cut-off frequency starting from 200 Hz can be chosen. Thus, in the present experimentation, we decided to filter the GRF raw signals with a low-pass, third-order zero-phase, Butterworth filter with a cut-off frequency of 200 Hz which is also consistent with previous experimentations utilizing the same FP (Morin, Slawinski, et al., 2015; Rabita et al., 2015; Samozino et al., 2016).

The same methodology was applied to the other variables computed from the other systems and the table 5 shows the cut-off frequencies chosen for all the parameters analyzed in the **studies #1, #2, #3 & #4**.

Table 5. Cut-off frequencies chosen after residual analysis for the filters applied to the raw signal in the different studies.

	Study #1	Studies #1 & #2	Study #3	Study #4
Parameters	$V_{V\ MIMU}, V_{A-P\ MIMU}$ & $V_{M-L\ MIMU}$	F_V, F_{A-P} & F_{M-L}	Hip, knee and ankle angles & angular velocities	All muscles
Cut-off frequency	20 Hz	200 Hz	15 Hz	20-450 Hz

4. Events detection

The beginning of the starting blocks pushing phase was defined as the instant when the change in F_V rose above 15 N of the BW (Rabita et al., 2015). The end of the starting blocks pushing phase was defined as the instant when the F_V first dropped below 20 N (Morin et al., 2019). After the starting blocks exit, the sprint events (touchdown and toe-off) were determined using a 20-N threshold on the F_V (Millot et al., 2023; Morin et al., 2019).

5. Stance times

The **starting blocks pushing time** (expressed in ms) was computed as the elapsed time between the beginning of the starting blocks pushing phase and the starting blocks exit. Afterwards, the **stance times** (expressed in ms) were computed as the elapsed time from the ipsilateral touchdown to the ipsilateral following take-off. The **swing times** (expressed in ms) on the other hand corresponded to the elapsed time from the take-off to the following ipsilateral touchdown. The **SF** (expressed in Hz) was defined as the number of steps per second and was computed as follow:

$$\text{Step frequency} = \frac{1}{\text{Stance time} + \text{Swing time}} \quad (5)$$

Finally, we averaged the **stance times**, the **swing times** and the **SF** over each distance (see figure 21) by making difference between the left and the right steps.

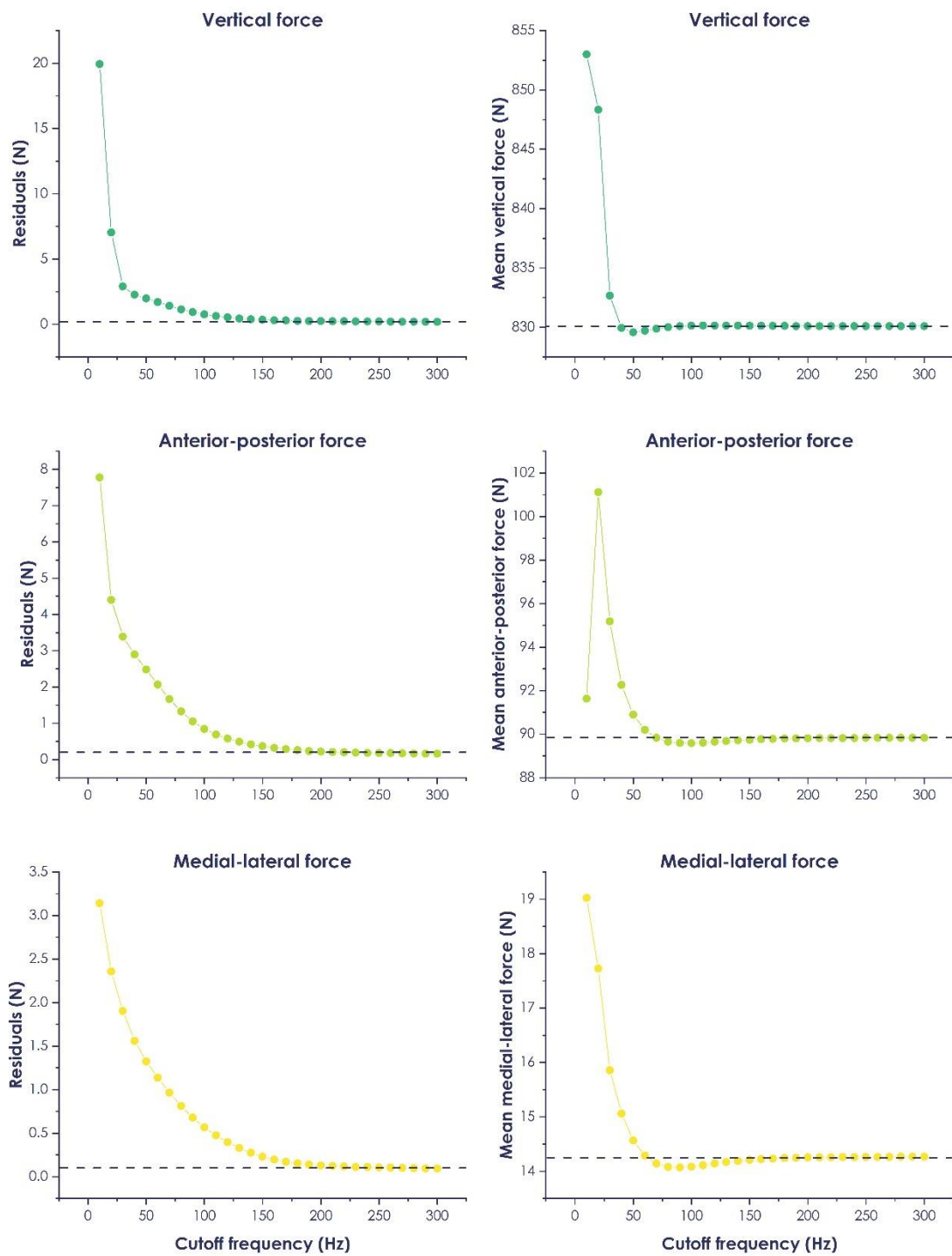


Figure 28. The left panels correspond to the plots of the residuals between the raw vertical, antero-posterior and medial-lateral ground reaction forces (GRF) and the filtered signals over 3 stances as a function of the filter cut-off frequency. For each panel, the horizontal dotted line corresponds approximately to the “stability point”. This means that starting from this cut-off frequency, choosing a higher cut-off frequency will result in negligible changes in the residuals. The right panels show the change in the mean vertical, antero-posterior and medial-lateral GRF over 3 stances as a function of the filter cut-off frequency. The horizontal dotted line also corresponds to the “stability point”, meaning that an increase in the cut-off frequency will not affect the mean GRF starting from this point.

6. Study 1: Comparison of the centre of mass velocity between a reference system and a MIMU-based system

1. Protocol

For the **study #1**, we only processed the 10-m sprints (corresponding to the 0-6 m distance on the FP; see figure 21) as we wanted to compare the V_{CM} between the FP and the MIMU-based system when the initial velocity was null and did not require an integration constant (*i.e.*, when the participants started from the starting blocks on the FP, with a stationary position). Indeed, for the 15-, 20-, 30- and 40-m sprints, the participants began their sprint outside of the FP and the initial conditions when entering the FP were not 0 which required an integration constant. In addition to that, for the analysis, the stances kept corresponded to all the consecutive “valid” stances. For example, if the participant A had the first four stances “valid”, they were all kept for analysis. In contrast, if the participant B had the first two stances “valid”, the third stance landed outside the FP and the fourth was “valid”, only the first two stances were kept for further analysis. The fourth stance was discarded as an integration constant was needed.

2. Global and local coordinate systems

Despite both the FP and the MIMU-based system axes were supposed to be aligned, it is very unlikely that they remain perfectly aligned due to sensors drift (Millot et al., 2023). Consequently, we computed the norm of the horizontal plane of the FP and the MIMU-based systems (V_{HFP} and V_{HMIMU} , see below for the computation details).

3. CM velocity computation using the force platforms

The instantaneous F_V , F_{A-P} & F_{M-L} (in N) were low-pass filtered, 200-Hz cut-off frequency, third-order zero-phase Butterworth filter chosen after residual analysis (Winter, 2009). Based on Newton's Second Law and according to previous literature (Cavagna, 1975; Elftman, 1939; Eng & Winter, 1993; Maus et al., 2011; Pavei et al., 2017, 2020; Rabita et al., 2015; Samozino et al., 2016) the three CM orthogonal instantaneous acceleration components (A_V , A_{A-P} and A_{M-L} , respectively, in $m \cdot s^{-2}$) were calculated by dividing the GRF by the body mass ($-m \cdot g$ for the A_V). Thereafter, we computed the instantaneous antero-posterior (V_{A-PFP}) and medial-lateral (V_{M-LFP}) velocities (in $m \cdot s^{-1}$) by integration of A_{A-P} and A_{M-L} , respectively, over each stance:

$$V_{A-P FP} = V_{0A-P FP} + \int \frac{F_{A-P}}{m} dt \quad (6)$$

$$V_{M-L FP} = V_{0M-L FP} + \int \frac{F_{M-L}}{m} dt \quad (7)$$

with m the participant's body mass (in kg), $V_{0V FP}$, $V_{0A-P FP}$ and $V_{0M-L FP}$ the initial velocity conditions (in $m \cdot s^{-1}$) taken as integration constants and set to 0 since the starting blocks were placed over the FP and the participants started from a stationary position. Afterwards, we computed the norm of the horizontal plane of the FP V_{CM} ($V_{H FP}$, in $m \cdot s^{-1}$):

$$V_{H FP} = \sqrt{V_{A-P FP}^2 + V_{M-L FP}^2} \quad (8)$$

Finally, the instantaneous vertical velocity ($V_{V FP}$, in $m \cdot s^{-1}$) was computed as follows:

$$V_{V FP} = V_{0V FP} + \int \frac{F_V - m \cdot g}{m} dt \quad (9)$$

The norm of the horizontal plane V_{CM} ($V_{H FP}$) and the vertical V_{CM} ($V_{V FP}$) were averaged over each "valid" stance.

4. MIMU-based CM velocity computation

The MIMU-based system's vertical, antero-posterior and medial-lateral instantaneous V_{CM} (respectively $V_{V MIMU}$, $V_{A-P MIMU}$ and $V_{M-L MIMU}$, in $m \cdot s^{-1}$) were retrieved directly from the MVN software. After data extraction, the $V_{V MIMU}$, the $V_{A-P MIMU}$ and the $V_{M-L MIMU}$ were low-pass filtered, 20-Hz cut-off frequency, third-order zero-phase Butterworth filter chosen after residual analysis (Winter, 2009). The whole process followed to determine the cut-off frequency was similar to that described in section 5.3.

Thereafter, we computed the norm of the horizontal plane of the MIMU-based system V_{CM} ($V_{H MIMU}$, in $m \cdot s^{-1}$):

$$V_{H MIMU} = \sqrt{V_{A-P MIMU}^2 + V_{M-L MIMU}^2} \quad (10)$$

Similar to the FP computation, the norm of the horizontal plane V_{CM} computed with the MIMU-based system ($V_{H MIMU}$) and the vertical V_{CM} ($V_{V MIMU}$) were averaged over each "valid" stance.

5. Data analysis

The mean V_{VFP} and V_{VMIMU} on one hand and the mean V_{HFP} and V_{HMIMU} on the other hand were computed over the same stances and compared between systems in the straight and in the curve.

The analysis was split within two conditions: a) the **starting blocks** (from the beginning of the starting blocks pushing phase to the starting blocks exit) and b) the **0-6 m phase** (from the first touchdown after the starting blocks pushing phase to the take-off of the last stance computed).

7. Study 2: Are the ground reaction forces altered by the curve and with the increasing sprinting velocity through the transition phase?

1. Protocol

For the **study #2**, the GRF from the 10-, 15-, 20-, 30- and 40-m sprints were used for the data processing.

2. Global coordinate system rotation

In the straight, the experimentations generally assume that the antero-posterior component (Y_{FP1} on the panel A of figure 29) of the FP GCS is aligned with the straight-line lane (dark blue lines on the panel A of the figure 29) (Colyer et al., 2018; Hunter et al., 2005; Kawamori et al., 2013; Morin, Slawinski, et al., 2015; Morin et al., 2019; Nagahara & Salo, 2018; Rabita et al., 2015; Samozino et al., 2016). In our study, the antero-posterior component of the FP used was also aligned with the straight-line lane (figure 29 panel A). In the curve, we applied the same assumption and aligned the antero-posterior component of the GCS (Y'_{FP} on the panel B of figure 29) to the curve lane. For that sake, we calculated the angle between the straight-line lane and the curve along the FP area every 10 cm using the DLT method (Abdel-Aziz & Karara, 1971).

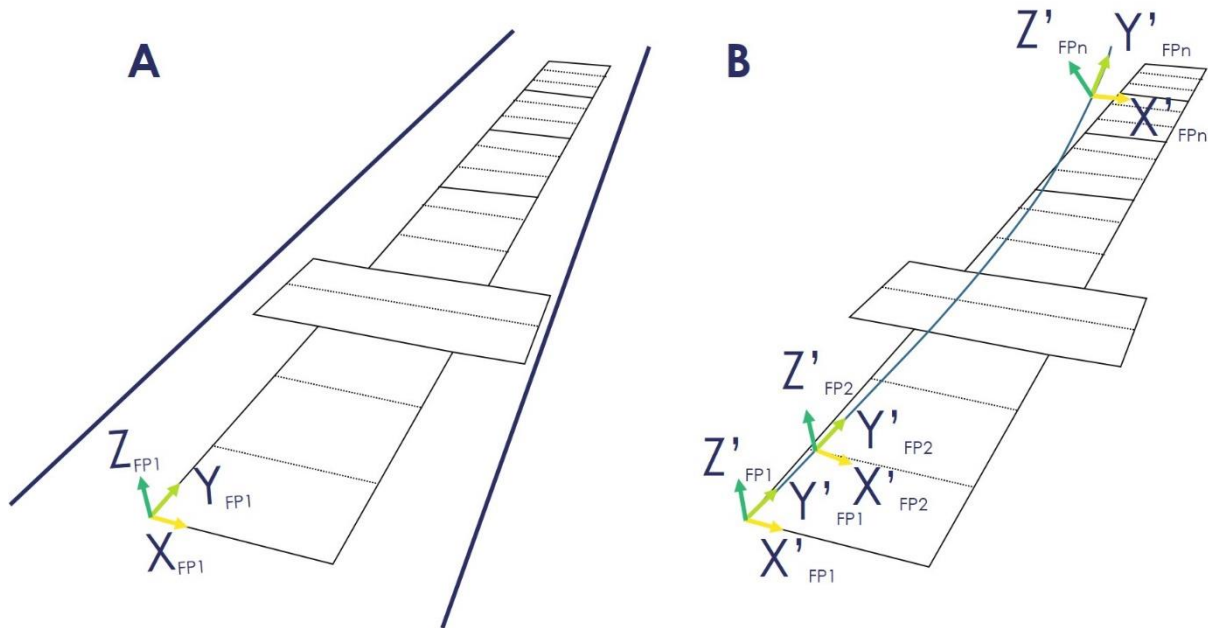


Figure 29. Panel A. In the straight, the force platforms' (FP) antero-posterior axis (Y_{FP}) is aligned with the straight-line lane (in dark blue). Panel B. In the curve, the FP's Y_{FP} (Y'_{FP1} , Y'_{FP2} , ..., Y'_{FPn}) was also aligned with the lane. For that sake, the FP's global coordinate system was rotated at each FP's areas (dashed lines) about the vertical axis.

3. Determination of the angle between the straight and the curve

The DLT technique is a video analysis method that consists on reconstructing points in space based on their 2D position in at least two different planes. In our study, these two planes correspond to two different camera views (see figure 30). This technique has been theorized by Abdel-Aziz & Karara (1971) and consists on two successive steps.

- **Calibration:** For the calibration, we positioned 18 retro-reflective markers (dark blue dots on figure 30 panels A & B) on known position corresponding to each corner of the 6 FP (see the points' coordinates between brackets next to each dark blue dot in figure 30 panel A & B). These positions were known thanks to the FP dimensions. Afterwards, each retro-reflective marker's LCS was obtained with manual digitation in each camera view (using Kinovea 0.9.5). This made it possible to compute the 11 relevant DLT parameters defining our DLT set up and calibration (Abdel-Aziz & Karara, 1971).
- **Analysis:** Following the calibration process, 78 retro-reflective markers (small dark blue dots in figure 30 panel B) were positioned at each ~0.10 m on the inside lane of the reconstructed curve (see figure 30 panel B) and filmed using two cameras (iPhone 11, Apple, California, USA). Each marker coordinate was then manually digitized on each camera view using Kinovea (0.9.5).

After the manual digitation, the angle θ between a vector following the FP antero-posterior axis (the black arrow) and the reconstructed curve (the blue arrow) with a radius of 41.58 m for each 0.10-m segment (see figure 31) was computed.

The angle evolution was approximatively $\sim 0.2^\circ$ for each 0.10 m. As each FP is 1.20-m long (except the second FP positioned perpendicularly that is 0.60-m long), each FP was then sub-divided within three 0.40-m long areas (except for the FP positioned perpendicularly, divided within two 0.30-m long areas), with an angle variation between two subsequent areas $< 0.8^\circ$.

Within an area, as the angle change between the proximal and the distal 0.10 m sub-areas was $< 0.8^\circ$ and as this will have small effects on the cosine and sine functions in the rotations matrices used to compute the GRF (Glaister et al., 2007), we decided to gather 4 successive 0.10 m areas.

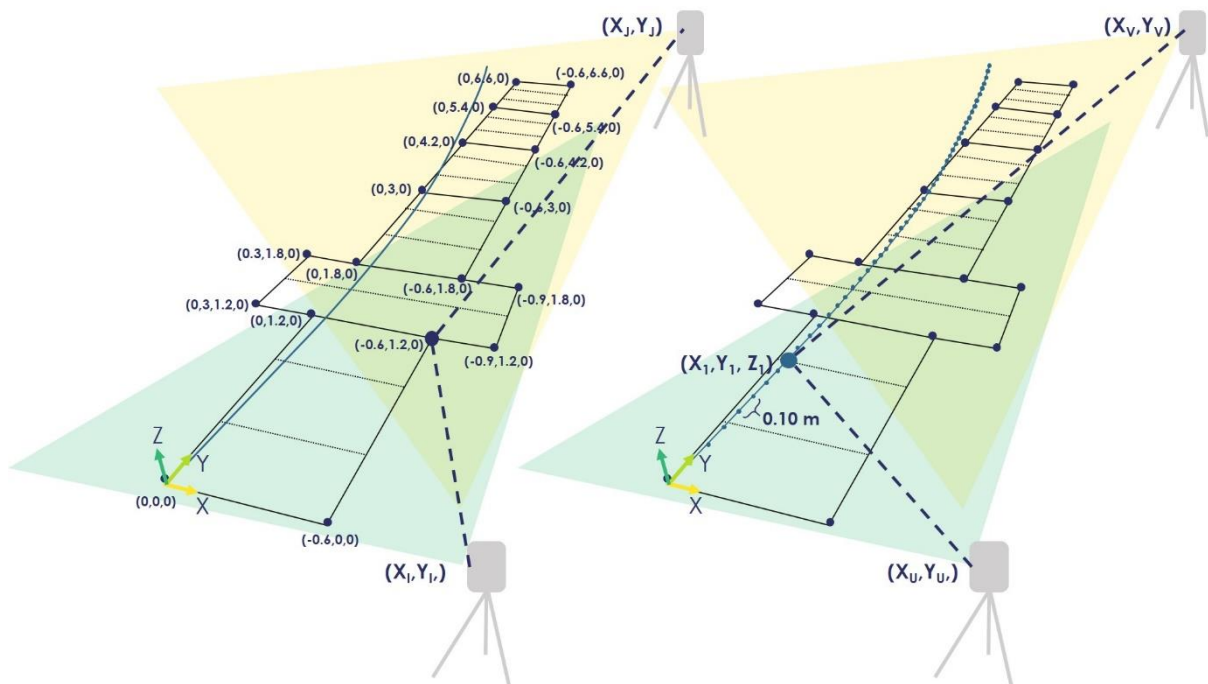


Figure 30. Representation of the setup used for the Direct Linear Transformation method. The panel A shows the calibration step where 18 retro-reflective markers (dark blue) are positioned on know coordinates and filmed by two cameras (light grey on tripods). The panel B shows 78 retro-reflective markers (blue) positioned along the inner lane (radius = 41.58 m) and filmed by the two same cameras. On each panel, the dark dashed lines correspond to the separation of each force platform's areas.

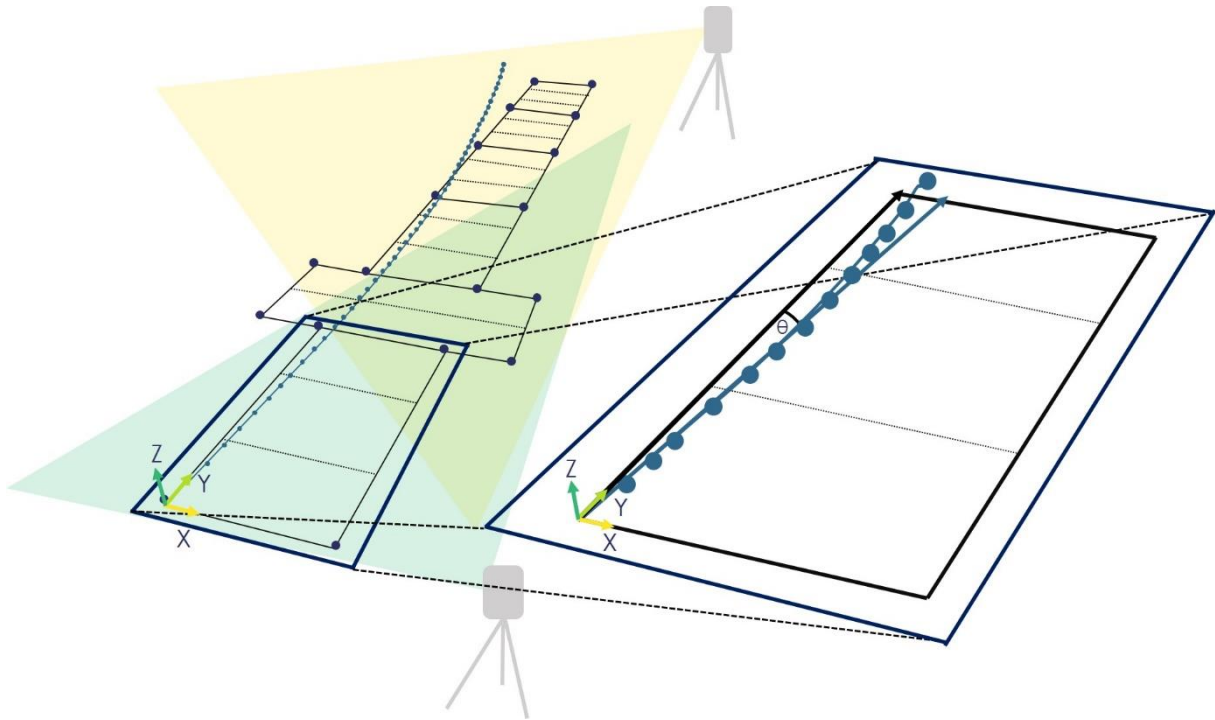


Figure 31. Graphical representation of the angle between the force platforms' (FP) global coordinate system and each zone's vector. The right-hand side of the figure is a zoom in of the first FP. The angle θ corresponds to the angle between the Y-axis of the FP (black arrow) and the curve (blue arrow). On each panel, the dark dashed lines correspond to the separation of each force platform's areas.

4. Rotating the global coordinate system

For each participant, the area of the FP on which the foot landed was checked with the video footages. Afterwards, at each stance, the FP GCS was aligned with the sprinting path by rotating F_{A-P} and F_{M-L} about the vertical axis (Glaister et al., 2007) for each area (see equation 11) using the angle θ that corresponds to the area where the foot landed (determined using the two video cameras):

$$\begin{bmatrix} F'_{A-P} \\ F'_{M-L} \end{bmatrix} = \begin{bmatrix} \cos \theta & \sin \theta \\ -\sin \theta & \cos \theta \end{bmatrix} \begin{bmatrix} F_{A-P} \\ F_{M-L} \end{bmatrix} \quad (11)$$

Where F_{A-P} and F_{M-L} are GRF outputs from the FP, F'_{A-P} and F'_{M-L} correspond respectively to the rotated F_{A-P} and F_{M-L} at each stance. For clarity sake, F'_{A-P} and F'_{M-L} will be referred to F_{A-P} and F_{M-L} respectively for the rest of this manuscript. The same process was applied for each zone, with the angle θ changing depending on the zone where the participant's foot landed.

5. GRF forces

Similar to the **study #1**, the instantaneous F_{TOT} , F_V , F_{A-P} & F_{M-L} (in N) were low-pass filtered, 200-Hz cut-off frequency, third-order zero-phase Butterworth filter chosen after

residual analysis (Winter, 2009). For either sprinting condition, F_{TOT} , F_V , F_{A-P} and F_{M-L} were averaged over each “valid” stance and expressed relative to the body mass (thus expressed in $N \cdot kg^{-1}$) with distinction being made between the left and the right limbs. Thereafter, F_{TOT} , F_V , F_{A-P} and F_{M-L} were averaged over each zone. As an example, a participant performing a 10-m sprint had 4 valid stances after the starting blocks exit with the left foot in contact with the ground during the stances 1 and 3; and the right foot in contact with the ground for the stances 3 and 4. Thus, the mean left F_{TOT} , F_V , F_{A-P} and F_{M-L} at 0-6 m corresponds to the mean F_{TOT} , F_V , F_{A-P} and F_{M-L} over the 2 left stances. On the other hand, the mean right F_{TOT} , F_V , F_{A-P} and F_{M-L} at 0-6 m corresponds to the mean F_{TOT} , F_V , F_{A-P} and F_{M-L} over the 2 right stances.

6. Stance times

The stance times were computed as the elapsed times between the touchdown and the following take-off.

7. GRF impulses

The IMP_{TOT} , the IMP_V , the IMP_{A-P} and the IMP_{M-L} were computed over the same stances as described above by integrating the GRF over each stance duration using the trapezium rule. IMP_V was computed by subtracting the impulse due to BW:

$$IMP_{TOT} = \int_0^t F_{TOT} dt \quad (12)$$

$$IMP_V = \int_0^t (F_V - m \cdot g) dt \quad (13)$$

$$IMP_{A-P} = \int_0^t F_{A-P} dt \quad (14)$$

$$IMP_{M-L} = \int_0^t F_{M-L} dt \quad (15)$$

Similar to the GRF forces, the impulses were averaged over the different sprinting zones and distinction was also made between left and right stances. The impulses were normalized to body mass (thus expressed in $m \cdot s^{-1}$), in order to reflect the changes in the V_{CM} (Churchill et al., 2016; Hunter et al., 2005; Judson et al., 2019; Kawamori et al., 2013; Morin, Slawinski, et al., 2015).

8. Data analysis

The mean **sprinting performance**, F_{TOT} , F_V , F_{A-P} and F_{M-L} , **stance times**, IMP_{TOT} , IMP_V , IMP_{A-P} and IMP_{M-L} over the **starting blocks pushing phase** and at **0-6 m**, **8-14 m**, **14-19 m**, **24-29 m** and **34-39 m** were used for further analysis and compared between the straight and the curve.

8. Study 3: Are the lower limb joint kinematics altered by the curve and with the increasing sprinting velocity through the transition phase?

1. Protocol

For the **study #3**, the lower body kinematic metrics from the 10-, 15-, 20-, 30- and 40-m sprints were selected based on the previous literature discussed in the **literature review** of this manuscript. With the synchronization between systems and using the .c3d files, we have analyzed separately the different variables over respectively the stance and the swing phases.

2. Joint angles and angular velocities

Robert-Lachaine et al. (2017) showed that the hip, the knee and the ankle joints were less sensitive to the errors due to anthropometrical model used. Thus, in the present study, the hip, the knee and the ankle joint angles (in °) and angular velocities (in °·s⁻¹) were directly retrieved from the MVN software. Both the raw joint angles and angular velocities were low-pass filtered, 15-Hz cut-off frequency, third-order zero-phase Butterworth filter chosen after residual analysis (Winter, 2009) following the process developed in the **section 5.3. of the general methodology**. For the present study, we investigated the sagittal plane of motion (see the joint angles' definition in figure 32) only. Indeed, a recent study showed low correlation coefficients of the hip, the knee and the ankle angles between the MIMU-based system and an OS system in the frontal and the transverse planes during jumping and change-of-direction tasks (Nijmeijer et al., 2023).

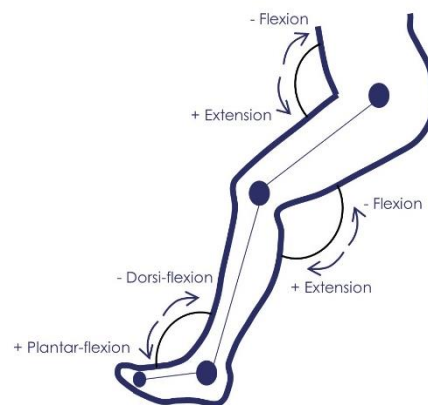


Figure 32. Graphical representation of the hip, the knee and the ankle joint angles' definition.

3. Data analysis

During the **late stance phase**, the **hip peak extension**, the **knee peak extension**, the **ankle peak plantarflexion angle** and **angular velocities** were identified (see figure 33). We chose these angles and angular velocities as they are meaningful in terms of performance as they result from the end of the extensions and plantarflexions during the stance (N. E. Bezodis, Willwacher, et al., 2019).

During the **mid-swing phase**, the **hip** and the **knee peak flexion angles** and **angular velocities** were determined as they relate how the thigh is repositioned forward during the swing. Finally, during the **late swing phase**, where the hamstrings are most susceptible to injury risks (Chumanov et al., 2007, 2012), the **hip** and the **knee peak extension** and the **ankle peak plantarflexion angles** and **angular velocities** were identified (see figure 33). The mean **swing times** and **step frequencies** were also kept for further analyses.

The **hip, knee** and **ankle peak angles** and **angular velocities** as well as the **swing times** and **step frequencies** were compared between the straight and the curve. Similar to the GRF, distinctions were made between the left and right limbs.

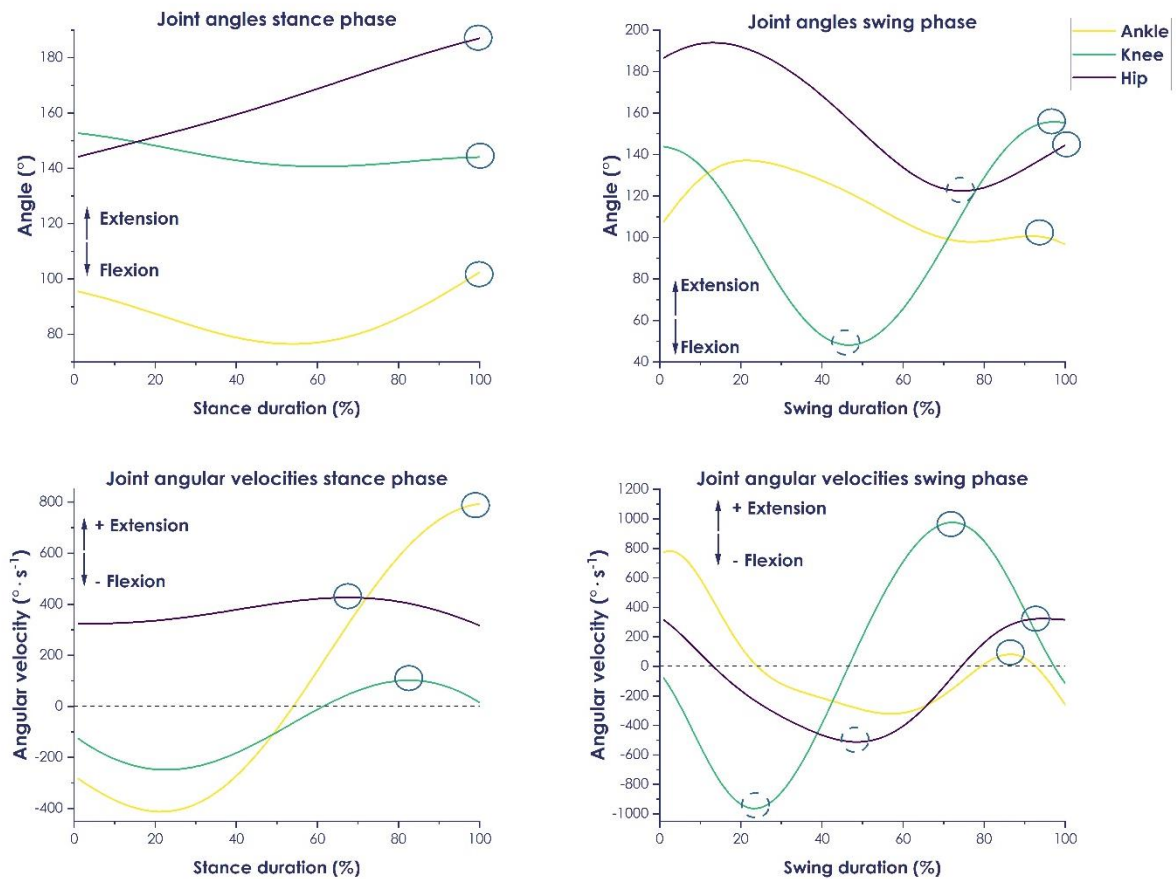


Figure 33. Graphical representation of the hip and knee peak extension and ankle plantarflexion angles and angular velocities (blue circles) and the peak flexion angles and angular velocities (dashed blue circles) computed.

9. Study 4: Are the muscular activities altered by the curve and with the increasing sprinting velocity through the transition phase?

1. Protocol

For the **study #4**, the sEMG from the 10-, 15-, 20-, 30- and 40-m sprints were used for data processing. In order to remove the low-frequency noise associated with electrode movement on the skin; and high-frequency noise associated with baseline drift, the sEMG signals were offline band-pass (20-450 Hz) filtered with a fourth-order zero-lag Butterworth filter and full-wave rectified (Hegyi, Gonçalves, et al., 2019; Higashihara et al., 2018). After visual inspection of each signal, a few channels were excluded from the analysis when clear detection of the event was challenging due to

poor signal detection and baseline noise (see the figure 34 showing an example of a high-quality signal and a low-quality signal).

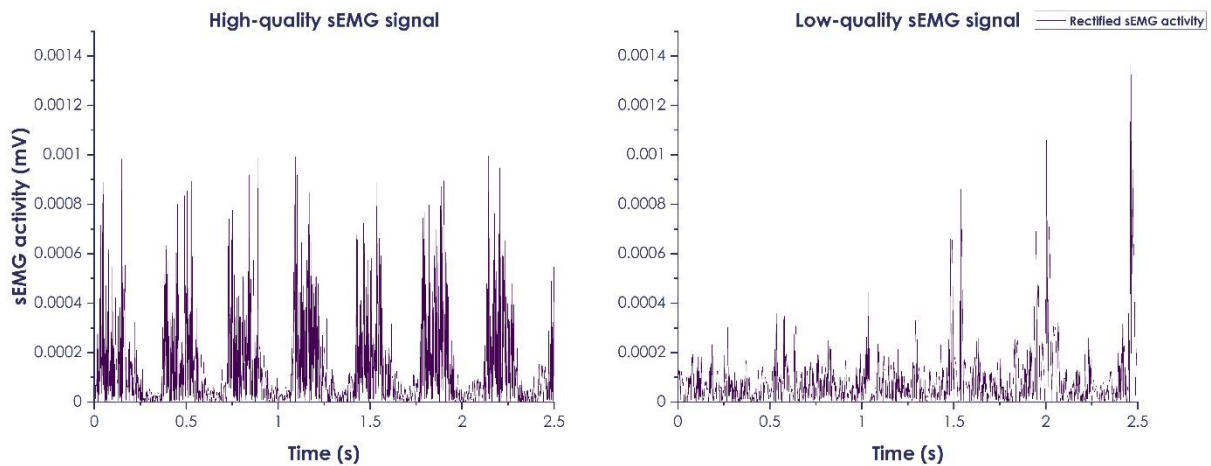


Figure 34. Example of a high-quality surface electromyographic (sEMG) signal (left panel) and a low quality sEMG signal (right panel). In this example, the low-quality sEMG signal would be discarded from the analysis.

2. How to determine whether a muscle is active or not?

Determining whether a muscle is active is a challenge that has engaged numerous debates in the EMG literature. While some experimentations determined the bursts onsets with visual inspection (Clancy et al., 2004; Pinniger et al., 2000), others attempted to reduce the operator-dependent errors by creating computerized algorithms (Hodges & Bui, 1996; Li et al., 2007; Li & Aruin, 2005; Staude et al., 2001; Staude & Wolf, 1999).

After being developed in the early 1990's, the Teager-Kaiser energy operator (TKEO) (Kaiser, 1990, 1993) has been applied to the sEMG signal processing (Li et al., 2007; Li & Aruin, 2005). In 2010, Solnik and his colleagues (Solnik et al., 2010) compared several methods to detect EMG bursts with and without applying the TKEO : "visual detection", "threshold-based" and "approximated generalized likelihood ratio" (AGLR). Overall, the accuracy of the onset detection clearly improved in all methods when the TKEO was applied during the signal processing. In the end, the AGLR method applied to the TKEO was found to yield the more robust burst detection on the EMG signal in comparison to the other methods and should preferentially be used to identify the muscle activity timings.

Thus, in the present study, the onset and offset of each muscle activity during a running cycle, were determined by applying the TKEO method on the rectified sEMG signal (Solnik et al., 2010) (equation 16) with the discrete TKEO ψ defined as:

$$\psi[x(n)] = x^2(n) - x(n + 1)x(n - 1) \quad (16)$$

where x is the EMG value and n is the sample number. Afterwards, the AGLR was applied on the TKEO signal to detect the sEMG bursts whereby two hypotheses were tested using a log-likelihood ratio test $b(n)$:

$$b(n) = \ln \left(\prod_{n=1}^k \frac{p_1(x_n)|H_1}{p_0(x_n)|H_0} \right) \begin{matrix} > \\ < \end{matrix} h \quad (17)$$

Where \ln represents natural logarithm, x_n represents series of EMG samples, p_1 and p_0 represent probability density functions associated with hypotheses H_1 and H_0 respectively. When the log-likelihood $b(n)$ becomes higher than the pre-set threshold h , then the hypothesis H_1 is more probable and a signal change is detected. The AGLR algorithm performs hypothesis testing on a sliding window of a size L , over the series of sEMG data. The log-likelihood ratio is calculated from L samples for every window step. After a signal change is detected, the estimated onset time t_1 is found by maximizing the likelihood estimators for each sample from the last window position (Solnik et al., 2010).

In order to choose the best window size and the best threshold, false detections (see the red arrows on the left panel of the figure 35) must be avoided. In the example of the “threshold too low” (see the left panel of the figure 35), the window size should be increased as well as the threshold in order to remove the false detections. However, if the window size is too high, the detection will resemble to the middle panel of the figure 35. By adjusting the window size and the threshold, the detections eventually look like the “good threshold” as depicted on the right-hand side of the figure 35. In the present study, the window size was set at $L = 43$ ms and the detected threshold was set at $h = 15$.

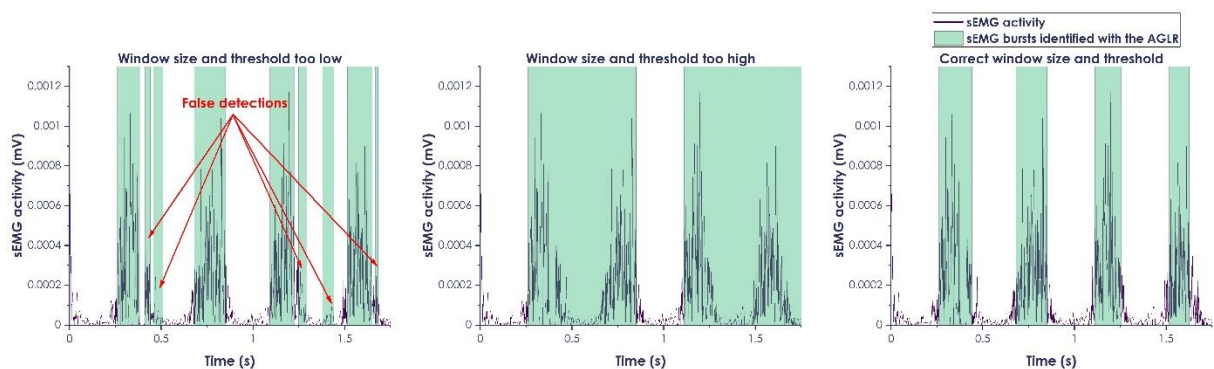


Figure 35. Examples of a) a window size and a threshold set too low inducing false detection (left panel); b) a window size and a threshold set too high; and c) a correct window size and a correct threshold.

After the onset and the offset detections (light green shaded areas in the figure 35), each signal was visually checked to ensure a correct identification was completed. Each muscle was analyzed separately and was considered active from the i th onset to the i th offset of the corresponding muscle. Inversely, each muscle was considered inactive from the i th offset, to the $i + 1$ th onset of the same muscle.

3. Normalization

As previously discussed in the **literature review**, the sEMG signals are often expressed as a normalized value (in %) in order to enable between muscles, between studies and between subjects' comparisons (De Luca, 1997). Such process requires a rescaling to a percentage of a given value (Ball & Scurr, 2013). According to Ball & Scurr (2013), high-velocity movements should be normalized to the task under investigation. Thus, in the present experimentation, we decided to use the straight-line 40-m sprints as the "reference condition" since we compared the curve to the straight.

Further, in order to reduce any potential impact of an outlier on the detection of the greatest muscular activity, we identified the three greatest mean sEMG bursts over the 40-m sprint (dark purple shaded areas in figure 36). Afterwards, we averaged these three greatest mean sEMG bursts. Therefore, in both the straight and the curve, we normalized each burst of sEMG activity to the average of the three greatest mean sEMG bursts (*i.e.*, the reference value) from the 40-m sprints in the straight.

After normalization to the reference value, the mean sEMG activity of the *BFlh*, the *RF*, the *VL* and the *GM* over each burst duration was computed in the straight and in the curve during both the stance and swing phases and distinction was made between left and right stances.

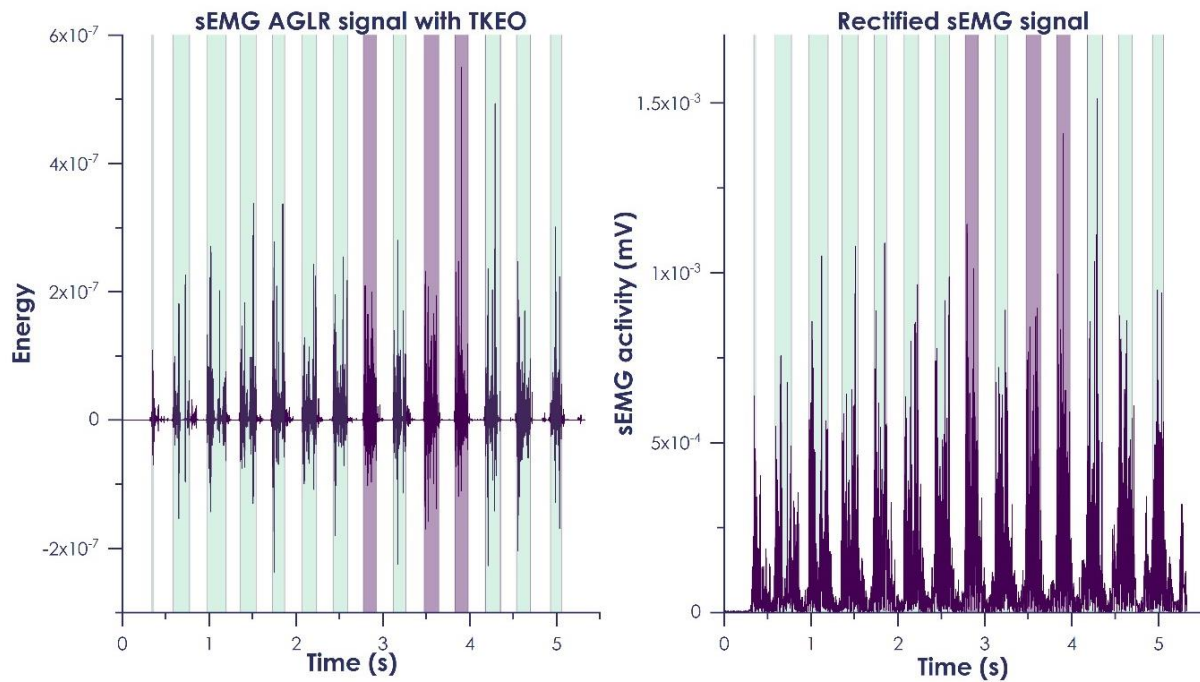


Figure 36. The left panel represents an example of the Approximated Generalized Likelihood Ratio (AGLR) signal from the Gastrocnemius Medialis used to identify each burst of muscle activity. The right panel shows the corresponding rectified surface electromyographic (sEMG) signal. From each identified burst (the light green shaded areas) during the 40-m sprint in the straight, we highlighted the 3 bursts with the greatest mean sEMG activity (dark purple shaded areas) through the 40-m sprint. Finally, the “reference” value was determined as the mean of the 3 greatest mean bursts.

4. Data analysis

After the onset and the offset of each muscle activity were identified, the **sEMG activity durations** were computed for the **BFH**, the **RF**, the **VL** and the **GM** by computing the elapsed times between the onset and the offset of each muscle activity with distinctions made between the **stance** and **swing phases**. In addition to that, the **sEMG activity amplitude** were computed as the mean sEMG activity over each burst both during the **stance** and **swing phases**.

10. Statistical analyses

For the **studies #1, #2, #3** and **#4**, the statistical analyses were performed using JASP (0.15.0.0).

In the **study #1**, the V_{H-L} and the V_V obtained with the FP and the MIMU-based system were compared using a) mean bias (mean differences between systems expressed in % in comparison to the FP) and 95% limits of agreement (Bland & Altman, 1986); and b) Pearson's correlation coefficients (r) with threshold values of 0.3, 0.5, 0.7 and 0.9

representing respectively low, moderate, high and very high relationships (Hopkins et al., 2009; Mukaka, 2012). For all statistical analyses, the alpha level was set as $\alpha = 0.05$. Values are reported as means \pm SD unless otherwise stated.

In the **study #2**, the normal distribution of the data was checked for each variable using the Shapiro-Wilk normality test. During the starting blocks pushing phase, the **starting blocks pushing phase duration** and the **mean F_{TOT} , F_V , F_{A-P} , F_{M-L} , IMP_{TOT} , IMP_V , IMP_{A-P} and IMP_{M-L}** were compared between the straight and the curve using paired t-tests. After the starting blocks exit, the effects of the condition (straight vs curve), the effects of the distance (0-6 m, 8-14 m, 14-19 m, 24-29 m & 34-39 m) and the condition x distance interactions of the **mean F_{TOT} , F_V , F_{A-P} , F_{M-L} , stance times, IMP_{TOT} , IMP_V , IMP_{A-P} and IMP_{M-L}** were tested using two-way analyses of variance (ANOVAs) with repeated measures. The homogeneity and the sphericity (Mauchly's test) were also checked and a Geisser-Greenhouse correction applied when necessary. The effect sizes were described with the omega squared (ω^2 , with $\omega^2 < 0.01$; $\omega^2 > 0.01$; $\omega^2 > 0.06$ and $\omega^2 > 0.14$ indicating respectively trivial, small, medium and large effect sizes). For all the statistical analyses, the alpha level was set as $\alpha = 0.05$. The values are reported as means \pm SD unless otherwise stated.

In the **study #3**, the normal distribution of the data for each variable was checked using the Shapiro-Wilk normality test ($p > 0.05$). Afterwards, a) the **hip** and the **knee peak extension** and the **ankle peak plantarflexion angles**; and b) the **hip** and the **knee peak extension** and the **ankle peak plantarflexion velocities** during the **stance** and the **swing phases**, the **swing times** and the **step frequencies** were compared between the straight and the curve using two-ways ANOVAs with repeated measures where condition (straight vs curve) and distance (0-6 m, 8-14 m, 14-19 m, 24-29 m & 34-39 m) effects and the condition x distance interaction were evaluated. The homogeneity and the sphericity (Mauchly's test) were also checked and a Geisser-Greenhouse correction applied when necessary. The effect sizes were described with the omega squared (ω^2 , with $\omega^2 < 0.01$; $\omega^2 > 0.01$; $\omega^2 > 0.06$ and $\omega^2 > 0.14$ indicating respectively trivial, small, medium and large effect sizes). For all the statistical analyses, the alpha level was set as $\alpha = 0.05$. The values are reported as means \pm SD unless otherwise stated.

In the **study #4**, the normal distribution of the data for each variable was checked using the Shapiro-Wilk normality test ($p > 0.05$). Afterwards, the **sEMG activity timings** and **amplitude** of the **BFlh**, **RF**, **VL** and **GM** during the **stance** and the **swing phases** were compared between the straight and the curve using two-ways ANOVAs with repeated measures where condition (straight vs curve) and distance (0-6 m, 8-14 m, 14-19 m, 24-29 m & 34-39 m) effects and the condition x distance interaction were

evaluated. The homogeneity and the sphericity (Mauchly's test) were also checked and a Geisser-Greenhouse correction applied when necessary. Effect sizes were described with the omega squared (ω^2 , with $\omega^2 < 0.01$; $\omega^2 > 0.01$; $\omega^2 > 0.06$ and $\omega^2 > 0.14$ indicating respectively trivial, small, medium and large effect sizes). For all the statistical analyses, the alpha level was set as $\alpha = 0.05$. The values are reported as means \pm SD unless otherwise stated.

EXPERIMENTAL CONTRIBUTIONS

STUDY 1

Centre of mass velocity comparison using a whole body magnetic inertial measurement unit system and force platforms in well trained sprinters in straight-line and curve sprinting

Associated publication

Millot, B., Blache, P., Dinu, D., Arnould, A., Jusseaume, J., Hanon, C. & Slawinski, J. (2022). Centre of mass velocity comparison using a whole body magnetic inertial measurement unit system and force platforms in well trained sprinters in straight-line and curve sprinting. *Gait Posture*. <https://doi.org/10.1016/j.gaitpost.2022.11.002>

Associated communication

Millot, B., Blache, P., Dinu, D., Arnould, A., Jusseaume, J., Hanon, C. & Slawinski, J. (2022). Centre of mass velocity comparison using a whole body magnetic inertial measurement unit system and force platforms in well trained sprinters in straight-line and curve sprinting. 27th European College of Sport Science, Sevilla, Spain. **Oral communication.**

1. Results

The number of valid stances for each participant varied between two (the starting blocks pushing-phase and the first stance) to five (the starting blocks pushing phase and the following four stances) for both sprinting conditions. Overall, 75 and 73 valid stances were computed respectively for the straight and the curve.

1. Starting blocks pushing phase

The mean $V_{H\ MIMU}$ during the starting blocks pushing phase was in average 0.26 and 2.03% lower than the $V_{H\ FP}$ respectively in the straight and in the curve (see table 6). On the other hand, the mean $V_{V\ MIMU}$ during the starting blocks pushing phase was in average 2.33 and 4.49% lower than the $V_{V\ FP}$ in the straight and in the curve, respectively (see table 6). For the starting blocks pushing phase, the correlation coefficients between both systems were greater than 0.917.

Table 6. Mean \pm SD of the centre of mass velocity with both systems, the variables retrieved from the Bland & Altman plots and the Pearson's correlation coefficients between both systems

		MIMU-based system ($m \cdot s^{-1}$)	FP ($m \cdot s^{-1}$)	Bias (%)	95% Agreement limits	Correlation coefficients
Starting blocks	V_H STR	1.28 \pm 0.14	1.29 \pm 0.14	0.26	(-7.49; 6.97)	0.943
	V_H CUR	1.24 \pm 0.14	1.27 \pm 0.16	2.03	(-10.02; 5.95)	0.957
	V_V STR	0.47 \pm 0.06	0.48 \pm 0.08	2.33	(-15.72; 11.06)	0.917
	V_V CUR	0.44 \pm 0.07	0.46 \pm 0.09	4.49	(-19.34; 10.37)	0.938
0-6 m	V_H STR	4.60 \pm 0.90	4.87 \pm 0.94	5.63	(-11.71; 0.45)	0.990
	V_H CUR	4.43 \pm 0.86	4.76 \pm 0.92	7.29	(-13.77; -0.81)	0.971
	V_V STR	0.21 \pm 0.09	0.21 \pm 0.10	1.44	(-98.63; 95.74)	0.499
	V_V CUR	0.20 \pm 0.09	0.24 \pm 0.08	19.95	(-108.62; 68.71)	0.423

MIMU-based system = Magnetic Inertial Measurement Unit system; FP = Force Platforms; SD = Standard Deviation; STR = Straight-Line sprints; CUR = Curve sprints; V_H = Norm of the horizontal plane of the CM velocity; V_V = CM vertical velocity.

2. 0-6 m

At 0-6 m, the mean $V_{H\ MIMU}$ was in average 5.63 and 7.29% lower than the $V_{H-L\ FP}$ respectively in the straight and in the curve and the correlation coefficients were greater than 0.971 (see table 6). The mean $V_{V\ MIMU}$ was in average 1.44 and 19.95% lower than the $V_{V\ FP}$ respectively in the straight and in the curve. However, the random errors reached 108% and the correlation coefficients between devices were lower than 0.499.

The figure 37 shows an example of the $V_{H\ MIMU}$ - and $V_{H\ FP}$ -time (left panel) and the $V_{V\ MIMU}$ - and $V_{V\ FP}$ -time (right panel) over the starting blocks pushing phase (green area) and the stances between 0-6 m (green shaded area). The mean bias between the MIMU-based system and the FP was lower in the straight than in the curve (see table 6). The table 6 presents the mean \pm SD for the sprint variables as well as the mean bias, 95% agreement limits and correlation coefficients for both systems within the straight and the curve conditions for the starting blocks and at 0-6 m.

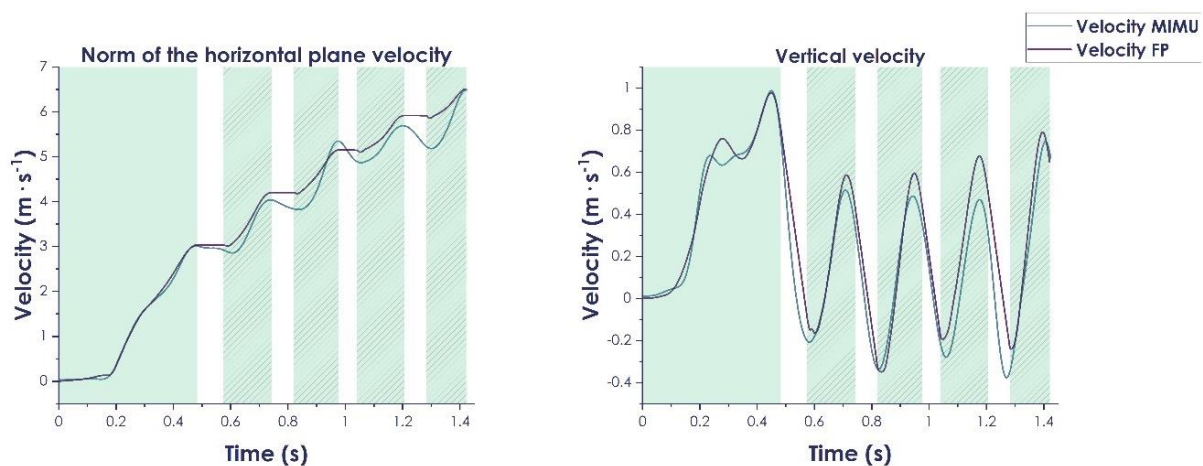


Figure 37. Typical example showing A) the norm of the horizontal plane of the centre of mass (CM) velocity (V_H) and B) the CM vertical velocity (V_V) computed respectively with the force platforms (FP) (purple) and the Magneto-Inertial Measurement Units (MIMU)-based system (blue). The light green area on the left of each panel represents the entire starting blocks phase. The light green shaded areas correspond to the stance phases between 0-6 m.

The figures 38 & 39 present the Bland & Altman plots of the $V_{H\ MIMU}$ and $V_{V\ MIMU}$ mean differences in comparison to the $V_{H\ FP}$ and $V_{V\ FP}$ during respectively the starting blocks pushing phase (see figure 38) and 0-6 m both in the straight and in the curve (see figure 39).

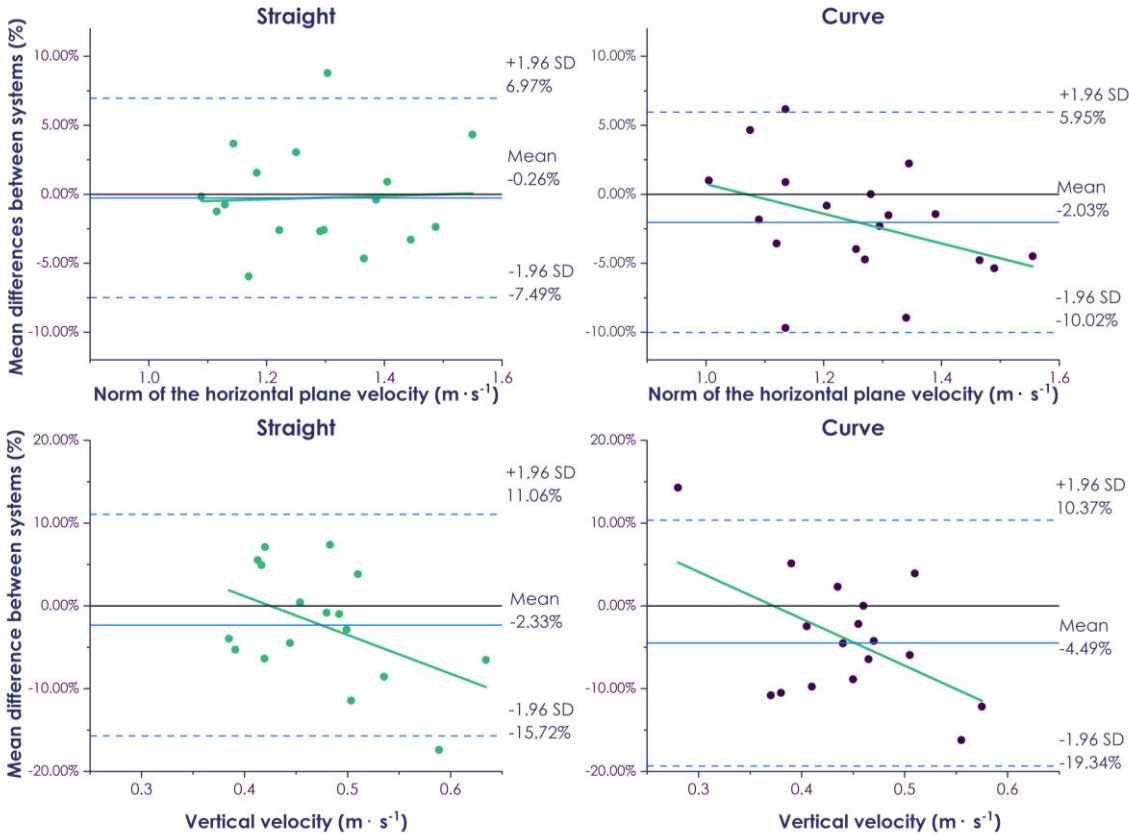


Figure 38. Bland & Altman plots presenting the mean differences (blue horizontal line) and 95% limits of agreement (dashed horizontal lines) between the norm of the horizontal plane velocity computed with the Magneto-Inertial Measurement Units (MIMU)-based system ($V_{H\ MIMU}$) and the force platforms ($V_{H\ FP}$); between the vertical velocity computed with the MIMU-based system ($V_{V\ MIMU}$) and the force platforms ($V_{V\ FP}$) during the starting blocks pushing phase both in the straight (panels on the left) and the curve (panels on the right). The green line is a linear fit from all individual points.

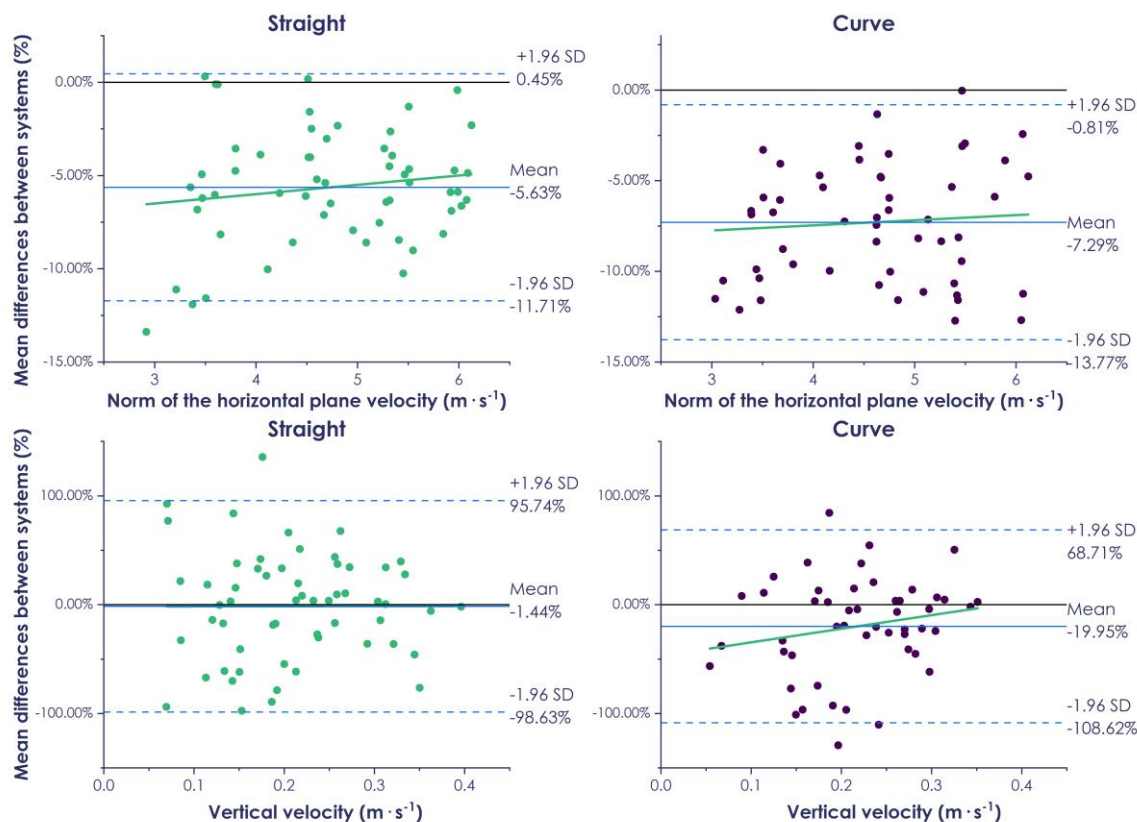


Figure 39. Bland & Altman plots presenting the mean differences (blue horizontal line) and 95% limits of agreement (dashed horizontal lines) between the norm of the horizontal plane velocity computed with the Magneto-Inertial Measurement Units (MIMU)-based system ($V_{H\ MIMU}$) and the force platforms ($V_{H\ FP}$) (panels A & B); between the vertical velocity computed with the MIMU-based system ($V_{V\ MIMU}$) and the force platforms ($V_{V\ FP}$) (panels C & D) for the stances at 0-6 m both in the straight (panels on the left) and the curve (panels on the right). The green line is a linear fit from all individual points.

2. Discussion

This experimentation compared the stance-averaged V_{CM} measured from a commercially available MIMU-based system to that computed from 6 FP over the a) starting blocks pushing phase; and b) the initial 1-to-4 stances that follow the starting blocks exit (between 0-6 m). We compared both the stance-averaged V_{CM} between both systems in the straight-line and in the curve among 19 experienced-to-elite curve sprinters with different anthropometric characteristics, sprinting expertise and mechanical capacities. Overall, the MIMU-based system underestimated by 5-to-7% the $V_{H\ MIMU}$ in comparison to the reference system with narrow random errors (< 14%). On the other hand, the $V_{V\ MIMU}$ showed larger differences up to ~20% in comparison to the reference system, with large random errors (up to ~108%).

1. The starting blocks pushing phase

i. Norm of the horizontal plane velocity

During the starting blocks pushing phase, the $V_{H\ MIMU}$ was close to the $V_{H\ FP}$ (mean bias $\leq 2.03\%$). In addition to that, the correlation coefficients were almost perfect ($r \geq 0.943$) meaning that a change of the $V_{H\ FP}$ magnitude was well associated with a similar change of the $V_{H\ MIMU}$ magnitude in both the straight and the curve. However, in the curve, the mean bias increased with the increasing $V_{H\ MIMU}$ (see figure 38). Consequently, we can consider that the $V_{H\ MIMU}$ can be accurately computed using this MIMU-based system in the straight. In the curve, on the other hand, further experimentations should probably be conducted in order to assess whether this system can be used accurately to compute the $V_{H\ MIMU}$.

ii. Vertical velocity

The $V_{V\ MIMU}$ was also slightly underestimated in comparison to the $V_{V\ FP}$ (mean bias $\leq 4.49\%$) during the starting blocks pushing phase and the correlation coefficients were very large ($r \geq 0.917$). However, the random errors were higher (up to 19.34%). The figure 38 (bottom panels) also suggests that the mean bias would increase with the increasing $V_{V\ MIMU}$ (as represented by the green linear fit). Additionally, despite the mean bias was limited at the group level, large random errors can be found at the individual level and could in turn challenge the data interpretation. Hence, we question the accuracy of this MIMU-based system to compute the $V_{V\ MIMU}$ during the starting-blocks pushing phase, both in the straight and in the curve.

2. 0-6 m

i. Norm of the horizontal plane velocity

During the 0-6 m, the $V_{H\ MIMU}$ mean bias was low in comparison to the reference system (i.e., $V_{H\ FP}$) (5.63 and 7.29% respectively for the straight and the curve). In addition to that, the correlation coefficients for the stance-averaged V_H were very high ($r > 0.971$) between systems. These correlation coefficients show that although slightly underestimated, a change of magnitude of $V_{H\ FP}$ was very well associated with a similar change of magnitude of $V_{H\ MIMU}$.

In addition to that, we did not find any trend for the mean bias between systems to increase with the increasing V_H . In the present study, the V_H reached over the last stances investigated was $\sim 5\text{-}6\ \text{m}\cdot\text{s}^{-1}$ which correspond to $\sim 60\text{-}70\%$ of the participants' $V_{A-P\ MAX}$. Those findings suggest that differences between systems would not increase

with velocity although further experimentations evaluating V_H later on during the transition phase or at $V_{A-P MAX}$ are needed to confirm our findings.

ii. Vertical velocity

Contrastingly, the $V_{V MIMU}$ showed a greater mean bias (up to ~20%) with large limits of agreement (up to ~108%) in comparison to the $V_{V FP}$. Additionally, the small correlation coefficients ($r \leq 0.499$) between both systems attest that a change of magnitude in the $V_{V FP}$ was poorly associated with a similar change of magnitude in the $V_{V MIMU}$ during the 0-6 m section of the sprint. Consequently, this MIMU-based system should not be used to compute the $V_{V MIMU}$ in overground sprinting with maximal effort.

3. Comparison to the literature and in-field application

The present experimentation's findings for $V_{H FP}$ over the starting blocks and the first stances were slightly below those reported by Nagahara et al. (2020) among male sprinters (100-m time PBs: 11.27 ± 0.27 s, corresponding to an average of 808 points at the IAAF scoring table) (Nagahara et al., 2020). In their experimentation, Nagahara et al. (2020) found a $V_{A-P FP}$ of respectively 3.92, 4.93, 5.70 and 6.30 $\text{m} \cdot \text{s}^{-1}$ for the first, second, third and fourth stances following the starting blocks pushing phase (Nagahara et al., 2020) while we found a $V_{H FP}$ of respectively 3.59, 4.62, 5.36 and 6.02 $\text{m} \cdot \text{s}^{-1}$ for the corresponding stances. Hence, considering the participants' PBs in both studies (in our study, the mean participants' PBs corresponded to 823 points at the IAAF scoring table) and that all the participants were male in Nagahara et al.'s (2020) experimentation, we can consider that our findings are in line with those of Nagahara et al. (2020). Regarding the $V_{V FP}$, to our knowledge, no experimentation investigated the stance-average $V_{V FP}$ over the first stances of a sprint. Slawinski et al. (2010) found a V_V of 0.52, 0.35 and 0.35 $\text{m} \cdot \text{s}^{-1}$ among elite sprinters using an OS respectively at the end of the starting blocks exit and at the first and second stances' toe-off (Slawinski, Bonnefoy Mazure, Levêque, et al., 2010) while we found a mean $V_{V FP}$ of 0.44, 0.19 and 0.24 $\text{m} \cdot \text{s}^{-1}$ for the corresponding stances.

To the best of our knowledge, only one study compared the step velocity between a MIMU-based system and FP during a 50-m sprint (van den Tillaar et al., 2021). These authors found that the MIMU-based system velocity was underestimated for all steps as these authors reported a mean bias ranging from 0.45 to over 0.60 $\text{m} \cdot \text{s}^{-1}$ in comparison to the FP as opposed to 0.33 $\text{m} \cdot \text{s}^{-1}$ in the present study. The discrepancies between both studies likely result from the different methods used to compute the velocity. In our study, $V_{H MIMU}$ was computed by retrieving the antero-posterior and the medial-lateral V_{CM} from the MIMU-based system software and $V_{H FP}$ was obtained from

integration of the GRF (see the **general methodology**) while. On the other hand, van den Tillaar et al. (2021) obtained V_{MIMU} from the product of the SL and the SF, determined from ankle angular velocity to identify the touchdown and the toeoff using MIMUs placed on both feet, yet based on currently unpublished algorithm (van den Tillaar et al., 2021). Finally, the V_{FP} was also obtained as the product of the SL (computed from the centre of pressure) and SF. Therefore, the computation methods differ between the two studies.

Moreover, when comparing the V_{HMIMU} to V_{HFP} , care must be taken with regards to the coordinate system orientation. The MIMU-based system antero-posterior axis is likely neither aligned with the FP coordinate system nor with the sprinting path due to sensors drift and regardless of a thorough calibration procedure. In their experimentation, Van den Tilaar et al. (2021) might have considered the antero-posterior axis only which can explain greater differences in comparison to our study. To ensure accurate computation when using a MIMU-based system, it is therefore mandatory to compute the norm of the horizontal plane velocity (V_{HMIMU} in the present study) which represents a limitation of this system if someone is willing to analyze each axis distinctly on the field.

Overall, the mean bias for the V_{HMIMU} in comparison to the V_{HFP} lies within a similar range to those reported by Samozino et al. (2016) in their field method validation for the F-v relationship computation. Samozino et al. (2016) found an absolute bias ranging from ~2 to 8% for the F-v mechanical variables when compared to the computation using FP (Samozino et al., 2016). These authors concluded that this bias was "low" and the field method for the F-v relationship computation is now widely used in sport science and in sprint trainings.

Similarly, differences between two reference systems (FP and OS) compared together for the CM trajectory reached ~9% when walking at a constant speed (Pavei et al., 2020). Those results show that even with two "reference systems", differences -likely resulting from the anthropometrical assumptions- greater than those reported in the present study can be found.

Hence, we can consider that this MIMU-based system can be used to compute the V_{HMIMU} and the present study provides hints regarding the choice of the optimal system when researchers and/or sport practitioners are willing to compute the V_{HCM} , considering each system's cost, accuracy and easy-of-use ratio that meet the requirement of the experimental conditions.

The V_{VMIMU} displayed the largest systematic bias (up to ~20%) and the largest random errors (up to ~108%). Those results are in contrast with the findings of Pavei et al. (2020)

who reported the lowest bias on the vertical axis (Pavei et al., 2020). However, these authors compared the point-by-point root mean square distance, range of motion, minimum and maximum positions on the 3 orthogonal axes (Pavei et al., 2020) while we analyzed the stance-averaged velocities in the present study. Further, Pavei et al. (2020) used a different system, sampling at 60 Hz, with wireless MIMUs and this can also account for some of the variance in the findings (Camomilla et al., 2018). Finally, their protocol also differed from ours since they analyzed walking strides with constant velocities of $0.79 \pm 1.94 \text{ m} \cdot \text{s}^{-1}$ (Pavei et al., 2020) while we evaluated maximal effort accelerated sprints (V_{HFP} up to $\sim 6 \text{ m} \cdot \text{s}^{-1}$). It is also important to note that since the V_{VFP} values are much lower than the V_{HFP} , an error of $0.05 \text{ m} \cdot \text{s}^{-1}$ would yield greater discrepancies when expressed in percentage. Nevertheless, when considering the large random errors as well as the small correlation coefficients, it must be acknowledged that this MIMU-based system is not fully mature yet for accurately computing the V_{VMIMU} in overground sprinting with maximal effort.

3. Limitations

Other points likely conducted to differences between the FP and the MIMU-based system and are worth discussing. First and foremost, the anthropometrical model used within the MIMU-based system represents one of the main source of errors (Robert-Lachaine et al., 2017), as it is also the case when using an OS (Pavei et al., 2017, 2020). Although not one of the aims of this study, the mean bias was greater for the females than for the males: 8.23% and 4.64%, respectively, at 0-6 m within the straight. While this sheds some light on the possibility that this MIMU-based system anthropometric model is more adapted for males, this must be interpreted cautiously since only 4 females participated in this study.

The differences between the FP and the MIMU-based system should also be balanced since this experimentation focussed on the early transition phase, where sprinters produce their greatest acceleration (Slawinski, Bonnefoy Mazure, Levêque, et al., 2010). In addition, within this phase of the sprint, participants are in a crouched-to-semi-straightened position which could also challenge the biomechanical model computation. Therefore, the V_{HMIMU} and V_{VMIMU} should also be compared to the FP latter during the transition phase, when the participants have straightened up (Nagahara et al., 2014).

Discrepancies between devices could also result from the systems' synchronization and the different sampling rates. Since the synchronization between systems was at the nearest MIMU-based system's frame, we have tested on two random participants what could be the differences for the V_{HMIMU} with plus or minus 1 frame. We found

mean discrepancies of ~3.5% and maximum differences reaching ~8.5%, meaning that the synchronization and the different sampling rates could also account for some of the variance between systems.

The MIMU-based system sensitivity to magnetic fields has also been widely discussed in the literature (Camomilla et al., 2018; Hughes et al., 2021). It is of importance to avoid ferromagnetic objects nearby the analysis area to limit the sensors drift and to follow guidelines for the MIMU-based system utilization (Camomilla et al., 2018). Nevertheless, the experimentations took place in an indoor wooden indoor facility and considering that the FP were embeded underneath the track surface, we can assume that this likely resulted in only little disturbances.

Finally, the last source of discrepancy between the MIMU-based system and the FP could result from the FP measurement errors. Albeit considered a reference system with pros well detailed by Pavei et al. (2017), FP can also be prone to measurement errors related mainly to a) integration with errors originating from the initial conditions and b) long recordings leading up to FP drift (Pavei et al., 2017).

4. Conclusion

Evaluating the CM kinematics within *in-field* environments is a challenging process, especially when seeking for portable system that you can use either inside or outside, with a simple setup and a wide range to capture the entire motion. The present study brought new insights into the use of this commercially available MIMU-based system as a valuable alternative of FP or OS for *in-field* computation of the V_H over the starting blocks pushing phase and the initial stances (*i.e.*, 0-6 m) be it in the straight or in the curve. Furthermore, considering its range, this MIMU-based system would provide the unique opportunity to access the V_H over an entire sprint, be it a 200- or 400-m sprint. Contrastingly, the V_V computation is not fully mature yet and further improvements must be made in the sensor-fusion algorithm in order for this MIMU-based system to become an alternative to reference systems for the V_V computation.

During this PhD thesis, we had the opportunity to conduct experimentations at the Japan Institute of Sport Sciences (Tokyo, Japan). From these experimentations, one of the objectives was to compare the V_V , the V_{A-P} and the V_{M-L} computed with the same MIMU-based system used in the present study to an OS, a marker less system and FP both during the first 1-to-4 stances and at $V_{A-P MAX}$. The data processing will begin after this PhD thesis.

We saw in the **literature review** that the V_{A-P} can strongly predict the sprinting performance (Slawinski, Bonnefoy Mazure, Levêque, et al., 2010; Slawinski et al., 2017). Based on Newton's Second Law of Motion, the change in the V_{A-P} results from the magnitude and the direction of the F_{TOT} vector during the stance phase. Thus, comparing the GRF in the straight and in the curve would provide a deeper understanding of the V_{A-P} -time kinetics in the curve.

STUDY 2

Are the ground reaction forces altered by the curve and with the increasing sprinting velocity through the transition phase?

Associated publication

Millot, B., Pradon, D., Blache, P., Dinu, D., Cecchelli, G., Arnould, A. & Slawinski, J. (2023). How the increase in the sprinting velocity affects the ground reaction forces in the curve. *To be submitted*.

Associated communication

Millot, B., Blache, P., Dinu, D., Arnould, A., Jusseaume, J., Hanon, C. & Slawinski, J. (2021). Kinetic analysis of curve sprinting in male and female track athletes. 19ème congrès de l'Association des Chercheurs en Activités Physiques et Sportives, Montpellier, France **Oral communication**

1. Results

1. Sprinting performance

In this **study #2**, the sprinting performance was measured using photocells (see **general methodology** 3.2.). The sprinting performance during the 10-m sprints was similar in the straight and in the curve (see table 7). However, starting from the 15-m sprint onwards, the sprinting performance in the curve was significantly poorer than in the straight (all $p < 0.026$, see table 7).

Table 7. Mean (\pm SD) sprinting performance (in s) in the straight and in the curve from the different sprinting distances measured with photocells. * indicates significantly different from the straight ($p < 0.05$).

Sprints (m)	Sprinting performance in the straight (s)	Sprinting performance in the curve (s)
10 m	1.98 \pm 0.06	1.99 \pm 0.07
15 m	2.63 \pm 0.09	2.65 \pm 0.10*
20 m	3.22 \pm 0.12	3.25 \pm 0.14*
30 m	4.37 \pm 0.19	4.40 \pm 0.21*
40 m	5.47 \pm 0.23	5.52 \pm 0.25*

2. Ground reaction forces

i. The starting blocks pushing phase

During the starting blocks pushing phase in the curve, the mean F_{M-L} was lower than in the straight (respectively -0.26 ± 0.57 vs -0.06 ± 0.53 N \cdot kg⁻¹; $p = 0.002$). In contrast, no differences were observed for the mean F_{TOT} , F_V and F_{A-P} (all $p \geq 0.712$) (see figure 40).

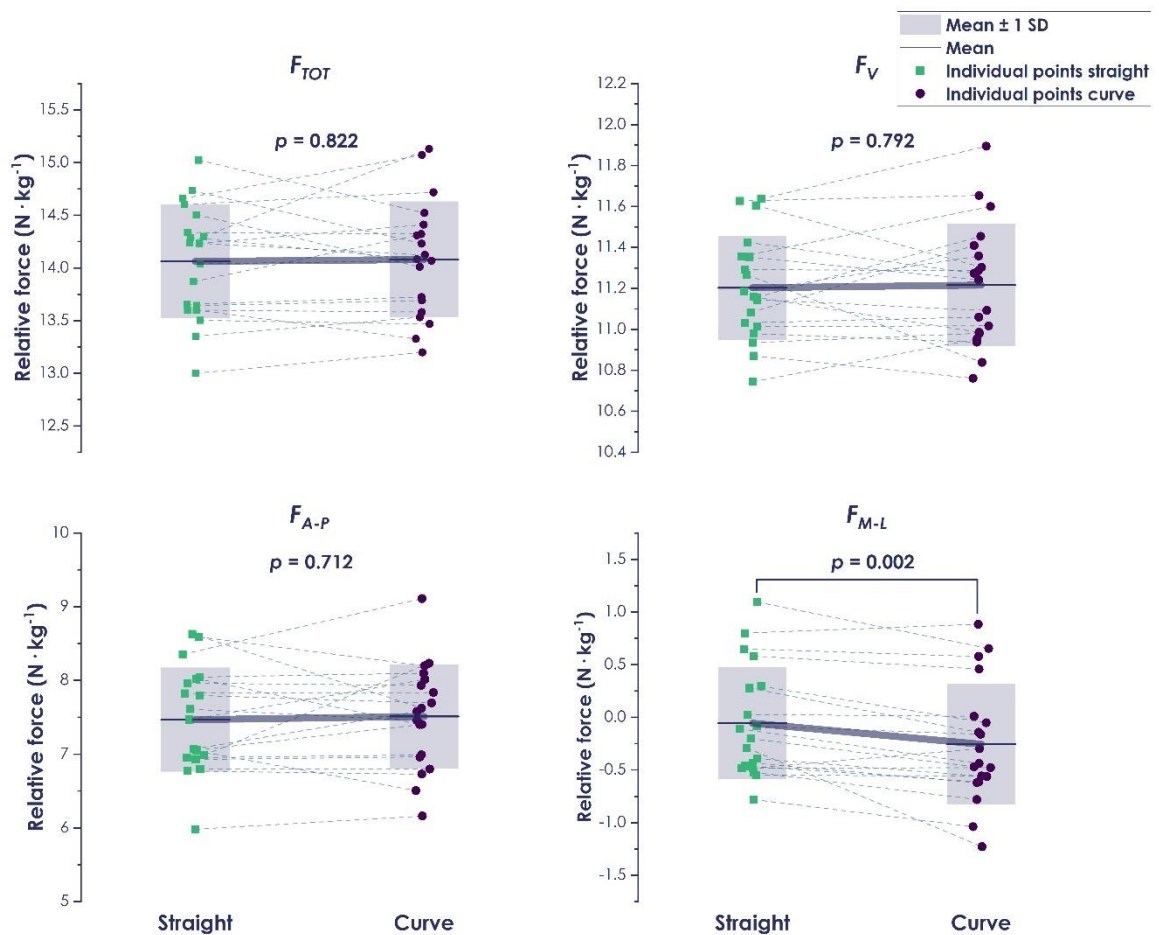


Figure 40. Individual values (each dot represent the mean value of a participant) of the resultant (F_{TOT}), vertical (F_V), antero-posterior (F_{A-P}) and medial-lateral (F_{M-L}) relative to body mass (expressed in $N \cdot kg^{-1}$) averaged over the starting blocks pushing phase. The bold traces connect the mean values of the whole sample ($n = 19$) in the two sprinting conditions. The box charts correspond to mean ± 1 SD and the dashed traces connect individual values between the two sprinting conditions.

ii. Transition phase

F_{TOT}

During the transition phase, the two-way ANOVA with repeated measures revealed a significant condition effect for the left F_{TOT} ($F_{(1, 12)} = 5.717$, $p = 0.034$, $\omega^2 = 0.024$). The post-hoc analysis with the Bonferroni correction indicated a lower left F_{TOT} in the curve in comparison to the straight (see figure 41).

F_V

A significant main effect for condition was also reported for the left F_V ($F_{(1,12)} = 8.018$, $p = 0.015$, $\omega^2 = 0.036$), with the left F_V being lower in the curve than in the straight (see figure 41).

 F_{A-P}

The left ($F_{(1,12)} = 45.001$, $p < 0.001$, $\omega^2 = 0.214$) and the right F_{A-P} ($F_{(1,8)} = 24.973$, $p = 0.001$, $\omega^2 = 0.143$) were lower in the curve in comparison to the straight (see figure 41). In addition to that, we observed a significant condition x distance interaction for the left ($F_{(1,12)} = 7.394$, $p < 0.001$, $\omega^2 = 0.145$) and the right F_{A-P} ($F_{(1,8)} = 2.861$, $p = 0.039$, $\omega^2 = 0.055$). The post-hoc analyses with the Bonferroni corrections showed that the F_{A-P} was lower in the curve than in the straight for the left stances starting from 24-29 m onwards; and for the right stances at 34-39 m (see figure 41).

 F_{M-L}

Moreover, the left ($F_{(1,10)} = 487.54$, $p < 0.001$, $\omega^2 = 0.846$) and the right F_{M-L} ($F_{(1,8)} = 438.822$, $p < 0.001$, $\omega^2 = 0.779$) were greater in the curve than in the straight. Finally, a significant condition x distance interaction for the left ($F_{(1,10)} = 8.716$, $p < 0.001$, $\omega^2 = 0.202$) and right F_{M-L} ($F_{(1,8)} = 5.727$, $p = 0.009$, $\omega^2 = 0.143$) were observed at each distance, showing that within the curve, the F_{M-L} was systematically greater than in the straight for both the left and right stances (all $p \leq 0.003$; see figure 41).

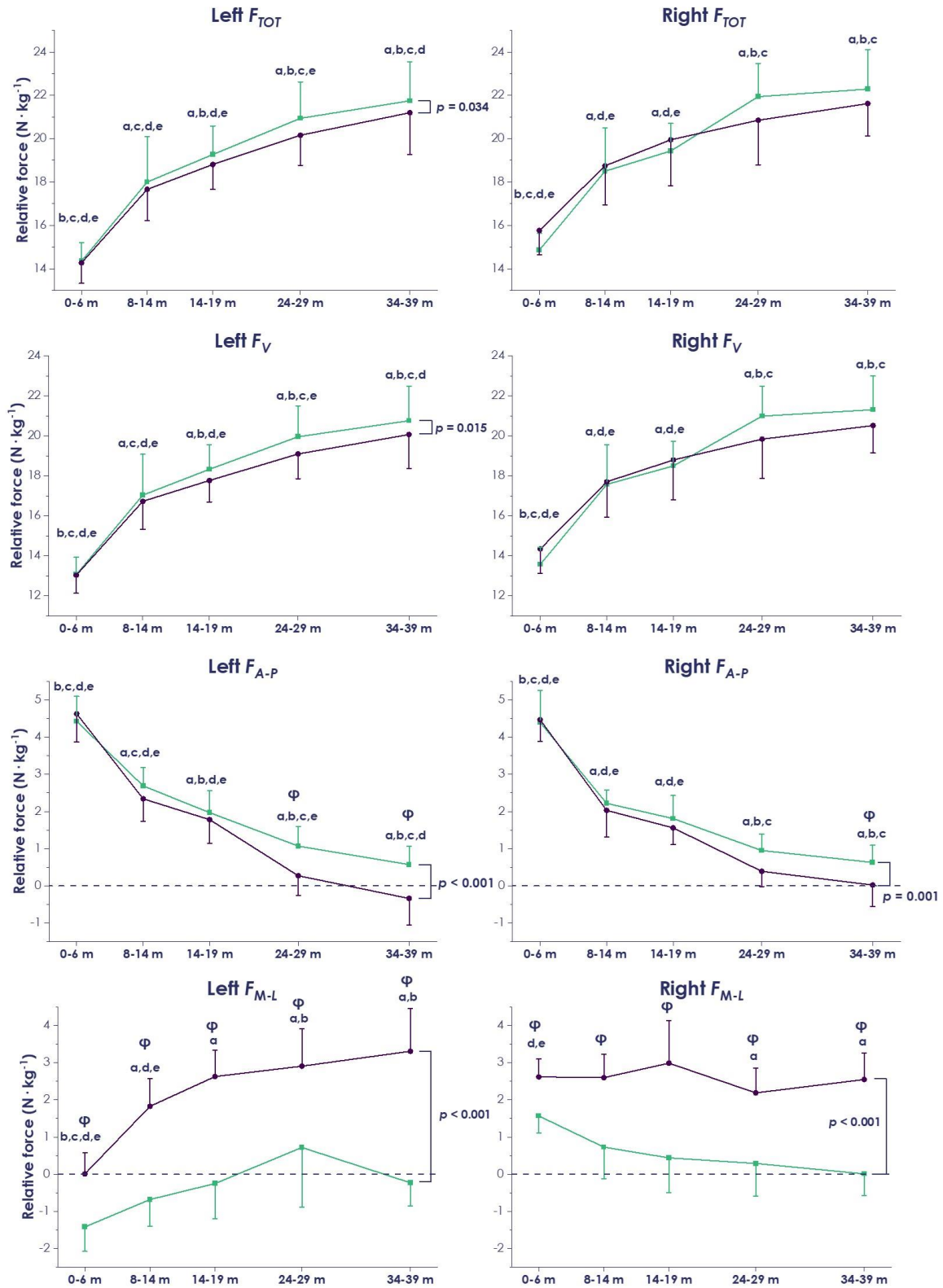


Figure 41. Mean (\pm SD) left and right resultant (F_{TOT}), vertical (F_V), antero-posterior (F_{A-P}) and medial-lateral (F_{M-L}) ground reaction forces averaged during the stances in the straight (green) and in the curve (purple) over each zone. For all panels, * indicates a significant main effect for condition ($p < 0.05$); a: different from 0-6 m; b: different from 8-14 m; c: different from 14-19 m; d: different from 24-29 m; e: different from 34-39 m ($p < 0.05$).

3. Stance times

i. Starting blocks pushing phase

No differences were observed between the straight and the curve for the starting blocks pushing-time ($p = 0.556$; see figure 42).

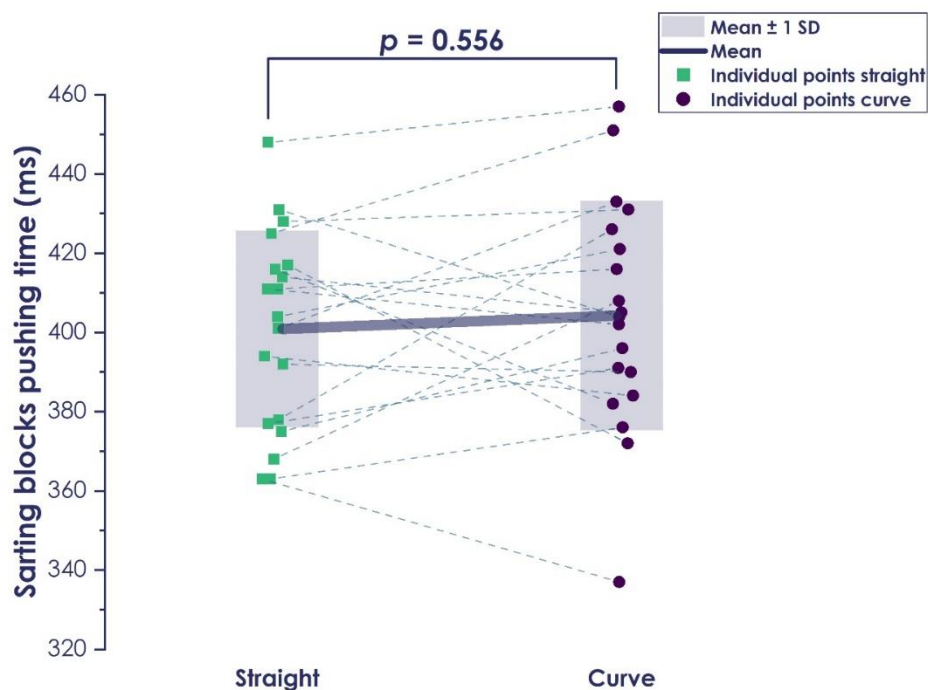


Figure 42. Mean (\pm SD) starting blocks pushing times (expressed in ms) in the straight (green) and in the curve (purple).

ii. Transition phase

After the starting blocks exit, the left stance times were longer in the curve than in the straight ($F_{(1,11)} = 42.009$, $p < 0.001$, $\omega^2 = 0.112$; see figure 43). In contrast, no differences were observed for the right stance times between the straight and the curve ($F_{(1,12)} = 0.224$, $p = 0.646$, $\omega^2 = 0.000$; see figure 43).

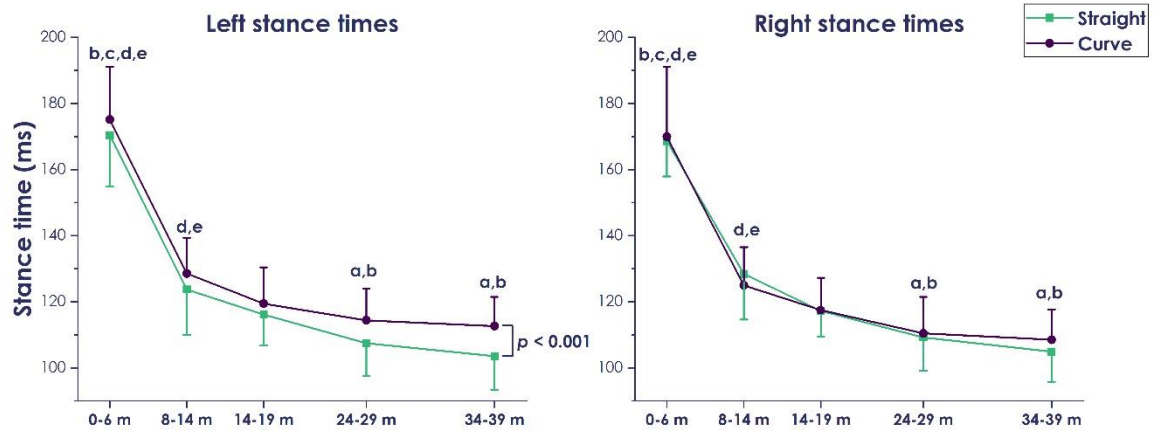


Figure 43. Mean (\pm SD) left and right stance times (expressed in ms) over each interval in the straight (green) and in the curve (purple). For all panels, * indicates a significant main effect for condition ($p < 0.05$); a: different from 0-6 m; b: different from 8-14 m; c: different from 14-19 m; d: different from 24-29 m; e: different from 34-39 m ($p < 0.05$).

4. Impulses

i. Starting blocks pushing phase

During the starting blocks pushing-phase in the curve, the relative mean IMP_{M-L} was greater than in the straight (-0.11 ± 0.23 vs -0.02 ± 0.21 $m \cdot s^{-1}$; $p = 0.001$; see figure 44). No other significant differences were observed on the other axes (all $p \geq 0.140$; see figure 44).

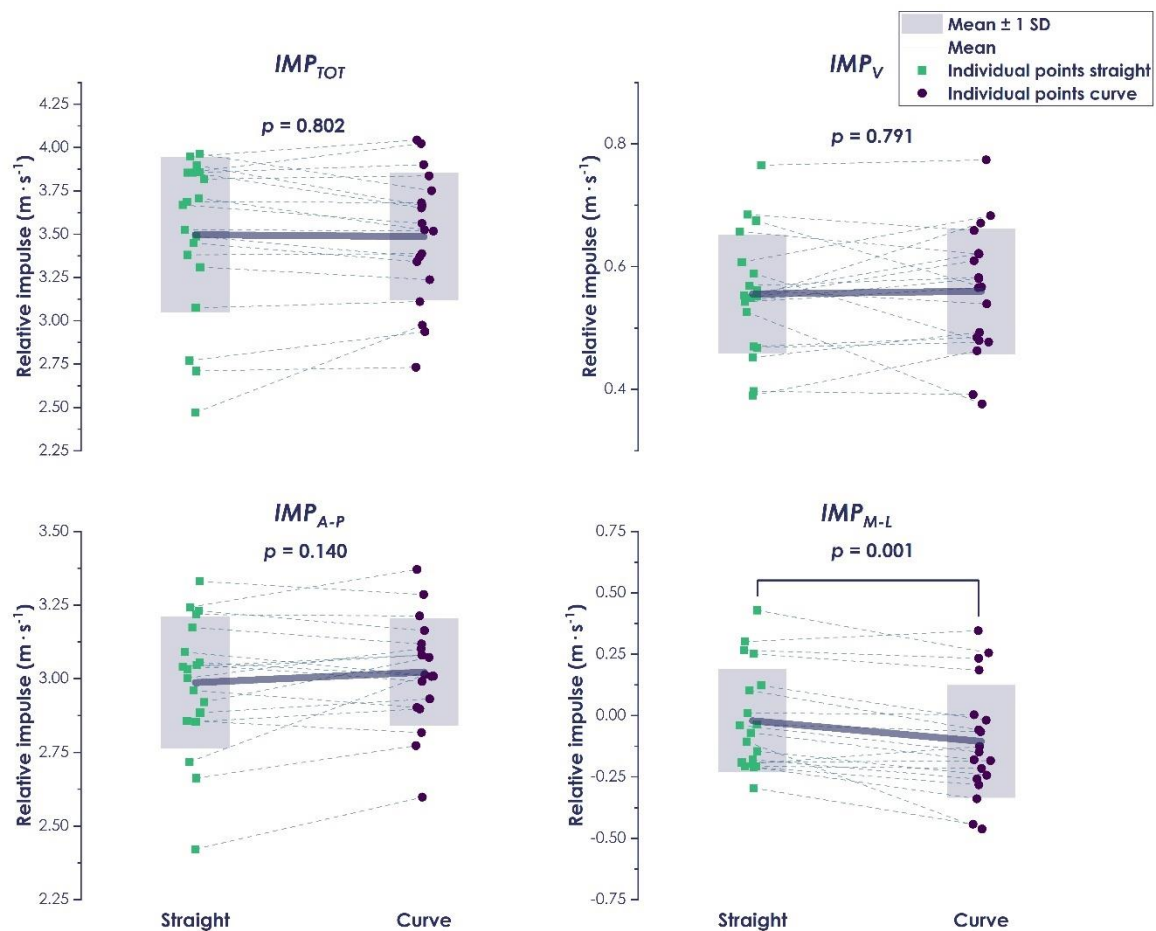


Figure 44. Individual values (each dot represent the value of a participant) of the resultant (IMP_{TOT}), vertical (IMP_V), antero-posterior (IMP_{A-P}) and medial-lateral (IMP_{M-L}) impulses expressed relative to body mass (in $\text{N} \cdot \text{kg}^{-1}$) over the starting blocks pushing phase. The bold traces connect the mean of the whole sample ($n = 19$) between the straight and the curve. The box charts correspond to the mean ± 1 SD and the dashed traces connect the individual values between the straight and the curve.

ii. Transition phase

IMP_{TOT}

No significant main effect for condition and no condition x distance interactions were found for the left ($p \geq 0.391$) and right ($p \geq 0.099$) IMP_{TOT} (see figure 45).

IMP_V

Similarly, no significant main effect for condition and no condition x distance interactions were found for the left ($p \geq 0.442$) and right ($p \geq 0.814$) IMP_V (see figure 45).

IMP_{A-P}

The left ($F_{(1,12)} = 39.808$, $p < 0.001$, $\omega^2 = 0.221$) and the right IMP_{A-P} ($F_{(1,8)} = 42.257$, $p < 0.001$, $\omega^2 = 0.165$) were lower in the curve than in the straight (see figure 9). In addition

to that, there was a significant condition x distance interaction for the left IMP_{A-P} ($F_{(1,12)} = 6.945, p < 0.001, \omega^2 = 0.145$) indicating that the left IMP_{A-P} was lower in the curve than in the straight starting from 24-29 m onwards ($p < 0.001$; see figure 45).

IMP_{M-L}

The left ($F_{(1,12)} = 453.279, p < 0.001, \omega^2 = 0.861$) and the right IMP_{M-L} ($F_{(1,8)} = 341.636, p < 0.001, \omega^2 = 0.792$) were greater in the curve than in the straight ($p < 0.001$; see figure 9). Lastly, we observed significant condition x distance interactions for the left ($F_{(1,12)} = 5.080, p < 0.001, \omega^2 = 0.112$) and the right IMP_{M-L} ($F_{(1,8)} = 3.975, p = 0.033, \omega^2 = 0.101$). The post-hoc analyses with the Bonferroni corrections showed that at each distance, the left and right IMP_{M-L} in the curve exceeded that of the straight ($p \leq 0.001$; see figure 45).

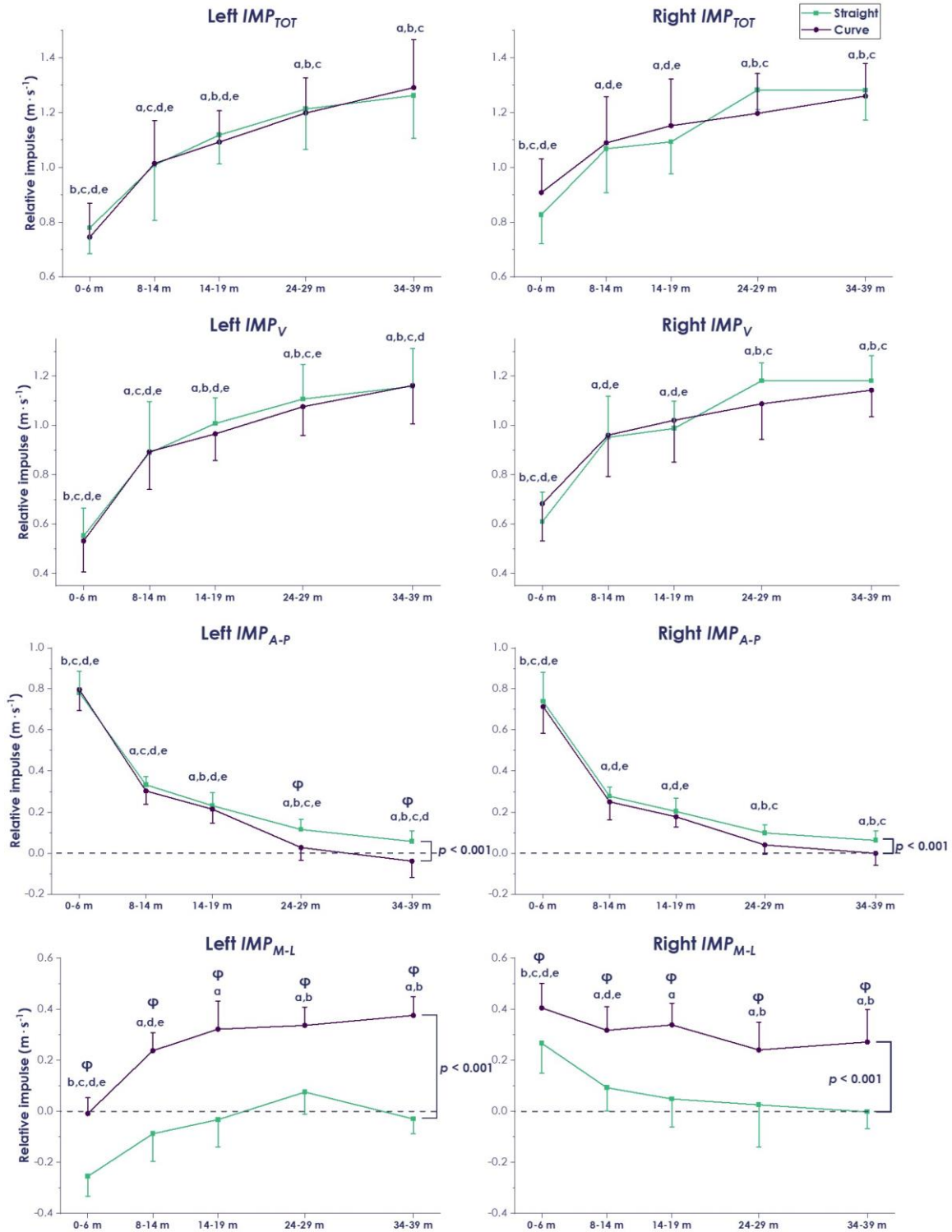


Figure 45. Mean (\pm SD) resultant (IMP_{TOT}), vertical (IMP_V), antero-posterior (IMP_{A-P}) and medial-lateral (IMP_{M-L}) impulses for the left and right stances in the straight (green) and in the curve (purple) averaged over each distance. For all panels, * indicates a significant main effect for condition ($p < 0.05$); a: different from 0-6 m; b: different from 8-14 m; c: different from 14-19 m; d: different from 24-29 m; e: different from 34-39 m ($p < 0.05$). Finally, ϕ indicates a significant condition x distance interaction ($p < 0.05$).

2. Discussion

1. Are the ground reaction forces affected by the curve?

The core novelty of the present experimentation was the ability to explore the GRF over 15-to-19 foot contacts in the curve (from the starting blocks on to $V_{A-P MAX}$) while previous studies investigated the GRF in the curve during a single stance at 13 m (Judson et al., 2019) or at $V_{A-P MAX}$ (Churchill et al., 2016). The main findings were that the mean F_{M-L} largely increased in the curve on both limbs. On the left limb, this large increase conducted to a reduction in the mean F_{TOT} , F_V and F_{A-P} (see table 8). Thus, in order to maintain an adequate sprinting motion, the left stance times increased to produce similar IMP_{TOT} and IMP_V to the straight (see table 9).

i. Starting blocks pushing phase

The mean F_{M-L} was lower in the curve than in the straight during the starting blocks pushing phase (respectively -0.26 ± 0.57 vs -0.06 ± 0.53 N · kg⁻¹; see figure 3), meaning that the participants were heading towards the outside of their lane (*i.e.*, laterally) after the starting blocks exit. In the present experimentation, 14 out of 19 participants started with their left foot on the front block. Among them, 13 participants produced a negative mean F_{M-L} and IMP_{M-L} over the starting blocks pushing phase in the curve, meaning that the participants were heading towards the outside of their lane. In contrast, 4 out of the 5 participants that started with their right leg on the front block produced a mean F_{M-L} and IMP_{M-L} positive in the curve, meaning that the participants were heading towards the inside of their lane. These findings further question the choice of the front and rear foot in the starting blocks in the curve as this choice will in turn impact the sprinter's direction after the starting blocks exit.

In the present study, the starting-blocks were positioned on the middle of the lane as the FP were narrower than the lane (0.60 vs 1.22 m, respectively). We are aware that this represents a limitation in the present study and might have impacted the GRF during the starting blocks pushing phase for some participants. From this standardized position and despite the athletes positioned their blocks such that they were heading towards the inside of their lane. Yet, the participants with the left foot on the front block headed laterally for the starting-blocks pushing phase, before heading medially in the following stances, which is unlikely to be optimal for the sprinting performance. Consequently, the present findings strengthen the idea that, in the curve, the starting-blocks should be positioned on the outside of the lane.

ii. Transition phase

Based on female and male 200-m times from the 2004 World Indoor Championships, Usherwood and Wilson (2006) postulated the “constant limb force” hypothesis. This model assumes that the peak F_{TOT} would not be modified in the curve in comparison to the straight, however, as the F_{M-L} increases in the curve, the stance times would increase as well in order to produce the necessary IMP_V . Churchill et al. (2016) previously rejected this assumption for the left limb as the peak F_{TOT} was lower during the left stance in the curve on lane 2 in comparison to the straight.

In the present study, we showed that the left mean F_{TOT} was lower in the curve than in the straight (see figure 41). This was caused by the lower left mean F_V and F_{A-P} and despite a large concomitant increase in the left mean F_{M-L} . Therefore, in line with Churchill et al.’s (2016) findings, we can further reject the “constant limb hypothesis” for the left limb, this time, throughout the transition phase. Previously, Judson et al. (2019) showed that the left limb push-off axis switched from transverse to oblique (see figure 16 in the **literature review**). Thus, we can hypothesize that the ability to produce F_{TOT} is altered with the oblique push-off axis.

On the other hand, the mean F_{TOT} was not altered for the right limb (see table 8), which is consistent with what was previously reported in lane 2 (Churchill et al., 2016) or at extremely tight radii (*i.e.*, ≤ 6 m) (Chang & Kram, 2007). For the right limb, only the horizontal plane was affected whereby we observed an increase in the mean F_{M-L} concomitantly with a decrease in the mean F_{A-P} , in comparison to the straight (see figure 41).

Table 8. Summary of the significant main effects for condition between the straight and the curve on the resultant (F_{TOT}), vertical (F_V), antero-posterior (F_{A-P}) and medial-lateral (F_{M-L}) ground reaction forces.

	Left	Right
	Curve vs straight	Curve vs straight
F_{TOT}	↓	→
F_V	↓	→
F_{A-P}	↓	↓
F_{M-L}	↑	↑

2. Are the stance times impacted by the curve?

No changes were observed between the straight and the curve for the starting blocks pushing phase duration (see figure 42). On the other hand, after the starting blocks

exit, the left mean stance times in the curve were longer than in the straight while no changes were reported for the right limb (see figure 43). In the curve, the left limb stance times were increased due to lower mean F_V and in an attempt to produce a similar IMP_V as in the straight in order to maintain an adequate sprinting motion.

3. Are the impulses impacted by the curve?

i. Starting-blocks pushing phase

In the present study, the IMP_{A-P} were similar both in the straight and in the curve with a velocity at the starting-blocks exit of $\sim 3 \text{ m} \cdot \text{s}^{-1}$. Additionally, the present findings are consistent with the literature with groups of similar expertise (Otsuka et al., 2014) and slightly below the values of $3.37 \text{ m} \cdot \text{s}^{-1}$ reported among elite sprinters (Morin, Slawinski, et al., 2015).

ii. Transition phase

As the left mean stance times increased in the curve in comparison to the straight, the left mean IMP_{TOT} and IMP_V were similar to the straight (see table 9). Therefore, likewise Churchill et al. (2016) reported: “The increased stance times enabled maintenance of the IMP_V in the curve compared with the straight in the presence of significantly reduced F_V ” (Churchill et al., 2016).

However, despite the increased left mean stance times, the left mean IMP_{A-P} remained lower in the curve than in the straight meaning that impulse changes were only observed in the horizontal plane (see table 9). The IMP_{A-P} was previously reported as a major parameter in overground sprinting performance (Hunter et al., 2005; Kawamori et al., 2013; Morin, Slawinski, et al., 2015). Thus, overall, the sprinting performance was reduced in the curve due to the decreased left and right IMP_{A-P} (see table 9).

Table 9. Summary of the significant main effects for condition between the straight and the curve on the resultant (IMP_{TOT}), vertical (IMP_V), antero-posterior (IMP_{A-P}) and medial-lateral (IMP_{M-L}) impulses as well as the stance times.

	Left	Right
	Curve vs straight	Curve vs straight
IMP_{TOT}	→	→
IMP_V	→	→
IMP_{A-P}	↓	↓
IMP_{M-L}	↑	↑
Stance times	↑	→

4. Are the ground reaction forces and impulses changing with the increasing velocity?

In the present study, the mean F_{TOT} , IMP_{TOT} , F_V and IMP_V increased progressively with the increasing distance, which is similar to what was previously reported in the existing literature (Morin, Slawinski, et al., 2015; Nagahara et al., 2018b; Rabita et al., 2015). In contrast, the mean F_{A-P} and IMP_{A-P} decreased with the increasing velocity both in the straight and in the curve, which is also consistent with what was previously reported (Morin, Slawinski, et al., 2015; Nagahara et al., 2018b; Rabita et al., 2015). In the curve, the mean IMP_{A-P} became negative for both the left and right limbs starting from 34-39 m while the mean IMP_{A-P} remained positive in the mean time in the straight (see figure 45). Consequently, the participants reached their $V_{A-P MAX}$ earlier in the curve although this is detrimental for sprinting performance as we have discussed in the **literature review** of this manuscript (Debaere, Jonkers, et al., 2013; Graubner & Nixdorf, 2009; Slawinski et al., 2017).

On the other hand, large discrepancies were observed between the straight and the curve regarding the mean F_{M-L} and IMP_{M-L} . Indeed, in the straight, these metrics decreased progressively which corresponds to what Nagahara et al. (2017) previously described. However, in the curve, these metrics strongly differed from the straight (see figure 5 & 9) with the left and right limbs responding differently to the curve.

5. Differences between left and right limbs within the curve

Although this was not a direct aim of the present study, the figure 46 illustrates the left and right mean F_{M-L} (left panel) and IMP_{M-L} (right panel) within the curve. The right mean F_{M-L} was $\sim 2.5 \text{ N} \cdot \text{kg}^{-1}$ at 0-6 m and plateaued afterwards (full line in figure 46). On the other hand, the left mean F_{M-L} and IMP_{M-L} were close to zero at 0-6 m and increased progressively subsequently. This means that during the first 14 m of the sprint in lane 5, the CM mainly turned thanks to the right leg's ability to generate F_{M-L} and IMP_{M-L} . At 14-19 m, both the left and right mean F_{M-L} and IMP_{M-L} were almost equal (represented by the red circles on the figure 46), meaning that both limbs similarly contributed to the CM rotation. Afterwards, the left mean F_{M-L} and IMP_{M-L} became visually greater. Although we have not conducted a statistical analysis on this specific point, we can assume that, starting from 24 m onwards, the left leg apparently made the CM turn more than the right leg. Those findings are consistent with previous research stipulating that more turning of the CM occurred during the right stances at 13 m (Judson, Churchill, Barnes, Stone, Brookes, et al., 2020) while more turning of the CM occurred during the left stances at 40 m (Churchill et al., 2015).

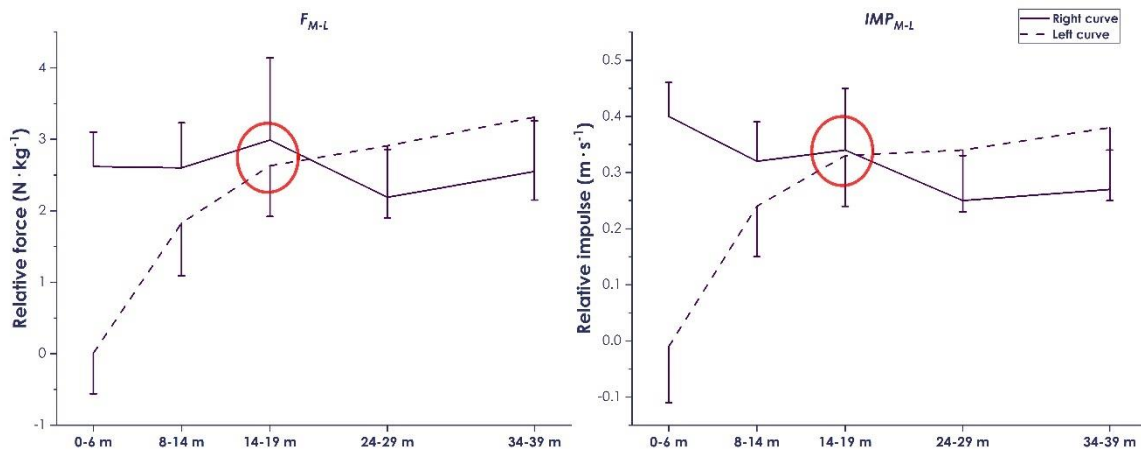


Figure 46. Mean (\pm SD) left (dashed) and right (full) medial-lateral ground reaction forces (F_{M-L} ; left panel) and impulses (IMP_{M-L} ; right panel) within the curve.

3. Limitations

In the present study, the starting blocks were kept in the middle of the lane for each participant in order to standardize the starting blocks position and to remove any bias implicated by the medial or lateral positioning of the starting blocks. We are aware that this represents a limitation and might have impacted the GRF during the starting blocks pushing phase for some participants. Yet, our findings strengthen a common statement among coaches postulating that the starting blocks should be positioned on the outside of the lane. Indeed, by positioning the starting blocks on the outside of their lane, the participants could avoid to produce a lateral F_{M-L} over the starting blocks pushing phase. Nevertheless, whether this technique is better in terms of performance remains to be investigated.

4. Conclusion

The present experimentation helped us to better comprehend the kinetic factors altering the sprinting performance in the curve. Overall, the left limb was the most affected in the curve and the sprinting performance was reduced in the curve mostly due to:

- The decreased left and right F_{A-P} and IMP_{A-P} that were likely caused by the concomitant increased left and right F_{M-L} and IMP_{M-L} , to adopt a curvilinear motion. Indeed, as the participants were not able to increase the F_{TOT} and due

to the additional requirement of the F_{M-L} , the participants inevitably decreased their F_{A-P} .

- The increased left stance times in the curve, likely due to the decreased F_{TOT} and F_V and in an attempt to produce a similar IMP_{TOT} and IMP_V in comparison to the straight, likely to maintain an adequate sprinting motion and balance.

The GRF and the impulses alterations in the curve eventually result from modifications in the sprinting technique (*i.e.*, body kinematics). In the curve, one of the most impacted kinematic metrics is the BLL. Thus, it is likely that changes in the frontal plane conduct to modifications in the sagittal plane.

STUDY 3

Are the sprinting kinematics altered by the curve and with the increasing sprinting velocity through the transition phase?

Associated publication

Millot, B., Pradon, D., Blache, P., Dinu, D., Cecchelli, G., Arnould, A. & Slawinski, J. (2023). How the increase in the sprinting velocity affects the lower limbs' joints kinematics in the curve. *To be submitted*

1. Results

1. Stance phase

i. Peak extension/plantarflexion angles during the stance phase

The two-way ANOVA with repeated measures revealed a significant main effect for condition for the left knee ($F_{(1,18)} = 10.982, p = 0.004, \omega^2 = 0.041$) and the right ankles ($F_{(1,18)} = 8.965, p = 0.009, \omega^2 = 0.040$). The post-hoc analyses with the Bonferroni corrections indicated a lower left knee peak extension angle ($p = 0.004$; see figure 47) and a greater right ankle peak plantarflexion angles ($p = 0.009$; see figure 47) during the stance phase in the curve in comparison to the straight (see figure 47).

There was also a significant condition x distance interaction for the right ankle ($F_{(1,18)} = 2.629, p = 0.041, \omega^2 = 0.021$) whereby the right ankle peak plantarflexion angle was greater in the curve than in the straight at 40 m ($p = 0.009$) during the stance phase (see figure 47). The main effects for distance are reported in the figure 47.

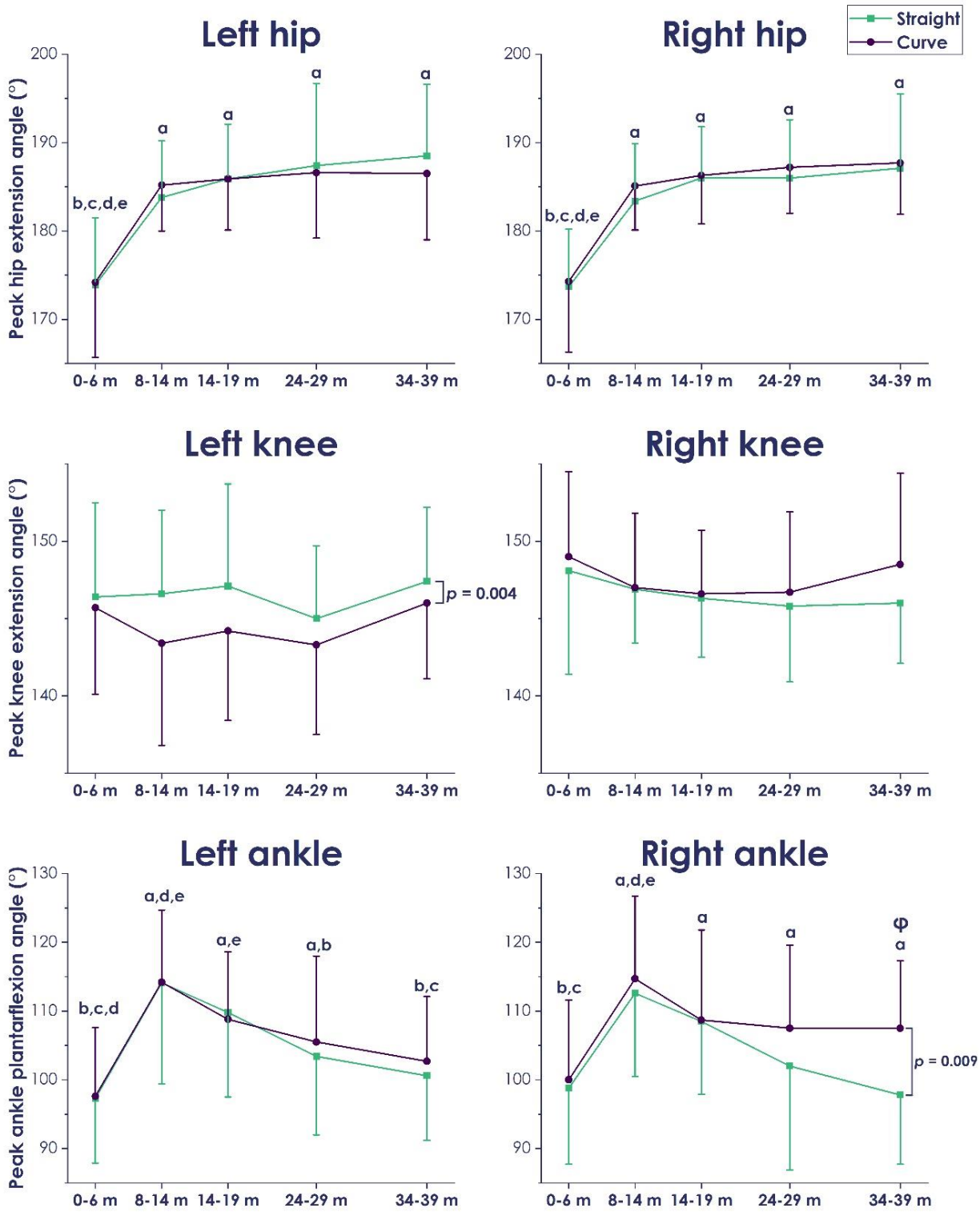


Figure 47. Mean (\pm SD) left and right hip and knee peak extension angles and ankle peak plantarflexion angles reached during the late stance phase. a: different from 0-6 m; b: different from 8-14 m; c: different from 14-19 m; d: different from 24-29 m; e: different from 34-39 m ($p < 0.05$). The brackets indicate a main effect for condition. Finally, ϕ indicates a significant condition x distance interaction. All significant differences reported are $p < 0.05$.

ii. Peak extension/plantarflexion velocities during the stance phase

The two-way ANOVA with repeated measures did not reveal any significant main effect for condition for the hip and the knee peak extension velocity and the ankle peak plantarflexion velocity during the stance phase (all $p \geq 0.215$, see figure 48). The main effects for distance are reported in the figure 48.

2. Swing phase

i. Peak extension/plantarflexion angles during the swing phase

The two-way ANOVA with repeated measures revealed a significant main effect for condition at the left ($F_{(1,18)} = 6.947$, $p = 0.017$, $\omega^2 = 0.044$) and the right ($F_{(1,18)} = 7.236$, $p = 0.015$, $\omega^2 = 0.043$) ankles. The post-hoc analyses with the Bonferroni corrections showed that the left ankle peak plantarflexion angle during the swing phase in the curve was lower than in the straight ($p = 0.017$; see figure 49). On the other hand, the right ankle peak plantarflexion angle was greater during the swing phase in the curve than in the straight ($p = 0.015$; see figure 49). The main effects for distance are reported in the figure 49.

ii. Peak flexion angles during the swing phase

The two-way ANOVA with repeated measures showed a significant main effect for condition at the left knee ($F_{(1,18)} = 5.629$, $p = 0.029$, $\omega^2 = 0.025$). The post-hoc analysis with the Bonferroni correction indicated that the left knee peak flexion angle in the curve was greater than in the straight ($p = 0.029$).

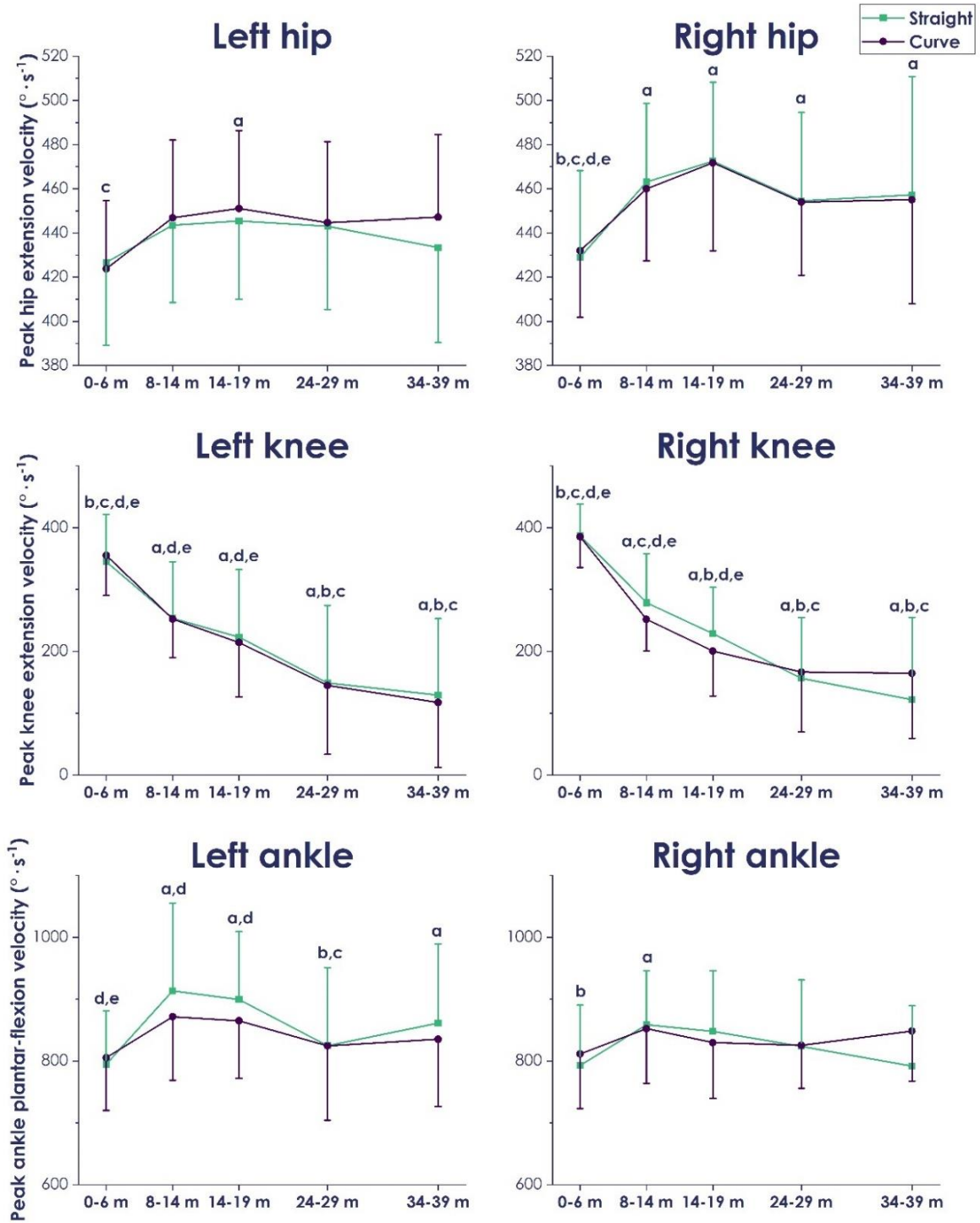


Figure 48. Mean (\pm SD) left and right hip and knee peak extension velocities and ankle peak plantarflexion velocities reached during the late stance phase. a: different from 0-6 m; b: different from 8-14 m; c: different from 14-19 m; d: different from 24-29 m; e: different from 34-39 m ($p < 0.05$). All significant differences reported are $p < 0.05$.

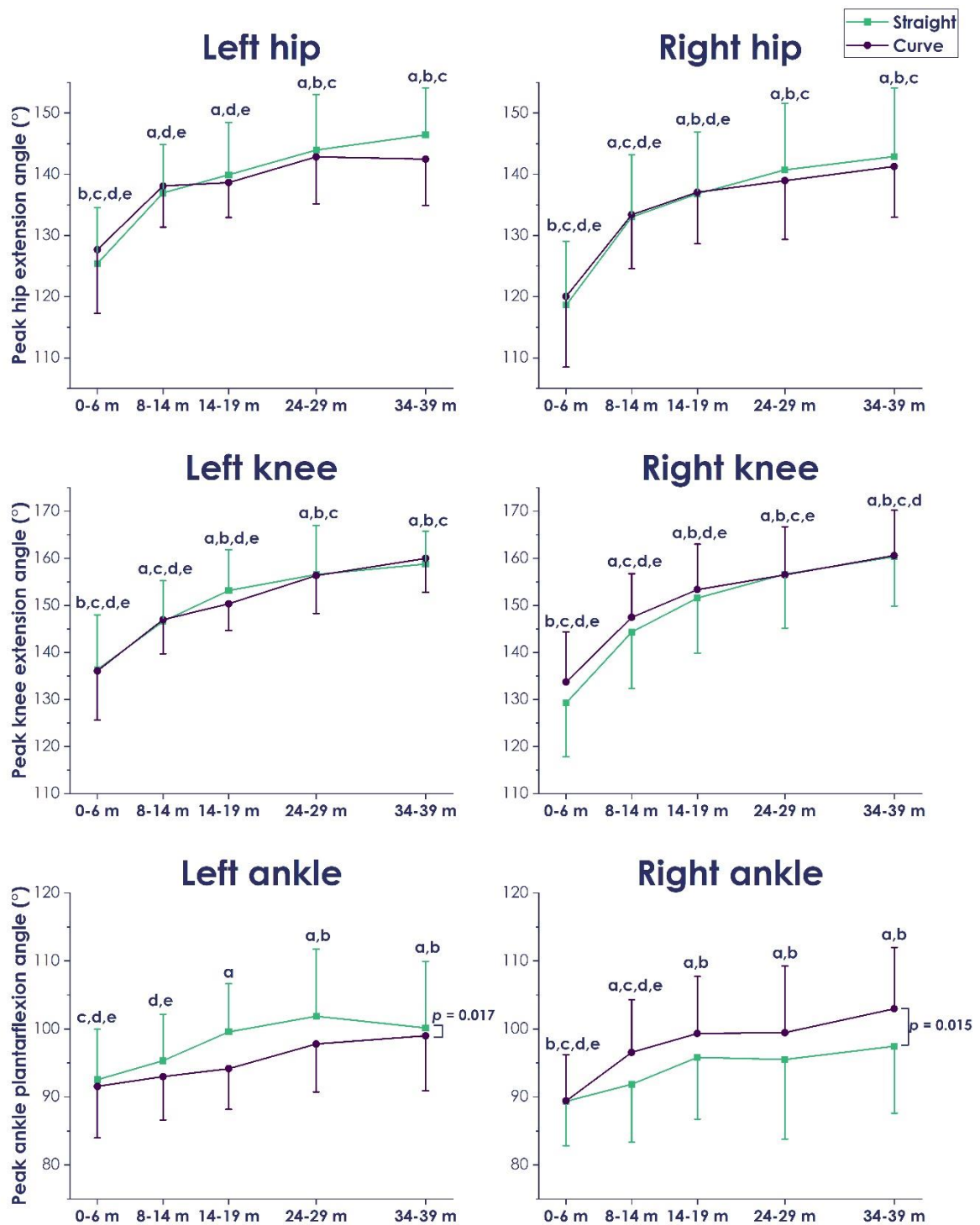


Figure 49. Mean (\pm SD) left and right hip and knee peak extension angles and ankle peak plantarflexion angles reached during the late swing phase. a: different from 0-6 m; b: different from 8-14 m; c: different from 14-19 m; d: different from 24-29 m; e: different from 34-39 m ($p < 0.05$). The brackets indicate a main effect for condition. All significant differences reported are $p < 0.05$.

3. Peak angular velocity during the swing phase

i. Peak extension/plantarflexion velocity

There was a main effect for condition at the left ($F_{(1,18)} = 4.772$, $p = 0.042$, $\omega^2 = 0.042$) and the right ($F_{(1,18)} = 9.180$, $p = 0.007$, $\omega^2 = 0.058$) ankles. The post-hoc analyses with the Bonferroni corrections showed that the left ankle peak plantarflexion velocity during the late swing phase was lower in the curve than in the straight ($p = 0.042$; see figure 50). In contrast, the right ankle peak plantarflexion velocity during the late swing phase was greater in the curve than in the straight ($p = 0.007$; see figure 50). No significant condition x distance interactions were observed at any joint (all $p \geq 0.143$, $\omega^2 \leq 0.002$; see figure 50). The main effects for distance are reported in the figure 50.

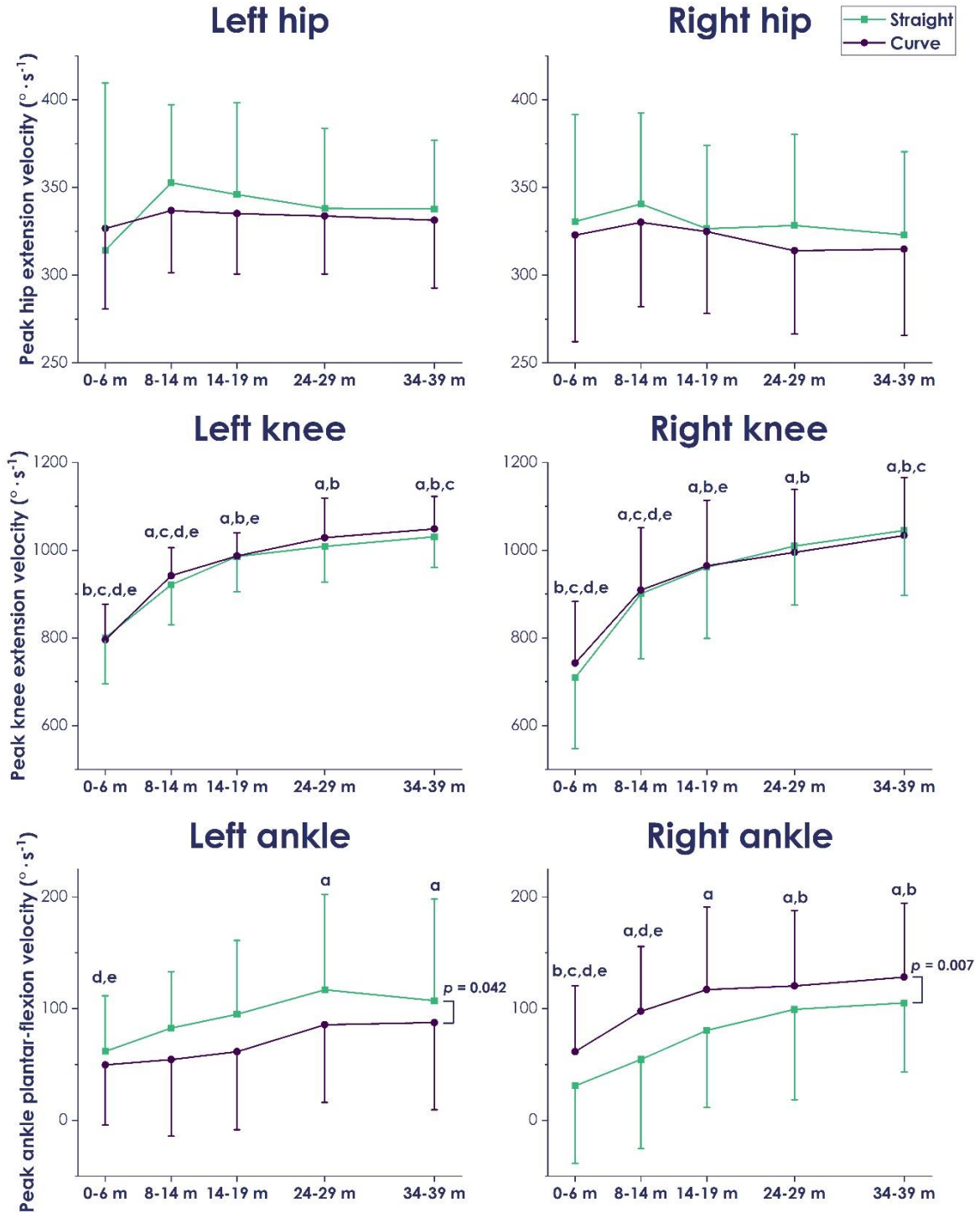


Figure 50. Mean (\pm SD) left and right hip and knee peak extension velocities and ankle peak plantarflexion velocities reached during the late swing phase. a: different from 0-6 m; b: different from 8-14 m; c: different from 14-19 m; d: different from 24-29 m; e: different from 34-39 m ($p < 0.05$). The brackets indicate a main effect for condition. All significant differences reported are $p < 0.05$.

ii. Peak flexion velocity

No significant main effect for condition were reported for the peak hip and knee flexion velocities (all $p \geq 0.098$). A main effect for distance was found for the left ($F_{(1,18)} = 25.269, p < 0.001, \omega^2 = 0.273$) and the right ($F_{(1,18)} = 40.393, p < 0.001, \omega^2 = 0.189$) knee peak flexion velocities. The post-hoc analyses with the Bonferroni corrections showed that the left and the right knee peak flexion velocities were greater starting from 8-14 m onwards in comparison to 0-6 m.

4. Swing times

The two-way ANOVA with repeated measures showed a significant main effect for condition for the right swing times ($F_{(1,18)} = 26.936, p < 0.001, \omega^2 = 0.058$). The post-hoc analysis with the Bonferroni correction showed that the right swing times were lower in the curve in comparison to the straight ($p < 0.001$; see figure 51).

We also reported a significant main effect for distance for the left ($F_{(1,18)} = 167.778, p < 0.001, \omega^2 = 0.766$) and the right ($F_{(1,18)} = 161.492, p < 0.001, \omega^2 = 0.779$) swing times. The post-hoc analyses with the Bonferroni corrections showed that the left and the right swing times increased successively from 0-6 m to 24-29 m and plateaued afterwards (see figure 51).

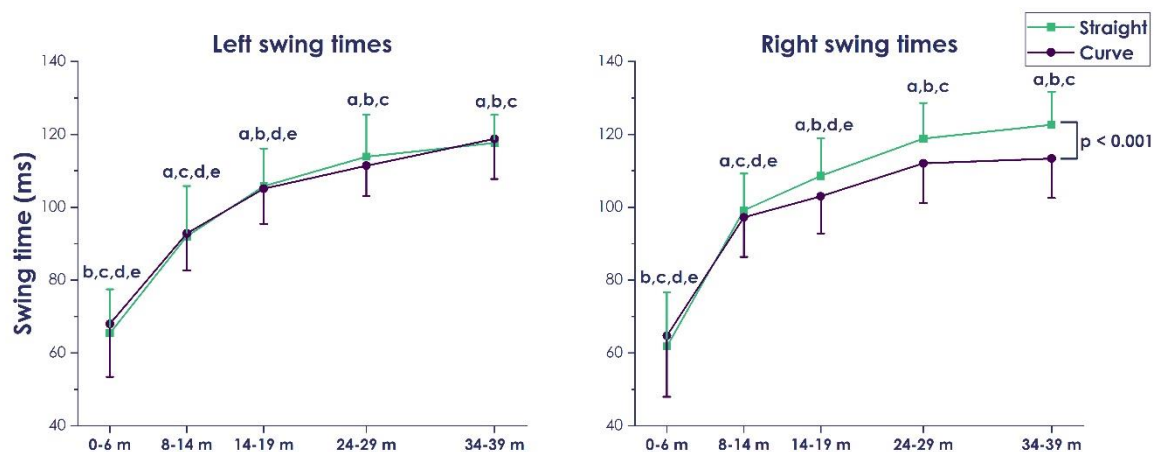


Figure 51. Mean (\pm SD) left and right swing times at each distance in the straight (green) and in the curve (purple). a: different from 0-6 m; b: different from 8-14 m; c: different from 14-19 m; d: different from 24-29 m; e: different from 34-39 m ($p < 0.05$). The brackets indicate a significant main effect for condition. All significant differences reported are $p < 0.05$.

5. Step frequency

The two-way ANOVA with repeated measures showed a significant main effect for condition for the left SF ($F_{(1,17)} = 17.489$, $p < 0.001$, $\omega^2 = 0.056$). The post-hoc analysis with the Bonferroni correction showed that the left SF was lower in the curve in comparison to the straight ($p < 0.001$; see figure 52). For the left and the right limbs, the SF increased from 0-6 m to 8-14 m and plateaued afterwards (see figure 52).

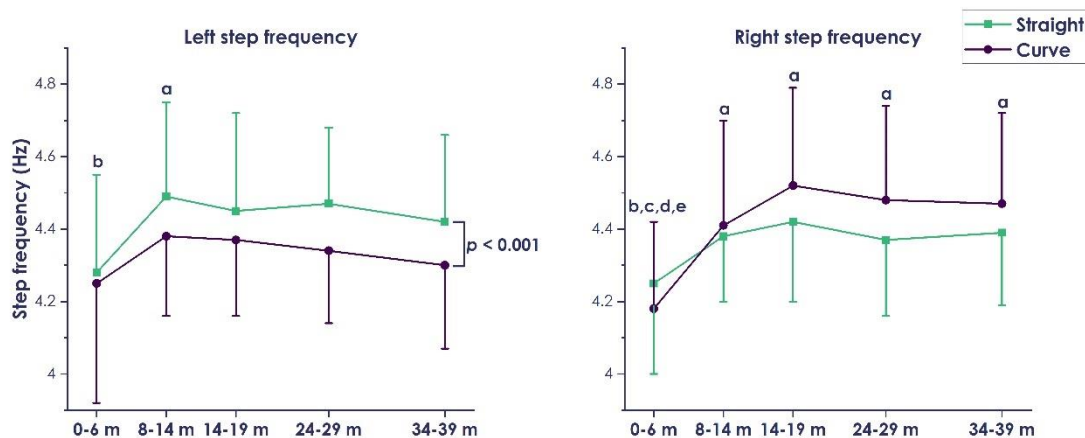


Figure 52. Mean (\pm SD) left and right step frequencies at each distance in the straight (green) and in the curve (purple). a: different from 0-6 m; b: different from 8-14 m; c: different from 14-19 m; d: different from 24-29 m; e: different from 34-39 m ($p < 0.05$). The brackets indicate a significant main effect for condition. All significant differences reported are $p < 0.05$.

2. Discussion

The core novelty of the present experimentation was the ability to process the hip, the knee and the ankle sagittal plane kinematics during the stance and the swing phases in both the straight and the curve from the first stance after the starting blocks exit to the $V_{A-P MAX}$. The main findings of the present study were that, likely due to the BLL, the participants flexed more their left knee and plantar-flexed more their right ankle during the stance in the curve in comparison to the straight, likely in an attempt to maintain the ankle-hip-shoulder alignment.

1. Are the lower limb joint kinematics affected by the curve?

The figure 53 shows the group's mean hip, knee and ankle angles (top panels) and angular velocities (bottom panels) over the stance (left panels) and swing (right panels) phases, both in the straight (full lines) and in the curve (dashed lines) at 34-39 m. This figure is provided to illustrate our findings throughout the discussion. Overall,

slight changes were observed at the peak extension/plantarflexion angles and the peak extension/plantar flexion velocities between the straight and the curve (which will be discussed below). Yet, the hip, the knee and the ankle joint sagittal plane kinematic curves were mostly similar in the straight and in the curve during both the stance and the swing phases (see figure 53). The joint angles and angular velocities reported in the present study well resembled to those previously reported in the existing literature at 0-6 m (N. E. Bezodis et al., 2014; Brazil et al., 2016; Charalambous et al., 2012; Debaere, Delecluse, et al., 2013; King et al., 2023; Slawinski, Bonnefoy Mazure, Ontanon, et al., 2010), 14-19 m (Johnson & Buckley, 2001) and at $V_{A-P MAX}$ (Belli et al., 2002; I. N. Bezodis et al., 2008).

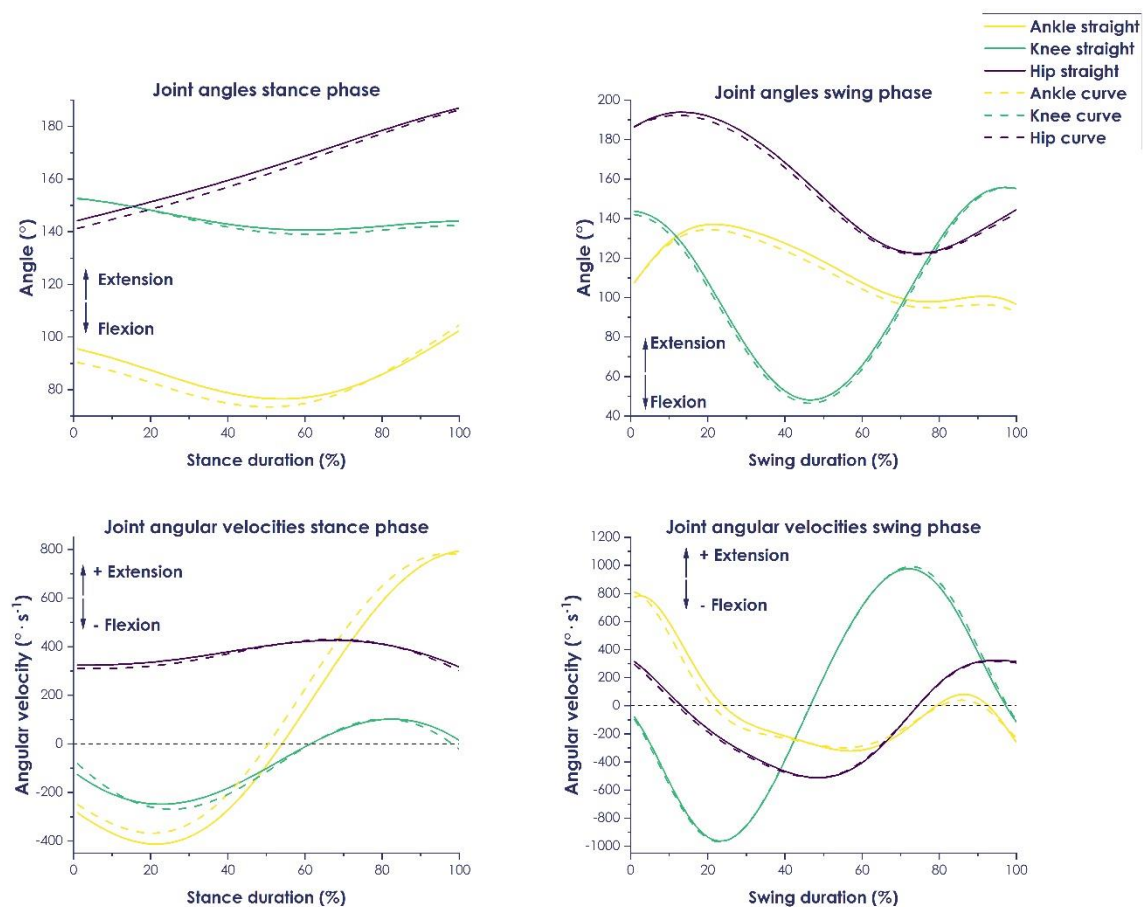


Figure 53. Graphical representation of the group's mean joint angles and angular velocities during the stance (left panels) and swing (right panels) phases, both in the straight (full lines) and in the curve (dashed lines) at 34-39 m. For clarity sake, we only displayed the left limb in the straight and in the curve.

i. Stance phase

Hip

No differences between the straight and the curve were observed for the left and the right hip peak extension angles during the stance phase (see table 10 and figure 47).

In both sprinting conditions, the hip was extending through the stance and reached the peak extension angle at the end of the stance, with the hip almost fully extended (see figure 53).

The hip peak extension velocity on the other hand was reached during the late stance phase (~70% of the stance duration; see figure 53). No differences between the straight and the curve were found, neither for the left, nor for the right hip peak extension velocities during the late stance phase ($p \geq 0.215$; see table 10 and figure 48). Therefore, our findings for the left hip contrast with those reported by Churchill et al. (2015) as these authors found a significantly lower left hip peak extension velocity during the stance phase in the curve in comparison to the straight at 40 m. The discrepancies between both studies could be explained by the different radii of curvature in the two studies. In the present experimentation, we reconstructed a lane 5 ($r = 41.58$ m) while Churchill et al. (2015) reconstructed a lane 2 ($r = 37.72$ m). Thus, it is likely that the tighter the radius of curvature, the lower the hip peak extension velocity during the stance phase.

Knee and ankle

In the curve, the left knee peak extension angle was in average 2° lower than in the straight during the stance ($p = 0.004$; see figure 47) while no differences were observed at the right knee ($p = 0.182$; see table 10 and figure 47). In contrast, the right ankle peak plantarflexion angle was in average 3.7° greater in the curve in comparison to the straight during the stance phase while no differences were observed on the left ankle ($p = 0.226$; see table 10 and figure 47). The figure 54 shows a graphical representation of the distance between the greater trochanter (dark blue circles) and the ground (horizontal black line) in order to illustrate those findings. From this figure 54, we can visually see that the distance between the right greater trochanter and the ground (L2) is greater than for the right limb (L2) (see figure 54, panel A). Thus, in order to adapt for the BLL in the curve (Churchill et al., 2015; Judson, Churchill, Barnes, Stone, Brookes, et al., 2020), maintain an ankle-hip-shoulder alignment and reach the ground, the participants necessarily plantar flexed more their right ankle. For the left limb, on the other hand, the ankle-hip-shoulder alignment was met by flexing more the left knee. In the present study, the participants sprinted on a flat track. It is likely that different results could be observed on a banked track as the distance L1' is increased while the distance L2' is decreased (see figure 54, panel B)), yet this was beyond the scope of the present study.

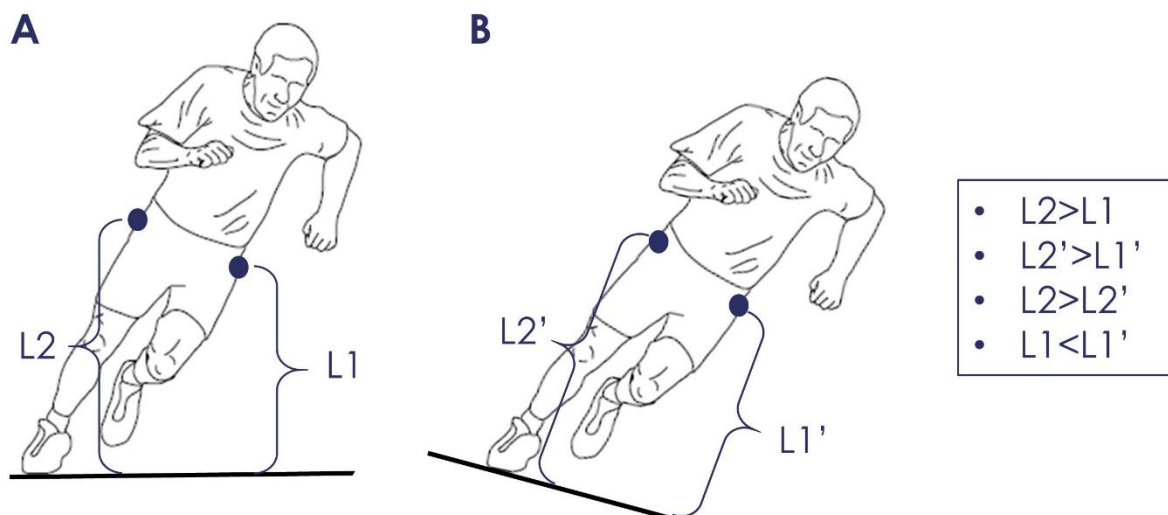


Figure 54. Graphical representation showing a sprinter leaning into the curve in the frontal plane A. on a flat track; B. on a banked track. The two dark blue dots show respectively the left and the right greater trochanter. $L1$ and $L2$ correspond to the distance between respectively the left and the right greater trochanter and the ground (dark horizontal line). Figure adapted from Chang and Kram (2007).

During the 0-6 m section of the sprint, no knee flexion was observed during the stance phase either in the straight or in the curve, which is similar to what King et al. (2023) previously reported during the first four stances in the straight. From 8-14 m into the sprint onwards, the knee was systematically flexing for the first ~40-70% of the stance phase (see figure 53). The knee was then extending through the end of the stance and the knee peak extension angle was reached around the take-off (see figure 53).

No difference in the left and the right knee peak extension velocities during the stance phase were found between the straight and the curve ($p \geq 0.795$; see figure 53). During the 0-6-m section, two peaks of knee extension velocities were reached: at touchdown and at ~90% of the stance duration (see figure 53). From 8-14 m onwards, the knee peak extension velocity was reached between ~70 and 90% of the stance duration (see figure 53).

At touchdown, the ankle was plantar-flexed between 80 and 90° (depending on the distance; see figure 53). The ankle dorsiflexed during the first ~50-70% of the stance phase, then plantarflexed afterwards and until the take-off (see figure 53). Consequently, two peaks of ankle plantarflexion angles were reached during the stance. In the present study, the second peak of ankle plantarflexion was investigated and we reported a greater right ankle peak plantar flexion angle in the curve ($p = 0.009$; see table 10 and figure 47).

Table 10. Summary of the significant main effects for condition between the straight and the curve on the hip, the knee and the ankle peak extension/plantarflexion angles and angular velocities.

		Left	Right
		Curve vs straight	Curve vs straight
Extension/Plantarflexion angle	Hip	→	→
	Knee	↓	→
	Ankle	→	↑
Extension/Plantarflexion velocity	Hip	→	→
	Knee	→	→
	Ankle	→	→

ii. Swing phase

Hip

After the take-off, the hip continued to extend during the first ~10% of the swing duration and the hip peak extension was reached (~180-190°; see figure 53). Afterwards, the hip flexed until ~70-80% of the swing duration (peak hip angle of ~100-120°; see figure 53) and then extended until the following touchdown. The hip peak flexion angles during the mid-swing phase were similar in the straight and in the curve (~105-120°; see table 11 and figure 49). The hip peak flexion velocity occurred during the mid-swing phase (at ~50% of the swing duration) with the participants reaching a hip peak flexion velocity of ~500 °·s⁻¹. We observed no differences between both sprinting conditions for the left and the right hip peak flexion velocities ($p \geq 0.098$; see table 11 and figure 53).

Afterwards, the hip extended until the following touchdown where a second hip peak extension was reached (~120-140°; see figure 53). In the present study, this second hip peak extension angle was of interest and we did not report any differences neither for the left, nor for the right hip peak extension angles between the straight and the curve ($p \geq 0.150$; see table 11 and figure 49). No differences in the left and right hip peak extension velocities between the straight and the curve were observed during the late swing phase either ($p \geq 0.127$; see table 11 and figure 50). Two peaks of hip extension velocities were observed during the swing phase (see figure 53). The first one occurred at the take-off (~300 °·s⁻¹) while the second one was reached between 90% of the swing duration and the following touchdown (~300 °·s⁻¹ as well; see figure 53).

Knee

After the take-off, almost all the participants started to flex their knee until 50-60% of the swing duration while the thigh was repositioned forward (see figure 53). In the curve, the left knee peak flexion angle was in average 1.7° greater than in the straight ($p = 0.029$; see table 11). On the other hand, no differences between the straight and the curve were observed for the right knee ($p = 0.550$; see table 11). Additionally, the knee peak flexion velocity was mostly observed at $\sim 20\%$ of the swing phase ($\sim 1000^\circ \cdot s^{-1}$). No differences between the straight and the curve were reported in the knee peak flexion velocity during the swing phase (all $p \geq 0.661$; see table 11).

From $\sim 60\%$ and until $\sim 98\%$ of the swing duration the knee extended. Thus, two peaks of knee extension angles were observed during the swing phase (*i.e.*, just after the take-off and in the late swing phase; see figure 53). In the present study, we compared the knee peak extension angle between the straight and the curve reached during the late swing phase as the hamstrings seem to be at a higher injury risk during this phase of the swing (Chumanov et al., 2012; Thelen, Chumanov, Hoerth, et al., 2005; Yu et al., 2008). We did not report significant differences in the knee peak extension angles and angular velocities between the straight and the curve during the late swing phase (respectively $p \geq 0.360$ and $p \geq 0.249$; see table 11 and figure 49-50). The knee peak extension velocity (between ~ 700 and $1050^\circ \cdot s^{-1}$) was reached at $\sim 70\text{-}80\%$ of the swing phase duration (see figure 53).

Ankle

After the take-off, the ankle kept plantar-flexing for the first $\sim 20\%$ of the swing duration (see figure 53). Afterwards, the ankle was dorsiflexing with the thigh being repositioned forward and until $\sim 80\%$ of the swing phase duration (see figure 53). In the late swing phase, some participants slightly plantar-flexed ($\sim 100^\circ \cdot s^{-1}$) their ankle before the following touchdown while others did not (see figure 53). The left ankle peak plantarflexion angle was in average 2.8° lower in the curve in comparison to the straight ($p = 0.017$; see table 11 and figure 49) while the right ankle peak plantarflexion angle was in average 3.5° greater in the curve ($p = 0.015$; see table 11 and figure 49). Similarly, the left ankle peak plantarflexion velocity was in average $25^\circ \cdot s^{-1}$ lower in the curve in comparison to the straight ($p = 0.042$; see table 11 and figure 50) while the right ankle peak plantarflexion angle was in average $31^\circ \cdot s^{-1}$ greater in the curve ($p = 0.007$; see table 11 and figure 48).

Table 11. Summary of the significant main effects for condition between the straight and the curve on the hip, knee and ankle peak extension/plantarflexion/flexion angles and angular velocities, step frequency and swing times.

		Left	Right
		Curve vs straight	Curve vs straight
Peak extension/Plantarflexion angle	Hip	→	→
	Knee	→	→
	Ankle	↓	↑
Peak extension/Plantarflexion velocity	Hip	→	→
	Knee	→	→
	Ankle	↓	↑
Peak flexion angle	Hip	→	→
	Knee	↑	→
Peak flexion velocity	Hip	→	→
	Knee	→	→
Step frequency		↓	→
Swing time		→	↓

2. Do the joint angles and angular velocities change with the increasing distance?

Overall, the hip, knee and ankle peak angles and angular velocities followed a similar time-course pattern with the increasing distance both in the straight and in the curve.

i. Stance phase

During the stance phase, most of the peak angles and angular velocities plateaued starting from 14-19 m (see figures 47 & 48). This instant was likely concomitant with the second “breakpoint” identified by Nagahara et al. (2014) whereby the sprinters have reached an erected posture and the CM vertical position almost plateaus afterwards. Thus, we hypothesize that most of the modifications at the lower limb joint angles and angular velocities during the stance phase are associated with the sprinters progressing from a crouched position towards an erected posture.

ii. Swing phase

To our knowledge, this was the first experimentation to record the knee peak extension angle and extension velocity during the late swing phase throughout the transition phase of overground maximal effort sprints. The left and the right knee peak extension

angles and extension velocities increased progressively until 24-29 m and plateaued afterwards (see figures 47 & 48). In addition to that, although this was not an aim of the present study, we investigated the knee angles at the knee peak extension velocities during the late swing phase as this could relate to the *BFIh* MTU length and in turn the injury risks (Chumanov et al., 2012; Schache et al., 2012, 2013; Thelen, Chumanov, Best, et al., 2005). The left and the right knees were progressively more extended when they reached their peak extension velocity (from $\sim 97^\circ$ at 0-6 m to $\sim 108^\circ$ at 34-39 m, see the **general discussion** for a more detailed analysis). Therefore, as the participants progressed into the sprint, straightened up and reached higher V_H , their knee extended at a progressively higher velocity with the knee progressively more extended during the late swing phase.

As the *BFIh* is likely at the highest injury risk during the late swing phase (Chumanov et al., 2012), we hypothesized that the greater the knee peak extension velocity at a greater knee extension angle, the greater the *BFIh* injury risk. Although further experimentations should be conducted to confirm those preliminary findings, track and field coaches should pay attention to limit the knee extension angles and extension velocities when performing sprints ≥ 25 m. For that sake, sprint trainings can be done in hills or with sleds (Guo et al., 2006; Okudaira et al., 2021). As the *BFIh* is bi-articular, the hip kinematics should also be discussed in order to have a broader overview of the *BFIh* injury risk. This will be debated in the **general discussion** of the present manuscript.

3. Spatiotemporal parameters

In the present study, we reported significantly shorter right swing times in comparison to the straight which is similar to what was previously reported in the curve at $V_{A-P MAX}$ (Churchill et al., 2015, 2016). Although the SL was not computed in the present study, we can further assume that the shorter right swing time would in turn reduce the right SL (Churchill et al., 2015, 2016).

We saw in the **study #2** that the left stance times increased in the curve in comparison to the straight. Hence, as the left swing time was unchanged, the left SF was reduced in the curve in comparison to the straight (see figure 52), which can further explain the reduced sprinting performance in the curve.

3. Limitations

The MIMU-based system used in the present experimentation can be used as an easy-to-use system. Considering its portability, it can be easily used for *in-field* experimentations (Dinu et al., 2020, 2023; Slawinski et al., 2020) to strengthen the ecological validity. In addition, this MIMU-based system provides valuable data for the sagittal plane kinematics in comparison to OS (Blair et al., 2018; Nijmeijer et al., 2023; Robert-Lachaine et al., 2017). However, the frontal and transverse planes kinematics computed with this MIMU-based system showed lower agreement in comparison to an OS (Nijmeijer et al., 2023; Robert-Lachaine et al., 2017). Consequently, we limited our analysis to the sagittal plane kinematics and we might have missed differences between the straight and the curve on the frontal and the transverse planes. In the future, other experimentations should target the frontal and transverse plane kinematics through the transition phase in the curve.

Finally, in the present study, we investigated the peak joint angles and angular velocities. However, the peaks only provide a partial understanding of the whole picture. Thus, investigating the entire joint angle and angular velocity signals during the stance and swing phases using a Statistical Parametric Mapping (Colyer et al., 2018, 2019; Hegyi, Gonçalves, et al., 2019) would be of great interest in the future.

4. Conclusion

Despite our initial thoughts based on the **study #2** findings, the sagittal plane kinematics were only slightly affected by the curve. During the stance phase, due to the BLL and in order to maintain an ankle-hip-shoulder alignment, the left knee peak extension was reduced and the right ankle plantarflexion was increased in comparison to the straight. Based on these findings, it is likely that the lower mean F_V at the left limb in the curve were related to the left knee being more flexed during the stance phase and the inability to produce F_V in this position. Conversely, the modifications in the mean F_{A-P} and F_{M-L} likely originate from transverse or frontal plane kinematics that we could not investigate.

The participants' knee peak extension velocity increased progressively and was reached with the knee being more extended during the late swing phase as the participants were at a progressively higher V_{A-P} . Those findings suggest that extending the knee more rapidly, with the knee being more extended, could increase the hamstring injury risk.

The kinematic differences observed on the sagittal plane likely have a muscular origin. Consequently, investigating the sEMG activity amplitude and activation timings would be of valuable interest. For example, as the knee peak extension was reduced in the curve during the stance phase in comparison to the straight, we can postulate that knee extensors (i.e., *RF* and *VL* among others) stopped their activity earlier in the curve in comparison to the straight and/or were less activated.

Furthermore, we saw that the knees were extending more rapidly during the late swing phase with the increasing distance. Was this related to a greater sEMG activity of the knee extensors as the participants progressed into the sprint? This would suggest that a greater *BFlh* activity could also increase the hamstring injury risks during the late swing phase.

STUDY 4

Are the muscle activities altered by the curve and with the increasing sprinting velocity through the transition phase?

Associated publication

Millot, B., Pradon, D., Blache, P., Dinu, D., Cecchelli, G., Arnould, A., Hegyi, A. & Slawinski, J. (2023). Muscle activity timings in the early acceleration phase of straight-line and curve sprinting. *To be submitted*

Associated communication

Millot, B., Pradon, D., Blache, P., Dinu, D., Cecchelli, G., Arnould, A., Hegyi, A. & Slawinski, J. (2023). Muscle activity timings in the early acceleration phase of straight-line and curve sprinting. 28th European College of Sport Science, Paris, France. **Oral communication.**

1. Results

After visual inspection of each sEMG raw signal, some participants were removed from the analysis due to the poor signal quality (see **general methodology**). For the left and the right VL, 15 participants were kept for the analysis. For the left and the right GM, 14 and 15 participants were conserved, respectively. For the left and the right RF, 10 and 12 participants were kept for data reduction, respectively. Finally, for the left and the right BFlh, 18 and 15 participants were kept, respectively.

1. Stance phase

i. Muscle activity duration

The two-way ANOVA with repeated measures ($F_{(1,14)} = 3.961$, $p = 0.066$, $\omega^2 = 0.041$) and the post-hoc analysis with the Bonferroni correction showed a tendency for the left VL to be activated longer (in % of the stance duration) during the stance phase in the curve in comparison to the straight ($p = 0.066$; see figure 55).

Apart from that, the two-way ANOVAs with repeated measures did not reveal any significant main effects for condition (all $p \geq 0.324$) or condition x distance interactions (all $p \geq 0.157$) for the other muscles.

The left VL and RF muscles were activated longer from 0-6 m to 24-29 m in comparison to 34-39 m (all $p \leq 0.044$). The right VL remained active for a longer duration activity at 0-6, 14-19 and 24-29 m in comparison to 34-39 m (all $p \leq 0.049$).

On the other hand, the left BFlh remained active for a longer duration starting from 8-14 m to 24-29 m in comparison to 0-6 m (all $p \leq 0.010$). Finally, the right BFlh sEMG activity was longer at 14-19 m and 24-29 m in comparison to 0-6 m (all $p < 0.001$).

ii. sEMG activity amplitude

The two-way ANOVA with repeated measures showed a significant main effect for condition for the left VL ($F_{(1,14)} = 5.377$, $p = 0.036$, $\omega^2 = 0.042$). The post-hoc analysis with the Bonferroni correction showed that the left VL sEMG activity was lower in the curve than in the straight during the stance phase ($p = 0.036$; see table 12 and figure 56). No other significant differences between the straight and the curve were reported for the other muscles (all $p \geq 0.377$; see table 12 and figure 56).

2. Swing phase

i. Muscle activity duration

During the swing phase, the two-way ANOVA with repeated measures revealed a significant condition effect for the left *BFlh* duration of activation ($F_{(1,15)} = 11.881$, $p = 0.004$, $\omega^2 = 0.091$). The post-hoc analysis with the Bonferroni correction showed that the left *BFlh* was active for a shorter duration during the swing phase in the curve in comparison to the straight ($p = 0.004$; see figure 55). For the other muscles, no significant condition effects were reported during the swing phase (all $p \geq 0.088$).

The two-way ANOVA with repeated measured showed a significant main effect for distance for the right GM duration of activation in the swing phase ($F_{(1,9)} = 5.017$, $p = 0.003$, $\omega^2 = 0.102$). The post-hoc analysis with the Bonferroni correction showed that the right GM was active for a longer duration at 8-14 m and 34-39 m in comparison to 0-6 m (both $p \leq 0.018$). In addition to that, the left *BFlh* was active for a shorter period starting from 14-19 m onwards in comparison to 0-6 m ($F_{(1,15)} = 3.939$, $p = 0.007$, $\omega^2 = 0.090$).

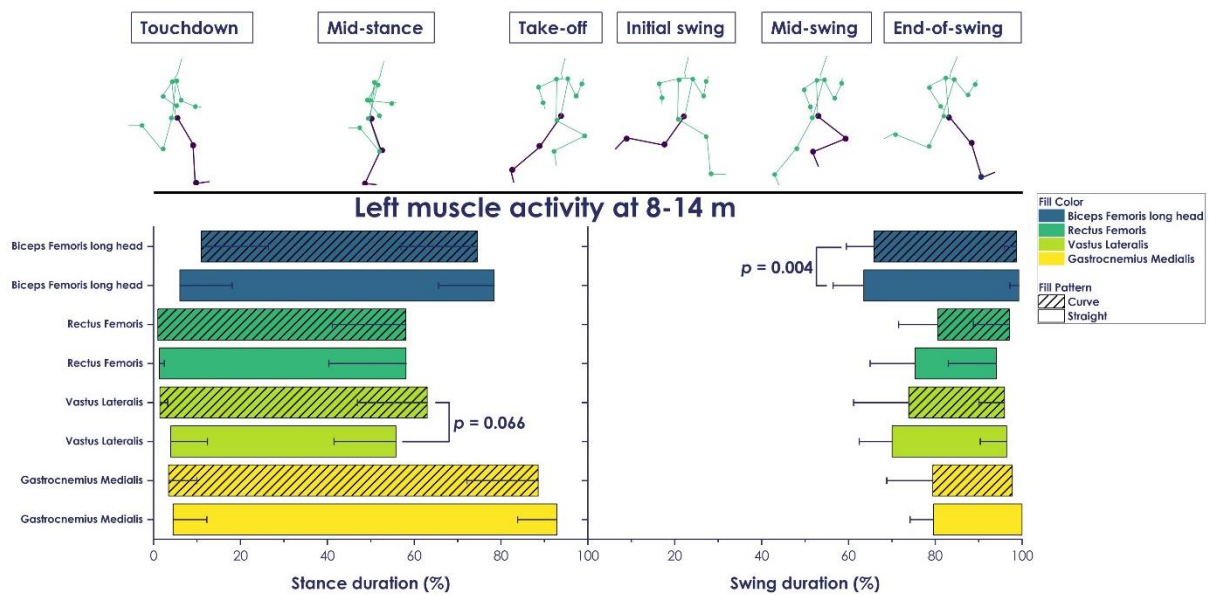


Figure 55. The mean \pm SD of the left muscle activation timings during the stance (left panel) and swing (right panel) phases at 8-14 m. The different full (straight) and dashed (curve) horizontal floating charts represent the periods where the muscles are active. The error bars represent the standard deviations of the mean onset and offset of each muscle activity. For clarity sake, we only provide one figure.

ii. sEMG activity amplitude

The two-way ANOVA with repeated measures did not reveal any significant main effects for condition, or condition x distance interactions for the sEMG activity amplitude during the swing phase (all $p \geq 0.066$ and $\omega^2 \leq 0.041$; see table 13 and figure 57).

During the swing phase, the left *BFlh* ($F_{(1,16)} = 4.982$, $p = 0.001$, $\omega^2 = 0.064$) showed a greater sEMG activity at 34-39 m in comparison to 0-6 m (see figure 57). On the other hand, the right *BFlh* showed a greater sEMG activity starting from 14-19 m onwards in comparison to 0-6 m ($F_{(1,14)} = 4.652$, $p = 0.013$, $\omega^2 = 0.064$) (see figure 57). That being said, both the left and the right *BFlh* sEMG activity amplitudes plateaued starting from 8-14 m (see table 12 and figure 57).

For the left *VL*, the mean sEMG activity was lower between 34-39 m in comparison to 0-6 m ($F_{(1,14)} = 2.831$, $p = 0.033$, $\omega^2 = 0.042$; see figure 56). Finally, for the left ($F_{(1,12)} = 5.712$, $p < 0.001$, $\omega^2 = 0.064$) and the right *GM* ($F_{(1,13)} = 8.722$, $p < 0.001$, $\omega^2 = 0.122$), the sEMG activity during the stance phase was greater starting from 24-29 m onwards in comparison to 0-6 m (see table 12 and figure 57).

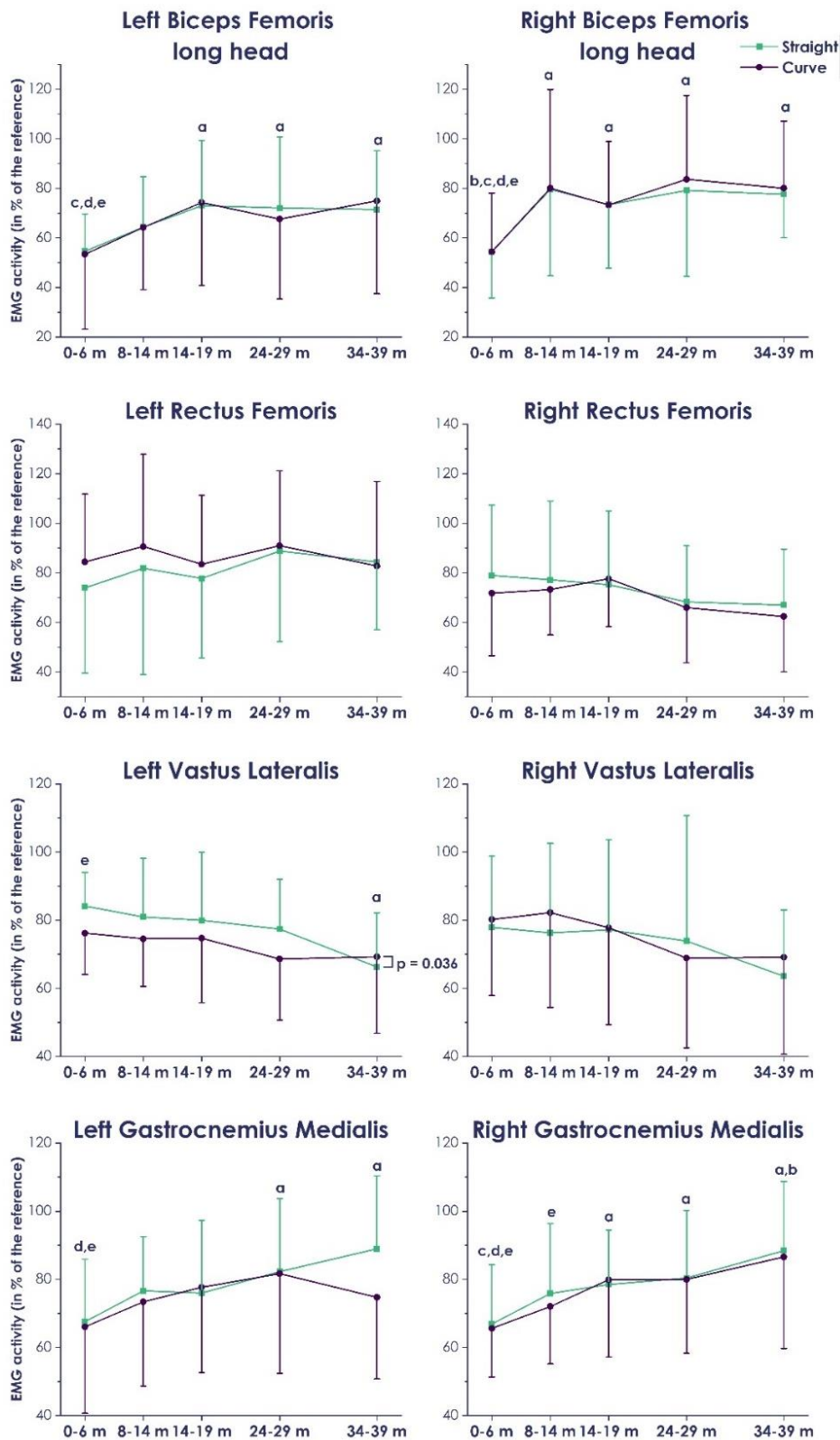


Figure 56. Mean (\pm SD) surface electromyographic activity (expressed relative to the reference) during the stance phase averaged over each zone for the left and right Biceps Femoris long head, Rectus Femoris, Vastus Lateralis & Gastrocnemius Medialis. For all panels, * indicates a significant main effect for condition ($p < 0.05$); a: different from 0-6 m; b: different from 8-14 m; c: different from 14-19 m; d: different from 24-29 m; e: different from 34-39 m ($p < 0.05$).

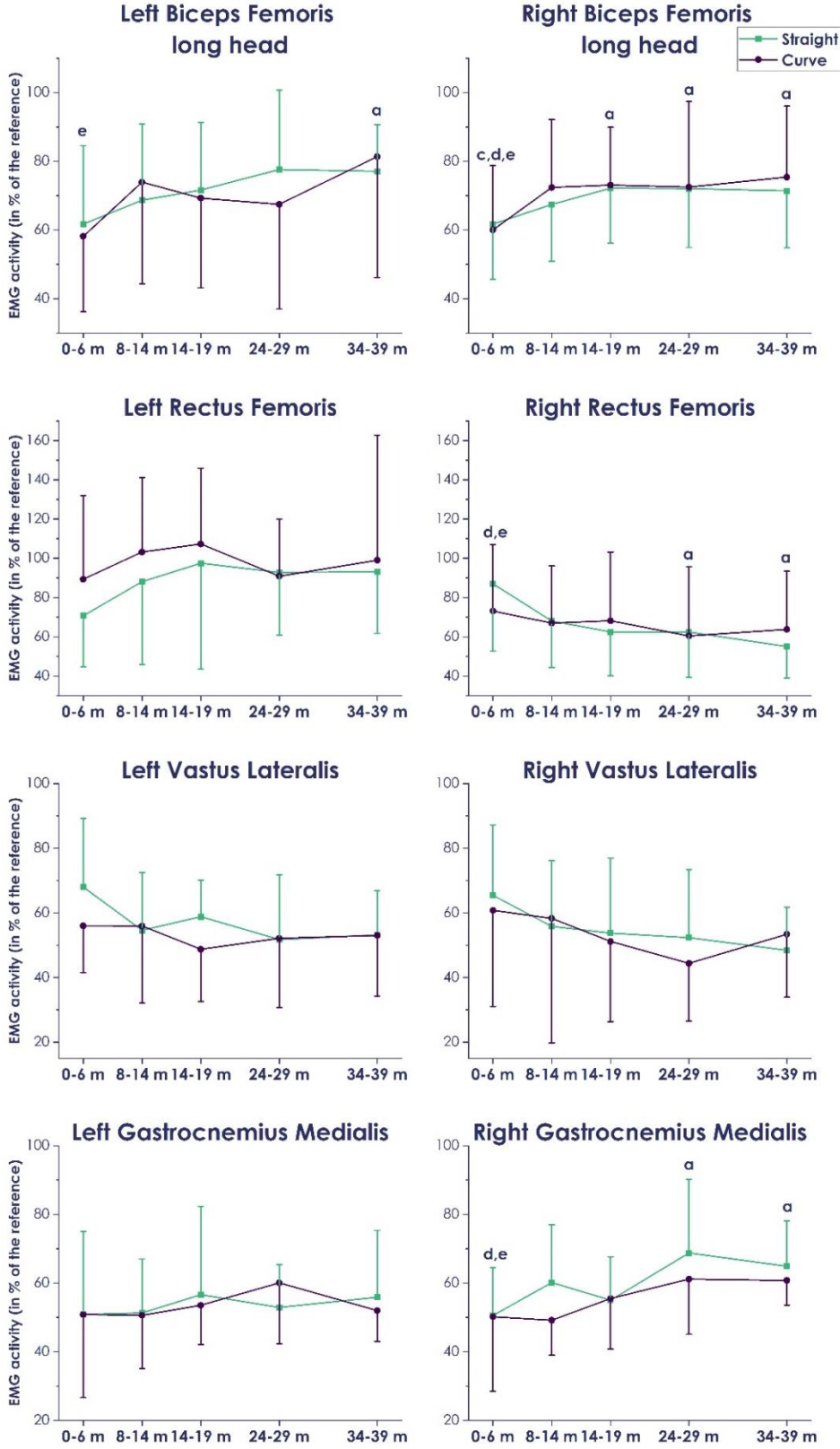


Figure 57. Mean (\pm SD) surface electromyographic amplitude (expressed relative to the reference) during the swing phase averaged over each distance for the left and right Biceps Femoris long head, Rectus Femoris, Vastus Lateralis & Gastrocnemius Medialis. For all panels, * indicates a significant main effect for condition ($p < 0.05$); a: different from 0-6 m; b: different from 8-14 m; c: different from 14-19 m; d: different from 24-29 m; e: different from 34-39 m ($p < 0.05$).

2. Discussion

To our knowledge, this is the first experimentation to investigate the sEMG activity in the curve at radii typical of outdoor track events. In this study, the main finding was that the left VL sEMG activity was lower in the curve in comparison to the straight. This could in turn explain the lower left knee peak extension (see **study #3**) which could itself explain the lower F_V in the left limb in the curve (see **study #2**).

1. Is the muscle activity affected by the curve?

i. Muscle activity duration during the stance phase

In the present study, we did not observe any modifications in the sEMG activity duration between the straight and the curve during the stance phase (see table 12). We only found a tendency ($p = 0.066$; see table 12) for the left VL to be active longer in the curve in comparison to the straight relative to the stance time. As the left stance times were longer in the curve than in the straight (**see study #2**), it is likely that when expressed in absolute terms, the left VL would be active longer in the curve than in the straight.

It is worth mentioning that, in the present study, we analyzed separately the stance and the swing phases in order to maintain the consistency with the **studies #2** and **#3**. Therefore, the TKEO and the AGLR (see the **general methodology**) were applied on the sEMG signals during either the stance or the swing phases, separately. By doing so, it appeared that some participants had two distinct bursts of sEMG activity through the stride (*i.e.*, one first sEMG activity during the stance phase and one second sEMG activity during the late swing phase; see an example on the figure 55). However, it is likely that if we had applied the TKEO and the AGLR on the entire stride cycle (as a single sEMG signal), we would have observed a single sEMG burst starting from the late swing phase and lasting until the following stance phase. In fact, this is what most of the participants showed. Indeed, only a few participants deactivated their muscles during the late swing phase, before the following touchdown, while the majority of the participants kept their muscles active from the late swing phase into the mid/late stance phase (see figure 57).

Overall, the sEMG activities were similar between the straight and the curve (see table 12 and figures 56-57) for the four muscles investigated in the present study. During the stance phase, the left and the right *BFlh*, *RF*, *VL* and *GM* were active at touchdown for almost all participants (the figure 55 shows the mean \pm SD of the left muscle activity at 8-14 m during the stance and swing phases). Afterwards, the left and the right *RF* and *VL* became inactive first among the muscles investigated (between ~50-70% of the

stance duration), followed by the *BFlh* (~70-80% of the stance duration) and finally the *GM* (~80-95% of the stance duration) (see figure 55). Interestingly, the *RF* and the *VL* (*i.e.*, two knee extensors), became inactive earlier than the knee peak extension velocity (reached at ~80% of the stance duration, see **study #3**) (see figure 55). Consequently, those findings suggest that other knee extensors (*i.e.*, for instance the *VM* or the *Vastus Intermedius*) remained active during the stance, after the *VL* and the *RF* became inactive, to continue to extend the knee.

ii. Muscle activity duration during the swing phase

During the swing phase, both in the straight and in the curve, the *RF* showed two clear bursts at 0-6 m for all the participants as it was previously described at $V_{A-P MAX}$ (Takehata et al., 2021) or during the deceleration phase (Takehata et al., 2022) in the straight. The first burst occurred in the mid-swing phase, with the *RF* acting as a hip flexor (Mero & Komi, 1987) to reposition the thigh forward (Takehata et al., 2021). In contrast, we did not observe a systematic activation of the *RF* during the mid-swing phase starting from 8-14 m onwards (see figure 55), both in the straight and in the curve, and this *RF* activation was apparently more participant-dependant. Indeed, some participants presented a clear activation of the *RF* (~1/3rd of the participants) while the others did not (~2/3rd of the participants). Those findings suggest that, while in a crouched position (*i.e.*, from 0 to 6 m) all the participants solicited their *RF* to flex their hip during the mid-swing phase. In contrast, as the sprinters straightened up, the hip flexion during the mid-swing phase resulted from individual muscle coordination both in the straight and in the curve. Consequently, starting from 8-14 m onwards, the participants that did not activate their *RF* during the mid-swing phase likely activated other hip flexors (*i.e.*, *Psoas*, *Iliacus*, *Sartorius*, *ADD*) to flex their hip.

At 0-6 m, during the swing phase in the curve, the left *RF* was active for 7% less time in comparison to the straight (during 22.1% vs 29.1% of the swing duration in the curve and in the straight, respectively; $p = 0.029$; see table 13). This was mainly caused by an earlier offset of the left *RF* in the curve. Indeed, the left *RF* became inactive at $50.8 \pm 5.9\%$ vs $55.5 \pm 7.8\%$ of the swing duration in the curve and in the straight, respectively. As we have previously seen in the **study #3**, someone sprinting in the curve leans inward (Churchill et al., 2015; Judson, Churchill, Barnes, Stone, Brookes, et al., 2020). Thus, it is likely that with the BLL, the left *RF* had "less room" to reposition the thigh forward (Churchill et al., 2016) and in turn became inactive earlier than in the straight. Consequently, other hip flexors were likely activated in this specific body position to continue to flex the left hip during the swing phase in the curve after the *RF* has become inactive (*i.e.*, *Psoas*, *Iliacus*, *Sartorius*, *Adductor*).

The second *RF* activation occurred during the late swing phase and started at ~75% of the swing duration. During the late swing phase, the *BFlh*, the *VL* and the *GM* showed a single activation. The *BFlh* became active first at ~60% of the swing duration, followed by the *VL* (at ~70%) and the *GM* (at ~80%) and these muscles remained active until the following touchdown for the majority of the participants. Those findings are in line with what previous research showed (Howard et al., 2018; Pinniger et al., 2000). As no differences were reported between the straight and the curve, we can hypothesize that the late swing phase is less affected by the BLL in the curve than the mid-swing phase.

Using musculoskeletal modeling or joint kinematics, different experimentations estimated the muscle lengthening or shortening in sprinting. Hence, according to these models, the *BFlh* is likely eccentrically contracted (Nagano et al., 2014; Schache et al., 2012; Yu et al., 2008) during the first half of the late swing phase, to slow the knee extension (Higashihara et al., 2010; Kyröläinen et al., 2005b). Afterwards, at the end of the late swing phase, the *BFlh* MTU is apparently shortening as the hip extends (Nagano et al., 2014; Schache et al., 2012). Concomitantly, the *RF* and the *VL* are likely concentrically activated to extend the knee. Hence, we can hypothesize that the *BFlh* and the *RF* (i.e., two antagonist muscles) are co-activated to create a high knee joint stiffness before the following touchdown (Belli et al., 2002; Hasan, 1986; Hortobagyi & DeVita, 2000; Latash, 2018; Nummela et al., 1994). Finally, despite the ankle was plantarflexed before the following touchdown, to produce the “pawing action” of the foot (Morin, Gimenez, et al., 2015), it is challenging to estimate whether the *GM* MTU is shortening or lengthening as this muscle is bi-articular and as the knee extends in the meantime.

iii. Muscle activity amplitude during the stance phase

In the curve, only the left *VL* sEMG activity amplitude was affected among the muscles investigated during the stance phase (see table 12 and figure 56). Indeed, we found that the left *VL* sEMG activity amplitude was ~5% lower in the curve, in comparison to the straight, during the stance phase. As the *VL* is a knee extensor, we can hypothesize that the lower *VL* sEMG activity amplitude in the curve could be related to the lower knee peak extension angle observed in the curve during the stance phase (see **study #3**), due to the BLL.

Table 12. Summary of the significant main effects for condition between the straight and the curve on the Biceps Femoris long head, the Rectus Femoris, the Vastus Lateralis and the Gastrocnemius Medialis activity duration and amplitude during the stance phase.

		Left	Right
		Curve vs straight	Curve vs straight
Duration	Biceps Femoris long head	→	→
	Rectus femoris	→	→
	Vastus Lateralis	↓ ($p = 0.066$)	→
	Gastrocnemius Medialis	→	→
Amplitude	Biceps Femoris long head	→	→
	Rectus femoris	→	→
	Vastus Lateralis	↓	→
	Gastrocnemius Medialis	→	→

iv. Muscle activity amplitude during the swing phase

On the other hand, no modifications were observed among the four muscles investigated in the sEMG activity amplitude between the straight and the curve during the swing phase (see table 13 and figure 57). As we did observe kinematic differences at the ankle joint in the late swing phase (see **study #3**) and as no differences were observed at the GM, the kinematic differences at the ankle could result from sEMG activity changes of other plantar flexor muscles (i.e., the Soleus or the Flexor Hallucis Longus) or foot muscles (i.e., Flexor Hallucis Longus or Flexor Hallucis Brevus (Tanaka et al., 2019)).

Table 13. Summary of the significant main effects for condition between the straight and the curve on the Biceps Femoris long head, the Rectus Femoris, the Vastus Lateralis and the Gastrocnemius Medialis activity duration and amplitude during the swing phase.

		Left	Right
		Curve vs straight	Curve vs straight
Duration	Biceps Femoris long head	↓	→
	Rectus femoris (0-6 m)	↓	→
	Vastus Lateralis	↓	→
	Gastrocnemius Medialis	→	→
Amplitude	Biceps Femoris long head	→	→
	Rectus femoris (0-6 m)	→	→
	Vastus Lateralis	→	→
	Gastrocnemius Medialis	→	↓ ($p = 0.066$)

2. Is the muscle activity affected by the increasing distance?

i. Muscle activity duration and amplitude during the stance phase

During the stance phase, we showed that the left and the right *RF* were active for a shorter duration at 34-39 m in comparison to 14-19 m and 24-29 m. In addition, the left and the right *VL* were active for a shorter duration at 34-39 m in comparison to the earlier parts of the sprint. In parallel, we demonstrated that the left and the right *RF* were activated maximally at 0-6 m as their activity did not increase afterwards. In contrast, the left *VL* activity was lower at 34-39 m in comparison to 0-6 m. As the sEMG activity amplitude of the knee extensors investigated in the present study did not markedly change and as their duration of activation was reduced at 34-39 m, we hypothesize that the knee extensors have a lesser role close to $V_{A-P MAX}$ in comparison to the earlier phases of the sprint.

On the other hand, for the left and the right *GM*, the mean sEMG activity during the stance phase was greater starting from 24-29 m onwards in comparison to 0-6 m. Those findings somehow contrast with the ankle kinematics we previously reported in the **study #3** as the ankle peak plantarflexion angle plateaued starting from 8-14 m. Finally, the left and the right *BFlh*, the sEMG activity plateaued starting from 8-14 m onwards. Those findings are in line with the hip kinematics we reported in the **study #3**. Indeed, we showed in the **study #3** that the hip peak extension angle during the stance increased from 0-6 m to 8-14 m and plateaued afterwards. Consequently, based on the present findings, we can assume that, with the increasing velocity, the hip extensor and the ankle plantar flexor muscles investigated in the present study underwent greater changes in their sEMG activity, in comparison to the knee extensors. Thus, the present findings suggest that the hip extension and the ankle plantarflexion demand increased more than the knee extension demand during the stance with the increasing velocity.

ii. Muscle activity amplitude during the swing phase

During the swing phase, with the increasing distance (and thus with the increasing velocity), the left and the right *BFlh* sEMG activity amplitudes plateaued starting from 8-14 m (see figure 57). Previously, experimentations reported an increase in the *BFlh* sEMG activity with the increasing velocity (Hegyi, Gonçalves, et al., 2019; Higashihara et al., 2010; Kyröläinen et al., 1999, 2005b). However, these authors compared different steady-states velocities with participants running or sprinting on a treadmill. In the **literature review** of the present manuscript, we have already discussed the differences between steady-state running at different velocities and maximal effort sprinting from

a kinematic aspect (Frishberg, 1983; Van Caekenberghe et al., 2013) meaning that both sprinting conditions are different. In the present study, we demonstrated that the *BFlh* sEMG activity amplitude did not increase after 8-14 m ($\sim 90\%$ of $V_{A-P MAX}$) in maximal effort overground sprinting either during the stance of the late swing phase. Therefore, we can hypothesize that, close to, or at the $V_{A-P MAX}$, the *BFlh* higher injury risk is not caused by a greater sEMG activity of this muscle. Rather than the *BFlh* sEMG activity amplitude, the *BFlh* could be at a higher injury risk due to changes at the hip and the knee kinematics and this will be further discussed in the **general discussion** of the present manuscript.

3. Limitations

In the present study, we investigated four muscles that are mainly involved in sagittal plane movements. However, due to the BLL in the curve (Churchill et al., 2015; Judson, Churchill, Barnes, Stone, Brookes, et al., 2020), we can also expect differences between the straight and the curve in the sEMG activity of muscles involved in the frontal or transverse planes.

In order to explore the sEMG activity of the *BFlh*, the *RF*, the *VL* and the *GM*, we used bipolar sEMG electrodes that were positioned on the middle of the muscle belly (Hermens et al., 2000). However, by using such devices positioned at a specific location along the muscle fiber, we cannot access the changes of the sEMG activity within the muscle (*i.e.*, proximal vs distal activity) (Hegyi, Gonçalves, et al., 2019). Although Hegyi et al. (2019) did not report any differences between muscle regions in the *BFlh* at three increasing velocities using high-density sEMG (HD sEMG), their study was conducted on a treadmill at three different steady-state velocities. In addition to that, the within muscle activity of the *VL*, *GM* & *RF* were not studied in their study. Therefore, it would be of great interest to replicate the protocol of the present study, this time using high-density sEMG in order to investigate the proximal-distal changes in the sEMG with the increasing V_{A-P} within a maximal effort sprint.

In addition to that, we investigated the mean sEMG activity over each period of activity. This differs from other processing methods whereby the entire signal was considered (Jacobs & van Ingen Schenau, 1992; Mero & Komi, 1986, 1987), or where the signal was averaged over either the stance or swing phases (Higashihara et al., 2018, 2019; Morin, Gimenez, et al., 2015). In addition to that, we are aware that by splitting the analysis within stance and swing phases have likely impacted the findings as the muscles investigated are active from the late swing phase and until the following late stance phase.

4. Conclusion

In this **study #4**, we reported a lower sEMG activity of the left VL and this muscle tended to be activated for a shorter period in the curve in comparison to the straight. In the curve, the left VL likely cannot be active in a similar way to the straight due to the BLL and due to the lower knee peak extension angle.

For the other muscles investigated, we reported little modifications in the sEMG activity duration and amplitude. Those findings suggest that sprinting in the curve only slightly affected the sEMG activity of the *BFlh*, *RF* and *GM*. However, these muscles are mostly involved in movements in the sagittal plane of motion. As little differences were observed in the sagittal plane kinematics between the straight and the curve, further experimentations should target muscles involved in the transverse and frontal planes.

GENERAL DISCUSSION

The first main objective of this PhD thesis was to deepen our understanding of the different factors altering the sprinting performance in the curve using a kinetic, a kinematic and a neuro-muscular approach. Using this multidisciplinary approach, we began at the “macroscopic” level with the CM analysis (**study #1**), then gradually progressed towards a more “microscopic” level. Indeed, the CM moves thanks to the GRF and the impulses (**study #2**) which itself is impacted by the joint and the segment kinematics (**study #3**), itself caused by the sEMG activities at the muscle level (**study #4**).

The second main objective of this PhD work was to investigate whether these parameters change as a sprinter progresses into the sprint (*i.e.*, with the increasing V_{A-P}) and whether the differences between the straight and the curve increase concomitantly.

Our main findings were that:

- The sprinting performance measured with photocells was reduced in the curve in comparison to the straight starting from 15 m onwards;
- The $V_{A-P\ MAX}$ was reached sooner in the curve in comparison to the straight;
- In the curve, the left and the right mean F_{M-L} largely increased in comparison to the straight, conducting to a reduction in the left and the right mean F_{A-P} as the participants were not able to increase the mean F_{TOT} ;
- The left mean F_{TOT} was also reduced in the curve due to a lower left mean F_V . Since the left F_V was lower in comparison to the straight, the left limb stance times increased in order to produce the required left IMP_V , to maintain an adequate sprinting motion;
- The left knee peak extension angle during the stance phase was reduced in the curve due to the BLL and this was caused by a lower left VL sEMG activity during the stance phase in the curve in comparison to the straight;
- With the increasing distance, the knee peak extension velocity during the late swing phase increased until 24-29 m and plateaued afterwards both in the

straight and in the curve. This sheds light upon the greater risk of hamstring injuries as the sprinter progresses into the sprint.

1. A pioneer exploration in the curve from the starting blocks on to the maximal antero-posterior velocity

Despite the fact that the curve represents ~58% of the total distance to run from the 200 m onwards, little is known regarding the performance determinants in this sprinting condition. Thus far, the two main group of researchers that aimed to compare the curve to the straight were limited to two steps at 13 m (Judson, Churchill, Barnes, Stone, Brookes, et al., 2020; Judson, Churchill, Barnes, Stone, & Wheat, 2020; Judson et al., 2019) and at 40 m (Churchill et al., 2015, 2016) after the starting blocks. Those limitations likely originated from the several challenges faced when attempting to analyze the GRF in the curve.

In the present PhD thesis, the main challenge was to collect the GRF in the curve over multiple stances. It is likely because of this methodological challenge that the previous experimentations investigating the GRF in the curve were limited to a single stance at either 13 (Judson et al., 2019) or 40 m (Churchill et al., 2016). In order to overcome these challenges, we had the privilege to access to an indoor venue where 6 FP are embedded within the track surface. Subsequently, we replicated a lane 5 ($r = 41.58$ m) overlapping the 6 FP. In order to collect the GRF over a large number of stances, we applied a previously used protocol (Cavagna et al., 1971; Rabita et al., 2015) into the curve. This protocol permitted to analyze almost all the stances of a 40-m sprint from the starting blocks on to the ~22nd stance (corresponding approximately to $V_{A-P MAX}$) both in the straight and in the curve.

1. The curvilinear motion begins during the starting blocks pushing phase

To our knowledge, this study is the first to examine the GRF during the starting blocks pushing phase in the curve. Based on our findings, we showed that the participants produced a more lateral mean F_{M-L} during the starting blocks pushing phase in the curve than in the straight (see **study #3**). Those findings are similar to what is usually observed in biking for example, whereby before entering a curve, riders position themselves on the outside of the lane. This is also a common advice among 400-m coaches whereby the sprinters are advised to be on the outside of the lane before entering the second curve of the 400 m.

In addition to that, we observed that the choice of the leg positioned on the front block directly influenced the trajectory at the starting blocks exit. Indeed, we found

that when the left foot was positioned on the front block, the participants were almost exclusively heading towards the outside of their lane. In contrast, when the right foot was positioned on the front block, the participants were almost all heading towards the inside of their lane. Therefore, despite individual preferences in the choice of the foot to place on the front block, the present findings question the strategy to adopt regarding the foot to position on the front block for 200-, 400-, 4*100- and 4*400-m races. Future experimentations should be conducted in that way in order to comprehend whether positioning the left or the right foot on the front block impacts the performance during the initial stances in the curve.

Between 0-6 m, the mean F_{M-L} was also greater in the curve than in the straight for both the left and the right limbs. However, this time the mean F_{M-L} was more medial, meaning that the participants were heading towards the inside of their lane. Therefore, contrary to a well-admitted empirical evidence, there is no linear motion over the first 4-to-5 stances that follow the starting blocks pushing-phase.

2. The left limb pleads guilty

In the present study, the straight was considered as the “reference condition” whereby we assumed that the mean F_{TOT} produced in the straight corresponded to the individual limits of each participant. The left leg in the curve showed a clear contrast with this “reference condition” since the participants produced less mean F_{TOT} than in the straight. This was caused by a reduced left mean F_V in the curve.

It is likely that the BLL (Churchill et al., 2015; Judson, Churchill, Barnes, Stone, Brookes, et al., 2020) and the foot push-off axis that switched from transverse to oblique (Judson et al., 2019) affected the sprinter's ability to produce a similar mean F_V in comparison to the straight. Indeed, Bojsen-Møller (1978) indicated that using the oblique axis conducted to several kinematic changes on the foot and the shank. Those kinematic changes could in turn alter the muscle function of a multitude of foot muscles that play a key role in sprinting such as the *Flexor Hallucis Longus* or *Flexor Hallucis Brevus* (Tanaka et al., 2019).

In addition to that, we saw in the **study #3** that the left knee peak extension was reduced in the curve, which was itself caused by a decreased activation of the left VL (see **study #4**). Previously, Hamner & Delp (2013) and Pandey et al. (2021) reported a “substantial contribution of the VL to the upward acceleration” during the stance, especially during the braking phase. Thus, it is likely that the lower left VL activity during the stance phase triggered a cascade of alterations whereby the left knee peak extension was reduced which in turn altered the mean F_V as well.

Based on these findings, we subsequently hypothesized that, when sprinting in the curve, the priority switches from “performance” to “maintaining an equilibrium” and an “adequate sprinting motion”. From that point onwards, the participants tried to maintain an adequate sprinting motion regardless of the performance, at least for the left limb. For that sake, the participants increased their left stance times in an attempt to maintain a similar IMP_V to the straight as mathematical models previously theorized (Greene, 1985; Usherwood & Wilson, 2006). However, the increased left limb stance times conducted to a reduced left limb SF. Although we did not investigate the SL in the present study, previous experimentations reported a decreased SL in the curve at 13 (Judson, Churchill, Barnes, Stone, Brookes, et al., 2020) and 40 m (Churchill et al., 2015) in the curve. Hence, the decreased left limb SF likely participated to the altered sprinting performance (Hunter et al., 2004) in the curve.

In addition, the left mean F_{A-P} were reduced in the curve, likely due to the large increase in the mean F_{M-L} as the participants were unable to increase the mean F_{TOT} . Despite the increased left stance times, the left mean IMP_{A-P} remained lower in the curve than in the straight, due to a larger decrease in the left mean F_{A-P} compared with the concomitant increase in the left stance times.

Several experimentations reported that the mean F_{A-P} and IMP_{A-P} were major sprinting performance determinants in the straight (Hunter et al., 2005; Kawamori et al., 2013; Morin, Slawinski, et al., 2015; Rabita et al., 2015). Thus, in the curve, the reduced mean F_{A-P} and IMP_{A-P} provide additional evidence regarding the metrics altering the sprinting performance. Yet, to date, no study reported the performance determinants in the curve and future studies should be conducted in that way.

On the other hand, our findings clearly demonstrated that the right limb was less affected in the curve. Indeed, the right VL sEMG activity was similar to the straight, which likely conducted to a similar knee peak extension, which itself likely permitted to produce a similar mean F_V in comparison to the straight. Our findings are thus in line with those previously reported by Churchill et al. (2016) at $V_{A-P MAX}$. Nonetheless, because of the large increase in the mean F_{M-L} , we observed decrease in the mean F_{A-P} as the participants were unable to increase the right mean F_{TOT} either. As the right limb stance times did not increase in the curve, the mean IMP_{A-P} remained lower than in the straight. The only kinematic differences reported were at the ankle whereby the right ankle was more plantar flexed in the curve without concomitant changes in the sEMG activity among the muscles investigated. However, although not investigated in the present study and quite challenging to capture, it is likely that changes in the sEMG activity of other plantar flexor muscles such as the *Flexor Hallucis Longus* and *Flexor Hallucis Brevus* could be observed.

- Overall, based on the present findings, the sprinting performance decreased in the curve due to a) a reduction in the left and the right leg mean F_{A-P} and IMP_{A-P} ; and b) a reduction in the left limb SF.

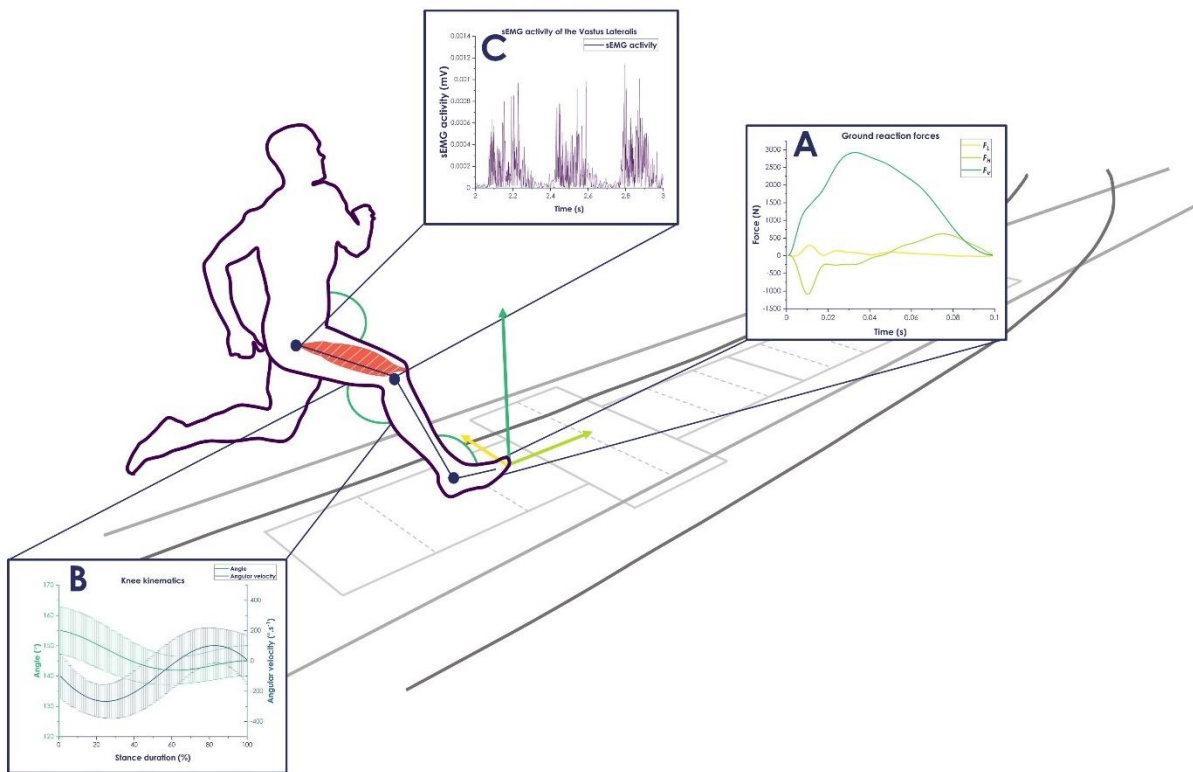


Figure 58. Sum-up figure of the “holistic” approach used in the present PhD thesis to compare the sprinting performance in the curve to the straight. This figure shows an example of the ground reaction forces (panel A), the knee joint kinematics (panel B) and the Vastus Lateralis surface electromyographic activity (panel C).

3. Injury prevention and training programs

As we have developed in the previous paragraphs, the additional requirement in F_{M-L} in the curve is likely the major factor altering the sprinting performance in comparison to the straight. In their exploratory study, Chang & Kram (2007) used a tether attached to the participant, close to the CM in order to externally apply the F_C to the participants. Although the participants ran at tight radii ($r \leq 6$ m) and despite this study lacked statistical power ($n = 5$), the findings were still interesting. In addition, even though the mean F_{M-L} was not reported, the peak F_{M-L} was lower when the participants used the tether than without (Chang & Kram, 2007). In addition to that, the V_{A-P} was systematically greater when the participants ran in the curve with the tether than without (Chang & Kram, 2007), which confirms our hypothesis stipulating that the sprinting V_{A-P} in the curve is reduced due to the additional requirement of F_{M-L} . In the future, an experimentation with a tether externally applying the F_C at a

radius typical of track events would provide insightful knowledge. In the same way, the mean GRF should be compared to sprinting at the same radius without the tether.

If the mean F_{M-L} applied by the sprinter is lower when using a tether, tethers could in turn be used during training sessions in order to reach higher V_{A-P} in the curve which could somehow resemble to “overspeed”. In addition, producing F_{M-L} on the left limb in the curve requires a greater left ankle eversion (Judson et al., 2019) which can in turn increase the foot injury risk (Beeson, 2014). Thus, we can hypothesize that using a tether during training sessions would reduce the strains at the left ankle and reduce the injury risks.

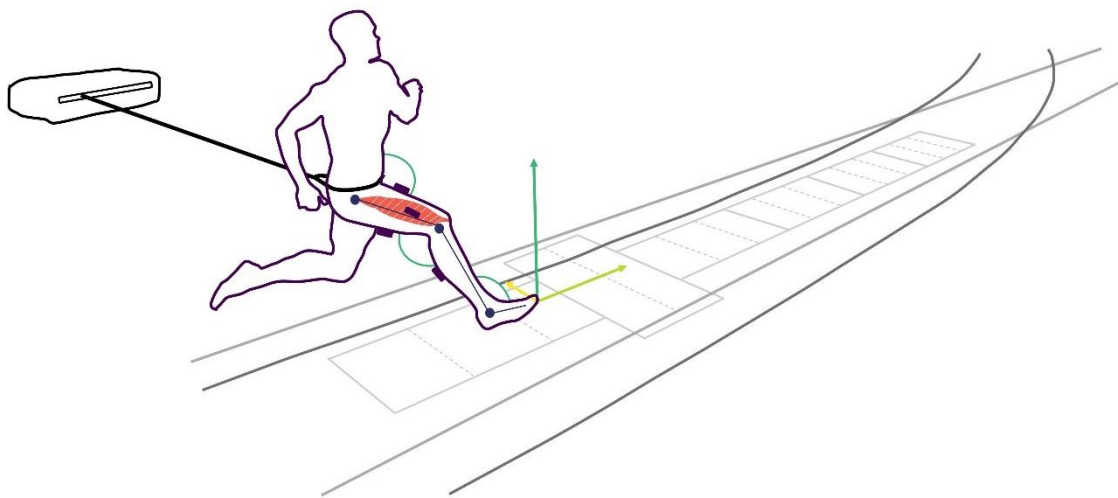


Figure 59. Graphical representation of a sprinter with a linear encoder (top left corner of the figure) positioned on the middle of the curve and attached to the sprinter at the waist to externally apply the centripetal force near the centre of mass in order to reduce the medial-lateral force (yellow arrow shorter than in the figure 58) and the left ankle eversion.

During sprinting and middle-distance training sessions, we often see the athletes warming-up and working out in the counterclockwise direction (*i.e.*, in the same direction as the competitions). However, we have seen throughout this manuscript that curve sprinting induces several alterations in comparison to the straight. In addition to that, an athlete sprinting in lane 1 will undergo greater modifications than the same sprinter, at the same velocity, in lane 8 because of the centripetal force. Finally, throughout the year, numerous of sprints are regularly done in the inner lanes by those athletes. Consequently, repetitive loading and exposure to curve sprinting at tight radii might sadly increase the injury risks, especially due to the left ankle eversion repetitions (Beeson, 2014; Hamill et al., 1987). Therefore, we suggest to limit the training load where the alterations are the greatest (*i.e.*, at the

tighter radii). For example, the warm-ups and the training sessions should preferentially be realized on the outermost lane.

4. Practical recommendations

- **Sprinting in the curve with a tether that externally applies the F_C at the CM should be implemented during training sessions as this might reduce the F_{M-L} the sprinter must produce in the curve. With the utilization of a tether, “overspeed” training sessions specifically in the curve could be implemented. In addition to that, the left ankle eversion would decrease which would result in lower ankle/foot injury risks.**
- **Promoting repetitions (especially when high velocities are reached) on the outermost lanes and alternating between the counterclockwise and the clockwise directions during the warm-up in order to reduce the overuse injury risks.**

2. An explanatory factor for the hamstrings' injury during the late swing phase?

Among the hamstrings, the *BFlh* is usually the most frequently injured (Askling et al., 2007; Koulouris & Connell, 2003) and these injuries likely occur during the late swing phase (Chumanov et al., 2011, 2012; Kenneally-Dabrowski et al., 2019; Schache et al., 2012), mostly at high sprinting velocities (Bramah et al., 2023; Gronwald et al., 2022). Although this was not a direct aim of the present thesis originally, we wanted to dig into the kinematic and sEMG metrics that evolve with the sprinting velocity and investigate whether these metrics could relate to the hamstring injury risk during the late swing phase.

Thanks to the MIMU-based system, we could investigate the lower limb joint kinematics from the starting blocks exit into the $V_{A-P MAX}$. As we have seen in the **study #3**, the knee peak extension velocity increased progressively through the early transition phase and plateaued starting from 24-29 m onwards (see figure 60). We saw in the **general methodology** that the *BFlh* is biarticular, with an origin proximally at the ischial tuberosity (Stępień et al., 2019) and distally on the styloid process of the fibula (Terry & LaPrade, 1996). Thus, the *BFlh* MTU length ultimately depends on the hip and the knee joint kinematics and their analysis should be conducted as the *BFlh* injury risks increase when the *BFlh* MTU is lengthened (Bramah et al., 2023; Danielsson et al., 2020). Therefore, in this third section of the **general discussion**, we will discuss about the hip and the knee joint kinematics throughout the transition phase together with the *BFlh* sEMG, in order to investigate whether those metrics can provide hints and could help to better understand the *BFlh* injury risks.

To begin with, the figure 60 shows a typical example of the knee angular velocity from the starting blocks pushing phase and until the $V_{A-P MAX}$ (22nd stance in this example). On this figure, we can clearly see that the knee peak extension velocity increases progressively with the $V_{H MIMU}$ and plateaus starting from the 14th stance (~25 m) around $1000 \text{ }^\circ \cdot \text{s}^{-1}$ (see the red dashed horizontal line in figure 60). We can also notice on this figure that the knee peak flexion velocities (negative peak angular velocities) were comparable in magnitude to the knee peak extension velocities. However, as the *BFlh* is very unlikely to sustain a strain injury with the knee flexing (Danielsson et al., 2020), we will focus on the phase of the swing where the knee extends. In addition to that, as the *BFlh* is bi-articular, the *BFlh* MTU length depends on the hip and the knee kinematics.

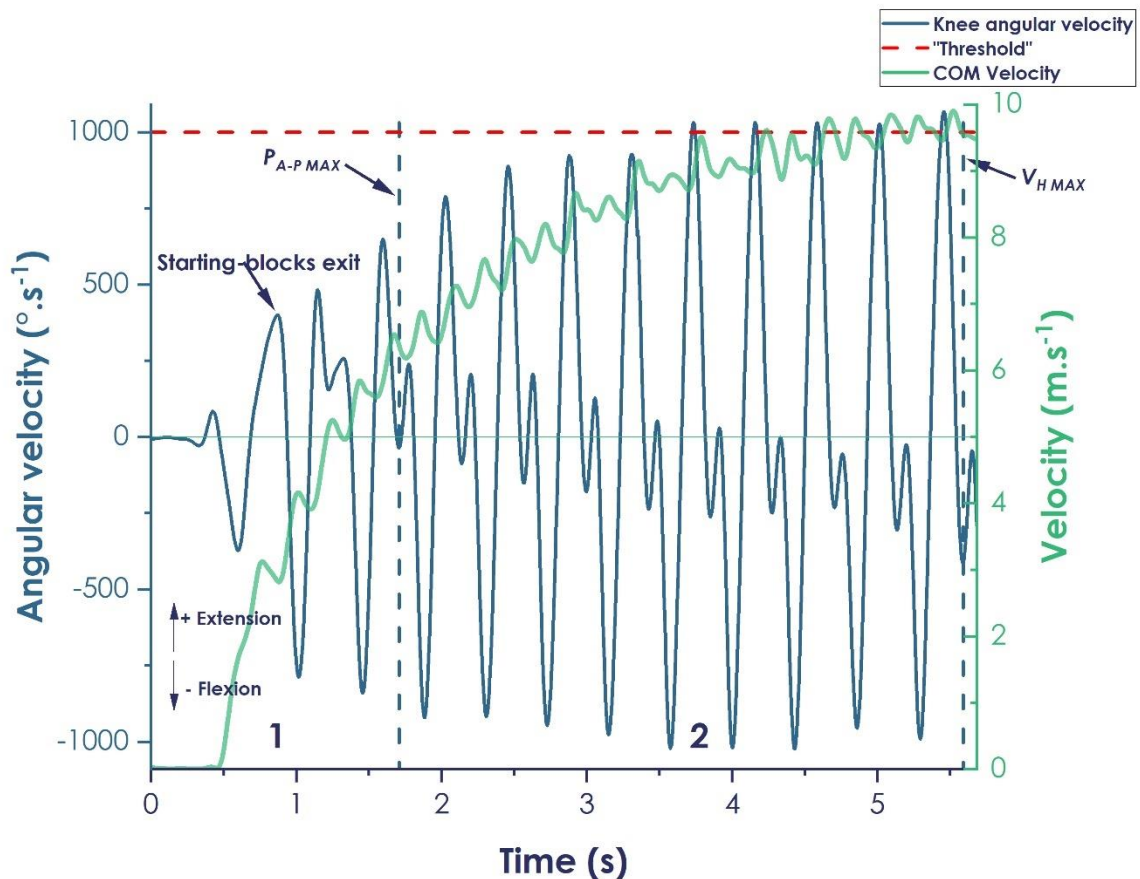


Figure 60. Example of the knee angular velocity time-course (in dark blue) of one participant on a 40-m sprint in the straight. The first blue vertical dashed line shows the maximal antero-posterior power ($P_{A-P MAX}$) and corresponds to the instant where the knee starts to flex (negative angular velocity) during the stance phase. The second blue vertical dashed line corresponds to the maximal horizontal velocity ($V_{H MAX}$) computed with the Magneto-Inertial Measurement Unit-based system. In this example the knee peak extension velocity reaches the “threshold” at the 12th stance (corresponding to ~23 m).

Thus, the figure 61 below shows a typical example of the knee (in blue) and hip (in green) angular velocities during the swing phase at 34-39 m. From this figure, we can identify two “zones” where the knee extended. In the “zone 1” (light red in figure 61), the hip was flexing while the knee was extending, meaning that the *BFlh* MTU was lengthening (see the dark purple line) (Higashihara et al., 2016; Schache et al., 2012; Thelen, Chumanov, Hoerth, et al., 2005). In addition to that, a recent systematic review stipulated that “a stretch-type injury to the hamstrings is caused by an extensive hip flexion with an extended knee” (Danielsson et al., 2020), meaning that this “zone 1” (between 48% and 74% of the swing duration in this example) would potentially place the *BFlh* under high injury risk. In addition to that, in this example, the *BFlh* sEMG activity started at 62% of the swing duration (the blue horizontal floating chart in the top right of the figure 61 indicates when the muscle is active during the swing). Since Danielsson et al. (2020) postulated that the hamstrings are most likely to sustain injury strains while

actively lengthened (i.e., with the muscle active) (Danielsson et al., 2020), the *BFlh* would most likely undergo a hamstring injury in the second half of the “zone 1” (between 62 and 74% of the swing duration in this example).

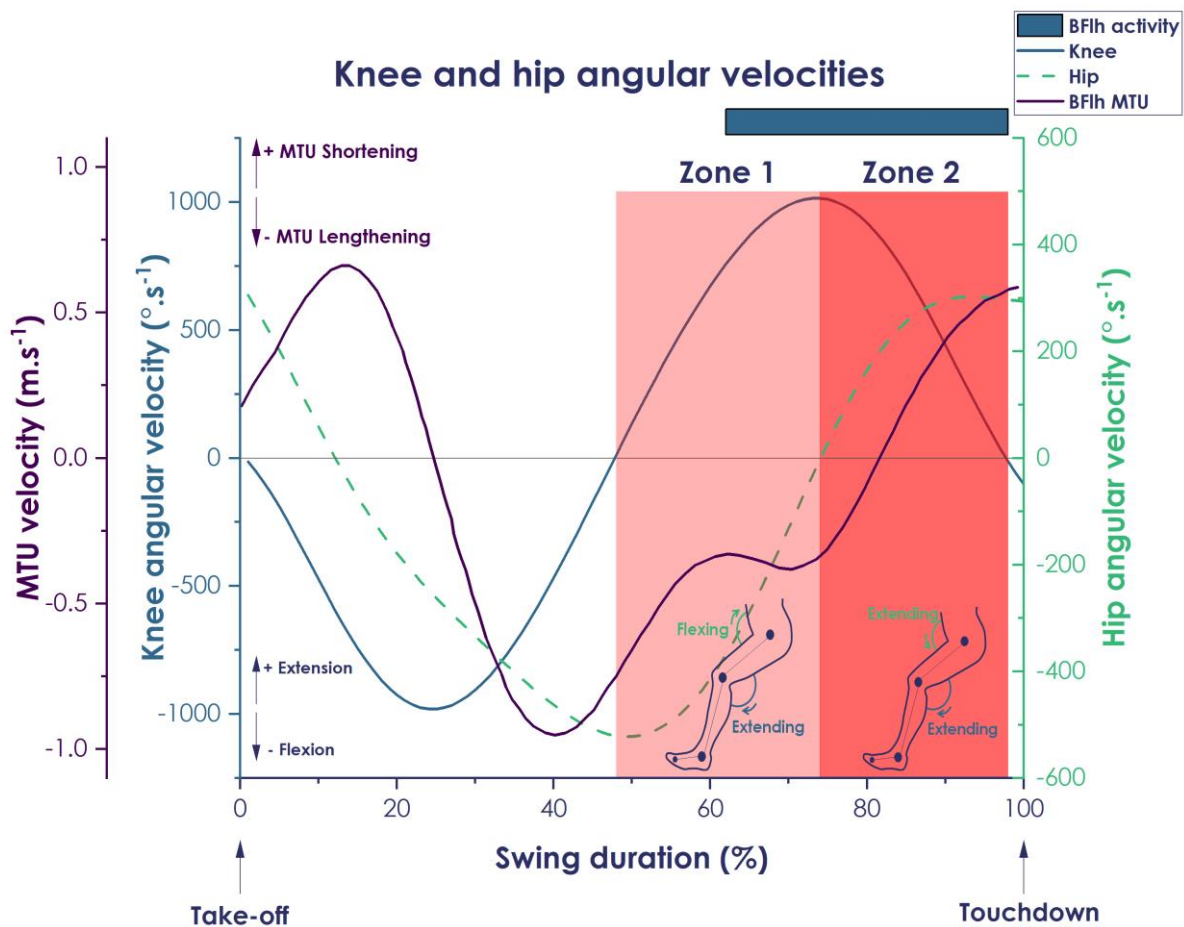


Figure 61. Typical example of the hip (dashed line in green) and the knee (in dark blue) angular velocities during the swing phase at 34-39 m. The light pink zone corresponds to the instant where the hip is flexing and the knee is extending. On the other hand, the red dashed zone corresponds to the instant where the hip is extending and the knee is extending. The surface electromyographic activity of the Biceps Femoris long head (*BFlh*) is also displayed in blue at the top of the figure. The *BFlh* muscle-tendon unit (MTU) velocity is displayed in dark purple and the data were retrieved from Schache et al. (2012). A positive MTU velocity indicates a *BFlh* MTU shortening. On the other hand, a negative MTU velocity indicates a *BFlh* MTU lengthening.

On the other hand, the “zone 2” (dark red) spanned from 74% to 98% of the swing duration in this example whereby the hip and the knee were extending concomitantly. In the “zone 2”, the *BFlh* MTU velocity decreased progressively and the peak *BFlh* MTU length was reached at ~80% of the swing duration (Chumanov et al., 2007, 2011; Higashihara et al., 2016; Nagano et al., 2014; Schache et al., 2012; Thelen, Chumanov, Best, et al., 2005; Thelen, Chumanov, Hoerth, et al., 2005). As a muscle is unlikely to sustain a strain injury while being shortened (Danielsson et al., 2020), we can postulate that the greatest hamstring injury risk in the “zone 2” would correspond to the *BFlh*

being lengthened (*i.e.*, between 74 and 81% of the swing duration). Several studies suggested that actively lengthening a muscle already elongated would increase the hamstring injury risk (Chumanov et al., 2011, 2012; Schache et al., 2012; Yu et al., 2008). Consequently, the *BFlh* would also be at a high injury risk in the beginning of the “zone 2”.

To summarize, the literature suggests that *BFlh* injury risks are the highest during the swing phase, while the *BFlh* is actively lengthened. Therefore, the figure 62 below shows the “zone of all the danger” (in red with the dashed lines in figure 62) where the *BFlh* injury risk could be the highest. This zone starts with the *BFlh* sEMG activity (blue floating horizontal bar on top of the figure 62) onset and terminates when the *BFlh* MTU starts to shorten (*BFlh* MTU lengthening velocity becoming positive). This zone eventually corresponds to the greatest knee extension velocities reached during the swing phase and strengthen the idea that reaching high knee peak extension velocities would increase the hamstring injury risk.

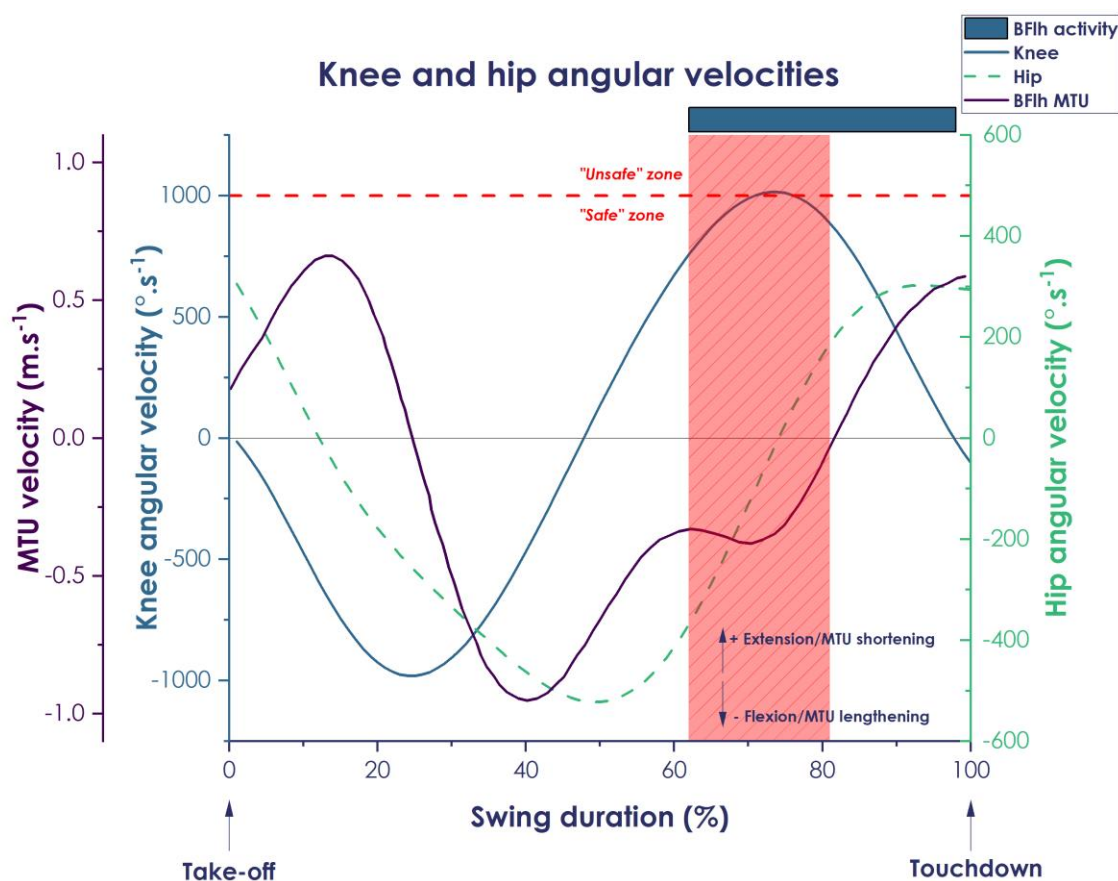


Figure 62. A typical of the hip (dashed line in green) and knee (in dark blue) angular velocities during the swing phase at 34-39 m. The mean surface electromyographic (sEMG) activity of the Biceps Femoris long head (*BFlh*) is also displayed in the blue floating chart at the top of the figure. The dark red zone in the middle of the figure initiates when the *BFlh* sEMG activity starts and terminates when the *BFlh* muscle-tendon unit (MTU) stops lengthening. The *BFlh* muscle-tendon unit (MTU) velocity is displayed in dark purple and the data were retrieved from Schache et al. (2012).

Therefore, from the hip and knee kinematics reported in the present thesis and according to the current literature, we can in turn hypothesize that a “threshold” (likely participant dependant) would exist: above a given knee extension velocity, the *BFlh* injury risk increases. This “threshold” would correspond approximately to the plateau of the knee peak extension velocity observed starting from 24-29 m onwards (see red horizontal dashed line in figure 62). In turn, the hamstrings injury risk would be increased at or above this “threshold”. It is also likely that increasing the time spent around the “threshold” would in turn increase the hamstring injury risk by “accumulating” the *BFlh* strains. This latter hypothesis suggests that the hamstrings would “deteriorate” due to successive rapid knee extensions (*i.e.*, rapid *BFlh* MTU lengthening) with a *BFlh* already elongated, until the muscle goes to failure and the sprinter undergoes a hamstring strain injury. As the so-called “threshold” is likely individual, sprinting kinematic screenings using a MIMU-based system (or a similar device allowing kinematic measurements over 40 m) should be performed throughout the season in order to investigate the individual responses in the lower limb kinematics with the increasing V_{A-P} .

From that point onward, two possibilities can be drawn from the present findings and can in turn be adapted to sprint trainings: a) either avoid placing a sprinter within or close to the “unsafe” zone, or b) progressively familiarize the sprinter to the required kinematic demands. The former would likely be the safer in terms of hamstring injury risk, though is not suitable for sprinting competitions. Indeed, anyone competing would anyway have to face those “unsafe” kinematic demands in competition and would likely undergo a hamstring injury instantly. Therefore, acclimating the sprinter to the kinematic demands of high-velocity sprinting would likely be the best option (Edouard et al., 2019, 2022).

Several injury prevention training programs have been used to adapt the sprinter to the hamstring MTU lengthening and eventually reduce the hamstring injury risk. Among them, eccentric exercises (Arnason et al., 2008) such as Nordic hamstring exercises (Brooks et al., 2006; Clark et al., 2005; Petersen et al., 2011) are often used. However, the peak extension velocities reached during these exercises are far from representing the sprinting demand ($<100 \text{ }^\circ \cdot \text{s}^{-1}$) (Alt et al., 2018; Nishida et al., 2022). In addition to that, previous research showed that these exercises do not replicate the “sprint-specific hamstring sEMG activity” (Edouard et al., 2019). For example, the *BFlh* reaches a sEMG activity comprised between ~15 and ~60% of the sprint-specific sEMG activity while performing various strengthening exercises (Hegyi, Csala, et al., 2019; Prince et al., 2021; van den Tillaar et al., 2017).

Rather than these isolated exercises, recent research suggest that familiarizing sprinters to the sprinting demand should preferentially be performed through specific activity such as high-intensity sprints (Edouard et al., 2019). For example, in Gaelic football, players who reached >95% of their $V_{A-P\ MAX}$ during training sessions were at a lower hamstring injury risk in comparison to those who reached <95% of their $V_{A-P\ MAX}$ during the same training sessions (Malone et al., 2017). These authors concluded their study by stipulating: “Coaches should expose players to high percentages of $V_{A-P\ MAX}$ within training situations as this offers a potential “vaccine” against subsequent soft tissue injury.” (Malone et al., 2017). A similar metaphor was used by Edouard et al. (2019) postulating that “adequate exposure to sprinting may be an effective “vaccine” against hamstring muscle injury”.

Thus, based on our findings and on the existing literature, we hypothesize that sprint training programs should progressively target the knee extension velocities associated with the “unsafe zone” and progressively increase the training load associated with these demands throughout the season (Edouard et al., 2022; Malone et al., 2017). In our example, we postulate that increasing progressively the training load with knee extension velocities $>1000\ ^\circ \cdot s^{-1}$ would likely prevent the sprinter from hamstring strain injuries. As the knee extension velocities reached $1000\ ^\circ \cdot s^{-1}$ at ~ 25 m (at the group level), we would advise to begin the sprint trainings with sprints < 25 m and progressively increase the distance sprinter. Obviously, these distances should be adapted to each individual's hip and knee kinematics and kinematic screenings should be scheduled throughout the season in order to investigate whether the “safe” and “unsafe” zones change. After a few training sessions, we assume that this “threshold” between the “safe” and “unsafe” zones would be shifted above $1000\ ^\circ \cdot s^{-1}$. Thereafter, the sprinter would be able to sprint “safely” with the sprinting demands associated with the previous “threshold” and the sprinting distance could progressively be increased. Yet, since an acute increase in the sprinting training load is associated with large increase in hamstring injury risk (Duhig et al., 2016), progressivity is the key here and sprint trainings should be implemented gradually throughout the season and the years to decrease the hamstring injury risk.

We are aware that the hip and knee kinematics during the swing phase likely do not explain 100% of the hamstring injuries and other metrics are likely of great importance such as the pelvic tilt or the forward trunk lean among others (Bramah et al., 2023; Nagano et al., 2014). In addition to that, we observed a plateau of the knee peak extension velocity in the present study after 24-29 m (see **study #3**). Yet, we stopped our analysis at 40 m and it would be interesting to investigate whether the knee peak extension velocity remains at a plateau afterwards or whether it decreases during the

deceleration phase. Finally, from the hip and knee kinematics, and the BFlh sEMG activity, it would be insightful to use a musculoskeletal modeling in order to investigate whether the BFlh MTU length and the lengthening velocity change after the knee peak extension velocity plateaued.

We are aware that this part of the discussion might seem out of the PhD scope at first sight. However, within this context of this PhD thesis conducted at the French Athletics Federation, 11 months ahead of the Olympics, we thought it would be meaningful for coaches and sport practitioners in general to put our findings in perspective with the existing literature and provide simple and practical recommendations.

It is also interesting to note that no differences were reported between the straight and the curve for the knee peak extension velocities. Thus, the present work is the first, to our knowledge, to indicate that sprinting in the curve apparently conducts to similar hamstring injury risk in comparison to the straight.

1. Practical recommendations

- Sprinting should be used as a mithridatization process throughout the season whereby the athletes should start sprinting early into the season and progressively increase the V_{A-P} and the training load associated. In other words, in the early season, athletes should not sprint for longer than ~25 m. After appropriate adaptation to the sprinting demand, sprinter can progressively increase the distance sprinted in order to reach higher sprinting V_{A-P} .
- Regular kinematic screenings should be scheduled throughout the season in order to investigate the hip and knee kinematics during the swing phase and consequently adapt the training program.

GENERAL CONCLUSION

Throughout this PhD thesis, we have identified two main factors altering the sprinting performance in the curve.

First and foremost, the left and the right F_{M-L} increased in comparison to the straight. However, this conducted to a reduction in the left and the right F_{A-P} as the participants were unable to increase the mean F_{TOT} concomitantly. Despite the left stance times increased in the curve, the left IMP_{A-P} remained lower than in the straight. On the right limb, we also reported a lower right IMP_{A-P} and this was caused by a lower right F_{A-P} in the curve and unchanged right stance times.

Thus, the decreased left and right IMP_{A-P} in the curve represent the main factors explaining the reduced sprinting performance in the curve.

Additionally, in the curve, the participants could not exert a similar left F_V as in the straight. This was caused by a greater left knee flexion during the stance, itself related to a lower VL sEMG activity, due to the inclined position. Consequently, as the left F_V was lower than in the straight, the participants likely switched from “performance” to “maintain the equilibrium”. For that sake, the left stance times increased in order to produce a left IMP_V and a left IMP_{TOT} similar to the straight and maintain the so-called “equilibrium”. Although we did not investigate the SL in the present study, previous experimentations reported decreased SL in the curve.

Therefore, the increased left stance times and the decreased left SF in the curve without concomitant increase in the left SL can further explain the decreased sprinting performance in the curve.

1. Research perspectives

The multi-disciplinary approach used in the present PhD thesis provided an interesting basis that we can build upon for future research. In addition to that, based on the present findings, we drew preliminary practical recommendations that can be directly applied to sprint trainings. Nevertheless, we are aware that we only captured a fragment of this overall picture.

- Indeed, the sagittal plane kinematic analysis did not permit to fully understand the reasons explaining the reduced performance in the curve. For the present work, our kinematic analysis focussed on the sagittal plane kinematics as the frontal and transverse planes computed from the MIMU-based system were

found to be less valid in comparison to an OS (Nijmeijer et al., 2023). However, these 3D kinematic comparisons were made during jumping and change of directions (Nijmeijer et al., 2023), stair ascent and stair descent (Zhang et al., 2013) or ergonomic tasks (Robert-Lachaine et al., 2017). Hence, none of these studies compared the 3D kinematics of this MIMU-based system to a reference system in overground sprinting. Consequently, in parallel to the studies conducted within the framework of this PhD thesis, I had the privilege to participate to experimentations that were led at the Japan Institute of Sport Sciences (Tokyo, Japan). The aim of these experimentations was to compare the 3D joints' kinematics of the MIMU-based system to an OS, FP and a marker less system in overground sprinting during a) the starting blocks pushing phase and the initial 1-to-4 stances; and b) the $V_{A-P MAX}$ phase.

I will contribute to the data processing after this PhD thesis. We discussed in the **study #1** the challenges faced to align the MIMU-based system antero-posterior axis with the GCS antero-posterior axis. In the experimentations conducted at the Japan Institute of Sport Sciences, it will be possible to investigate each V_{CM} axis distinctly thanks to the OS.

Additionally, if the MIMU-based system accurately computes the lower limb joint 3D kinematics in overground sprinting, I will process the 3D kinematics in the straight and in the curve using the data from the experimentations conducted within of the scope of this PhD thesis.

Finally, if the MIMU-based yields accurate 3D kinematics in overground sprinting, we will investigate the lower limb joint kinetics by using the inverse dynamics approach to better comprehend the net demand of the hip, the knee and the ankle joints.

- A secondary research perspective emerges from the practical recommendations developed in the **general discussion**. We saw that the F_{M-L} was lower and the V_{A-P} was greater when the F_C was externally applied to the sprinter thanks to a tether (Chang & Kram, 2007). We would like to replicate a similar experimentation, this time at a radius typical of track events. If the F_{M-L} is confirmed to be lower and if the V_{A-P} is confirmed to be greater when a tether is used to externally apply the F_C , training sessions could eventually be considered with a linear encoder attached to the sprinter's waist in order to externally apply the F_C . The objective behind those sessions would be to reduce the strains at the ankles in the curve (Bojsen-Møller, 1978; Judson et al., 2019) and to realize "overspeed" training sessions in the curve.

- Finally, together with the experimental work that I have conducted throughout this PhD thesis, I had the opportunity to collect *in-field* data for French athletes during 3 National indoor Championships, 3 National outdoor Championships, 2 Diamond Leagues and 18 international track meets. The main objective was then to provide feedbacks to the athletes regarding their performances within a competition environment. Nonetheless, among the data collected in competitions, an extensive work remains to be realized, especially from the GPS data in order to better comprehend the sprinting demand in these events.

REFERENCES

- Abdel-Aziz, Y. I., & Karara, H. M. (1971). Direct Linear Transformation from Comparator Coordinates into Object Space Coordinates in Close-Range Photogrammetry. *Photogrammetric Engineering & Remote Sensing*, 81(2), 103–107. <https://doi.org/10.14358/PERS.81.2.103>
- Aerenhouts, D., Delecluse, C., Hagman, F., Taeymans, J., Debaere, S., Van Gheluwe, B., & Clarys, P. (2012). Comparison of anthropometric characteristics and sprint start performance between elite adolescent and adult sprint athletes. *European Journal of Sport Science*, 12(1), 9–15. <https://doi.org/10.1080/17461391.2010.536580>
- Albertus-Kajee, Y., Tucker, R., Derman, W., Lamberts, R. P., & Lambert, M. I. (2011). Alternative methods of normalising EMG during running. *Journal of Electromyography and Kinesiology*, 21(4), 579–586. <https://doi.org/10.1016/j.jelekin.2011.03.009>
- Alt, T., Heinrich, K., Funken, J., & Potthast, W. (2015). Lower extremity kinematics of athletics curve sprinting. *Journal of Sports Sciences*, 33(6), 552–560. <https://doi.org/10.1080/02640414.2014.960881>
- Alt, T., Nodler, Y. T., Severin, J., Knicker, A. J., & Strüder, H. K. (2018). Velocity-specific and time-dependent adaptations following a standardized Nordic Hamstring Exercise training. *Scandinavian Journal of Medicine & Science in Sports*, 28(1), 65–76. <https://doi.org/10.1111/sms.12868>
- Arnason, A., Andersen, T. E., Holme, I., Engebretsen, L., & Bahr, R. (2008). Prevention of hamstring strains in elite soccer: An intervention study. *Scandinavian Journal of Medicine & Science in Sports*, 18(1), 40–48. <https://doi.org/10.1111/j.1600-0838.2006.00634.x>
- Askling, C. M., Tengvar, M., Saartok, T., & Thorstensson, A. (2007). Acute First-Time Hamstring Strains during Slow-Speed Stretching: Clinical, Magnetic Resonance Imaging, and Recovery Characteristics. *The American Journal of Sports Medicine*, 35(10), 1716–1724. <https://doi.org/10.1177/0363546507303563>
- Ball, N., & Scurr, J. (2013). Electromyography Normalization Methods for High-Velocity Muscle Actions: Review and Recommendations. *Journal of Applied Biomechanics*, 29(5), 600–608. <https://doi.org/10.1123/jab.29.5.600>
- Beeson, P. (2014). *Plantar fasciopathy: Revisiting the risk factors*. 20(3), 160–165.
- Belli, A., Kyröläinen, H., & Komi, P. V. (2002). Moment and Power of Lower Limb Joints in Running. *International Journal of Sports Medicine*, 23(2), 136–141. <https://doi.org/10.1055/s-2002-20136>
- Bezodis, N. E., Kerwin, D. G., & Salo, A. I. T. (2008). Lower-Limb Mechanics during the Support Phase of Maximum-Velocity Sprint Running. *Medicine & Science in Sports & Exercise*, 40(4), 707–715. <https://doi.org/10.1249/MSS.0b013e318162d162>
- Bezodis, N. E., Salo, A. I. T., & Trewartha, G. (2014). Lower limb joint kinetics during the first stance phase in athletics sprinting: Three elite athlete case studies. *Journal of Sports Sciences*, 32(8), 738–746. <https://doi.org/10.1080/02640414.2013.849000>
- Bezodis, N. E., Trewartha, G., & Salo, A. I. T. (2015). Understanding the effect of touchdown distance and ankle joint kinematics on sprint acceleration performance through computer simulation. *Sports Biomechanics*, 14(2), 232–245. <https://doi.org/10.1080/14763141.2015.1052748>
- Bezodis, N. E., Walton, S. P., & Nagahara, R. (2019). Understanding the track and field sprint start through a functional analysis of the external force features which contribute to higher levels of block phase performance. *Journal of Sports Sciences*, 37(5), 560–567. <https://doi.org/10.1080/02640414.2018.1521713>
- Bezodis, N. E., Willwacher, S., & Salo, A. I. T. (2019). The Biomechanics of the Track and Field Sprint Start: A Narrative Review. *Sports Medicine*, 49(9), 1345–1364. <https://doi.org/10.1007/s40279-019-01138-1>

- Blair, S., Duthie, G., Robertson, S., Hopkins, W., & Ball, K. (2018). Concurrent validation of an inertial measurement system to quantify kicking biomechanics in four football codes. *Journal of Biomechanics*, *73*, 24–32. <https://doi.org/10.1016/j.jbiomech.2018.03.031>
- Bland, M. J., & Altman, D., G. (1986). Statistical methods for assessing agreement between two methods of clinical measurement. *The Lancet*, *327*(8476), 307–310. [https://doi.org/10.1016/S0140-6736\(86\)90837-8](https://doi.org/10.1016/S0140-6736(86)90837-8)
- Bojsen-Møller, F. (1978). *Calcaneocuboid joint and stability of the longitudinal arch of the foot at high and low gear push off*. *129*(1), 165–176.
- Bramah, C., Mendiguchia, J., Dos'Santos, T., & Morin, J. B. (2023). Exploring the Role of Sprint Biomechanics in Hamstring Strain Injuries: A Current Opinion on Existing Concepts and Evidence. *Sports Medicine*. <https://doi.org/10.1007/s40279-023-01925-x>
- Brazil, A., Exell, T., Wilson, C., Willwacher, S., Bezodis, I. N., & Irwin, G. (2016). Lower limb joint kinetics in the starting blocks and first stance in athletic sprinting. *Journal of Sports Sciences*, 1–7. <https://doi.org/10.1080/02640414.2016.1227465>
- Brooks, J. H. M., Fuller, C. W., Kemp, S. P. T., & Reddin, D. B. (2006). Incidence, Risk, and Prevention of Hamstring Muscle Injuries in Professional Rugby Union. *The American Journal of Sports Medicine*, *34*(8), 1297–1306. <https://doi.org/10.1177/0363546505286022>
- Burden, A. (2010). How should we normalize electromyograms obtained from healthy participants? What we have learned from over 25 years of research. *Journal of Electromyography and Kinesiology*, *20*(6), 1023–1035. <https://doi.org/10.1016/j.jelekin.2010.07.004>
- Burden, A., & Bartlett, R. (1999). Normalisation of EMG amplitude: An evaluation and comparison of old and new methods. *Medical Engineering & Physics*, *21*(4), 247–257. [https://doi.org/10.1016/S1350-4533\(99\)00054-5](https://doi.org/10.1016/S1350-4533(99)00054-5)
- Camomilla, V., Bergamini, E., Fantozzi, S., & Vannozzi, G. (2015). In-field use of wearable magneto-inertial sensors for sports performance evaluation. *Paper Presented at 33rd International Conference on Biomechanics in Sports*.
- Camomilla, V., Bergamini, E., Fantozzi, S., & Vannozzi, G. (2018). Trends Supporting the In-Field Use of Wearable Inertial Sensors for Sport Performance Evaluation: A Systematic Review. *Sensors*, *18*(3), 873. <https://doi.org/10.3390/s18030873>
- Cavagna, G. A. (1975). Force platforms as ergometers. *Journal of Applied Physiology*, *39*(1), 174–179. <https://doi.org/10.1152/jappl.1975.39.1.174>
- Cavagna, G. A., Komarek, L., & Mazzoleni, S. (1971). The mechanics of sprint running. *The Journal of Physiology*, *217*(3), 709–721. <https://doi.org/10.1113/jphysiol.1971.sp009595>
- Cavagna, G. A., Saibene, F. P., & Margaria, R. (1963). External work in walking. *Journal of Applied Physiology*, *18*(1), 1–9. <https://doi.org/10.1152/jappl.1963.18.1.1>
- Cavanagh, P. R., & LaFortune, M. A. (1980). Ground reaction forces in distance running. *Journal of Biomechanics*, *13*(5), 397–406. [https://doi.org/10.1016/0021-9290\(80\)90033-0](https://doi.org/10.1016/0021-9290(80)90033-0)
- Chang, Y.-H., & Kram, R. (2007). Limitations to maximum running speed on flat curves. *Journal of Experimental Biology*, *210*(6), 971–982. <https://doi.org/10.1242/jeb.02728>
- Charalambous, L., Irwin, G., Bezodis, I. N., & Kerwin, D. (2012). Lower limb joint kinetics and ankle joint stiffness in the sprint start push-off. *Journal of Sports Sciences*, *30*(1), 1–9. <https://doi.org/10.1080/02640414.2011.616948>
- Chumanov, E. S., Heiderscheit, B. C., & Thelen, D. G. (2007). The effect of speed and influence of individual muscles on hamstring mechanics during the swing phase of sprinting. *Journal of Biomechanics*, *40*(16), 3555–3562. <https://doi.org/10.1016/j.jbiomech.2007.05.026>
- Chumanov, E. S., Heiderscheit, B. C., & Thelen, D. G. (2011). Hamstring Musculotendon Dynamics during Stance and Swing Phases of High-Speed Running. *Medicine & Science in Sports & Exercise*, *43*(3), 525–532. <https://doi.org/10.1249/MSS.0b013e3181f23fe8>
- Chumanov, E. S., Schache, A. G., Heiderscheit, B. C., & Thelen, D. G. (2012). Hamstrings are most susceptible to injury during the late swing phase of sprinting. *British Journal of Sports Medicine*, *46*(2), 90–90. <https://doi.org/10.1136/bjsports-2011-090176>

- Churchill, S. M., Salo, A. I. T., & Trewartha, G. (2015). The effect of the bend on technique and performance during maximal effort sprinting. *Sports Biomechanics*, 14(1), 106–121. <https://doi.org/10.1080/14763141.2015.1024717>
- Churchill, S. M., Trewartha, G., Bezodis, I. N., & Salo, A. I. T. (2016). Force production during maximal effort bend sprinting: Theory vs reality: Force production during bend sprinting. *Scandinavian Journal of Medicine & Science in Sports*, 26(10), 1171–1179. <https://doi.org/10.1111/sms.12559>
- Ciacchi, S., Merni, F., Bartolomei, S., & Di Michele, R. (2016). Sprint start kinematics during competition in elite and world-class male and female sprinters. *Journal of Sports Sciences*, 35(13), 1270–1278. <https://doi.org/10.1080/02640414.2016.1221519>
- Clancy, E. A., Cairns, K. D., Riley, P. O., Meister, M., & Kerrigan, D. C. (2004). Effects of Treadmill Walking Speed on Lateral Gastrocnemius Muscle Firing: *American Journal of Physical Medicine & Rehabilitation*, 83(7), 507–514. <https://doi.org/10.1097/01.PHM.0000130033.91894.5A>
- Clark, R., Bryant, A., Culgan, J.-P., & Hartley, B. (2005). The effects of eccentric hamstring strength training on dynamic jumping performance and isokinetic strength parameters: A pilot study on the implications for the prevention of hamstring injuries. *Physical Therapy in Sport*, 6(2), 67–73. <https://doi.org/10.1016/j.ptsp.2005.02.003>
- Colyer, S. L., Graham-Smith, P., & Salo, A. I. T. (2019). Associations between ground reaction force waveforms and sprint start performance. *International Journal of Sports Science & Coaching*, 14(5), 658–666. <https://doi.org/10.1177/1747954119874887>
- Colyer, S. L., Nagahara, R., Takai, Y., & Salo, A. I. T. (2018). How sprinters accelerate beyond the velocity plateau of soccer players: Waveform analysis of ground reaction forces. *Scandinavian Journal of Medicine & Science in Sports*, 28(12), 2527–2535. <https://doi.org/10.1111/sms.13302>
- Danielsson, A., Horvath, A., Senorski, C., Alentorn-Geli, E., Garrett, W. E., Cugat, R., Samuelsson, K., & Hamrin Senorski, E. (2020). The mechanism of hamstring injuries – a systematic review. *BMC Musculoskeletal Disorders*, 21, 641. <https://doi.org/10.1186/s12891-020-03658-8>
- de Leva, P. (1996). Adjustments to Zatsiorsky-Seluyanov's segment inertia parameters. *Journal of Biomechanics*, 29(9), 1223–1230. [https://doi.org/10.1016/0021-9290\(95\)00178-6](https://doi.org/10.1016/0021-9290(95)00178-6)
- De Luca, C. J. (1997). The Use of Surface Electromyography in Biomechanics. *Journal of Applied Biomechanics*, 13(2), 135–163. <https://doi.org/10.1123/jab.13.2.135>
- Debaere, S., Delecluse, C., Aerenhouts, D., Hagman, F., & Jonkers, I. (2013). From block clearance to sprint running: Characteristics underlying an effective transition. *Journal of Sports Sciences*, 31(2), 137–149. <https://doi.org/10.1080/02640414.2012.722225>
- Debaere, S., Jonkers, I., & Delecluse, C. (2013). The Contribution of Step Characteristics to Sprint Running Performance in High-Level Male and Female Athletes. *The Journal of Strength & Conditioning Research*, 27(1), 116. <https://doi.org/10.1519/JSC.0b013e31825183ef>
- Dinu, D., Delaveau, G., Blache, P., Slawinski, J., & Millot, B. (2023). Étude des contraintes biomécaniques exercées sur les articulations de l'épaule et de la hanche chez le pongiste de haut niveau. *Journal de Traumatologie du Sport*, 40(3), 184–191. <https://doi.org/10.1016/j.jts.2023.06.008>
- Dinu, D., Millot, B., Slawinski, J., & Louis, J. (2020). An Examination of the Biomechanics of the Cross, Hook and Uppercut between Two Elite Boxing Groups. *Proceedings*, 49(1), 61. <https://doi.org/10.3390/proceedings2020049061>
- Drillis, R., Contini, R., & Bluestein, M. (1966). *Body segment parameters*. 1166–03.
- Duhig, S., Shield, A. J., Opar, D., Gabbett, T. J., Ferguson, C., & Williams, M. (2016). Effect of high-speed running on hamstring strain injury risk. *British Journal of Sports Medicine*, 50(24), 1536–1540. <https://doi.org/10.1136/bjsports-2015-095679>
- Dumas, R., Chèze, L., & Verriest, J.-P. (2007). Adjustments to McConville et al. And Young et al. Body segment inertial parameters. *Journal of Biomechanics*, 40(3), 543–553. <https://doi.org/10.1016/j.jbiomech.2006.02.013>
- Edouard, P., Mendiguchia, J., Guex, K., Lahti, J., Prince, C., Samozino, P., & Morin, J. B. (2022). Sprinting: A key piece of the hamstring injury risk management puzzle. *British Journal of Sports Medicine*, bjsports-2022-105532. <https://doi.org/10.1136/bjsports-2022-105532>

- Edouard, P., Mendiguchia, J., Guex, K., Lahti, J., Samozino, P., & Morin, J. B. (2019). *Sprinting: A potential vaccine for hamstring injury? 2*.
- Elftman, H. (1939). The force exerted by the ground in walking. *Arbeitsphysiologie*, 10(5), 485–491. <https://doi.org/10.1007/BF02012165>
- Eng, J., & Winter, D. (1993). Estimations of the horizontal displacement of the total body centre of mass: Considerations during standing activities. *Gait & Posture*, 1(3), 141–144. [https://doi.org/10.1016/0966-6362\(93\)90055-6](https://doi.org/10.1016/0966-6362(93)90055-6)
- Fenn, W. O. (1930). FRICTIONAL AND KINETIC FACTORS IN THE WORK OF SPRINT RUNNING. *American Journal of Physiology-Legacy Content*, 92(3), 583–611. <https://doi.org/10.1152/ajplegacy.1930.92.3.583>
- Filter, A., Olivares-Jabalera, J., Santalla, A., Morente-Sánchez, J., Robles-Rodríguez, J., Requena, B., & Loturco, I. (2020). Curve Sprinting in Soccer: Kinematic and Neuromuscular Analysis. *International Journal of Sports Medicine*, a-1144-3175. <https://doi.org/10.1055/a-1144-3175>
- Frishberg, B. A. (1983). An analysis of overground and treadmill sprinting. *Medicine & Science in Sports & Exercise*, 15(6), 478.
- Giroux, C., Rabita, G., Chollet, D., & Guilhem, G. (2014). What is the Best Method for Assessing Lower Limb Force-Velocity Relationship? *International Journal of Sports Medicine*, 36(02), 143–149. <https://doi.org/10.1055/s-0034-1385886>
- Glaister, B. C., Orendurff, M. S., Schoen, J. A., & Klute, G. K. (2007). Rotating horizontal ground reaction forces to the body path of progression. *Journal of Biomechanics*, 40(15), 3527–3532. <https://doi.org/10.1016/j.jbiomech.2007.05.014>
- Graubner, R., & Nixdorf, E. (2009). *The Sprint and Hurdles Events at the 2009 IAAF World Championships in Athletics*. 1, 35.
- Greene, P. R. (1985). Running on Flat Turns: Experiments, Theory, and Applications. *Journal of Biomechanical Engineering*, 107(2), 96–103. <https://doi.org/10.1115/1.3138542>
- Gronwald, T., Klein, C., Hoenig, T., Pietzonka, M., Bloch, H., Edouard, P., & Hollander, K. (2022). Hamstring injury patterns in professional male football (soccer): A systematic video analysis of 52 cases. *British Journal of Sports Medicine*, 56(3), 165–171. <https://doi.org/10.1136/bjsports-2021-104769>
- Guissard, N., Duchateau, J., & Hainaut, K. (1992). EMG and mechanical changes during sprint starts at different front block obliquities. *Medicine & Science in Sports & Exercise*, 24(11), 1257.
- Guo, L.-Y., Su, F.-C., Yang, C.-H., Wang, S.-H., Chang, J.-J., Wu, W.-L., & Lin, H.-T. (2006). EFFECTS OF SPEED AND INCLINE ON LOWER EXTREMITY KINEMATICS DURING TREADMILL JOGGING IN HEALTHY SUBJECTS. *Biomedical Engineering: Applications, Basis and Communications*, 18(02), 73–79. <https://doi.org/10.4015/S1016237206000142>
- Halaki, M., & Gi, K. (2012). Normalization of EMG Signals: To Normalize or Not to Normalize and What to Normalize to? In G. R. Naik (Ed.), *Computational Intelligence in Electromyography Analysis—A Perspective on Current Applications and Future Challenges*. InTech. <https://doi.org/10.5772/49957>
- Hamner, S. R., & Delp, S. L. (2013). Muscle contributions to fore-aft and vertical body mass center accelerations over a range of running speeds. *Journal of Biomechanics*, 46(4), 780–787. <https://doi.org/10.1016/j.jbiomech.2012.11.024>
- Hanon, C., & Gajer, B. (2009). Velocity and Stride Parameters of World-Class 400-Meter Athletes Compared With Less Experienced Runners. *Journal of Strength and Conditioning Research*, 23(2), 524–531. <https://doi.org/10.1519/JSC.0b013e318194e071>
- Hanon, C., Thépaut-Mathieu, C., & Vandewalle, H. (2005). Determination of muscular fatigue in elite runners. *European Journal of Applied Physiology*, 94(1), 118–125. <https://doi.org/10.1007/s00421-004-1276-1>
- Hasan, Z. (1986). Optimized movement trajectories and joint stiffness in unperturbed, inertially loaded movements. *Biological Cybernetics*, 53(6), 373–382.
- Hegyí, A., Csala, D., Péter, A., Finni, T., & Cronin, N. J. (2019). High-density electromyography activity in various hamstring exercises. *Scandinavian Journal of Medicine & Science in Sports*, 29(1), 34–43. <https://doi.org/10.1111/sms.13303>

- Hegyí, A., Gonçalves, B. A. M., Finni, T., & Cronin, N. J. (2019). Individual Region- and Muscle-specific Hamstring Activity at Different Running Speeds. *Medicine & Science in Sports & Exercise*, 51(11), 2274–2285. <https://doi.org/10.1249/MSS.0000000000002060>
- Hermens, H. J., Freriks, B., Disselhorst-Klug, C., & Rau, G. (2000). Development of recommendations for SEMG sensors and sensor placement procedures. *Journal of Electromyography and Kinesiology*, 10(5), 361–374. [https://doi.org/10.1016/S1050-6411\(00\)00027-4](https://doi.org/10.1016/S1050-6411(00)00027-4)
- Higashihara, A., Nagano, Y., Ono, T., & Fukubayashi, T. (2016). Relationship between the peak time of hamstring stretch and activation during sprinting. *European Journal of Sport Science*, 16(1), 36–41. <https://doi.org/10.1080/17461391.2014.973913>
- Higashihara, A., Nagano, Y., Ono, T., & Fukubayashi, T. (2018). Differences in hamstring activation characteristics between the acceleration and maximum-speed phases of sprinting. *Journal of Sports Sciences*, 36(12), 1313–1318. <https://doi.org/10.1080/02640414.2017.1375548>
- Higashihara, A., Ono, T., Kubota, J., Okuwaki, T., & Fukubayashi, T. (2010). Functional differences in the activity of the hamstring muscles with increasing running speed. *Journal of Sports Sciences*, 28(10), 1085–1092. <https://doi.org/10.1080/02640414.2010.494308>
- Higashihara, A., Ono, T., Tokutake, G., Kuramochi, R., Kunita, Y., Nagano, Y., & Hirose, N. (2019). Hamstring muscles' function deficit during overground sprinting in track and field athletes with a history of strain injury. *Journal of Sports Sciences*, 37(23), 2744–2750. <https://doi.org/10.1080/02640414.2019.1664030>
- Hodges, P. W., & Bui, B. H. (1996). A comparison of computer-based methods for the determination of onset of muscle contraction using electromyography. *Electroencephalography and Clinical Neurophysiology*.
- Hopkins, W. G., Marshall, S. W., Batterham, A. M., & Hanin, J. (2009). Progressive Statistics for Studies in Sports Medicine and Exercise Science. *Medicine & Science in Sports & Exercise*, 41(1), 3–12. <https://doi.org/10.1249/MSS.0b013e31818cb278>
- Hortobagyi, T., & DeVita, P. (2000). Muscle pre- and coactivity during downward stepping are associated with leg stiffness in aging. *Journal of Electromyography and Kinesiology*.
- Howard, R. M., Conway, R., & Harrison, A. J. (2018). Muscle activity in sprinting: A review. *Sports Biomechanics*, 17(1), 1–17. <https://doi.org/10.1080/14763141.2016.1252790>
- Hughes, G. T. G., Camomilla, V., Vanwanseele, B., Harrison, A. J., Fong, D. T. P., & Bradshaw, E. J. (2021). Novel technology in sports biomechanics: Some words of caution. *Sports Biomechanics*, 1–9. <https://doi.org/10.1080/14763141.2020.1869453>
- Hunter, J. P., Marshall, R. N., & McNair, P. J. (2004). Interaction of Step Length and Step Rate during Sprint Running. *Medicine & Science in Sports & Exercise*, 36(2), 261–271. <https://doi.org/10.1249/01.MSS.0000113664.15777.53>
- Hunter, J. P., Marshall, R. N., & McNair, P. J. (2005). Relationships between Ground Reaction Force Impulse and Kinematics of Sprint-Running Acceleration. *Journal of Applied Biomechanics*, 21(1), 31–43. <https://doi.org/10.1123/jab.21.1.31>
- Jacobs, R., & van Ingen Schenau, G. J. (1992). Intermuscular coordination in a sprint push-off. *Journal of Biomechanics*, 25(9), 953–965. [https://doi.org/10.1016/0021-9290\(92\)90031-U](https://doi.org/10.1016/0021-9290(92)90031-U)
- Jain, P. C. (1980). On a Discrepancy in Track Races. *Research Quarterly for Exercise and Sport*, 51(2), 432–436. <https://doi.org/10.1080/02701367.1980.10605212>
- Jaskólski, A., Veenstra, B., Goossens, P., Jaskólska, A., & Skinner, J. S. (1996). Optimal resistance for maximal power during treadmill running. *Sports Medicine, Training and Rehabilitation*, 7(1), 17–30. <https://doi.org/10.1080/15438629609512067>
- Johnson, M., & Buckley, J. G. (2001). Muscle power patterns in the mid-acceleration phase of sprinting. *Journal of Sports Sciences*, 19(4), 263–272. <https://doi.org/10.1080/026404101750158330>
- Judson, L. J., Churchill, S. M., Barnes, A., Stone, J. A., Brookes, I. G. A., & Wheat, J. (2019). Horizontal force production and multi-segment foot kinematics during the acceleration phase of bend sprinting. *Scandinavian Journal of Medicine & Science in Sports*, 29(10), 1563–1571. <https://doi.org/10.1111/sms.13486>
- Judson, L. J., Churchill, S. M., Barnes, A., Stone, J. A., Brookes, I. G. A., & Wheat, J. (2020). Kinematic modifications of the lower limb during the acceleration phase of bend

- sprinting. *Journal of Sports Sciences*, 38(3), 336–342.
<https://doi.org/10.1080/02640414.2019.1699006>
- Judson, L. J., Churchill, S. M., Barnes, A., Stone, J. A., & Wheat, J. (2020). Joint moments and power in the acceleration phase of bend sprinting. *Journal of Biomechanics*, 101, 109632. <https://doi.org/10.1016/j.jbiomech.2020.109632>
- Kaiser, J. F. (1990). On a simple algorithm to calculate the 'energy' of a signal. *International Conference on Acoustics, Speech, and Signal Processing*, 381–384 vol.1.
<https://doi.org/10.1109/ICASSP.1990.115702>
- Kaiser, J. F. (1993). Some useful properties of Teager's energy operators. *IEEE International Conference on Acoustics Speech and Signal Processing*, 149–152 vol.3.
<https://doi.org/10.1109/ICASSP.1993.319457>
- Kakehata, G., Goto, Y., Iso, S., & Kanosue, K. (2021). Timing of Rectus Femoris and Biceps Femoris Muscle Activities in Both Legs at Maximal Running Speed. *Medicine & Science in Sports & Exercise*, 53(3), 643–652. <https://doi.org/10.1249/MSS.0000000000002497>
- Kakehata, G., Goto, Y., Iso, S., & Kanosue, K. (2022). The Timing of Thigh Muscle Activity Is a Factor Limiting Performance in the Deceleration Phase of the 100-m Dash. *Medicine & Science in Sports & Exercise*, 54(6), 1002–1012.
<https://doi.org/10.1249/MSS.0000000000002876>
- Kawamori, N., Nosaka, K., & Newton, R. U. (2013). Relationships Between Ground Reaction Impulse and Sprint Acceleration Performance in Team Sport Athletes. *Journal of Strength and Conditioning Research*, 27(3), 568–573.
<https://doi.org/10.1519/JSC.0b013e318257805a>
- Kenneally-Dabrowski, C. J. B., Brown, N. A. T., Lai, A. K. M., Perriman, D., Spratford, W., & Serpell, B. G. (2019). Late swing or early stance? A narrative review of hamstring injury mechanisms during high-speed running. *Scandinavian Journal of Medicine & Science in Sports*, 29(8), 1083–1091. <https://doi.org/10.1111/sms.13437>
- King, D., Burnie, L., Nagahara, R., & Bezodis, N. E. (2023). Relationships between kinematic characteristics and ratio of forces during initial sprint acceleration. *Journal of Sports Sciences*, 0(0), 1–9. <https://doi.org/10.1080/02640414.2023.2172797>
- Koulouris, G., & Connell, D. (2003). Evaluation of the hamstring muscle complex following acute injury. *Skeletal Radiology*, 32(10), 582–589. <https://doi.org/10.1007/s00256-003-0674-5>
- Kuitunen, S., Komi, P. V., & Kyröläinen, H. (2002). Knee and ankle joint stiffness in sprint running: *Medicine & Science in Sports & Exercise*, 34(1), 166–173.
<https://doi.org/10.1097/00005768-200201000-00025>
- Kyröläinen, H., Avela, J., & Komi, P. V. (2005a). Changes in muscle activity with increasing running speed. *Journal of Sports Sciences*, 23(10), 1101–1109.
<https://doi.org/10.1080/02640410400021575>
- Kyröläinen, H., Avela, J., & Komi, P. V. (2005b). Changes in muscle activity with increasing running speed. *Journal of Sports Sciences*, 23(10), 1101–1109.
<https://doi.org/10.1080/02640410400021575>
- Kyröläinen, H., Komi, P. V., & Belli, A. (1999). Changes in Muscle Activity Patterns and Kinetics With Increasing Running Speed. *The Journal of Strength & Conditioning Research*, 13(4), 400.
- Latash, M. L. (2018). Muscle coactivation: Definitions, mechanisms, and functions. *Journal of Neurophysiology*, 120(1), 88–104. <https://doi.org/10.1152/jn.00084.2018>
- Li, X., & Aruin, A. (2005). Muscle activity onset time detection using teager-kaiser energy operator. *Conference Proceedings: ... Annual International Conference of the IEEE Engineering in Medicine and Biology Society. IEEE Engineering in Medicine and Biology Society. Annual Conference, 2005*, 7549–7552.
<https://doi.org/10.1109/IEMBS.2005.1616259>
- Li, X., Zhou, P., & Aruin, A. S. (2007). Teager–Kaiser Energy Operation of Surface EMG Improves Muscle Activity Onset Detection. *Annals of Biomedical Engineering*, 35(9), 1532–1538.
<https://doi.org/10.1007/s10439-007-9320-z>
- Malone, S., Roe, M., Doran, D. A., Gabbett, T. J., & Collins, K. (2017). High chronic training loads and exposure to bouts of maximal velocity running reduce injury risk in elite

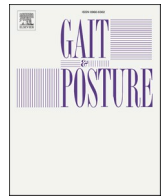
- Gaelic football. *Journal of Science and Medicine in Sport*, 20(3), 250–254.
<https://doi.org/10.1016/j.jsams.2016.08.005>
- Matsuo, A., Mizutani, M., Nagahara, R., Fukunaga, T., & Kanehisa, H. (2019). External mechanical work done during the acceleration stage of maximal sprint running and its association with running performance. *Journal of Experimental Biology*, 222(5), jeb189258. <https://doi.org/10.1242/jeb.189258>
- Maus, H.-M., Seyfarth, A., & Grimmer, S. (2011). Combining forces and kinematics for calculating consistent centre of mass trajectories. *Journal of Experimental Biology*, 214(21), 3511–3517. <https://doi.org/10.1242/jeb.057422>
- Merletti, R., Rainoldi, A., & Farina, D. (2001). Surface Electromyography for Noninvasive Characterization of Muscle. *Exercise and Sport Sciences Reviews*, 29(1), 20.
- Mero, A. (1988). Force-Time Characteristics and Running Velocity of Male Sprinters during the Acceleration Phase of Sprinting. *Research Quarterly for Exercise and Sport*, 59(2), 94–98. <https://doi.org/10.1080/02701367.1988.10605484>
- Mero, A., & Komi, P. V. (1986). Force-, EMG-, and elasticity-velocity relationships at submaximal, maximal and supramaximal running speeds in sprinters. *European Journal of Applied Physiology and Occupational Physiology*, 55(5), 553–561.
<https://doi.org/10.1007/BF00421652>
- Mero, A., & Komi, P. V. (1987). Electromyographic activity in sprinting at speeds ranging from sub-maximal to supra-maximal. *Medicine & Science in Sports & Exercise*, 19(3), 266.
- Mero, A., & Komi, P. V. (1990). Reaction time and electromyographic activity during a sprint start. *European Journal of Applied Physiology and Occupational Physiology*, 61(1–2), 73–80. <https://doi.org/10.1007/BF00236697>
- Mero, A., Komi, P. V., & Gregor, R. J. (1992). Biomechanics of Sprint Running: A Review. *Sports Medicine*, 13(6), 376–392. <https://doi.org/10.2165/00007256-199213060-00002>
- Millot, B., Blache, P., Dinu, D., Arnould, A., Jusseaume, J., Hanon, C., & Slawinski, J. (2023). Center of mass velocity comparison using a whole body magnetic inertial measurement unit system and force platforms in well trained sprinters in straight-line and curve sprinting. *Gait & Posture*, 99, 90–97.
<https://doi.org/10.1016/j.gaitpost.2022.11.002>
- Moravec, P., Ruzicka, J., Susanka, P., Kodejs, M., & Nosek, M. (1988). The 1987 International Athletic Foundation/IAAF Scientific Project Report: Time analysis of the 100 Metres events at the II World Championships in Athletics. *New Studies in Athletics*, 3, 61–96.
- Morin, J. B., Bourdin, M., Edouard, P., Peyrot, N., Samozino, P., & Lacour, J.-R. (2012). Mechanical determinants of 100-m sprint running performance. *European Journal of Applied Physiology*, 112(11), 3921–3930. <https://doi.org/10.1007/s00421-012-2379-8>
- Morin, J. B., Edouard, P., & Samozino, P. (2011). Technical Ability of Force Application as a Determinant Factor of Sprint Performance. *Medicine & Science in Sports & Exercise*, 43(9), 1680–1688. <https://doi.org/10.1249/MSS.0b013e318216ea37>
- Morin, J. B., Gimenez, P., Edouard, P., Arnal, P., Jiménez-Reyes, P., Samozino, P., Brughelli, M., & Mendiguchia, J. (2015). Sprint Acceleration Mechanics: The Major Role of Hamstrings in Horizontal Force Production. *Frontiers in Physiology*, 6.
<https://doi.org/10.3389/fphys.2015.00404>
- Morin, J. B., & Samozino, P. (2016). Interpreting Power-Force-Velocity Profiles for Individualized and Specific Training. *International Journal of Sports Physiology and Performance*, 11(2), 267–272. <https://doi.org/10.1123/ijsp.2015-0638>
- Morin, J. B., Samozino, P., Bonnefoy, R., Edouard, P., & Belli, A. (2010). Direct measurement of power during one single sprint on treadmill. *Journal of Biomechanics*, 43(10), 1970–1975. <https://doi.org/10.1016/j.jbiomech.2010.03.012>
- Morin, J. B., Samozino, P., Murata, M., Cross, M. R., & Nagahara, R. (2019). A simple method for computing sprint acceleration kinetics from running velocity data: Replication study with improved design. *Journal of Biomechanics*, 94, 82–87.
<https://doi.org/10.1016/j.jbiomech.2019.07.020>
- Morin, J. B., & Sève, P. (2011). Sprint running performance: Comparison between treadmill and field conditions. *European Journal of Applied Physiology*, 111(8), 1695–1703.
<https://doi.org/10.1007/s00421-010-1804-0>

- Morin, J. B., Slawinski, J., Dorel, S., Sàez-de-Villarreal, E., Couturier, A., Samozino, P., Brughelli, M., & Rabita, G. (2015). Acceleration capability in elite sprinters and ground impulse: Push more, brake less? *Journal of Biomechanics*, *48*(12), 3149–3154. <https://doi.org/10.1016/j.jbiomech.2015.07.009>
- Mukaka, M. (2012). A guide to appropriate use of Correlation coefficient in medical research. *Malawi Medical Journal: The Journal of Medical Association of Malawi*, *24*(3), 69–71.
- Nagahara, R., & Girard, O. (2021). Alterations of spatiotemporal and ground reaction force variables during decelerated sprinting. *Scandinavian Journal of Medicine & Science in Sports*, *31*(3), 586–596. <https://doi.org/10.1111/sms.13884>
- Nagahara, R., Kanehisa, H., & Fukunaga, T. (2020). Ground reaction force across the transition during sprint acceleration. *Scandinavian Journal of Medicine & Science in Sports*, *30*(3), 450–461. <https://doi.org/10.1111/sms.13596>
- Nagahara, R., Kanehisa, H., Matsuo, A., & Fukunaga, T. (2019). Are peak ground reaction forces related to better sprint acceleration performance? *Sports Biomechanics*, *20*(3), 360–369. <https://doi.org/10.1080/14763141.2018.1560494>
- Nagahara, R., Matsubayashi, T., Matsuo, A., & Zushi, K. (2014). Kinematics of transition during human accelerated sprinting. *Biology Open*, *3*(8), 689–699. <https://doi.org/10.1242/bio.20148284>
- Nagahara, R., Mizutani, M., Matsuo, A., Kanehisa, H., & Fukunaga, T. (2017). Association of Step Width with Accelerated Sprinting Performance and Ground Reaction Force. *International Journal of Sports Medicine*, *38*(07), 534–540. <https://doi.org/10.1055/s-0043-106191>
- Nagahara, R., Mizutani, M., Matsuo, A., Kanehisa, H., & Fukunaga, T. (2018a). Association of Sprint Performance With Ground Reaction Forces During Acceleration and Maximal Speed Phases in a Single Sprint. *Journal of Applied Biomechanics*, *34*(2), 104–110. <https://doi.org/10.1123/jab.2016-0356>
- Nagahara, R., Mizutani, M., Matsuo, A., Kanehisa, H., & Fukunaga, T. (2018b). Step-to-step spatiotemporal variables and ground reaction forces of intra-individual fastest sprinting in a single session. *Journal of Sports Sciences*, *36*(12), 1392–1401. <https://doi.org/10.1080/02640414.2017.1389101>
- Nagahara, R., & Salo, A. I. T. (2018). Kinetic demands of sprinting shift across the acceleration phase: Novel analysis of entire force waveforms. *Scandinavian Journal of Medicine & Science in Sports*, *28*(7), 1784–1792. <https://doi.org/10.1111/sms.13093>
- Nagano, Y., Higashihara, A., Takahashi, K., & Fukubayashi, T. (2014). Mechanics of the muscles crossing the hip joint during sprint running. *Journal of Sports Sciences*, *32*(18), 1722–1728. <https://doi.org/10.1080/02640414.2014.915423>
- Nijmeijer, E. M., Heuvelmans, P., Bolt, R., Gokeler, A., Otten, E., & Benjaminse, A. (2023). Concurrent validation of the Xsens IMU system of lower-body kinematics in jump-landing and change-of-direction tasks. *Journal of Biomechanics*, *154*, 111637. <https://doi.org/10.1016/j.jbiomech.2023.111637>
- Nilsson, J., & Thorstensson, A. (1989). Ground reaction forces at different speeds of human walking and running. *Acta Physiologica Scandinavica*, *136*(2), 217–227. <https://doi.org/10.1111/j.1748-1716.1989.tb08655.x>
- Nilsson, J., Thorstensson, A., & Halbertsma, J. (1985). Changes in leg movements and muscle activity with speed of locomotion and mode of progression in humans. *Acta Physiologica Scandinavica*, *123*(4), 457–475. <https://doi.org/10.1111/j.1748-1716.1985.tb07612.x>
- Nishida, S., Nakamura, M., Kiyono, R., Sato, S., Yasaka, K., Yoshida, R., & Nosaka, K. (2022). Relationship between Nordic hamstring strength and maximal voluntary eccentric, concentric and isometric knee flexion torque. *PLOS ONE*, *17*(2), e0264465. <https://doi.org/10.1371/journal.pone.0264465>
- Novacheck, T. F. (1998). The biomechanics of running. *Gait and Posture*.
- Nummela, A., Rusko, H., & Mero, A. (1994). EMG activities and ground reaction forces during fatigued and nonfatigued sprinting. *Medicine & Science in Sports & Exercise*, *26*(5), 605.

- Okudaira, M., Willwacher, S., Kawama, R., Ota, K., & Tanigawa, S. (2021). Sprinting kinematics and inter-limb coordination patterns at varying slope inclinations. *Journal of Sports Sciences*, 39(21), 2444–2453. <https://doi.org/10.1080/02640414.2021.1939949>
- Otsuka, M., Shim, J. K., Kurihara, T., Yoshioka, S., Nokata, M., & Isaka, T. (2014). Effect of Expertise on 3D Force Application During the Starting Block Phase and Subsequent Steps in Sprint Running. *Journal of Applied Biomechanics*, 30(3), 390–400. <https://doi.org/10.1123/jab.2013-0017>
- Pandy, M. G., Lai, A. K. M., Schache, A. G., & Lin, Y.-C. (2021). How muscles maximize performance in accelerated sprinting. *Scandinavian Journal of Medicine & Science in Sports*, 31(10), 1882–1896. <https://doi.org/10.1111/sms.14021>
- Pavei, G., Salis, F., Cereatti, A., & Bergamini, E. (2020). Body center of mass trajectory and mechanical energy using inertial sensors: A feasible stride? *Gait & Posture*, 80, 199–205. <https://doi.org/10.1016/j.gaitpost.2020.04.012>
- Pavei, G., Seminati, E., Cazzola, D., & Minetti, A. E. (2017). On the Estimation Accuracy of the 3D Body Center of Mass Trajectory during Human Locomotion: Inverse vs. Forward Dynamics. *Frontiers in Physiology*, 8. <https://doi.org/10.3389/fphys.2017.00129>
- Petersen, J., Thorborg, K., Nielsen, M. B., Budtz-Jørgensen, E., & Hölmich, P. (2011). Preventive Effect of Eccentric Training on Acute Hamstring Injuries in Men's Soccer: A Cluster-Randomized Controlled Trial. *The American Journal of Sports Medicine*, 39(11), 2296–2303. <https://doi.org/10.1177/0363546511419277>
- Pietraszewski, P., Gołaś, A., & Krzysztofik, M. (2021). Comparison of Muscle Activity During 200 m Indoor Curve and Straight Sprinting in Elite Female Sprinters. *Journal of Human Kinetics*, 80, 309–316. <https://doi.org/10.2478/hukin-2021-0111>
- Pinniger, G. J., Steele, J. R., & Groeller, H. (2000). Does fatigue induced by repeated dynamic efforts affect hamstring muscle function?: *Medicine & Science in Sports & Exercise*, 32(3), 647–653. <https://doi.org/10.1097/00005768-200003000-00015>
- Prince, C., Morin, J. B., Mendiguchia, J., Lahti, J., Guex, K., Edouard, P., & Samozino, P. (2021). Sprint Specificity of Isolated Hamstring-Strengthening Exercises in Terms of Muscle Activity and Force Production. *Frontiers in Sports and Active Living*, 2, 609636. <https://doi.org/10.3389/fspor.2020.609636>
- Rabita, G., Dorel, S., Slawinski, J., Sàez-de-Villarreal, E., Couturier, A., Samozino, P., & Morin, J. B. (2015). Sprint mechanics in world-class athletes: A new insight into the limits of human locomotion: Sprint mechanics in elite athletes. *Scandinavian Journal of Medicine & Science in Sports*, 25(5), 583–594. <https://doi.org/10.1111/sms.12389>
- Rahmani, A., Viale, F., Dalleau, G., & Lacour, J.-R. (2001). Force/velocity and power/velocity relationships in squat exercise. *European Journal of Applied Physiology*, 84(3), 227–232. <https://doi.org/10.1007/PL00007956>
- Robert-Lachaine, X., Mecheri, H., Larue, C., & Plamondon, A. (2017). Validation of inertial measurement units with an optoelectronic system for whole-body motion analysis. *Medical & Biological Engineering & Computing*, 55(4), 609–619. <https://doi.org/10.1007/s11517-016-1537-2>
- Roetenberg, D., Luinge, H., & Slycke, P. (2013). *Xsens MVN: Full 6DOF Human Motion Tracking Using Miniature Inertial Sensors*. 10.
- Samozino, P., Rabita, G., Dorel, S., Slawinski, J., Peyrot, N., Sàez-de-Villarreal, E., & Morin, J. B. (2016). A simple method for measuring power, force, velocity properties, and mechanical effectiveness in sprint running: Simple method to compute sprint mechanics. *Scandinavian Journal of Medicine & Science in Sports*, 26(6), 648–658. <https://doi.org/10.1111/sms.12490>
- Schache, A. G., Dorn, T. W., Blanch, P. D., Brown, N. A. T., & Pandy, M. G. (2012). Mechanics of the Human Hamstring Muscles during Sprinting. *Medicine & Science in Sports & Exercise*, 44(4), 647–658. <https://doi.org/10.1249/MSS.0b013e318236a3d2>
- Schache, A. G., Dorn, T. W., Wrigley, T. V., Brown, N. A. T., & Pandy, M. G. (2013). Stretch and activation of the human biarticular hamstrings across a range of running speeds. *European Journal of Applied Physiology*, 113(11), 2813–2828. <https://doi.org/10.1007/s00421-013-2713-9>
- Schepers, M., Giuberti, M., & Bellusci, G. (2018). *Xsens MVN: Consistent Tracking of Human Motion Using Inertial Sensing*. <https://doi.org/10.13140/RG.2.2.22099.07205>

- Segers, V., Aerts, P., Lenoir, M., & De Clercq, D. (2006). Spatiotemporal characteristics of the walk-to-run and run-to-walk transition when gradually changing speed. *Gait & Posture*, 24(2), 247–254. <https://doi.org/10.1016/j.gaitpost.2005.09.006>
- Segers, V., Lenoir, M., Aerts, P., & De Clercq, D. (2007). Kinematics of the transition between walking and running when gradually changing speed. *Gait & Posture*, 26(3), 349–361. <https://doi.org/10.1016/j.gaitpost.2006.10.013>
- Slawinski, J., Bonnefoy Mazure, A., Levêque, J. M., Ontanon, G., Riquet, A., Dumas, R., & L, L. (2010). Kinematic and Kinetic Comparisons of Elite and Well-Trained Sprinters During Sprint Start. *Journal of Strength and Conditioning Research*, 24(4), 896–905. <https://doi.org/10.1519/JSC.0b013e3181ad3448>
- Slawinski, J., Bonnefoy Mazure, A., Ontanon, G., Levêque, J. M., Miller, C., Riquet, A., Chèze, L., & Dumas, R. (2010). Segment-interaction in sprint start: Analysis of 3D angular velocity and kinetic energy in elite sprinters. *Journal of Biomechanics*, 43(8), 1494–1502. <https://doi.org/10.1016/j.jbiomech.2010.01.044>
- Slawinski, J., Dorel, S., Hug, F., Couturier, A., Fournel, V., Morin, J. B., & Hanon, C. (2008). Elite Long Sprint Running: A Comparison between Incline and Level Training Sessions. *Medicine & Science in Sports & Exercise*, 40(6), 1155–1162. <https://doi.org/10.1249/MSS.0b013e3181676681>
- Slawinski, J., Dumas, R., Chèze, L., Ontanon, G., Miller, C., & Bonnefoy Mazure, A. (2012). 3D kinematic of bunched, medium and elongated sprint start. *International Journal of Sports Medicine*, 33(7), 555–560. <https://doi.org/10.1055/s-0032-1304587>
- Slawinski, J., Millot, B., Houel, N., & Dinu, D. (2020). Use of an Inertial Measurement System to Calculate Maximal Power during Running Sprint Acceleration: Comparison with the Radar System. *Proceedings*, 49(1), 23. <https://doi.org/10.3390/proceedings2020049023>
- Slawinski, J., Termoz, N., Rabita, G., Guilhem, G., Dorel, S., Morin, J. B., & Samozino, P. (2017). How 100-m event analyses improve our understanding of world-class men's and women's sprint performance. *Scandinavian Journal of Medicine & Science in Sports*, 27(1), 45–54. <https://doi.org/10.1111/sms.12627>
- Solnik, S., Rider, P., Steinweg, K., DeVita, P., & Hortobágyi, T. (2010). Teager–Kaiser energy operator signal conditioning improves EMG onset detection. *European Journal of Applied Physiology*, 110(3), 489–498. <https://doi.org/10.1007/s00421-010-1521-8>
- Staupe, G., Flachenecker, C., Daumer, M., & Wolf, W. (2001). Onset Detection in Surface Electromyographic Signals: A Systematic Comparison of Methods. *EURASIP Journal on Advances in Signal Processing*, 2001(2), 2. <https://doi.org/10.1155/S1110865701000191>
- Staupe, G., & Wolf, W. (1999). Objective motor response onset detection in surface myoelectric signals. *Medical Engineering & Physics*, 21(6), 449–467. [https://doi.org/10.1016/S1350-4533\(99\)00067-3](https://doi.org/10.1016/S1350-4533(99)00067-3)
- Stępień, K., Śmigielski, R., Mouton, C., Cizek, B., Engelhardt, M., & Seil, R. (2019). Anatomy of proximal attachment, course, and innervation of hamstring muscles: A pictorial essay. *Knee Surgery, Sports Traumatology, Arthroscopy: Official Journal of the ESSKA*, 27(3), 673–684. <https://doi.org/10.1007/s00167-018-5265-z>
- Tanaka, T., Suga, T., Imai, Y., Ueno, H., Misaki, J., Miyake, Y., Otsuka, M., Nagano, A., & Isaka, T. (2019). Characteristics of lower leg and foot muscle thicknesses in sprinters: Does greater foot muscles contribute to sprint performance? *European Journal of Sport Science*, 19(4), 442–450. <https://doi.org/10.1080/17461391.2018.1534991>
- Terry, G. C., & LaPrade, R. F. (1996). The posterolateral aspect of the knee. Anatomy and surgical approach. *The American Journal of Sports Medicine*, 24(6), 732–739. <https://doi.org/10.1177/036354659602400606>
- Thelen, D. G., Chumanov, E. S., Best, T. M., Swanson, S. C., & Heiderscheit, B. C. (2005). Simulation of Biceps Femoris Musculotendon Mechanics during the Swing Phase of Sprinting. *Medicine & Science in Sports & Exercise*, 37(11), 1931–1938. <https://doi.org/10.1249/01.mss.0000176674.42929.de>
- Thelen, D. G., Chumanov, E. S., Hoerth, D. M., Best, T. M., Swanson, S. C., Li, L., Young, M., & Heiderscheit, B. C. (2005). Hamstring Muscle Kinematics during Treadmill Sprinting: *Medicine & Science in Sports & Exercise*, 37(1), 108–114. <https://doi.org/10.1249/01.MSS.0000150078.79120.C8>

- Thorstensson, A., & Roberthson, H. (1987). Adaptations to changing speed in human locomotion: Speed of transition between walking and running. *Acta Physiologica Scandinavica*, *131*(2), 211–214. <https://doi.org/10.1111/j.1748-1716.1987.tb08228.x>
- Usherwood, J. R., & Wilson, A. M. (2006). Accounting for elite indoor 200 m sprint results. *Biology Letters*, *2*(1), 47–50. <https://doi.org/10.1098/rsbl.2005.0399>
- Van Caekenberghe, I., Segers, V., Aerts, P., Willems, P., & De Clercq, D. (2013). Joint kinematics and kinetics of overground accelerated running versus running on an accelerated treadmill. *Journal of the Royal Society Interface*, *10*(84), 20130222. <https://doi.org/10.1098/rsif.2013.0222>
- van den Tillaar, R., Nagahara, R., Gleadhill, S., & Jiménez-Reyes, P. (2021). Step-to-Step Kinematic Validation between an Inertial Measurement Unit (IMU) 3D System, a Combined Laser+IMU System and Force Plates during a 50 M Sprint in a Cohort of Sprinters. *Sensors*, *21*(19), 6560. <https://doi.org/10.3390/s21196560>
- van den Tillaar, R., Solheim, J. A. B., & Bencke, J. (2017). COMPARISON OF HAMSTRING MUSCLE ACTIVATION DURING HIGH-SPEED RUNNING AND VARIOUS HAMSTRING STRENGTHENING EXERCISES. *International Journal of Sports Physical Therapy*, *12*(5), 718–727. <https://doi.org/10.26603/ijsppt20170718>
- Vandewalle, H., Peres, G., Heller, J., Panel, J., & Monod, H. (1987). Force-velocity relationship and maximal power on a cycle ergometer: Correlation with the height of a vertical jump. *European Journal of Applied Physiology and Occupational Physiology*, *56*(6), 650–656. <https://doi.org/10.1007/BF00424805>
- Volkov, N. I., & Lapin, V. I. (1979). Analysis of the velocity curve in sprint running: *Medicine & Science in Sports & Exercise*, *11*(4), 332–337. <https://doi.org/10.1249/00005768-197901140-00004>
- Weyand, P. G., Sandell, R. F., Prime, D. N. L., & Bundle, M. W. (2010). The biological limits to running speed are imposed from the ground up. *Journal of Applied Physiology*, *108*(4), 950–961. <https://doi.org/10.1152/jappphysiol.00947.2009>
- Weyand, P. G., Sternlight, D. B., Bellizzi, M. J., & Wright, S. (2000). Faster top running speeds are achieved with greater ground forces not more rapid leg movements. *Journal of Applied Physiology*, *89*(5), 1991–1999. <https://doi.org/10.1152/jappphysiol.2000.89.5.1991>
- Winter, D. A. (2009). *Biomechanics and motor control of human movement* (4th ed). Wiley.
- Yeadon, M. R., & Morlock, M. (1989). The appropriate use of regression equations for the estimation of segmental inertia parameters. *Journal of Biomechanics*, *22*(6–7), 683–689. [https://doi.org/10.1016/0021-9290\(89\)90018-3](https://doi.org/10.1016/0021-9290(89)90018-3)
- Yu, B., Queen, R. M., Abbey, A. N., Liu, Y., Moorman, C. T., & Garrett, W. E. (2008). Hamstring muscle kinematics and activation during overground sprinting. *Journal of Biomechanics*, *41*(15), 3121–3126. <https://doi.org/10.1016/j.jbiomech.2008.09.005>
- Zhang, J.-T., Novak, A. C., Brouwer, B., & Li, Q. (2013). Concurrent validation of Xsens MVN measurement of lower limb joint angular kinematics. *Physiological Measurement*, *34*(8), N63–N69. <https://doi.org/10.1088/0967-3334/34/8/N63>



Center of mass velocity comparison using a whole body magnetic inertial measurement unit system and force platforms in well trained sprinters in straight-line and curve sprinting

Benjamin Millot^{a,b,*}, Paul Blache^a, Daniel Dinu^a, Axelle Arnould^a, Jérémy Jusseaume^a, Christine Hanon^b, Jean Slawinski^a

^a Laboratory Sport, Expertise and Performance (EA7370), French Institute of Sport (INSEP), 11, Avenue du Tremblay, 75012 Paris, France

^b French Athletics Federation (FFA), 33, Avenue Pierre de Coubertin, 75013 Paris, France

ARTICLE INFO

Keywords:

Magneto-Inertial Measurement Units
Curve sprinting
Acceleration
Force platforms
Sprint running

ABSTRACT

Background: Sprint performance can be characterized through the centre of mass (COM) velocity over time. *In-field* computation of the COM is key in sprint training.

Research question: To compare the stance-averaged COM velocity computation from a Magneto-Inertial Measurement Units (MIMU) to a reference system: force platforms (FP), over the early acceleration phase in both straight and curve sprinting.

Methods: Nineteen experienced-to-elite track sprinters performed 1 maximal sprint on both the straight and the curve (radius = 41.58 m) in a randomized order. Utilizing a MIMU-based system (Xsens MVN Link) and compared to FP (Kistler), COM velocity was computed with both systems. Averaged stance-by-stance COM velocity over straight-line and curve sprinting following the vertical axis (respectively V_{zMIMU} and V_{zFP}) and the norm of the two axes lying on the horizontal plane: x and y, approximately anteroposterior and mediolateral (respectively V_{xyMIMU} and V_{xyFP}) over the starting-blocks (SB) and initial acceleration (IA – composed out of the first four stances following the SB) were compared using mean bias, 95 % limits of agreements and Pearson's correlation coefficients.

Results: 148 stances were analyzed. V_{xyMIMU} mean bias was comprised between 0.26 % and 2.03 % (expressed in % with respect to the FP) for SB, 5.63 % and 7.29 % over IA respectively on the straight and the curve. Pearson's correlation coefficients ranged between 0.943 and 0.990 for V_{xy} , 0.423 and 0.938 for V_z . On the other hand, V_{zMIMU} mean bias ranged between 2.33 % and 4.69 % for SB, between 1.44 % and 19.95 % over IA respectively on the straight and the curve

Significance: The present findings suggest that the MIMU-based system tested slightly underestimated V_{xyMIMU} , though within narrow limits which supports its utilization. On the other hand, V_{zMIMU} computation in sprint running is not fully mature yet. Therefore, this MIMU-based system represents an interesting device for *in-field* V_{xyMIMU} computation either for straight-line and curve sprinting.

1. Introduction

Sprint performance can be characterized through the centre of mass (COM) velocity over time [1,2]. For this reason, it is of interest to easily evaluate COM kinematics with accuracy within the athletes' ecological environment to preserve the measures' ecological validity. Yet, analyzing accurately the human movement *in-field* remains an everyday

challenge especially within the curve. In fact, sprinting in the curve represents ~58 % of the total distance for all track events starting from the 200 m [3]. Unfortunately, within the curve, systems such as radars or lasers become immediately inoperable. A few experimentations have described COM velocity in curve sprinting at specific instants [4–7]; however, the literature describing the COM velocity within this sprinting condition remains limited. Therefore, it is of importance to look for

* Correspondence to: 11, Avenue du Tremblay, 75012 Paris, France.

E-mail addresses: benjamin.millot@insep.fr, benjamin.millot@athle.fr (B. Millot), paulblache91@gmail.com (P. Blache), daniel.dinu@insep.fr (D. Dinu), aarnould.insep@gmail.com (A. Arnould), j.jusseaume92@gmail.com (J. Jusseaume), christine.hanon@athle.fr (C. Hanon), jean.slawinski@insep.fr (J. Slawinski).

<https://doi.org/10.1016/j.gaitpost.2022.11.002>

Received 20 July 2022; Received in revised form 24 October 2022; Accepted 2 November 2022

Available online 4 November 2022

0966-6362/© 2022 Elsevier B.V. All rights reserved.

in-field devices able to quickly evaluate the COM velocity within the curve over an entire sprint. Outside the laboratory, deciding which device to use relies on a trade-off between accuracy and feasibility. Considering their portability, convenience and range, full-body magneto-inertial measurement unit systems (MIMU) have become popular over the past decade. Yet, several authors have highlighted the limitations of such systems and overall there is no consensus regarding MIMU-based system's concurrent validity against reference systems for joints and segments kinematics [8–15].

At the COM, comparison between a MIMU-based system and an optoelectronic systems (OS) COM position while standing still showed a difference in the measurement from 0.73 mm (vertical axis) to 5.45 mm (medio-lateral axis) as well as very high correlations ($r > 0.99$; $p < 0.001$) [16].

Based on Newton's second law, force platforms (FP) have been considered as the reference system for COM velocity computation in sprint running [17–21], since correct computation does not rely on either accurate marker positioning or assumptions regarding the anthropometrical properties [22–25].

Using FP, Pavei et al. (2020) computed the COM displacement during overground walking and compared to a MIMU-based system [26]. They found differences between systems up to 98.7 ± 60.2 % [26], likely resulting from the sensors drift and the anthropometrical assumptions.

In sprint running, computations of the force-velocity profiles (FVP) from a MIMU-based system to a radar showed good agreements between both systems for the maximal velocity and the maximal theoretical force, velocity and power ($0.81 < r < 0.97$) [27]. However, despite their broad utilization for straight-line sprinting velocity computation [28–31], radars do not estimate neither the COM nor the frontal plane velocity, but only the participants' horizontal velocity [32,33]. Moreover, measurement can be impaired with such devices since radars detect all moving objects within their field of view.

Other authors used a single MIMU attached to the lumbar region to compute the participants' velocity [34] and compared the FVP variables obtained with those from the FP. Although these authors found “very large” to “extremely large” correlations for all but one FVP variable, they did not investigate the stance-averaged velocity itself. They also evaluated a point close to the COM, probably leading to erroneous COM estimation [22,25,33,35].

Recently, van den Tillaar et al. (2021) compared the step-velocity over 50-m sprints from a MIMU-based system to FP [36]. However, they multiplied step length and step rate rather than comparing the COM velocity, even though this parameter was found to be determinant for sprinting performance [2] and can be used to adapt training programs through FVP computation [21,37].

To our knowledge, no study compared the stance-averaged COM velocity computed from a MIMU-based system to a reference system. Additionally, the few experimentations that compared a MIMU-based system to the reference systems for other parameters only investigated the straight, notwithstanding the curve. Considering the prevalence of this sprinting condition in athletics, it appears mandatory to look for *in-field* devices able to easily evaluate the COM velocity within ecological environment.

Thus, the aim of the present study was to compare the stance-averaged COM velocity computed from a MIMU-based system to FP over the starting-blocks pushing phase and the initial acceleration during both straight-line and curve sprinting.

2. Methods

2.1. Participants

Nineteen (15 male and 4 female) experienced-to-elite curve sprinters (mean \pm SD: age = 23.9 ± 3.7 years; body mass = 73.9 ± 7.4 kg; height = 1.78 ± 0.07 m) volunteered to participate in this study. The mean

personal bests (PB) of the 6 male 200-m specialists, the 9 male 400-m specialists, the 2 female 200-m specialists and the 2 female 400-m specialists were respectively: 22.89, 49.56, 26.30 and 57.67 s. After an explanation of the protocol, the participants signed the informed consent to participate in the experimentation, conducted in accordance with the declaration of Helsinki and approved by the local ethical committee (IRB00012476–2021–29–04–107).

2.2. Materials

2.2.1. Concurrent system

The participants were equipped with a MIMU-based system MVN Link (Xsens Technologies, Enschede, Netherlands, 240 Hz). This system is composed of 17 MIMUs ($36 \times 24.5 \times 10$ mm: 10 g) fixed to the participants with straps. Each sensor contains a 3D gyroscope ($\pm 2000^\circ/s$), a 3D accelerometer (scale: ± 160 m/s²) and a 3D magnetometer (± 1.9 Gauss). Sensors were placed according to the manufacturer's recommendations (see Fig. 1). Participants' height and foot length were measured and inputted into the MVN software which estimated segment lengths with regression equations [38,39]. The calibration process was then performed according to the manufacturer instructions and general guidelines [9,10,12] to generate sensor-to-segment alignment [38].

2.3. Reference system

Using OS, errors can originate from marker positioning, movement on soft tissues and assumptions associated with anthropometric models [22,25,26]. Therefore, in the present experimentation we used a

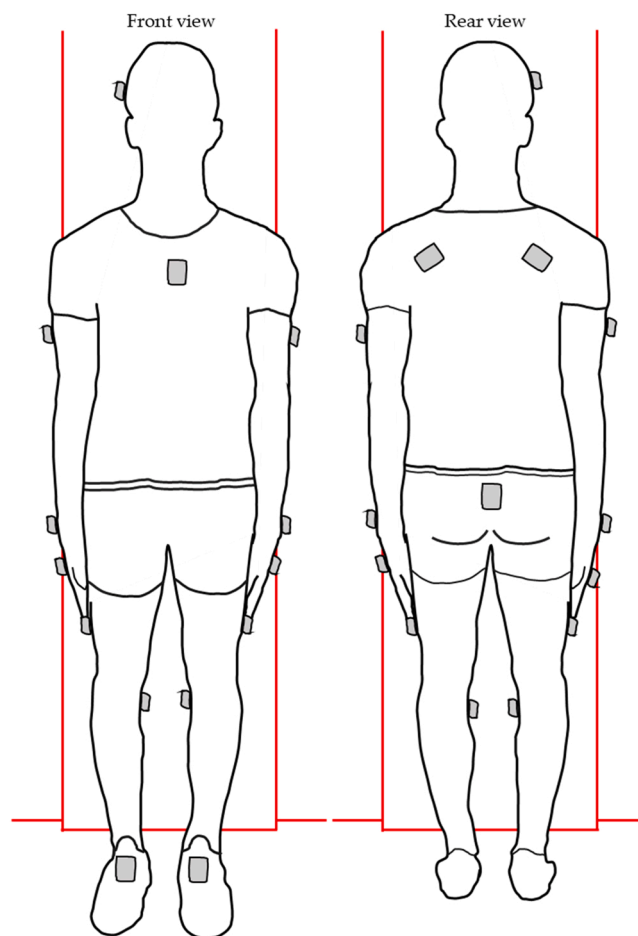


Fig. 1. Position of the inertial measurement units (in gray) with the athlete standing in the N-pose.

6.60 m-long FP composed out of 6 individual FP (5 length-wise and 1 sideways; 1.2×0.6 m each, KI 9067; Kistler, Wintherthu, Switzerland, 1 000 Hz) as the reference system. FP were connected in series, covered with a tartan mat and embedded within the track, thus making them invisible to the participants. This set-up allowed for a quasi *in-field* experimentation. Anteroposterior, mediolateral and vertical components (respectively F_x , F_y and F_z) of the GRF were computed from these FP.

The MIMU-based system and FP signals were synchronized to the nearest MIMU-based system frame using a customised cable with the MIMU-based system software triggering the FP. Accurate synchronization between devices has been confirmed during pilot experimentations by gently pressing on one MIMU positioned over the FP and by checking temporal events of vertical GRF and the MIMU accelerations.

2.4. Protocol

The recordings took place on an indoor track between June and July 2021, which corresponded to the competition period. The participants began with at least a 45-min self-managed warm-up. They were then equipped with the MIMUs and had a 10-min additional familiarization period with the MIMUs on. Subsequently, participants performed a maximal “valid” 10-m sprint within two conditions in a randomized order: straight and curve. A replicated curve corresponding to the lane 5 (radius 41.58 m) of a standard athletics track (World Athletics, 2019) overlapped the FP area.

A sprint was considered “valid” when at least the first stance out of the blocks fully landed within the FP area [20,21]. All participants used starting-blocks (SB) that were positioned on the FP which allowed the GRF computation over the SB pushing-phase.

2.5. Data analysis

2.5.1. Concurrent system

Using the temporal synchronization between systems, touchdown (TD) and toe-off (TO) for both systems were determined from the FP data using a 20-N threshold on F_z [37].

MIMU-based system anteroposterior, mediolateral and vertical instantaneous COM velocities (respectively V_{xMIMU} , V_{yMIMU} and V_{zMIMU}) based on the manufacturer’s proprietary sensor fusion algorithm were retrieved directly from the MVN software. V_{xMIMU} , V_{yMIMU} and V_{zMIMU} were low-pass filtered (20-Hz cut-off, third-order zero-phase Butterworth filter) chosen after residual analysis [40].

Thereafter, although the MIMU-based system calibration was realized such that its coordinate system coincides with that of FP, both devices’ coordinate systems are unlikely to be perfectly aligned. Consequently, we computed the norm of the horizontal plane of the MIMU-based system COM velocity (V_{xyMIMU}):

$$V_{xyMIMU} = \sqrt{V_{xMIMU}^2 + V_{yMIMU}^2} \quad (1)$$

2.6. Reference system

GRF raw signals were low-pass filtered (200-Hz cut-off, third-order zero-phase Butterworth filter) chosen after residual analysis [40].

Based on Newton’s Second Law and according to previous literature [17,19–21,23,25,26,41] the three COM orthogonal acceleration components were calculated by dividing GRF by the body mass ($-m \cdot g$ for the vertical acceleration). Thereafter, we computed instantaneous anteroposterior (V_{xFP}), mediolateral (V_{yFP}) and vertical (V_{zFP}) velocities by simple integration of the three orthogonal acceleration components over each stance:

$$V_{xFP} = V_{0xFP} + \int \frac{F_x}{m} dt \quad (2)$$

$$V_{yFP} = V_{0yFP} + \int \frac{F_y}{m} dt \quad (3)$$

$$V_{zFP} = V_{0zFP} + \int \frac{F_z - m \cdot g}{m} dt \quad (4)$$

with, m the participant’s body mass, V_{0xFP} , V_{0yFP} and V_{0zFP} the initial velocity conditions taken as integration constants and set to 0 since SB were placed over the FP and the sprinters started from a stationary position.

Finally, we computed the norm of the horizontal plane of the FP COM velocity (V_{xyFP}):

$$V_{xyFP} = \sqrt{V_{xFP}^2 + V_{yFP}^2} \quad (5)$$

Analysis was split within two conditions (Fig. 3), a) the SB phase (which includes only the starting-blocks pushing phase) and b) the initial acceleration, thereafter referred as IA (beginning at the first touchdown after the SB phase and ending at toe-off of the last stance computed).

The norm of the horizontal plane COM velocity (V_{xy}) and the vertical COM velocity (V_z) computed from both the FP and the MIMU-based system were averaged over each “valid” stance.

2.7. Statistical analysis

All descriptive statistics are presented as means \pm standard deviations (SD). Normality of the distribution was verified using the Shapiro-Wilk test. Then, V_{xy} and V_z obtained with both devices were compared using a) mean bias (expressed in % in comparison to the FP) and 95 % limits of agreement [42]; b) Pearson’s correlation coefficient (r) with threshold values of 0.3, 0.5, 0.7 and 0.9 representing respectively low, moderate, high and very high relationships [43,44]. For all statistical analyses, the alpha level was set as $p = 0.05$.

3. Results

The number of valid stances for each participant varied between two (SB and the following stance) to five (SB and the following four stances) for both sprinting conditions. Overall, 75 and 73 valid stances were computed respectively for the straight and the curve.

Table 1 presents the mean \pm SD for the sprint variables of both systems within the straight and the curve conditions for the SB and IA phases as well as the mean bias, 95 % agreement limits and correlation coefficients.

Figs. 2 and 3 display the Bland & Altman plots respectively for SB and IA. Mean bias between the MIMU-based system and the FP was lower on the straight than the curve. Mean V_{zMIMU} showed a bias of 1.44 % and 19.95 % respectively on the straight and the curve with random errors up to 108 %. Correlation coefficients between devices ranged between $r = 0.943 < r < 0.990$ for V_{xy} and $0.423 < r < 0.938$ for V_z Figs 4 and 5.

4. Discussion

This experimentation compared the COM stance-averaged velocity measured from a MIMU-based system to 6 FP over the early acceleration phase in both straight-line and curve sprinting among 19 experienced-to-elite curve sprinters with different anthropometric characteristics, sprinting expertise and mechanical capacities. V_{xyMIMU} mean bias either for SB (respectively 0.26 % and 2.03 % for the straight and the curve) and IA (respectively 5.63 % and 7.29 % for the straight and the curve) was low. Further, correlation coefficients for V_{xy} were very high for both SB and IA ($r > 0.943$). These correlation coefficients show that although slightly underestimated, a change of magnitude of V_{xyFP} is very well associated with a similar change of magnitude of V_{xyMIMU} either during SB and IA.

Table 1
Mean (\pm SD) values of the variables, Bland & Altman and correlation coefficients.

		MIMU (\pm SD) ($\text{m}\cdot\text{s}^{-1}$)	FP (\pm SD) ($\text{m}\cdot\text{s}^{-1}$)	Bias (%)	95 % Agreement limits	Correlation coefficients (r)
Starting blocks	V_{xy} STR	1.28 (\pm 0.14)	1.29 (\pm 0.14)	0.26	(-7.49; 6.97)	0.943
	V_{xy} CUR	1.24 (\pm 0.14)	1.27 (\pm 0.16)	2.03	(-10.02; 5.95)	0.957
	V_z STR	0.47 (\pm 0.06)	0.48 (\pm 0.08)	2.33	(-15.72; 11.06)	0.917
	V_z CUR	0.44 (\pm 0.07)	0.46 (\pm 0.09)	4.49	(-19.34; 10.37)	0.938
Initial accelerations	V_{xy} STR	4.60 (\pm 0.90)	4.87 (\pm 0.94)	5.63	(-11.71; 0.45)	0.990
	V_{xy} CUR	4.43 (\pm 0.86)	4.76 (\pm 0.92)	7.29	(-13.77; -0.81)	0.971
	V_z STR	0.21 (\pm 0.09)	0.21 (\pm 0.10)	1.44	(-98.63; 95.74)	0.499
	V_z CUR	0.20 (\pm 0.09)	0.24 (\pm 0.08)	19.95	(-108.62; 68.71)	0.423

MIMU = Magnetic Inertial Measurement Unit; FP = Force Platforms; SD = Standard Deviation; STR = Straight-Line Sprints; CUR = Curve Sprints; V_{xy} = Norm of the horizontal plane of the COM velocity; V_z = Vertical velocity.

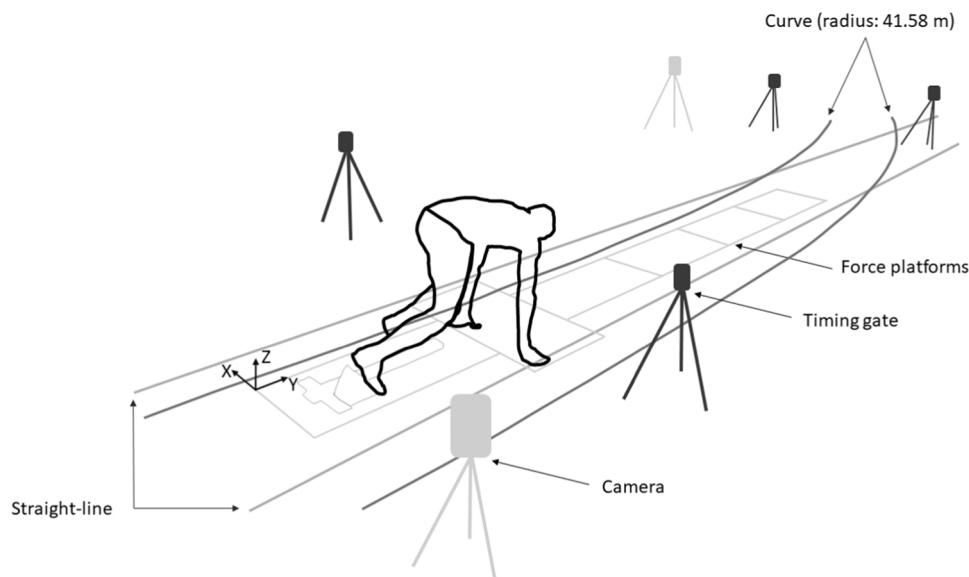


Fig. 2. Typical experimental set-up for the curve sprinting condition showing the force platforms, the straight-line and curve lanes, two video cameras (line grey on the tripods) and the timing gates (dark grey on the tripods). For the straight-line condition, the top right corner timing gate was moved outside of the straight-line lane and placed such at 10 m from the starting timing gates.

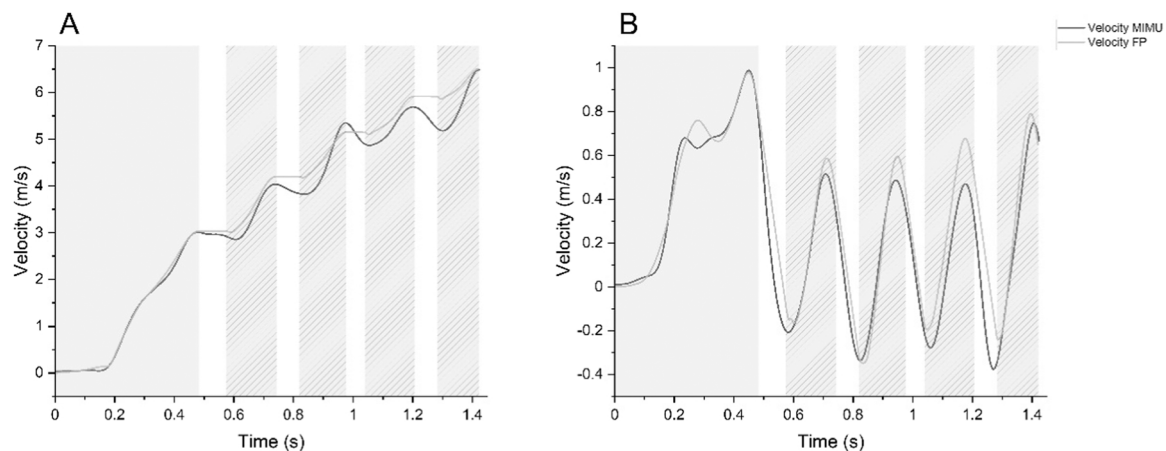


Fig. 3. Typical example showing A) the norm of the horizontal and lateral velocities and B) the vertical velocities computed respectively from the FP (light grey) and the MIMU-based (dark grey). The grey area on the left of each panel displays the entire starting-blocks phase. The grey shaded areas display the successive initial acceleration stance phases.

Throughout IA, we did not find any trend for the mean bias with increasing V_{xy} . The last stances' V_{xy} were $\sim 5\text{--}6 \text{ m}\cdot\text{s}^{-1}$ which corresponded to $\sim 60\text{--}70\%$ of the participants' maximal velocity. Those

findings suggest that differences between systems would not increase with velocity although further experimentations evaluating V_{xy} later on during the acceleration phase or at maximal velocity are needed to

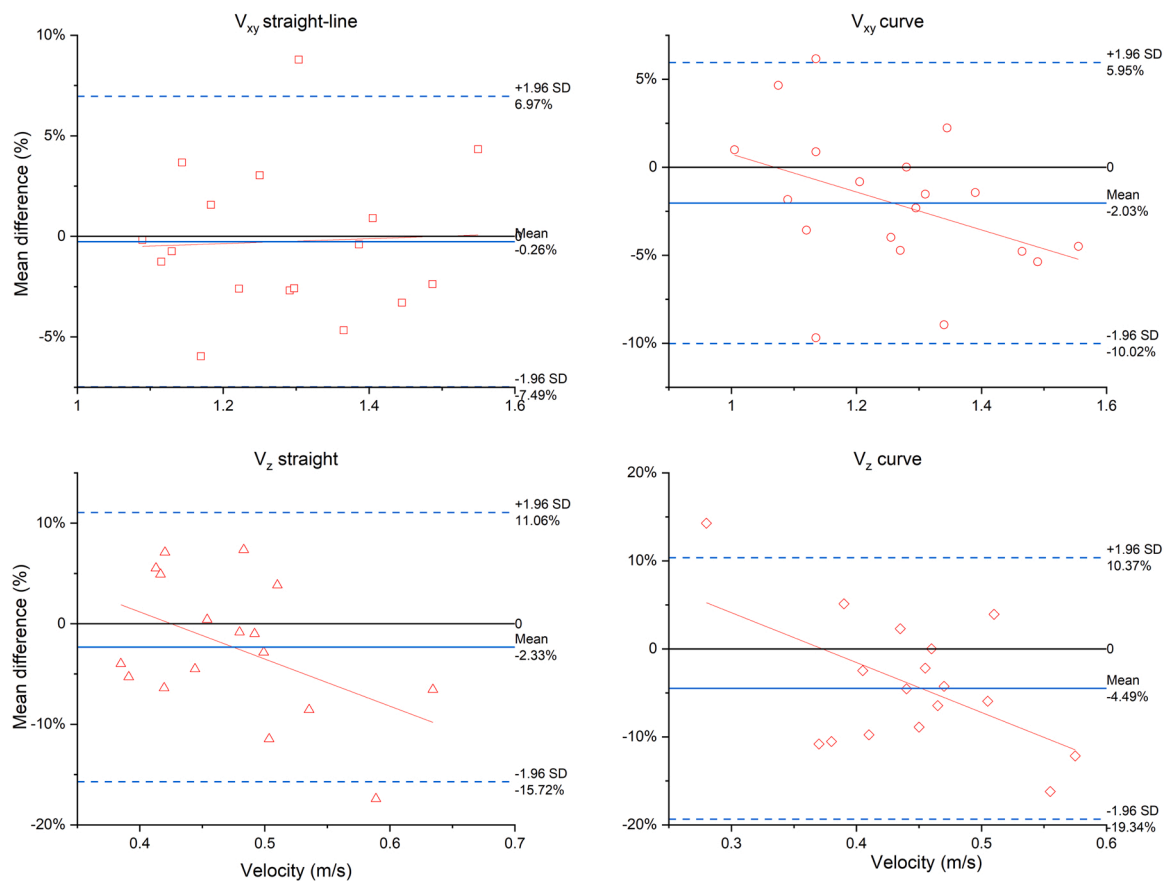


Fig. 4. Bland & Altman plots presenting the mean bias and 95 % limits of agreement between FP and MIMU for the starting-blocks pushing phase V_{xy} (top panels) and V_z (bottom panels) on both the straight-line (left panels) and the curve (right panels).

confirm our findings.

Contrastingly, V_{zMIMU} showed a greater mean bias (up to ~20 %) with large limits of agreement (up to ~108 %). Despite very high correlation coefficients for the SB between devices, IA showed small correlation coefficients meaning that a change of magnitude in V_{zFP} is poorly associated with a change of magnitude in V_{zMIMU} over the IA.

The findings of the present experimentation for V_{xyFP} over the SB and the first two stances are slightly below those reported by Nagahara et al. (2020) among male sprinters (100-m time PBs: 11.27 ± 0.27 s) [45]. In their experimentation, Nagahara et al. (2020) found a V_{xyFP} of respectively 3.92, 4.93, 5.70 and 6.30 $\text{m}\cdot\text{s}^{-1}$ for the first, second, third and fourth stances following the SB phase [45] while we found a V_{xyFP} of respectively 3.59, 4.62, 5.36 and 6.02 $\text{m}\cdot\text{s}^{-1}$ for the corresponding stances. Considering their athletes' PBs and that all participants were male in their experimentation, the findings of the present experimentation are thus in line with those of Nagahara et al. (2020). Regarding V_{zFP} , to our knowledge, no experimentation investigated the mean vertical velocity over the first stances. Slawinski et al. (2020) found vertical velocities of 0.52, 0.35 and 0.35 $\text{m}\cdot\text{s}^{-1}$ among elite sprinters respectively at SB clearing, first and second stances toe-off [27] while we found mean V_{zFP} of 0.44, 0.19 and 0.24 $\text{m}\cdot\text{s}^{-1}$ for the corresponding stances.

To the best of our knowledge, only one study compared the step velocity between a MIMU-based system and FP [36]. These authors found that the MIMU-based system velocity was underestimated for all steps. They reported a mean bias from 0.45 to over 0.60 $\text{m}\cdot\text{s}^{-1}$ as opposed to 0.26 $\text{m}\cdot\text{s}^{-1}$ in the present study. These discrepancies likely result from the different methods used to compute the velocity. While we have simply retrieved the COM velocity from the MIMU-based system software, these authors have multiplied step length and step frequency, determined from ankle angular velocity to identify TD and TO

using MIMUs placed on both feet, yet based on currently unpublished algorithm [36].

Moreover, when comparing data computed from a MIMU-based system and to those obtained with FP, care must be taken with regards to the coordinate system orientation. The MIMU-based system antero-posterior axis is likely neither aligned with the FP coordinate system nor with the sprinting path. Van den Tilaar et al. (2021) may have considered the antero-posterior axis only. To ensure accurate calculation it is therefore mandatory to compute the norm of the horizontal and mediolateral velocities (V_{xyMIMU} in the present study) which represents a limitation of this system if someone is willing to analyze each axis distinctly on the field.

Overall, the mean bias found in the present experimentation lies within similar range to those reported by Samozino et al. (2016) in their field method validation. They found absolute bias ranging from ~2–8 % against FP [21]. These authors concluded that this bias was “low” and this method is widely used in sport science and sprint training since. Similarly, differences between two reference systems (FP and OS) compared together for the COM trajectory reached ~9 % in walking at constant speed [26]. Those results show that even with two “reference systems”, differences - likely due to anthropometrical assumptions - comparable to the present findings can be found. Therefore, the present experimentation provides hints in the choice of the optimal system considering their cost, accuracy and easy-of-use ratio that meet the requirement of the experimental conditions.

V_{zMIMU} displayed the largest systematic bias (up to ~20 %) and random errors (up to ~108 %). Those results are in contrast with the findings of Pavei et al. (2020) who found the lowest bias on the vertical axis [26]. However, they compared the point-by-point root mean square distance, range of motion, minimum and maximum positions on the 3

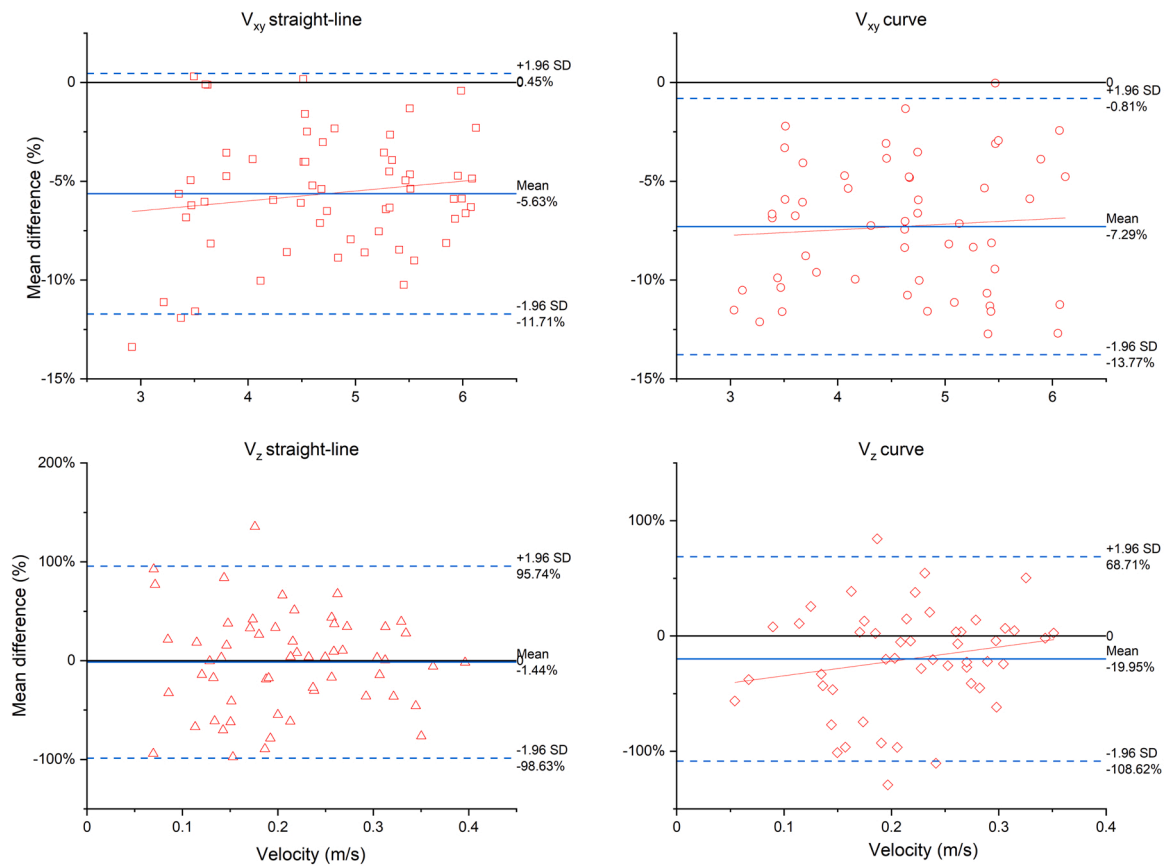


Fig. 5. Bland & Altman plots presenting the mean bias and 95 % limits of agreement between FP and MIMU for the initial acceleration V_{xy} (top panels) and V_z (bottom panels) on both the straight-line (left panels) and the curve (right panels).

orthogonal axes [26] while we analyzed the stance-averaged velocities in the present experimentation. Further, these authors have used a different system, sampling at 60 Hz with wireless MIMUs which can account for some of the variance between the experimentations [10]. Finally, their protocol also differed from ours since they analyzed walking strides with constant velocities of $0.79 \div 1.94 \text{ m}\cdot\text{s}^{-1}$ [26] while we evaluated accelerated sprinting (velocities up to $\sim 6 \text{ m}\cdot\text{s}^{-1}$). It is also important to note that since V_{zFP} values are much lower than V_{xyFP} , an error of $0.05 \text{ m}\cdot\text{s}^{-1}$ would yield greater discrepancies when expressed in percentage. However, considering the large random errors as well as the small correlation coefficients, it must be acknowledged that this MIMU-based system is not fully mature yet for accurately computing V_{zMIMU} in sprint running.

Other points likely resulting in differences between the FP and the MIMU-based system are worth mentioning. First and foremost, the anthropometrical model used with the MIMU-based system represents one of the main source of errors arising from either OS or MIMU-based systems in comparison to FP [15,25,26]. Although not one of the aims of this study, mean bias was greater for female than male: 4.64 % for male and 8.23 % for female over IA within the straight. While this shed some light on the possibility that this MIMU-based system anthropometric model is more adapted to male, this must be interpreted cautiously since only 4 females participated in this study.

The differences between the FP and the MIMU-based system should also be balanced since this experimentation focussed on the early acceleration phase, where sprinters produce their greatest acceleration [2]. In addition, at this very time of the sprint, participants are in a crouched-to-semi-straightened position which could challenge the biomechanical model computation. Therefore, the COM velocity of both systems should also be compared when the participant has straightened up.

Discrepancies between devices could also result from the systems' synchronization and the different sampling rate. Since synchronization between systems was at the nearest MIMU-based system's frame, we have tested on two random participants what could be the differences for V_{xyMIMU} with plus or minus 1 frame. We found mean discrepancies of $\sim 3.5\%$ and maximum differences reaching $\sim 8.5\%$, which could also account for some of the differences between systems.

MIMU-based system sensitivity to magnetic fields has also been widely discussed [10,12]. It is of importance to avoid ferromagnetic objects nearby the analysis area to limit sensors drift and ensure following guidelines for MIMU-based system use [10]. Considering the wooden indoor stadium where the experimentation took place and that the FP were embedded underneath the track surface, we can assume that this likely resulted in little disturbances.

The last source of discrepancy between the MIMU-based system and the FP could result from FP measurement errors. Albeit considered a reference system with pros well detailed by Pavei et al. (2017), FP can also be prone to measurement errors related mainly to a) integration with errors originating from the initial conditions and b) long recordings leading up to FP drift [25].

5. Conclusion

Evaluating the COM kinematics within *in-field* environments is a challenging process, especially when seeking for portable system you can use either inside or outside, with a simple setup and a wide range to capture the entire motion. This experimentation brings new insight into the use of this MIMU-based system as a valuable alternative of FP or OS for *in-field* computation of V_{xy} over the starting-blocks and the initial acceleration phase be it on the straight or the curve. Further, this MIMU-based system would provide the unique opportunity to access V_{xy} over

an entire sprint, be it a 200 or 400-m sprint. Contrastingly, V_{zMIMU} computation is not fully mature yet and further improvement must be made in order for this MIMU-based system to become an alternative to reference system for this parameter.

CRedit authorship contribution statement

Benjamin Millot: Conceptualization, Methodology, Software, Validation, Formal analysis, Investigation, Resources, Data curation, Writing – original draft, Writing – review & editing, Visualization, Project administration, Funding acquisition. **Paul Blache:** Investigation, Data curation. **Daniel Dinu:** Conceptualization, Resources. **Axelle Arnould:** Investigation. **Jeremy Jusseaume:** Investigation. **Christine Hanon:** Conceptualization, Methodology, Project administration, Funding acquisition. **Jean Slawinski:** Conceptualization, Validation, Resources, Methodology, Supervision, Project administration, Funding acquisition.

Conflict of interest statement

None.

Acknowledgments

The authors give special thanks to Vincent Guyot and Iwen Diuron for their assistance with data collection for this study and Sarah Chaudard for their help with English editing. We would also like to thank DimaSport for their support in reconstructing the curve and all the athletes from the present experimentation for their thorough involvement over each one's session. Benjamin Millot received a Ph.D. scholarship (CIFRE contract no. 2019/1904) founded by the French Athletics Federation and the French Agency of Research and Technology.

References

- J.P. Hunter, R.N. Marshall, P.J. McNair, Relationships between ground reaction force impulse and kinematics of sprint-running acceleration, *J. Appl. Biomech.* vol. 21 (1) (2005) 31–43, <https://doi.org/10.1123/jab.21.1.31>.
- J. Slawinski, et al., Kinematic and kinetic comparisons of elite and well-trained sprinters during sprint start, *J. Strength Cond. Res.* vol. 24 (4) (2010) 896–905, <https://doi.org/10.1519/JSC.0b013e3181ad3448>.
- D. Wilson, IAAF, 2008. Eds., Track and field facilities manual: 2008 edition; IAAF requirements for planning, constructing, equipping and maintaining. Monaco: Editions EGC, 2008.
- S.M. Churchill, A.I.T. Salo, G. Trewartha, The effect of the bend on technique and performance during maximal effort sprinting, *Sports Biomech.* vol. 14 (1) (2015) 106–121, <https://doi.org/10.1080/14763141.2015.1024717>.
- S.M. Churchill, A.I.T. Salo, G. Trewartha, The effect of the bend on technique and performance during maximal effort sprinting', *Sports Biomech.* vol. 14 (1) (2015) 106–121, <https://doi.org/10.1080/14763141.2015.1024717>.
- K. Ishimura, S. Sakurai, Asymmetry in determinants of running speed during curved sprinting, *J. Appl. Biomech.* vol. 32 (4) (2016) 394–400, <https://doi.org/10.1123/jab.2015-0127>.
- L.J. Judson, S.M. Churchill, A. Barnes, J.A. Stone, I.G.A. Brookes, J. Wheat, Horizontal force production and multi-segment foot kinematics during the acceleration phase of bend sprinting, *Scand. J. Med. Sci. Sports* vol. 29 (10) (2019) 1563–1571, <https://doi.org/10.1111/sms.13486>.
- S. Blair, G. Duthie, S. Robertson, W. Hopkins, K. Ball, Concurrent validation of an inertial measurement system to quantify kicking biomechanics in four football codes, *J. Biomech.* vol. 73 (2018) 24–32, <https://doi.org/10.1016/j.jbiomech.2018.03.031>.
- V. Camomilla, E. Bergamini, S. Fantozzi, G. Vannozzi, 2015. 'In-field use of wearable magneto-inertial sensors for sports performance evaluation', *ISBS*, 2015.
- V. Camomilla, E. Bergamini, S. Fantozzi, G. Vannozzi, Trends supporting the in-field use of wearable inertial sensors for sport performance evaluation: a systematic review, *Sensors* vol. 18 (3) (2018) 873, <https://doi.org/10.3390/s18030873>.
- A.I. Cuesta-Vargas, A. Galán-Mercant, J.M. Williams, The use of inertial sensors system for human motion analysis, *Phys. Ther. Rev.* vol. 15 (6) (2010) 462–473, <https://doi.org/10.1179/1743288x11Y.0000000006>.
- G.T.G. Hughes, V. Camomilla, B. Vanwanseele, A.J. Harrison, D.T.P. Fong, E. J. Bradshaw, Novel technology in sports biomechanics: some words of caution, *Sports Biomech.* (2021) 1–9, <https://doi.org/10.1080/14763141.2020.1869453>.
- P. Macadam, J. Cronin, J. Neville, S. Diwald, Quantification of the validity and reliability of sprint performance metrics computed using inertial sensors: a systematic review, *Gait Posture* vol. 73 (2019) 26–38, <https://doi.org/10.1016/j.gaitpost.2019.07.123>.
- B. Pedro, S. Cabral, A.P. Veloso, Concurrent validity of an inertial measurement system in tennis forehand drive, *J. Biomech.* vol. 121 (2021), 110410, <https://doi.org/10.1016/j.jbiomech.2021.110410>.
- X. Robert-Lachaine, H. Mecheri, C. Larue, A. Plamondon, Validation of inertial measurement units with an optoelectronic system for whole-body motion analysis, *Med Biol. Eng. Comput.* vol. 55 (4) (2017) 609–619, <https://doi.org/10.1007/s11517-016-1537-2>.
- D. Dinu, M. Fayolas, M. Jacquet, E. Leguy, J. Slavinski, N. Houel, Accuracy of postural human-motion tracking using miniature inertial sensors, *Procedia Eng.* vol. 147 (2016) 655–658, <https://doi.org/10.1016/j.proeng.2016.06.266>.
- G.A. Cavagna, Force platforms as ergometers, *J. Appl. Physiol.* vol. 39 (1) (1975) 174–179, <https://doi.org/10.1152/jappl.1975.39.1.174>.
- G.A. Cavagna, L. Komarek, S. Mazzoleni, The mechanics of sprint running, *J. Physiol.* vol. 217 (3) (1971) 709–721, <https://doi.org/10.1113/jphysiol.1971.sp009595>.
- H. Elftman, The force exerted by the ground in walking, *Arbeitsphysiologie* vol. 10 (5) (1939) 485–491, <https://doi.org/10.1007/BF02012165>.
- G. Rabita, et al., Sprint mechanics in world-class athletes: a new insight into the limits of human locomotion: sprint mechanics in elite athletes, *Scand. J. Med. Sci. Sports* vol. 25 (5) (2015) 583–594, <https://doi.org/10.1111/sms.12389>.
- P. Samozino, et al., A simple method for measuring power, force, velocity properties, and mechanical effectiveness in sprint running: Simple method to compute sprint mechanics, *Scand. J. Med. Sci. Sports* vol. 26 (6) (2016) 648–658, <https://doi.org/10.1111/sms.12490>.
- S.A. Gard, S.C. Miff, A.D. Kuo, Comparison of kinematic and kinetic methods for computing the vertical motion of the body center of mass during walking, *Hum. Mov. Sci.* vol. 22 (6) (2004) 597–610, <https://doi.org/10.1016/j.humov.2003.11.002>.
- H.-M. Maus, A. Seyfarth, S. Grimmer, Combining forces and kinematics for calculating consistent centre of mass trajectories, *J. Exp. Biol.* vol. 214 (21) (2011) 3511–3517, <https://doi.org/10.1242/jeb.057422>.
- A.E. Minetti, C. Cisotti, O.S. Mian, The mathematical description of the body centre of mass 3D path in human and animal locomotion, *J. Biomech.* vol. 44 (8) (2011) 1471–1477, <https://doi.org/10.1016/j.jbiomech.2011.03.014>.
- G. Pavei, E. Seminati, D. Cazzola, A.E. Minetti, On the estimation accuracy of the 3D body center of mass trajectory during human locomotion: inverse vs. forward dynamics, *Front. Physiol.* vol. 8 (2017), <https://doi.org/10.3389/fphys.2017.00129>.
- G. Pavei, F. Salis, A. Cereatti, E. Bergamini, Body center of mass trajectory and mechanical energy using inertial sensors: a feasible stride, *Gait Posture* vol. 80 (2020) 199–205, <https://doi.org/10.1016/j.gaitpost.2020.04.012>.
- J. Slawinski, B. Millot, N. Houel, D. Dinu, Use of an inertial measurement system to calculate maximal power during running sprint acceleration: comparison with the radar system, *Proceedings* vol. 49 (1) (2020) 23, <https://doi.org/10.3390/proceedings2020049023>.
- P.E. di Prampero, S. Fusi, L. Sepulcri, J.B. Morin, A. Belli, G. Antonutto, Sprint running: a new energetic approach, *J. Exp. Biol.* vol. 208 (14) (2005) 2809–2816, <https://doi.org/10.1242/jeb.01700>.
- J.-B. Morin, T. Jeannin, B. Chevallier, A. Belli, Spring-Mass model characteristics during sprint running: correlation with performance and fatigue-induced changes, *Int J. Sports Med.* vol. 27 (2) (2006) 158–165, <https://doi.org/10.1055/s-2005-837569>.
- J.-B. Morin, P. Edouard, P. Samozino, Technical ability of force application as a determinant factor of sprint performance, *Med. Sci. Sports Exerc.* vol. 43 (9) (2011) 1680–1688, <https://doi.org/10.1249/MSS.0b013e318216ea37>.
- J.-B. Morin, P. Sève, Sprint running performance: comparison between treadmill and field conditions, *Eur. J. Appl. Physiol.* vol. 111 (8) (2011) 1695–1703, <https://doi.org/10.1007/s00421-010-1804-0>.
- N. Bezodis, A.I. Salo, G. Trewartha, Measurement error in estimates of sprint velocity from a laser displacement measurement device, *Int. J. Sports Med.* vol. 33 (6) (2012) 439–444, <https://doi.org/10.1055/s-0031-1301313>.
- J. Slawinski, V. Billat, J.-P. Koralsztein, M. Tavernier, Use of lumbar point for the estimation of potential and kinetic mechanical power in running, *J. Appl. Biomech.* vol. 20 (3) (2004) 324–331, <https://doi.org/10.1123/jab.20.3.324>.
- I. Setuain, P. Lecumberri, J.P. Ahtiainen, A.A. Mero, K. Häkkinen, M. Izquierdo, Sprint mechanics evaluation using inertial sensor-based technology: a laboratory validation study', *Scand. J. Med. Sci. Sports* vol. 28 (2) (2018) 463–472, <https://doi.org/10.1111/sms.12946>.
- M.H.A. Eames, A. Cosgrove, R. Baker, Comparing methods of estimating the total body centre of mass in three-dimensions in normal and pathological gaits, *Hum. Mov. Sci.* vol. 18 (5) (1999) 637–646, [https://doi.org/10.1016/S0167-9457\(99\)00022-6](https://doi.org/10.1016/S0167-9457(99)00022-6).
- R. van den Tillaar, R. Nagahara, S. Gleadhill, P. Jiménez-Reyes, Step-to-Step kinematic validation between an Inertial Measurement Unit (IMU) 3D system, a combined laser-imu system and force plates during a 50 M sprint in a cohort of sprinters, *Sensors* vol. 21 (19) (2021) 6560, <https://doi.org/10.3390/s21196560>.
- J.-B. Morin, P. Samozino, M. Murata, M.R. Cross, R. Nagahara, A simple method for computing sprint acceleration kinetics from running velocity data: Replication study with improved design, *J. Biomech.* vol. 94 (2019) 82–87, <https://doi.org/10.1016/j.jbiomech.2019.07.020>.
- D. Roetenberg, H. Luinge, P. Slycke, Xsens MVN: full 6DOF human motion tracking using miniature inertial, *Sensors* (2013) 10.

- [39] M.R. Yeadon, M. Morlock, The appropriate use of regression equations for the estimation of segmental inertia parameters, *J. Biomech.* vol. 22 (6–7) (1989) 683–689, [https://doi.org/10.1016/0021-9290\(89\)90018-3](https://doi.org/10.1016/0021-9290(89)90018-3).
- [40] D.A. Winter, 2009. *Biomechanics and motor control of human movement*, 4th ed. Hoboken, N.J: Wiley, 2009.
- [41] J. Eng, D. Winter, Estimations of the horizontal displacement of the total body centre of mass: considerations during standing activities, *Gait Posture* vol. 1 (3) (1993) 141–144, [https://doi.org/10.1016/0966-6362\(93\)90055-6](https://doi.org/10.1016/0966-6362(93)90055-6).
- [42] M.J. Bland, G. D. Altman, Statistical methods for assessing agreement between two methods of clinical measurement, *Lancet* vol. 327 (8476) (1986) 307–310, [https://doi.org/10.1016/S0140-6736\(86\)90837-8](https://doi.org/10.1016/S0140-6736(86)90837-8).
- [43] W.G. Hopkins, S.W. Marshall, A.M. Batterham, J. Hanin, Progressive statistics for studies in sports medicine and exercise science, *Med. Sci. Sports Exerc.* vol. 41 (1) (2009) 3–12, <https://doi.org/10.1249/MSS.0b013e31818cb278>.
- [44] M. Mukaka, A guide to appropriate use of correlation coefficient in medical research, *Malawi Med. J.* vol. 24 (3) (2012) 69–71.
- [45] R. Nagahara, H. Kanehisa, T. Fukunaga, Ground reaction force across the transition during sprint acceleration, *Scand. J. Med. Sci. Sports* vol. 30 (3) (2020) 450–461, <https://doi.org/10.1111/sms.13596>.

RÉSUMÉ SUBSTANTIEL EN LANGUE FRANÇAISE

En athlétisme, lors du 100 m, la femme et l'homme qui franchissent la ligne d'arrivée dans le temps le plus court à partir du coup de feu du starter seront couronnés. Puisque la vitesse antéropostérieure moyenne atteinte sur ce 100 m est définie par le temps écoulé sur cette distance, cette vitesse antéropostérieure moyenne est le paramètre le plus déterminant de la performance et celui-ci doit être amélioré.

Quelques décennies de recherche appliquées au sprint ont permis de dresser de manière assez globale les différents paramètres qui influencent cette vitesse antéropostérieure moyenne et donc la performance sur le 100 m. En utilisant des données issues de lasers, radars ou de vidéos, Slawinski et al. (2017) ont montré que la vitesse antéropostérieure maximale atteinte sur un 100 m permettait de très bien prédire la performance sur ce 100 m parmi des sprinteurs de niveau mondial (coefficient de corrélation de -0.90). D'ailleurs, lors de son record du monde en 9.59 s, Usain Bolt a atteint une vitesse antéropostérieure maximale de $12.34 \text{ m} \cdot \text{s}^{-1}$ (Graubner & Nixdorf, 2009). Ainsi, quiconque tentera de battre ce record du monde devra certainement atteindre une vitesse antéropostérieure maximale encore plus élevée.

La vitesse antéropostérieure maximale du centre de masse, bien que plus difficile à mesurer, est également un paramètre déterminant de la performance et un témoin de l'expertise de l'athlète en sprint. Ainsi, plus cette vitesse antéropostérieure du centre de masse est élevée, plus l'athlète est expérimenté. En s'appuyant sur la deuxième loi de Newton, la vitesse du centre de masse peut être décrite grâce à l'application des forces au sol (Kawamori et al., 2013). Dans la ligne droite, il a été montré que la capacité d'un athlète à produire des plus hauts niveaux de force antéropostérieure serait un élément clé afin d'améliorer la performance (Hunter et al., 2005; Kawamori et al., 2013; Morin et al., 2012; Rabita et al., 2015). Ainsi, au sein d'un groupe de sprinteurs, les plus expérimentés sont capables de produire des plus hauts niveaux de force antéropostérieure que leurs partenaires moins expérimentés (Rabita et al., 2015). En revanche, puisque le 100 m est supposé être couru strictement en ligne droite, la force médiolatérale est généralement négligée, ou pas étudiée, bien que sa grandeur soit d'environ 1/3 du poids du corps sur les premiers appuis.

À l'inverse, dans le virage, la force médiolatérale devient centrale puisque le sprinteur doit suivre une trajectoire curviligne (Chang & Kram, 2007). Cette trajectoire curviligne est d'ailleurs un élément central du sprint puisque, en athlétisme, la course de sprint en virage représente 58% de la distance totale de course à parcourir dans toutes les disciplines sur piste à partir du 200 m. De plus, aux prochains Jeux olympiques de Paris 2024, 11 disciplines de sprint sont courues en virage : le 4*100 m, le 200 m, le 400 m, le 400 m haies, le 4*400 m et le 4*400 m mixte. Ainsi, sur les 45 médailles qui seront distribuées sur les disciplines de sprint, 33 concerneront la course de sprint en virage, ce qui témoigne de l'omniprésence de cette condition de course en athlétisme. En outre, il est assez largement admis que la course de sprint en virage entraîne une diminution de la performance en comparaison à la ligne droite. Il est donc paradoxal que la plupart des recherches menées jusqu'à présent en sprint se soient intéressées quasi exclusivement à la course de sprint en ligne droite.

Quelques études ont étudié différents paramètres mécaniques dans le virage afin de comprendre les raisons de la réduction de la performance dans cette condition de course. Cependant, parmi cette minorité d'études, certaines ont été menées dans des conditions trop éloignées de la pratique du sprint en athlétisme (*i.e.*, rayons de courbures trop petits, vitesses sous-maximales étudiées). De ce fait, seules quelques études ont étudié l'application des forces au sol (Churchill et al., 2016; Judson et al., 2019) ainsi que la cinématique de course (Churchill et al., 2015; Judson, Churchill, Barnes, Stone, Brookes, et al., 2020; Judson, Churchill, Barnes, Stone, & Wheat, 2020) dans le virage, à des rayons de courbure spécifiques de l'athlétisme, et avec des efforts maximaux. Malheureusement, leur analyse était limitée à 2 instants spécifiques du sprint : à 13 m (Judson, Churchill, Barnes, Stone, Brookes, et al., 2020; Judson, Churchill, Barnes, Stone, & Wheat, 2020; Judson et al., 2019) et 40 m (Churchill et al., 2015, 2016). Or, dans le virage, la force centripète appliquée au centre de masse est fortement influencée par la vitesse antéropostérieure de l'athlète (Greene, 1985). Il semble donc nécessaire de comparer le virage à la ligne droite, non pas à des instants isolés du virage, mais sur l'intégralité de la phase d'accélération.

L'application des forces au sol, nous l'avons vu, permet de décrire la vitesse du centre de masse. En outre, cette application des forces au sol dépend de la technique de course de l'athlète, et plus globalement des mouvements des segments de l'athlète, eux-mêmes dépendants de l'activité musculaire. Ainsi, afin d'avoir une compréhension globale de la performance en sprint, il est nécessaire d'établir une approche globale des facteurs de la performance à travers une approche expérimentale multifactorielle.

Ainsi, l'objet de cette thèse était de comparer l'application des forces au sol, la cinématique articulaire, ainsi que l'activité musculaire de certains muscles du bas du corps, entre le virage et la ligne droite, depuis les starting-blocks et jusqu'à l'atteinte de la vitesse antéropostérieure maximale.

Au cours de la dernière décennie, différentes améliorations technologiques ont permis de conduire des expérimentations *in situ* afin d'étudier la cinématique lors de différents mouvements sportifs de manière précise (Blair et al., 2018; Nijmeijer et al., 2023). D'autre part, les systèmes d'électromyographie sont désormais portables, permettant l'utilisation en sprint. En parallèle, des protocoles expérimentaux innovants (Cavagna et al., 1971; Rabita et al., 2015) permettent d'étudier l'application des forces au sol, la cinématique de course ainsi que l'activité musculaire sur l'intégralité d'un sprint dans des conditions écologiques, afin d'améliorer la validité de ces expérimentations. Dans le cadre de ce travail de thèse, nous avons souhaité réaliser ces expérimentations dans des conditions écologiques afin d'étudier le mouvement sportif dans son cadre de pratique. Nous avons divisé ce travail en quatre contributions expérimentales, toutes issues des mêmes expérimentations et rejoignant le même objectif *in fine* : l'amélioration de la compréhension des paramètres limitant de la performance lors de la course de sprint en virage.

Dans ce cadre, 4 femmes et 15 hommes, toutes et tous d'un niveau expérimenté à élite en course de sprint en virage ont réalisé 5 sprints en ligne droite et 5 sprints en virage (10 m, 15 m, 20 m, 30 m et 40 m) en utilisant des starting-blocks. Pour ces expérimentations, nous avons utilisé un système composé de 17 centrales à inertie, 6 plateformes de forces intégrées dans une piste d'athlétisme et 8 électrodes d'électromyographie de surface. Ce protocole nous a permis, en reculant successivement la position des starting-blocks par rapport aux plateformes de force, d'avoir des appuis consécutifs sur ces plateformes de force sur les différents sprints (0-6 m, 8-14 m, 14-19 m, 24-29 m et 34-39 m), et ainsi reconstruire presque intégralement les appuis d'un 40 m sur ces plateformes de force. Les trois systèmes étant synchronisés, cela nous a également permis d'étudier les paramètres cinématiques et musculaires sur les phases d'appuis et de vol, distinctement, et de manière précise.

La première étude de ce travail de thèse avait pour objectif de déterminer si la vitesse du centre de masse pouvait être mesurée de manière précise dans les starting-blocks et les 4 premiers appuis qui suivent, en utilisant un système composé de plusieurs centrales à inertie, et en le comparant à un système de référence (plateformes de force dans ce

cas). Dans cette étude, nous avons pu montrer que la norme de la vitesse horizontale était légèrement sous-estimée avec ce système de centrales à inertie, en ligne droite (5.63% de différence entre les deux systèmes ; 4.60 ± 0.90 vs 4.87 ± 0.94 m · s⁻¹) et en virage (7.29% de différence entre les deux systèmes ; 4.43 ± 0.86 vs 4.76 ± 0.92 m · s⁻¹). Les résultats de cette première étude ouvrent les possibilités d'utiliser ce système à l'avenir pour étudier la norme de la vitesse horizontale dans des conditions écologiques, en sprint. D'autre part, la vitesse verticale du centre de masse présentait des différences inférieures à 20% en ligne droite (1.44% de différence entre les deux systèmes ; 0.21 ± 0.09 vs 0.21 ± 0.10 m · s⁻¹) et en virage (19.95% de différence entre les deux systèmes ; 0.20 ± 0.09 vs 0.24 ± 0.08 m · s⁻¹). Cependant, même si les différences entre les deux systèmes à l'échelle du groupe étaient inférieures à 20%, de très larges différences en fonction des individus ont pu être soulignées (erreurs aléatoires allant jusqu'à 108.62%). Ce système ne doit donc pas être utilisé afin d'évaluer la vitesse verticale du centre de masse en sprint à l'heure actuelle.

La deuxième étude de ce travail de thèse s'est intéressée à l'application des forces au sol ainsi que les impulsions entre la ligne droite et le virage dans un objectif de meilleure compréhension de l'adoption de cette trajectoire curviligne dans le virage. Les forces et impulsions médiolatérales, antéropostérieures, verticales et totales étaient mesurées en utilisant 6 plateformes de force qui étaient situées dans le sol d'une piste d'athlétisme. Nous avons étudié à la fois l'effet condition de course (ligne droite vs virage), ainsi que l'effet vitesse de course (0-6 m, 8-14 m, 14-19 m, 24-29 m et 34-39 m). Les résultats majeurs concernaient l'augmentation de la force ($p < 0.001$) et de l'impulsion ($p < 0.001$) médiolatérales à la fois sur la jambe intérieure et extérieure dans le virage, en comparaison à la ligne droite. Cela était accompagné conjointement par une diminution de la force ($p < 0.001$) et de l'impulsion ($p < 0.001$) antéropostérieures dans le virage alors même que ces paramètres sont déterminants de la performance en ligne droite. Il est possible que cette diminution de la force et de l'impulsion antéropostérieures soit le résultat de l'impossibilité de l'athlète d'augmenter la force totale produite lors de l'appui, alors même que la force médiolatérale augmente fortement dans le virage. En outre, la force verticale était diminuée sur la jambe intérieure dans le virage. Dans cette deuxième étude, nous avons donc mis en avant le fait que la performance était diminuée dans le virage à cause d'une diminution de la force et de l'impulsion antéropostérieures, à la fois lors du contact de la jambe intérieure et extérieure dans le virage.

La troisième étude de ce travail de thèse s'est quant à elle intéressée à la cinématique articulaire (angles et vitesses angulaires en flexion et en extension) de la hanche, du genou et de la cheville dans le plan sagittal lors de la phase d'appuis et lors de la phase de vol. Pour cela, nous avons utilisé le même système de centrales à inertie que dans la première étude. Nous avons étudié à la fois l'effet condition de course (ligne droite vs virage), ainsi que l'effet vitesse de course (0-6 m, 8-14 m, 14-19 m, 24-29 m et 34-39 m). Dans cette troisième étude, nous avons pu souligner une diminution de l'angle maximal d'extension du genou de la jambe intérieure lors de la phase d'appuis ($p = 0.004$), ainsi qu'une augmentation de la flexion plantaire de la cheville extérieure dans le virage ($p = 0.009$), en comparaison à la ligne droite. Cette modification de la cinématique articulaire du bas du corps était possiblement due à l'inclinaison du tronc vers l'intérieur du virage, et dans un souci de conserver l'alignement cheville-hanche-épaule lors de l'appui.

Enfin, dans la **quatrième étude de ce travail de thèse**, nous avons étudié l'activité musculaire du chef long du *Biceps Femoris*, du *Rectus femoris*, du *Vastus Lateralis* et enfin du *Gastrocnemius Medialis* lors de la phase d'appuis ainsi que pendant la phase de vol, sur les deux jambes, en utilisant de l'électromyographie de surface. Nous avons étudié l'effet condition de course (ligne droite vs virage) ainsi que l'effet vitesse de course (0-6 m, 8-14 m, 14-19 m, 24-29 m et 34-39 m) sur la quantité d'activité musculaire ainsi que les durées d'activation de ces muscles. Dans le virage, nous avons pu mettre en évidence une plus faible activation du *Vastus Lateralis* de la jambe intérieure lors de la phase d'appuis. Puisque ce muscle est extenseur du genou, il est vraisemblable que la diminution de l'extension du genou de la jambe intérieure observée lors de la phase d'appuis dans le virage, dans la troisième étude, soit liée à la plus faible activation de ce muscle de la jambe intérieure dans le virage. En outre, puisque le *Vastus Lateralis* contribue à l'accélération verticale du centre de masse lors de la phase d'appuis, il est possible qu'une plus faible activation de ce muscle sur la jambe intérieure dans le virage impacte la production de force verticale.

D'une manière globale, nous avons pu démontrer à travers ce travail de thèse que la performance était réduite dans le virage à cause d'une diminution des forces et impulsions antéropostérieures lors de la phase d'appuis en comparaison à la ligne droite. Cela était certainement lié à l'augmentation des forces médiolatérales dans le virage afin d'adopter une trajectoire curviligne, et en l'absence d'une augmentation des forces totales produites lors de l'appui. La force verticale était également diminuée sur la jambe intérieure dans le virage. Cela était possiblement causé par une diminution de l'extension

du genou de la jambe intérieure, lui-même lié à une plus faible activation du *Vastus Lateralis* de cette même jambe intérieure dans le virage.

En quelques mots, ce travail de thèse a montré que la performance était diminuée lors de la course de sprint en virage à cause d'une diminution de la force et de l'impulsion antéropostérieures, sur les jambes intérieures et extérieures, en comparaison à la ligne droite.

What are the factors altering the sprinting performance in the curve?

Abstract: Curve sprinting represents ~58% of the total distance to run for all track events starting from the 200 m onwards. However, this sprinting condition has not been thoroughly analyzed in the existing literature. In overground sprinting with maximal effort, several factors affect the performance and among them, the ground reaction forces (GRF), the joint kinematics and the surface electromyography (sEMG). Therefore, the aims of this PhD thesis were to describe the modifications of these parameters in the curve in comparison to the straight from the starting blocks pushing phase and until the maximal velocity. For that sake, we have used a multidimensional approach during *in-field* experimentations with experienced curve sprinters (*i.e.*, 200 & 400 m). This PhD work has been divided within four studies, all emerging from the same experimentations. The first study aimed to compare the centre of mass (CM) velocity computed from a magneto-inertial measurement unit (MIMU)-based system to that of a reference system (*i.e.*, force platforms). The results showed that the norm of the horizontal plane CM velocity computed with the MIMU-based system was slightly under-estimated (< ~7%) in comparison to the reference system. These differences between systems likely originated from the anthropometrical model. The second study investigated the GRF and impulses from the starting blocks pushing phase and until the maximal velocity in the straight and in the curve using force platforms embedded within the track. The results demonstrated that within the curve, the participants were unable to produce a similar magnitude of anterior-posterior GRF and this was markedly pronounced on the inside leg. This was mainly due to a large increase in the medial-lateral force to maintain a curvilinear motion. In order to counter this, the participants increased their left stance times to produce resultant and vertical impulses similar to the straight. The third study explored the hip, the knee and the ankle joint kinematics using the MIMU-based system. Our main findings were that during the stance phase, the left knee was less extended and the right ankle was more plantar-flexed in the curve than in the straight, caused by the body lateral lean. Finally, the fourth study addressed the timings and amplitude of four lower limb muscles using sEMG. We reported a lower *Vastus Lateralis* (a knee extensor) activity in the curve in comparison to the straight. Apart from this muscle, the muscle activity timings and amplitude were in general similar to the straight. Overall, using this multidisciplinary approach, we could better elucidate some reasons for the poorer sprinting performance in the curve in comparison to the straight. Based on our findings, we could address some practical recommendations in a double objective of performance improvement and injury risks reduction.

Keywords: Curve sprinting, ground reaction forces, kinematics, surface electromyography, sprint, performance, injury prevention.

Quels sont les facteurs explicatifs de la diminution de la performance lors de la course de sprint en virage ?

Résumé : La course en virage représente ~58% de la distance totale à parcourir pour toutes les disciplines sur piste à partir du 200 m. Malgré la prévalence de cette condition de course, elle a été peu analysée jusqu'à présent dans la littérature. En sprint, différents facteurs impactent la performance, parmi eux, l'application des forces au sol (GRF), la cinématique articulaire ainsi que l'électromyographie de surface (sEMG). Ainsi, les objectifs de cette thèse de doctorat étaient de décrire les éventuelles modifications qui surviennent lors du virage en comparaison à la ligne droite à partir de la phase de starting blocks et jusqu'à l'atteinte de la vitesse maximale. Nous avons menées des expérimentations *in-situ* avec des participants expérimentés de la course de sprint en virage (200 et 400 m). Ce travail de thèse a ensuite été scindé en quatre études différentes, issues d'un même protocole expérimental. La première étude avait pour objectif de comparer l'utilisation d'un système à navigation inertielle à un système de référence (*i.e.*, plateformes de forces) pour la mesure de la vitesse du centre de masse (CM). La vitesse du plan horizontal du CM était légèrement sous-estimée (< ~7%) avec le système à navigation inertielle. Ces différences entre les deux systèmes étaient probablement liées au modèle anthropométrique. La deuxième étude s'intéressait à la comparaison des GRF et des impulsions entre la ligne droite et le virage à l'aide de plateformes de force. Les résultats de cette étude ont démontré que, dans le virage, les participants n'étaient pas en mesure de produire des niveaux de force antéro-postérieure similaire à la ligne droite, notamment sur la jambe intérieure. Cela était dû à une augmentation marquée de la force médio-latérale dans le virage. Pour contrecarrer cela, les participants augmentaient leur temps d'appuis sur la jambe intérieure afin de produire des niveaux d'impulsions résultante et verticale similaires à la ligne droite. La troisième étude explorait quant à elle la cinématique articulaire de la hanche, du genou et de la cheville lors du virage, en comparaison à la ligne droite. Lors de la phase d'appuis, nous avons principalement rapporté une diminution de l'extension de genou de la jambe intérieure et une augmentation de la flexion plantaire de la cheville extérieure, dues à l'inclinaison vers l'intérieur du virage. Enfin, la quatrième et dernière étude explorait les chronologies de mise en action ainsi que les niveaux d'activation de quatre muscles des membres inférieurs grâce à sEMG. Nous avons rapporté un plus faible niveau d'activation du *Vastus Lateralis* (VL, un extenseur de genou) de la jambe intérieure dans le virage en comparaison à la ligne droite. Ainsi, d'un point de vue global, la performance était diminuée dans le virage à cause d'une diminution de la force verticale sur la jambe gauche, elle-même due à une plus grande flexion du genou gauche à cause d'une plus faible activation du VL gauche dans le virage. Ces résultats dans leur globalité nous permettent de mieux comprendre les raisons pour lesquelles la performance est diminuée lors de la course de sprint en virage en comparaison à la ligne droite. Basées sur ces résultats, nous avons dressé des recommandations pratiques dans un double objectif d'amélioration de la performance et de réduction des risques de blessures.

Mots clés : Course en virage, application des forces au sol, cinématique, électromyographie de surface, sprint, optimisation de la performance, prévention des blessures.